UC Riverside

UC Riverside Electronic Theses and Dissertations

Title

Analysis of Capsid Dynamics Among Multipartite Bromoviruses

Permalink

https://escholarship.org/uc/item/6wq0s22x

Author

Chakravarty, Antara

Publication Date

2021

Copyright Information

This work is made available under the terms of a Creative Commons Attribution-NonCommercial-NoDerivatives License, availalbe at https://creativecommons.org/licenses/by-nc-nd/4.0/

Peer reviewed|Thesis/dissertation

eScholarship.org Powered by the California Digital Library
University of California

UNIVERSITY OF CALIFORNIA
RIVERSIDE

Analysis of Capsid Dynamics Among Multipartite Bromoviruses

A Dissertation submitted in partial satisfaction
of the requirements for the degree of

Doctor of Philosophy

in

Plant Pathology

by

Antara Chakravarty

June 2021

Dissertation Committee:
Dr. A. L. N. Rao, Chairperson
Dr. Shou-wei Ding
Dr. Rong Hai
Dr. Roya Zandi

Copyright by
Antara Chakravarty
2021

The Dissertation of Antara Chakravarty is approved:

_____

_____

_____

_____

Committee Chairperson

University of California, Riverside

ACKNOWLEDGEMENTS

It is a great pleasure to express my gratitude towards my Ph.D. supervisor, Professor ALN Rao, for his generous support and mentorship throughout my studies at UCR. I am thankful to him for allowing me to pursue projects of my interests and for teaching me many skills about scientific presentation and grantsmanship. His scholarly advice and rigorous attention to detail decidedly helped me to complete this degree. I thank my dissertation committee members Dr. Shou-wei Ding, Dr. Rong Hai, and Dr. Roya Zandi. They were always there to help with their constructive inputs, encouragement, and insightful comments on my work. I am very thankful for all the support I have received from my dear friend and labmate, Dr. Areeje Almasary.

I extend my gratitude and acknowledgment to the Chair of the Dept. of Microbiology and Plant Pathology, Dr. Katherine Borkovich, for her generous support towards my teaching goals and to Dr. Laura McGeehan, my Graduate Student Advisor, for her guidance, kindness, and prompt answers to any questions I had. I am grateful to Dr. James Ng and his lab members Dr. Jaclyn Zhou, Dr. James Peng, Dr. Angel Chen, and Chien-Hao, for their support throughout these years. I acknowledge past and present staff members at BMPN administration Nancy Ferguson, Sarah Acrey, Joann Braga, and Maggie Flores for answering many logistical questions about purchasing, order delivery, and conference

travels. I am very thankful for the support and guidance from Dr. Jie Zhou and Matthew Dickson for my MALDI and EM analysis work. I am grateful to Dr. David Pearson, the Director for Office of Technology Partnerships at UCR, Dr. Jay Gilberg, the lead instructor at the NSF I-Corps program, and my wonderful mentor Steve Sharp at Innova'R workshops for many thought-provoking discussions about the practical applications of my research. Dr. William Gelbert and Dr. Charles Knobler of UCLA provided much constructive criticism to enhance the quality of this dissertation, which I am very thankful for.

My Ph.D. journey would not have been half as meaningful and productive if I had not met Dr. Hillary Jenks, the Director of GradSuccess at UCR. Her faith in my ability to mentor other teaching assistants at UCR helped me develop as a teacher and scholar. Her resourcefulness, empathy, vast knowledge in graduate student professional development, and her way of leading by example, helped me successfully perform in my role at GradSuccess, which I gratefully thank her for. I also thank other members of my work family at GradSuccess: Dr. Yelda Serin, Christina Trujillo, Sarah, Kyla, Jessica, Songling, Kristoffer, Kelly, Ruihan, Beth, John, Patrick, Tyler, Lin, and Iris for making our time at work so memorable and fun. I also thank my friends at UCR and beyond for their willingness to help me, to guide me, to question me, and to believe in me: Dr. Meenakshi Kagda, Neerja Katiyar, Dr. Heba Zagloul, Fazeelu Fazhaludheen, and Shruti Kulkarni.

To my family, I can never thank them enough for their enduring support in achieving my dreams. My father, Arun, whom I lost during the third year of my Ph.D. never stopped having the optimistic belief in my aspirations. His blessings light up my ways even on the darkest of days. My mother Sarbari, and brother Shouvik, never failed to say that they were proud of me. I am grateful for the love I have received in abundance from my grandma Indira, my aunts Chandana and Ranjana, my uncle Biswanath, and my cousins Ananya, Kumarjit, and Kumarika. And I would not have persisted on this journey if I did not have the never-failing, selfless love of my husband, Rajesh. Having him beside me in this life's expedition has been and will forever be the greatest honor of my life. And above all, I am thankful to dear God, whose blessings I cannot finish counting!

DEDICATION

To my Grandma Indira Ganguly, the brightest light of my life

ABSTRACT OF THE DISSERTATION

Analysis of Capsid Dynamics Among Multipartite Bromoviruses

by

Antara Chakravarty

Doctor of Philosophy, Graduate Program in Plant Pathology
University of California, Riverside, June 2021
Dr. A. L. N. Rao, Chairperson

Viruses are intracellular parasites that can invade the cells of all known organisms. All viruses contain two components: a DNA or RNA genome and the capsid. Although the essential role of a viral capsid is to protect its genome, it must also release its genome for replication. To meet these two contesting requirements, viral capsids undergo a dynamic and reversible reorganization of biologically relevant surface peptides critical for their infectivity. Plant RNA viruses in the family *Bromoviridae* have a single-strand, positive-sense RNA genome divided among three genomic RNAs. These RNAs and subgenomic RNA get packaged into three homogeneous or four heterogeneous virion particles. In bromoviruses, the three virions, each carrying unique RNA species, have been physically inseparable by known separation techniques due to their particle homogeneity. Therefore, whether essential structural dynamism existed in these morphologically indistinguishable virions which could be of biological importance was unknown. **Chapter 1** of this dissertation focused on investigating the stability

and capsid dynamics of the three virions of brome mosaic virus (BMV), the type species of the genus *Bromovirus*, assembled autonomously in *Nicotiana benthamiana* using a robust agroinfiltration strategy. As the three virion types in BMV are identical in their morphology and electrophoretic mobility patterns, the use of a thermal denaturation assay and limited proteolysis followed by peptide mass mapping with MALDI-TOF enabled us to identify qualitative differences in capsid dynamics of three virions in BMV. **Chapter 2** focused on understanding the comparative capsid dynamics among the three virions of BMV and cowpea chlorotic mottle virus (CCMV), a member of the family Bromoviridae that shares an identical genome organization and packaging scheme as BMV. **Chapter 3** analyzed the relative dynamics of BMV and CCMV capsids assembled in the presence of heterologous replicase. **Chapter 4** investigated the biological significance of co-packaging of a genetically redundant subgenomic RNA4 in BMV. **Chapter 5** characterized Virus-like Particles (VLPs) assembled from the Gag protein of human immunodeficiency virus (HIV-1) in *N. benthamiana*. Finally, **Chapter 6** attempted to silence the NbSKP1 gene in *N. benthamiana* using virus-induced gene silencing (VIGS) and studied the following effect on cucumber mosaic virus-Q strain accumulation.

TABLE OF CONTENTS

LIST OF FIGURES

CHAPTER 2

CHAPTER 3

CHAPTER 4

CHAPTER 5

CHAPTER 6

LIST OF TABLES

INTRODUCTION

Viruses are obligate intracellular parasites that can invade and infect the cells of effectively all known organisms. They reproduce by confiscating the cell's biochemical machinery, energy, and building blocks of biomolecules to replicate viral genetic material and translate viral proteins, generally damaging or killing the host cell in the process. Then a large number (up to several thousand) of newly synthesized progeny viruses go on to infect neighboring cells, with the resulting exponential growth causing catastrophic damage in the host system within hours. Viruses are responsible for various virulent human diseases, ranging from poliomyelitis, hepatitis B liver infection, influenza to Zika, AIDS, and Ebola hemorrhagic fever. A novel coronavirus called SARS-CoV-2 (Zhou et al., 2020) has been responsible for the ongoing COVID-19 pandemic. As of the beginning of May 2021, SARS-CoV-2 has caused ~154 million cases of mild to acute respiratory distress and ~3 million deaths globally since December 2019 (https://covid19.who.int/). Similarly, many plant RNA viruses like the *Cucumber mosaic virus* (CMV), *Tobacco streak virus* (TSV), and *Alfalfa mosaic virus* (AMV) cause severe crop loss worldwide (Bol, 2005; Jacquemond, 2012; Pallas et al., 2012). Several genetically engineered (e.g., lentiviruses and adenoviruses) and attenuated (e.g., polio and yellow fever) human viral pathogens have been exploited for gene and vaccine delivery purposes, and several viruses that are not dangerous to humans (e.g., plant and bacterial viruses) are being used in biotechnology and nanomedicine applications.

All viruses contain at least two components: the capsid (a protein shell), and a genome, consisting of either DNA or RNA. Although one of the essential roles of a viral capsid is to *protect* its genome, it must also *release* its genome for replication. In the case of most double-stranded (ds) DNA viruses, the capsid remains intact, and the genome is ejected by the internal pressure of the virus that has been built up during its packaging into a preformed capsid (Gelbart & Knobler, 2009). However, for most single-stranded (ss) RNA viruses, which make up the majority of virulent human, plant, and animal pathogens, the capsid must be flexible enough to release its genome by disassembly (Suomalainen & Greber, 2013) or to allow ribosomes to translate its genes while remaining intact (Bakker et al., 2012). In this thesis, *Brome mosaic virus* (BMV) and *Cowpea chlorotic mottle virus* (CCMV) are used to elucidate how the unique *structures and accompanying dynamics* of the capsids of eukaryotic RNA viruses facilitate the exquisitely controlled order of their gene translation and replication processes.

MONOCOMPONENT AND MULTICOMPONENT VIRUSES

One class of plant viruses is characterized by having the genetic information required to initiate infection in a given host plant encoded by a single nucleic acid molecule. One of the notable examples is the *Tobacco mosaic virus* (TMV). In the second class of viruses, this required genetic information is divided among two or more nucleic acid molecules. Consequently, the former category is mono-component while the latter is multicomponent viruses (Sicard, Michalakis,

Gutiérrez, & Blanc, 2016). However, it should be noted that mono or multicomponent refers to the number of nucleic acid species but not the number of virions required to initiate the infection. A recent study highlighted a significant difference between the arrangement of RNA inside a multicomponent virion vs. that of a monocomponent virion. In multicomponent virions, the RNA genome is highly disordered inside the virion and mainly situated at the capsid shell. In monocomponent viruses like MS2, the genome is highly ordered with a dominant RNA conformation inside the virion. This difference is a result of the different lifecycle of the two groups of viruses. The monocomponent viruses package their genome using the packaging signals present throughout their genome, whereas the multicomponent viruses like BMV package their genome using the non-specific electrostatic interactions between RNA and capsid protein inside the virus-induced vesicles (Beren et al., 2020).

This thesis will focus on members of the family *Bromoviridae,* consisting *of* an agronomically important family of tripartite plant viruses. Viruses in this family exhibit the following characteristics:

- These viruses are pathogenic to vegetables like tomato, pepper (Jacquemond, 2012), in fruit crops like cherry, plum, peach (Pallas et al., 2012), as well as in fodder crops, ornamentals, herbaceous, and woody hosts.

- They are transmitted between susceptible hosts horizontally by mechanical inoculation to experimental hosts and non-persistently by insect vectors or vertically by pollen grains under natural settings (Jacquemond, 2012).
- They are characterized by having their genomes segmented into three linear single-stranded, positive(+)-sense RNAs packaged in three or four separate virions varying in morphology.
- Type species of the genera, *Bromovirus, Cucumovirus,* and *Alfamovirus,* serve as model systems in understating the mechanism of replication, genome packaging, translation, and recombination (Rao, 2006).

BROME MOSAIC VIRUS (BMV)

I. Genome Organization

Brome mosaic virus (BMV) is the type species of the genus *Bromovirus* (Bujarski et al., 2019). BMV ranks among the best-studied multipartite, positive-strand RNA viruses with respect to replication and genome packaging (Rao, Chaturvedi, & Garmann, 2014; Rao & Cheng Kao, 2015). The largest two genomic RNAs of BMV– RNA1 (B1) and RNA2 (B2)– are monocistronic, encoding non-structural replicase proteins 1a and 2a, which are methyltransferase-like (MT)/ Helicase-like (HEL) and RNA-dependent RNA Polymerase (RdRp), respectively (Kao & Sivakumaran, 2000). Genomic RNA3 (B3) is bicistronic and encodes another non-structural protein– the movement protein (MP)– at its 5' end, along with a 3' structural capsid protein (CP) (Kao & Sivakumaran, 2000). CP is

translated from replication-derived subgenomic RNA4 (B4), synthesized from minus-strand B3 by an internal initiation mechanism (Miller, Dreher, & Hall, 1985). The three virions of BMV (one each packaging B1 and B2 and the third co-packaging B3 and B4) are assembled from 180 copies of the CP and appear physically identical in shape and size (Lucas, Larson, & McPherson, 2002). In addition to protecting the progeny RNA from the cellular environment, virion assembly in BMV is intimately associated with other functions such as modification of the endoplasmic reticulum (ER) (Bamunusinghe, Chaturvedi, Seo, & Rao, 2013), symptom expression (Rao & Grantham, 1995) and cell-to-cell spread (Schmitz & Rao, 1996). Indeed, disruption of virion assembly results in failed ER modification (Bamunusinghe et al., 2013), blocked cell-to-cell spread (Schmitz & Rao, 1996), and onset of hypersensitive response (Rao & Grantham, 1995). The 3′-end of each genomic and sgRNA in BMV forms a tRNA-like structure (TLS) that mimics several tRNA-associated functions such as binding tyrosine and interaction with nucleotidyltransferase to maintain an intact -CCA_{OH} in telomeric fashion (Rao & Cheng Kao, 2015). i.e., if -CCA nucleotides are removed by the cellular ribonuclease, the intact -CCA's resynthesis occurs by the action of tRNA nucleotidyaltransferase.

II. Virion Characteristics

Purified virions of BMV contain a mixture of three virions. Physical and biochemical studies suggested that genomic RNA1 and RNA2 are packaged

separately into two particles while the genomic RNA3 and sgRNA4 are co-packaged into a third virion (Rao, 2006). The three virions of BMV are physically indistinguishable and are assembled from 180 coat protein subunits, measuring about 26 nm diameter with T=3 symmetry (Lucas et al., 2002). The virion structure of BMV has been resolved to ~3.4 Å and was found to be highly homologous (Lucas et al., 2002; Smith, Chase, Schmidt, & Perry, 2000). Since the three virions of BMV are physically indistinguishable, the reported crystallographic structure represents the average of three virions.

III. Genome Packaging

The mechanism of genome packaging was extensively studied in BMV (Rao, 2006). The ease with which BMV virions could be assembled *in vitro* has dramatically advanced in delineating various domains of the CP and RNA involved in the assembly of infectious virions (Rao, 2006). Application of *in vitro* assembly studies revealed that (i) a highly conserved 3' TLS is essential to initiate packaging of BMV RNAs into virions (Choi, Dreher, & Rao, 2002); (ii) packaging core of BMV RNA3 is bipartite constituting a 3' TLS and a *cis*-acting, position-dependent packaging element of 187 nucleotides (nt) present in the non-structural movement protein gene (Choi & Rao, 2003) and (iii) selective co-packaging of sgRNA-4 into virions containing RNA-3 is determined by the arginine residues located in the N-proximal region of BMV capsid protein (Choi & Rao, 2000). Subsequent application of the *Agrobacterium*-mediated transient expression system further identified that

genome packaging in BMV and most likely in other positive-strand RNA viruses is functionally coupled to replication.

IV. Replication Characteristics

Replication of BMV requires forming a functional RNA-dependent RNA polymerase (RdRp) complexed with a wide range of host factors (He, Zhang, Sathanantham, Diaz, & Wang, 2021). In principle, viral RNA replication involves initiating (-)-strand synthesis by the functional RdRp followed by asymmetric synthesis of progeny (+)-RNA. The initiation of the (-)-strand synthesis takes place at the penultimate cytidylate of the 3'-CCA_{OH} of the (+)-strand genomic RNA (Miller et al., 1985). The resulting (-)-strand progeny RNA serves as a template for the asymmetric synthesis of genomic (+)-strand RNA. RNA elements promoting (-)- and (+)-strand synthesis have been mapped using *in vitro* and *in vivo* replication assays (de Wispelaere, Sivanandam, & Rao, 2020).

The 200 nucleotide-long 3' TLS is highly conserved in three genomic as well as in the sgRNA in BMV, disruption of which results in a robust reduction in the genomic RNA1, 2 and less substantial decrease in the translation of the genomic RNA3 in wheat germ system. In contrast, the same disruption doesn't have any effect on CP expression from sgRNA4. This deficient translation was partially restored by providing the TLS in *trans* or was almost fully restored by providing a subdomain of TLS with only the hairpin structure of B2, C, and D regions (Barends et al., 2004). In BMV, in addition to RdRp, viral CP has been shown to play a critical

role in asymmetric replication, specifically in stimulating the (+)-strand synthesis (de Wispelaere et al., 2020).

Regarding the subcellular sites of replication, all member viruses of the family *Bromoviridae* are on either tonoplast or ER membranes (Bamunusinghe, Seo, & Rao, 2011; Bol, 2005; Jacquemond, 2012). Studies performed using yeast (den Boon, Chen, & Ahlquist, 2001) as a surrogate non-host system and as well as *Nicotiana benthamiana* revealed that BMV replicase protein 1a (p1a) reorganizes the endoplasmic reticulum (ER), inducing large assemblies of membrane vesicles to house replication-related functions. In addition to p1a, in *N. benthamiana* but not in yeast, an assembly competent viral CP modifies the ER to induce vesicles, accentuating a link between viral replicase and CP during the replication (Bamunusinghe et al., 2013).

COWPEA CHLOROTIC MOTTLE VIRUS (CCMV)

Like BMV, *Cowpea chlorotic mottle virus* (CCMV) is another member of the genus *Bromovirus* (Bujarski et al., 2019). It has a tripartite genome that consists of three single-stranded RNA, the first two being monocistronic and the last one being bicistronic. It follows a similar genome organization and packaging scheme as BMV. However, unlike BMV, which infects monocot hosts in a natural environment, CCMV was initially isolated from dicotyledonous host cowpea (Lane, 1981). *N. benthamiana* is a symptomless host for both BMV and CCMV. Symptomatic host *Chenopodium quinoa* is used to distinguish BMV from CCMV since the former

induces chlorotic local lesions followed by systemic mottling. In contrast, the latter induces only local necrotic lesions.

Heterologous expression of CCMV CP in suitable systems like *Pseudomonas fluorescens* and *Pichia pastoris* results in a high yield of soluble protein and *in vivo* assembly of virus-like particles (VLP, eCCMV) that were morphologically indistinguishable from the CCMV virions produced in natural plant hosts (Brumfield et al., 2004; Phelps, Dao, Jin, & Rasochova, 2007). The ability of eCCMV to encapsulate various host RNAs in a non-specific manner (Brumfield et al., 2004) and easy attachment of a wide variety of ligands on the capsid surface (Barwal, Kumar, Kateriya, Dinda, & Yadav, 2016) highlights the therapeutic potential of the CCMV VLP system. These findings are further encouraging as CCMV protein cages demonstrated broader tissue distribution and rapid clearance *in vivo* in a nonpathogenic mice model (Kaiser et al., 2007).

CCMV virions undergo a dramatic structural transition in response to changes in pH resulting in metal ion-dependent disassembly (at higher pH 7.5) and self-assembly (at lower pH 5.0). Changes in pH, combined with ionic strength and divalent cation concentration resulting in swelling of the virion volume by 10%. Speir et al. (Speir et al., 2006) compared the capsid dynamics between the closed and swollen forms of the wild type (WT CCMV) and a salt stable mutant of CCMV (SS-CCMV). Surprisingly, although a swollen state is expected to expose more trypsin cleavage sites, it was observed that SS-CCMV was less susceptible to

trypsin protease treatment than the WT CCMV. Matrix-assisted laser desorption ionization-time of flight (MALDI-TOF) analysis showed that cleavage of the tryptic peptide regions is localized in the N-terminus of the CP and the virions remained intact.

Studies involving BMV and CCMV show that the requirement of CP in cell-to-cell trafficking of monocot- vs. dicot-adapted members in genus *Bromovirus* was distinct (Weber & Bujarski, 2015). Biologically active RNA3 of BMV and CCMV where the CP was substituted with a reporter gene showed that, unlike BMV, epidermal cell-to-cell movement of CCMV could occur without a functional CP (Rao, 1997). However, neither BMV CP nor CCMV CP was found to harbor host-specific determinants for systemic spread when chimeric RNA3 expressing heterologous CP from both viruses were studied (Osman, Grantham, & Rao, 1997).

THE INTERPLAY BETWEEN CAPSID DYNAMICS AND PATHOGENESIS IN VIRUSES

Successful dissemination of almost all RNA viruses to eukaryotic cells requires stably assembled infectious virions. The assembly of viral capsids is regulated by sequence-specific and non-specific interaction between the CP subunits and the viral nucleic acid and the assistance of other scaffolding proteins (Mateu, 2013). Also, viral capsids have different primary roles like receptor binding, cellular entry, navigating the intracellular environment, and viral genome release.

To meet these requirements, virions must be stable enough to withstand the physicochemical environment they encounter and undergo a reversible reorganization of biologically relevant surface peptides critical for their infectivity (Doerschuk, Gong, Xu, Domitrovic, & Johnson, 2016).

Although information gleaned from the Cryo-EM and X-ray crystallographic studies shows that viral capsid as static structures, biochemical and physical studies reveal that viral capsids are conformationally dynamic assemblies fluctuating from inside to outside the particle. These fluctuations or the protein subunits' dynamism manifest the breathing of the particles and play an essential role in infectivity (Johnson, 2003).

FLUCTUATING DYNAMIC PROPERTIES OF VIRUSES

(i) Animal viruses

Virus assembly and genome packaging in RNA viruses is a highly orchestrated process to ensure only the progeny RNA is preferentially packaged (Rao, 2006). Information concerning the existence of fluctuating dynamic properties of virions was obtained from research on poliovirus.

A combination of experiments involving polypeptide fragments of the VP1 subunits of poliovirus and their antibodies' neutralizing properties revealed that infectivity was mapped to the antigenic epitopes of the virus (Chow, Yabrov, Bittle, Hogle, & Baltimore, 1985). Subsequent analysis of the poliovirus virion structure

confirmed that most peptides identified as antigenic epitopes were found on the particle (Hogle, Chow, & Filman, 1985). However, one N-proximal peptide sequence that was internal in the X-ray structure was able to elicit antibodies, suggesting this N-terminal peptide is intermittently exposed on the capsid (Roivainen, Piirainen, Rysä, Närvänen, & Hovi, 1993).

A more quantitative approach was used to map the dynamics of the crystallographically indistinguishable virions of wild type *Flock house virus* (FHV). The method used limited proteolysis followed by MALDI-TOF. X-ray structural analysis of FHV virions revealed that the N- and C-terminal regions of the CP are localized internally (Bothner, Dong, Bibbs, Johnson, & Siuzdak, 1998; Bothner et al., 1999). A time-course proteolytic analysis of intact wild type FHV virions revealed that the first digestion products were from the N- and C-terminal regions of the CP subunit, suggesting the transient exposure polypeptides on the surface of the viral capsid (Bothner et al., 1999). The approach extended to analyze the wild type FHV virions' dynamics containing the authentic viral genome and VLPs of FHV containing the cellular RNA assembled in a baculovirus expression system. Although both the VLPs and wild type FHV virions are structurally indistinguishable, the VLPs were significantly more susceptible to CP's proteolytic cleavage than wild type FHV virions. These observations suggested that packaged RNA has a regulatory role in protein stability during virus assembly (Bothner et al., 1999).

Adeno-associated viruses (AAV) that efficiently replicate in the presence of a helper virus like *Adenovirus* or *Herpesvirus* have T=1 icosahedral symmetry and several serotypes based on the viral capsid protein (VP) sequence and antigenicity. A study focusing on biophysical properties of AAV VLPs containing heterologous cellular RNA and GFP-gene containing virions of four serotypes, AAV1, AAV2, AAV5, and AAV8, revealed the serotypes to have distinct thermal denaturation profile and capsid dynamics. The most stable serotype was AAV5 with a melting temperature (T_m) ~5, ~17, and ~20°C, respectively, higher than AAV1, AAV8, and AAV2. Limited proteolysis followed by peptide mass mapping showed each serotype has a specific banding pattern, yet the kinetically favored first cleavage sites are mapped around the icosahedral 3-fold axes of symmetry. This region has been shown to play a crucial role in receptor binding in AAV2 and AAV8. This study also suggested that VP domains in AAV serotypes are dynamic and internal domains can be transiently exposed on the capsid surface (Rayaprolu et al., 2013).

(ii) Plant viruses

Plant viruses do not require receptor-mediated pathways to enter their hosts, and their systemic spread is mediated through intercellular connections. Since these inherent features of plant viruses are distinct from those of animal viruses, virions of plant viruses need not be dynamic. Indeed, virions of comoviruses, a group of plant viruses belonging to the picornavirus subgroup, are

similar to the picornavirus capsids but are less dynamic in solution (Lomonossoff & Johnson, 1991). Interestingly, a contrasting scenario was observed in the genus *Bromovirus*, a group of tripartite plant RNA viruses. Two members of the genus *Bromovirus*, BMV and CCMV, are well characterized by structure and capsid dynamics (Beren et al., 2020; Rao, 2006). BMV and CCMV are tripartite, icosahedral plant RNA viruses with T=3 symmetry. The genome of BMV and CCMV is divided among three single-strand, positive-sense RNAs (Kao & Sivakumaran, 2000). In these two viruses, the replication-derived progeny RNA is packaged in three homogeneous virion particles (Annamalai, Rofail, Demason, & Rao, 2008).

FLUCTUATING DYNAMIC PROPERTIES OF BMV AND CCMV VIRIONS

The advent of limited proteolysis followed by MALDI-TOF allowed us to analyze the fluctuating dynamics of BMV and CCMV virions. CCMV and BMV are known to undergo a dramatic structural transition in response to changes in pH, ionic strength, and divalent cation concentration resulting in swelling of the virion volume by 10%. Capitalizing on these features, Speir et al. (2006) compared the capsid dynamics between closed and swollen forms of wild type CCMV (WT CCMV) and a salt-stable mutant of CCMV (SS-CCMV). Surprisingly, although a swollen state is expected to expose more trypsin cleavage sites, it was observed that SS-CCMV was less susceptible to trypsin protease treatment than WT CCMV. MALDI-TOF analysis showed that cleavage of the tryptic peptide regions is

localized in the N-terminus of the CP, and the virion remained intact when examined under an electron microscope (Speir et al., 2006).

Interestingly, a study of the capsid dynamics in BMV, using approaches similar to those applied for CCMV, revealed a different scenario. In BMV CP, an N-terminal peptide ^{41}KAIKAIA^{47} functions as a molecular switch regulating T=3 virion symmetry (Calhoun, Speir, & Rao, 2007). This peptide (Δ7aa) deletion resulted in the assembly of polymorphic virions that preferentially packaged the truncated genomic RNAs over full-length and in the capsid dynamics fluctuation. For example, in wild-type BMV virions, residues 86-87 are on the particle interior but next to the quasi-3-fold axis. The deletion of the molecular switch region made the residues 86-87 more accessible to protease. This altered capsid dynamics manifestation is reflected in symptom phenotype by preventing the virus's systemic spread in barley plants. Interestingly, engineering the same deletion in CCMV had no detectable effect on either virion packaging or symptom expression, suggesting that the deleted molecular switch region can exert distinctly different outcomes despite being structurally similar viruses. These observations collectively indicated that BMV and CCMV exhibit distinct capsid dynamics despite being structurally very similar.

SCOPE OF THE THESIS

The three virions in either BMV or CCMV are homogeneous, therefore physically inseparable by known separation techniques like $CsCl_2$ buoyant density centrifugation and sucrose density gradient centrifugation. As a result, the reported crystallographic structure for these viruses is an average of all three virion types. Additionally, the previous studies investigating capsid dynamics in these viruses used either WT viruses or a CP mutant, both of which contained a mixture of three types of virions. Therefore, it was previously unknown whether the three virion types in the members of genus *Bromovirus* are structurally identical and how local and global dynamic conformational changes of the viral capsids modulate functions of biological relevance. As these virions were impossible to isolate in pure form, the reason for subgenomic RNA co-packaging in bromoviruses was also unknown.

Thus, in Chapter 1 of this thesis, we have established a robust agroinfiltration-based strategy to obtain, in pure form, each virion type of BMV, free from the remaining two counterparts. Using these pure virion types, we have shown that qualitatively different capsid dynamics exist in these individual virion types that may have important implications in the pathogenesis of bromoviruses.

Chapter 2 analyzes the comparative capsid dynamics among the three virions of CCMV and BMV using individual pure virion types of each virus,

assembled in a shared experimental host *Nicotiana benthamiana* that both viruses infect asymptomatically.

Chapter 3 analyzes the comparative thermal stability and dynamics of BMV and CCMV RNA3+4 containing virions assembled in the presence of heterologous replicase.

Chapter 4 investigates the answer to a critical question that why CP-independent bromoviruses co-package the subgenomic RNA4 with RNA3 in a separate virion? This chapter describes the role of sub-genomic RNA packaging in BMV capsid dynamics and pathogenesis by using RNA3+4 and RNA3 only containing virions of BMV.

The following two chapters describe the assembly of plant-based virus-like particles and the effect of a targeted host-gene silencing on viral replication. Chapter 5 sheds light on the *in vivo* self-assembly of *Human Immunodeficiency Virus-1* (HIV-1) Gag protein in *N. benthamiana* and characterizes the assembled VLPs isolated from plants. This chapter discusses the benefits of using plant-derived capsids of human viral pathogens as a tool to study virus assembly and maturation.

Chapter 6 studies the effect of silencing of a host gene S-phase kinase-related protein-1 (SKP1), an essential part of the SCF (SKP1-CUL1-F-box protein) ubiquitin ligase complex, on the accumulation of *Cucumber mosaic virus* (CMV).

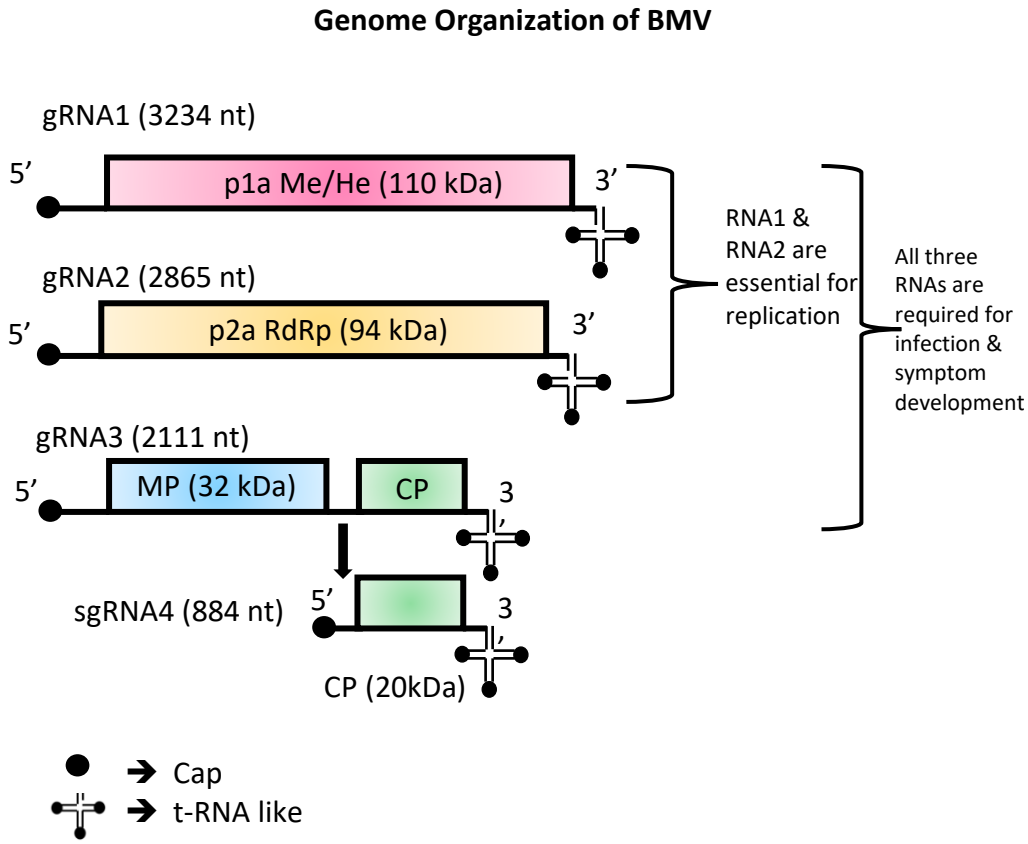

Figure 1. Genome organization of *Brome mosaic virus* (BMV)

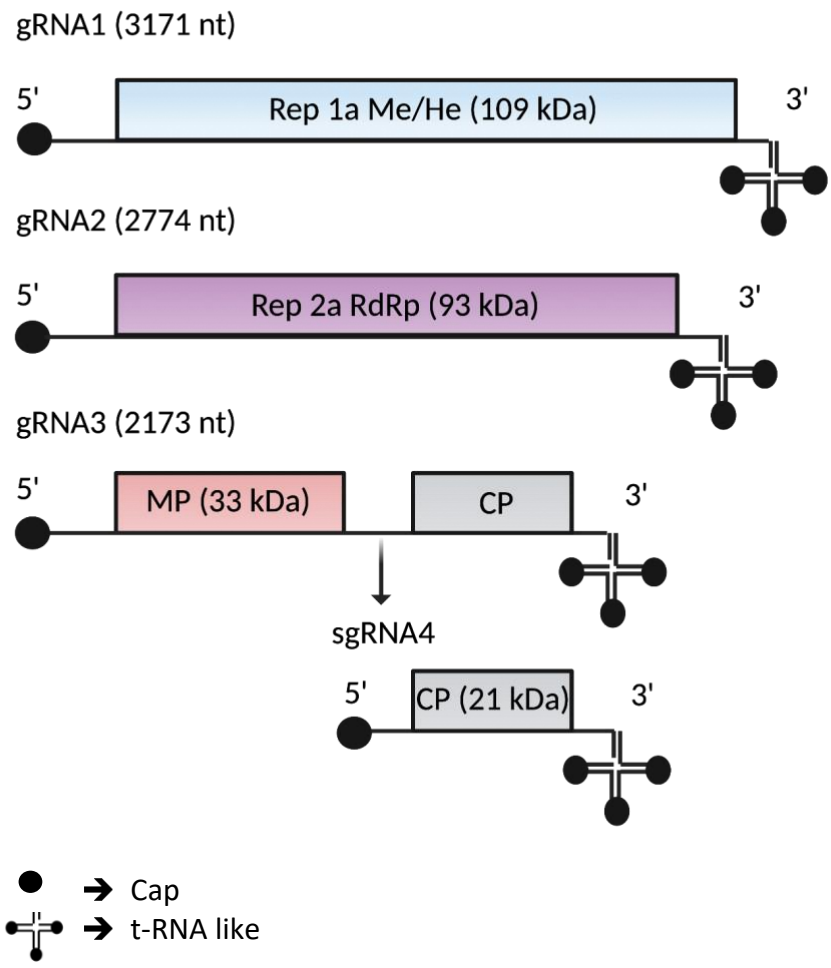

Figure 2. Genome organization of *Cowpea chlorotic mottle virus* (CCMV)

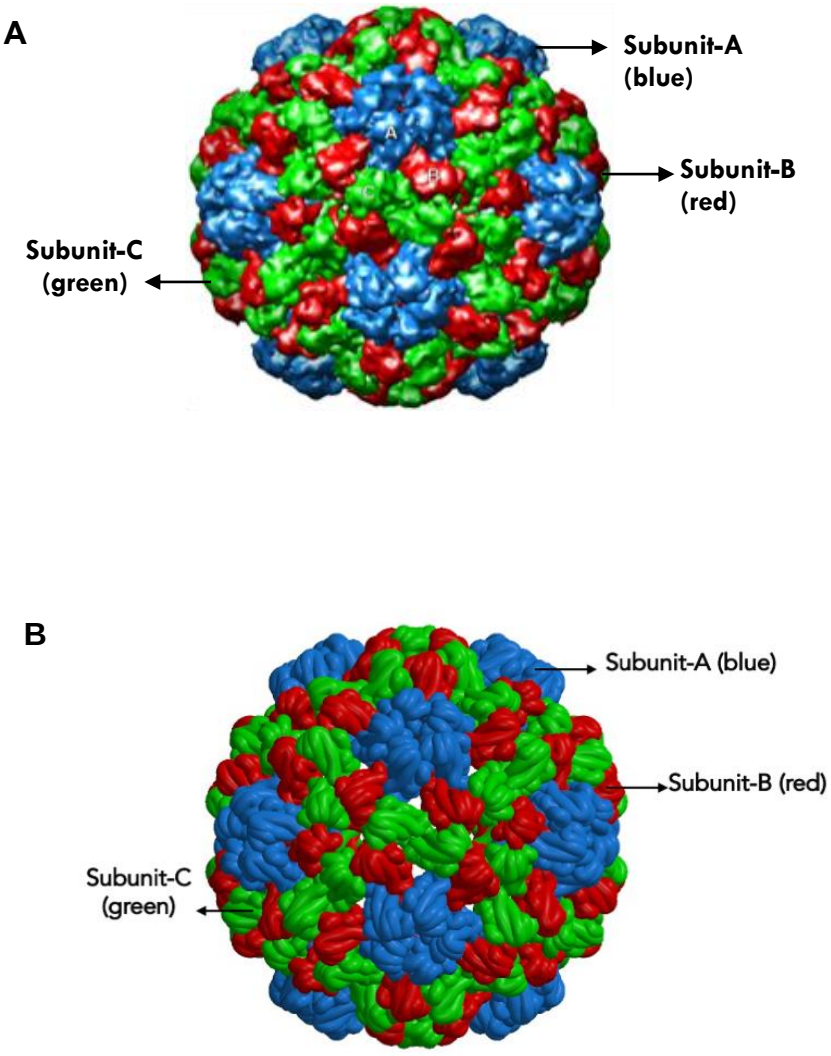

Figure 3. Structure of the BMV and CCMV virions. (A) The structure of the BMV capsid based on the PDB entry 1JS9 shows the A, B, and C subunits. (B) Structure of CCMV capsid based on the PDB entry 1CWP shows A, B, and C subunits.

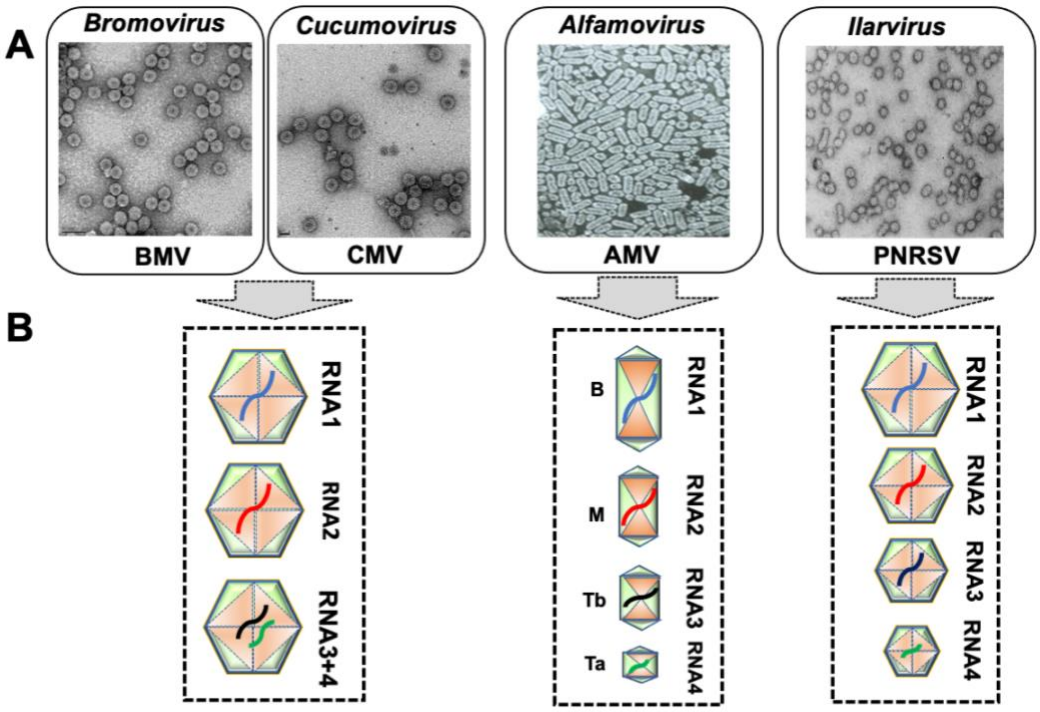

Figure 4. (A) Electron micrographs and (B) packaging scheme of the member viruses in the family *Bromoviridae* showing either three homogeneous or four heterogeneous virions.

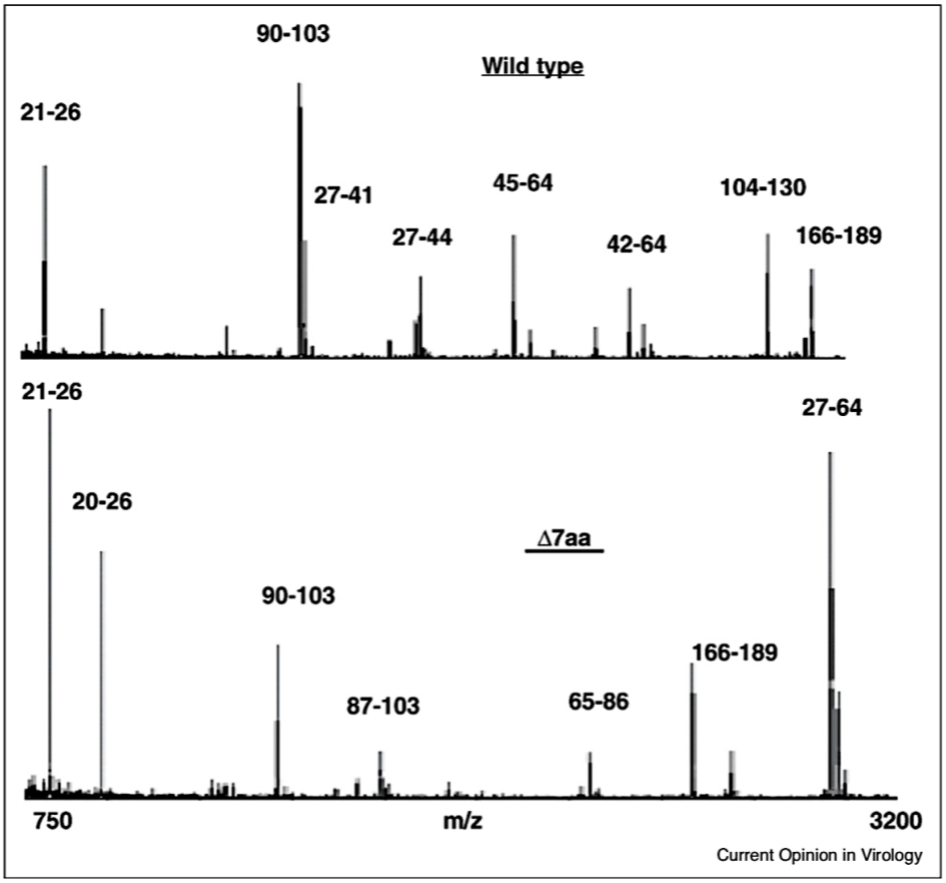

Figure 5. Capsid dynamics in BMV. MALDI-TOF analysis of BMV CP peptides released from the wild type and a mutant characterized by the deletion of seven amino acid residues (Δ7aa) controlling the molecular switch. Purified virions of WT BMV and mutant Δ7aa were treated with trypsin protease, and the MALDI-TOF identified the resulting peptides. The prominent peaks are labeled with corresponding polypeptide fragments of indicated amino acid residues (Calhoun et al., 2007)

REFERENCES

Annamalai, P., Rofail, F., Demason, D. A., & Rao, A. L. (2008). Replication-coupled packaging mechanism in positive-strand RNA viruses: synchronized coexpression of functional multigenome RNA components of an animal and a plant virus in Nicotiana benthamiana cells by agroinfiltration. *J Virol, 82*(3), 1484-1495. doi:10.1128/JVI.01540-07

Bakker, S. E., Ford, R. J., Barker, A. M., Robottom, J., Saunders, K., Pearson, A. R., . . . Stockley, P. G. (2012). Isolation of an asymmetric RNA uncoating intermediate for a single-stranded RNA plant virus. *J Mol Biol, 417*(1-2), 65-78. doi:10.1016/j.jmb.2012.01.017

Bamunusinghe, D., Chaturvedi, S., Seo, J. K., & Rao, A. L. (2013). Mutations in the Capsid Protein of Brome Mosaic Virus Affecting Encapsidation Eliminate Vesicle Induction In Planta: Implications for Virus Cell-to-Cell Spread. *Journal of Virology, 87*(16), 8982-8992. doi:10.1128/JVI.01253-13

Bamunusinghe, D., Seo, J. K., & Rao, A. L. (2011). Subcellular localization and rearrangement of endoplasmic reticulum by Brome mosaic virus capsid protein. *J Virol, 85*(6), 2953-2963. doi:10.1128/JVI.02020-10

Barends, S., Rudinger-Thirion, J., Florentz, C., Giegé, R., Pleij, C. W., & Kraal, B. (2004). tRNA-like structure regulates translation of Brome mosaic virus RNA. *J Virol, 78*(8), 4003-4010. doi:10.1128/jvi.78.8.4003-4010.2004

Barwal, I., Kumar, R., Kateriya, S., Dinda, A. K., & Yadav, S. C. (2016). Targeted delivery system for cancer cells consist of multiple ligands conjugated genetically modified CCMV capsid on doxorubicin GNPs complex. *Sci Rep, 6*, 37096. doi:10.1038/srep37096

Beren, C., Cui, Y., Chakravarty, A., Yang, X., Rao, A. L. N., Knobler, C. M., . . . Gelbart, W. M. (2020). Genome organization and interaction with capsid protein in a multipartite RNA virus. *Proc Natl Acad Sci U S A, 117*(20), 10673-10680. doi:10.1073/pnas.1915078117

Bol, J. F. (2005). Replication of alfamo- and ilarviruses: role of the coat protein. *Annu Rev Phytopathol, 43*, 39-62. doi:10.1146/annurev.phyto.43.101804.120505

Bothner, B., Dong, X. F., Bibbs, L., Johnson, J. E., & Siuzdak, G. (1998). Evidence of viral capsid dynamics using limited proteolysis and mass spectrometry. *J Biol Chem, 273*(2), 673-676. doi:10.1074/jbc.273.2.673

Bothner, B., Schneemann, A., Marshall, D., Reddy, V., Johnson, J. E., & Siuzdak, G. (1999). Crystallographically identical virus capsids display different properties in solution. *Nat Struct Biol, 6*(2), 114-116. doi:10.1038/5799

Brumfield, S., Willits, D., Tang, L., Johnson, J. E., Douglas, T., & Young, M. (2004). Heterologous expression of the modified coat protein of Cowpea chlorotic mottle bromovirus results in the assembly of protein cages with altered architectures and function. *J Gen Virol, 85*(Pt 4), 1049-1053. doi:10.1099/vir.0.19688-0

Bujarski, J., Gallitelli, D., García-Arenal, F., Pallás, V., Palukaitis, P., Reddy, M. K., . . . Ictv Report Consortium. (2019). ICTV Virus Taxonomy Profile: Bromoviridae. *J Gen Virol, 100*(8), 1206-1207. doi:10.1099/jgv.0.001282

Calhoun, S. L., Speir, J. A., & Rao, A. L. (2007). In vivo particle polymorphism results from deletion of a N-terminal peptide molecular switch in brome mosaic virus capsid protein. *Virology, 364*(2), 407-421. doi:10.1016/j.virol.2007.03.034

Choi, Y. G., Dreher, T. W., & Rao, A. L. (2002). tRNA elements mediate the assembly of an icosahedral RNA virus. *Proc Natl Acad Sci U S A, 99*(2), 655-660. doi:10.1073/pnas.022618199

Choi, Y. G., & Rao, A. L. (2000). Molecular studies on bromovirus capsid protein. VII. Selective packaging on BMV RNA4 by specific N-terminal arginine residuals. *Virology, 275*(1), 207-217. doi:10.1006/viro.2000.0513

Choi, Y. G., & Rao, A. L. (2003). Packaging of brome mosaic virus RNA3 is mediated through a bipartite signal. *J Virol, 77*(18), 9750-9757. doi:10.1128/jvi.77.18.9750-9757.2003

Chow, M., Yabrov, R., Bittle, J., Hogle, J., & Baltimore, D. (1985). Synthetic peptides from four separate regions of the poliovirus type 1 capsid protein VP1 induce neutralizing antibodies. *Proc Natl Acad Sci U S A, 82*(3), 910-914. doi:10.1073/pnas.82.3.910

de Wispelaere, M., Sivanandam, V., & Rao, A. L. N. (2020). Regulation of Positive-Strand Accumulation by Capsid Protein During Brome Mosaic

Virus Infection *in planta*. *Phytopathology, 110*(1), 228-236. doi:10.1094/PHYTO-07-19-0236-FI

den Boon, J. A., Chen, J., & Ahlquist, P. (2001). Identification of sequences in Brome mosaic virus replicase protein 1a that mediate association with endoplasmic reticulum membranes. *J Virol, 75*(24), 12370-12381. doi:10.1128/JVI.75.24.12370-12381.2001

Doerschuk, P. C., Gong, Y., Xu, N., Domitrovic, T., & Johnson, J. E. (2016). Virus particle dynamics derived from CryoEM studies. *Curr Opin Virol, 18*, 57-63. doi:10.1016/j.coviro.2016.02.011

Gelbart, W. M., & Knobler, C. M. (2009). Virology. Pressurized viruses. *Science, 323*(5922), 1682-1683. doi:10.1126/science.1170645

He, G., Zhang, Z., Sathanantham, P., Diaz, A., & Wang, X. (2021). Brome Mosaic Virus (Bromoviridae). *Encyclopedia of Virology*, 252-259. doi:10.1016/B978-0-12-809633-8.21294-6

Hogle, J. M., Chow, M., & Filman, D. J. (1985). Three-dimensional structure of poliovirus at 2.9 A resolution. *Science, 229*(4720), 1358-1365. doi:10.1126/science.2994218

Jacquemond, M. (2012). Cucumber mosaic virus. *Adv Virus Res, 84*, 439-504. doi:10.1016/B978-0-12-394314-9.00013-0

Johnson, J. E. (2003). Virus particle dynamics. *Adv Protein Chem, 64*, 197-218. doi:10.1016/s0065-3233(03)01005-2

Kaiser, C. R., Flenniken, M. L., Gillitzer, E., Harmsen, A. L., Harmsen, A. G., Jutila, M. A., . . . Young, M. J. (2007). Biodistribution studies of protein cage nanoparticles demonstrate broad tissue distribution and rapid clearance in vivo. *Int J Nanomedicine, 2*(4), 715-733.

Kao, C. C., & Sivakumaran, K. (2000). Brome mosaic virus, good for an RNA virologist's basic needs. *Molecular plant pathology, 1*(2), 91-97. doi:10.1046/j.1364-3703.2000.00017.x

Lane, L. C. (1981). Bromoviruses. In K. E (Ed.), *Hand book of plant virus infections and comparative diagnosis* (pp. 333-376): Elsevier Biomedical Press, Amsterdam, Netherlands.

Lomonossoff, G. P., & Johnson, J. E. (1991). The synthesis and structure of comovirus capsids. *Prog Biophys Mol Biol, 55*(2), 107-137. doi:10.1016/0079-6107(91)90003-b

Lucas, R. W., Larson, S. B., & McPherson, A. (2002). The crystallographic structure of brome mosaic virus. *J Mol Biol, 317*(1), 95-108. doi:10.1006/jmbi.2001.5389

Mateu, M. G. (2013). Assembly, stability and dynamics of virus capsids. *Arch Biochem Biophys, 531*(1-2), 65-79. doi:10.1016/j.abb.2012.10.015

Miller, W. A., Dreher, T. W., & Hall, T. C. (1985). Synthesis of brome mosaic virus subgenomic RNA in vitro by internal initiation on (-)-sense genomic RNA. *Nature, 313*(5997), 68-70.

Osman, F., Grantham, G. L., & Rao, A. L. (1997). Molecular studies on bromovirus capsid protein. IV. Coat protein exchanges between brome mosaic and cowpea chlorotic mottle viruses exhibit neutral effects in heterologous hosts. *Virology, 238*(2), 452-459. doi:10.1006/viro.1997.8849

Pallas, V., Aparicio, F., Herranz, M. C., Amari, K., Sanchez-Pina, M. A., Myrta, A., & Sanchez-Navarro, J. A. (2012). Ilarviruses of Prunus spp.: a continued concern for fruit trees. *Phytopathology, 102*(12), 1108-1120. doi:10.1094/PHYTO-02-12-0023-RVW

Phelps, J. P., Dao, P., Jin, H., & Rasochova, L. (2007). Expression and self-assembly of cowpea chlorotic mottle virus-like particles in Pseudomonas fluorescens. *J Biotechnol, 128*(2), 290-296. doi:10.1016/j.jbiotec.2006.10.005

Rao, A. L. (1997). Molecular studies on bromovirus capsid protein. III. Analysis of cell-to-cell movement competence of coat protein defective variants of cowpea chlorotic mottle virus. *Virology, 232*(2), 385-395. doi:10.1006/viro.1997.8579

Rao, A. L. (2006). Genome packaging by spherical plant RNA viruses. *Annu Rev Phytopathol, 44*, 61-87. doi:10.1146/annurev.phyto.44.070505.143334

Rao, A. L., Chaturvedi, S., & Garmann, R. F. (2014). Integration of replication and assembly of infectious virions in plant RNA viruses. *Curr Opin Virol, 9*, 61-66. doi:10.1016/j.coviro.2014.09.008

Rao, A. L., & Cheng Kao, C. (2015). The brome mosaic virus 3' untranslated sequence regulates RNA replication, recombination, and virion assembly. *Virus Res, 206*, 46-52. doi:10.1016/j.virusres.2015.02.007

Rao, A. L., & Grantham, G. L. (1995). Biological significance of the seven amino-terminal basic residues of brome mosaic virus coat protein. *Virology, 211*(1), 42-52. doi:S0042-6822(85)71377-3 10.1006/viro.1995.1377

Rayaprolu, V., Kruse, S., Kant, R., Venkatakrishnan, B., Movahed, N., Brooke, D., . . . Bothner, B. (2013). Comparative analysis of adeno-associated virus capsid stability and dynamics. *J Virol, 87*(24), 13150-13160. doi:10.1128/JVI.01415-13

Roivainen, M., Piirainen, L., Rysä, T., Närvänen, A., & Hovi, T. (1993). An immunodominant N-terminal region of VP1 protein of poliovirion that is buried in crystal structure can be exposed in solution. *Virology, 195*(2), 762-765. doi:10.1006/viro.1993.1427

Schmitz, I., & Rao, A. L. (1996). Molecular studies on bromovirus capsid protein. I. Characterization of cell-to-cell movement-defective RNA3 variants of brome mosaic virus. *Virology, 226*(2), 281-293. doi:S0042-6822(96)90656-X [pii] 10.1006/viro.1996.0656

Sicard, A., Michalakis, Y., Gutiérrez, S., & Blanc, S. (2016). The Strange Lifestyle of Multipartite Viruses. *PLoS Pathog, 12*(11), e1005819. doi:10.1371/journal.ppat.1005819

Smith, T. J., Chase, E., Schmidt, T., & Perry, K. L. (2000). The structure of cucumber mosaic virus and comparison to cowpea chlorotic mottle virus. *J Virol, 74*(16), 7578-7586.

Speir, J. A., Bothner, B., Qu, C., Willits, D. A., Young, M. J., & Johnson, J. E. (2006). Enhanced local symmetry interactions globally stabilize a mutant virus capsid that maintains infectivity and capsid dynamics. *J Virol, 80*(7), 3582-3591. doi:10.1128/JVI.80.7.3582-3591.2006

Suomalainen, M., & Greber, U. F. (2013). Uncoating of non-enveloped viruses. *Curr Opin Virol, 3*(1), 27-33. doi:10.1016/j.coviro.2012.12.004

Weber, P. H., & Bujarski, J. J. (2015). Multiple functions of capsid proteins in (+) stranded RNA viruses during plant-virus interactions. *Virus Res, 196*, 140-149. doi:10.1016/j.virusres.2014.11.014

Zhou, P., Yang, X. L., Wang, X. G., Hu, B., Zhang, L., Zhang, W., . . . Shi, Z. L. (2020). A pneumonia outbreak associated with a new coronavirus of probable bat origin. *Nature, 579*(7798), 270-273. doi:10.1038/s41586-020-2012-7

CHAPTER 1

Unravelling the Stability and Capsid Dynamics of the Three Virions of Brome Mosaic Virus Assembled Autonomously In Vivo

Reprinted from Journal of Virology 94:e01794-19. Chakravarty A, Reddy VS, Rao ALN. 2020. Unravelling the stability and capsid dynamics of the three virions of brome mosaic virus assembled autonomously in vivo.

Copyright © American Society of Microbiology, Journal of Virology 94:e01794-19 (2020)

ABSTRACT

Viral capsids are dynamic assemblies that undergo controlled conformational transitions to perform various biological functions. The replication-derived four-molecule RNA progeny of Brome mosaic virus (BMV) is packaged by a single capsid protein (CP) into three types of morphologically indistinguishable icosahedral virions with T3 quasisymmetry. Type 1 ($B1^V$) and type 2 ($B2^V$) virions package genomic RNA1 and RNA2, respectively, while type 3 ($B3+4^V$) virions copackage genomic RNA3 (B3) and its subgenomic RNA4 (sgB4). In this study, the application of a robust *Agrobacterium*-mediated transient expression system allowed us to assemble each virion type separately in planta. Experimental approaches analyzing the morphology, size, and electrophoretic mobility failed to distinguish between the virion types. Thermal denaturation analysis and protease-based peptide mass mapping experiments were used to analyze stability and the conformational dynamics of the individual virions, respectively. The crystallographic structure of the BMV capsid shows four trypsin cleavage sites (K65, R103, K111, and K165 on the CP subunits) exposed on the exterior of the capsid. Irrespective of the digestion time, while retaining their capsid structural integrity, $B1^V$ and $B2^V$ released a single peptide encompassing amino acids 2 to 8 of the N-proximal arginine-rich RNA binding motif. In contrast, $B3+4^V$ capsids were unstable with trypsin, releasing several peptides in addition to the peptides encompassing four predicted sites exposed on the capsid exterior. These results,

demonstrating qualitatively different dynamics for the three types of BMV virions, suggest that the different RNA genes they contain may have different translational timing and efficiency and may even impart different structures to their capsids.

IMPORTANCE

The majority of viruses contain RNA genomes protected by a shell of capsid proteins. Although crystallographic studies show that viral capsids are static structures, accumulating evidence suggests that, in solution, virions are highly dynamic assemblies. The three genomic RNAs (RNA1, -2, and -3) and a single subgenomic RNA (RNA4) of Brome mosaic virus (BMV), an RNA virus pathogenic to plants, are distributed among three physically homogeneous virions. This study examines the thermal stability by differential scanning fluorimetry (DSF) and capsid dynamics by matrix-assisted laser desorption ionization–time of flight (MALDI-TOF) analyses following trypsin digestion of the three virions assembled separately in vivo using the *Agrobacterium*-mediated transient expression approach. The results provide compelling evidence that virions packaging genomic RNA1 and -2 are distinct from those copackaging RNA3 and -4 in their stability and dynamics, suggesting that RNA-dependent capsid dynamics play an important biological role in the viral life cycle.

KEYWORDS

capsid dynamics, stability, genome packaging, RNA virus, MALDI-TOF

INTRODUCTION

Assembly of infectious virions is an essential step in the life cycle of RNA viruses pathogenic to eukaryotic organisms (Johnson, 2003; Mateu, 2013; Rao, 2006). Once assembled, a virion must fulfill two stringent requirements. First, it must be stable enough to withstand physicochemical aggression in the extracellular environment. Second, it must be flexible enough to release the viral genome in the host cell for subsequent replication. In order to meet these two competing demands, virions undergo dynamical fluctuations leading to biologically relevant surface conformational changes.

Brome mosaic virus (BMV), a prototype of the plant virus family Bromoviridae, ranks among the best-studied multipartite, positive-sense RNA viruses with respect to replication, virus assembly, and genome packaging (Rao, Chaturvedi, & Garmann, 2014; Rao & Cheng Kao, 2015). The genome of BMV is divided among three RNAs: the largest two genomic RNAs of BMV, RNA1 (B1) and RNA2 (B2), are monocistronic, encoding nonstructural replicase proteins 1a (p1a) and 2a (p2a), respectively (Kao & Sivakumaran, 2000). The third genomic RNA, RNA3 (B3), is dicistronic, encoding at its 5’ end a nonstructural movement

protein (MP) and at its 3' end a structural capsid protein (CP) (Kao & Sivakumaran, 2000). CP is translated from a replication-derived subgenomic RNA4 (sgB4), which is synthesized from a minus-strand B3 by an internal initiation mechanism (Miller, Dreher, & Hall, 1985). A single CP packages the three genomic RNAs (B1, B2, and B3) and the one subgenomic RNA (sgB4) into three types of morphologically indistinguishable icosahedral virions (Kao & Sivakumaran, 2000; Rao, 2006). Genomic RNAs B1 and B2 are packaged separately into two virion types, $B1^V$ and $B2^V$, respectively, while genomic B3 and sgB4 are copackaged into a third virion type, $B3+4^V$. Remarkably, all three virion types are physically homogeneous in size and morphology and are partially resolved by buoyant density sedimentation (Lane, 1981).

The structure of the BMV virion has been determined at 3.4-Å resolution showing a T=3 icosahedral symmetric capsid composed of 180 identical subunits of a single 20-kDa CP (Lucas, Larson, & McPherson, 2002) (Fig. 1.1A). In the BMV virion, pentameric capsid protein subunit A contains ordered amino acid (aa) residues 41 to 189, while hexameric subunits B and C contain residues 25 to 189 and 1 to 189, respectively (Lucas et al., 2002) (Fig. 1.1A). The first N-proximal 25-aa region of BMV CP contains an arginine-rich motif (ARM) and is not visible in the electron density map, since the N-ARM is disordered and interacts with RNA inside the capsid (Lucas et al., 2002).

In addition to protecting the progeny RNA from the cellular environment, virion assembly in BMV is intimately associated with other functions such as

modification of endoplasmic reticulum (ER) (Bamunusinghe, Chaturvedi, Seo, & Rao, 2013), symptom expression (Rao & Grantham, 1995), and cell-to-cell spread (Schmitz & Rao, 1996). Therefore, it is reasonable to assume that all three virion types should exhibit physical and structural homogeneity to promote optimal interaction with the host machinery for establishing a successful infection in a given host system. Since the three virions of BMV are physically inseparable, the reported crystallographic structure of BMV virions (Lucas et al., 2002) is an average of the three virion types. Therefore, it is not known whether the three virion types are structurally identical and how local and global dynamical conformational changes of the stable states of the viral capsids modulate functions of biological relevance. Thus, it is imperative to obtain, in pure form, each virion type, free from the remaining two counterparts. A previous attempt to separate each virion type using $CsCl_2$ buoyant density centrifugation has resulted in samples that are enriched in one type of virion but not free from the remaining two virion types (Ni, Vaughan, Tragesser, Hoover, & Kao, 2014; Vaughan et al., 2014).

To understand the mechanism of RNA packaging and virion assembly in BMV, we have developed an *Agrobacterium*-mediated transient expression (agroinfiltration) system amenable for dissecting events involving RNA replication and packaging (Annamalai & Rao, 2005, 2006; Annamalai, Rofail, Demason, & Rao, 2008). A series of agroinfiltration experiments performed in the last decade revealed that although BMV RNA packaging is independent of replication, coexpression of viral replicase components enhances packaging specificity

(Annamalai & Rao, 2006). Also, a physical interaction between CP and viral replicase, more specifically, replicase protein 2a, is obligatory in regulating RNA packaging specificity (Chaturvedi & Rao, 2014). Based on this collective information, in this study, we report a facile and robust agroinfiltration approach to separately assemble each virion type of BMV in planta. Further characterization of each virion type with respect to physical morphology by negative-stain electron microscopy (EM) and electrophoretic mobility profiles revealed that all three virion types are remarkably indistinguishable. However, examination of the viral surface structure using matrix-assisted laser desorption ionization–time of flight (MALDI-TOF) mass spectrometry, an approach that can identify viral proteolysis products to examine the viral surface structure (Bothner, Dong, Bibbs, Johnson, & Siuzdak, 1998), revealed that virions of type 1 and 2 are dynamically distinct from those of type 3. The biological significance of the observed variation in the dynamics of the three different virions of BMV is discussed.

RESULTS

Throughout this study, virion types $B1^V$, $B2^V$, and $B3+4^V$ represent individual virions packaging genomic RNA1, RNA2, and RNA3 plus -4, respectively. Wild type (wt) represents a constellation of three virions of BMV, each containing RNA1, RNA2, and RNA3 plus -4 purified from infected barley or *Nicotiana benthamiana* plants.

Determining the quantitative distribution of virion types in wt BMV

To estimate the percent distribution of each virion type, RNA was isolated from purified wt virions and subjected to denaturing agarose gel electrophoresis. Following ethidium bromide staining, the percent distribution of each of the four RNAs was estimated using ImageJ analysis (Fig. 1.1B). The results (an average from three independent assays) show that the three virion types accumulated disproportionately, with the most prevalent species (~60%) being virion type 3 that copackaged RNA3 plus -4, followed by virion type 2 packaging RNA2 (~30%), and virion type 1 packaging RNA1 (~10%) (Fig. 1.1C). Consequently, without separating each virion type—as described below—the mixed nature of BMV virions obscures the interpretation of biochemical (Ni et al., 2014; Vaughan et al., 2014) and structural studies (Lucas et al., 2002).

Strategy for in vivo assembly of three independent virion types of BMV

Figure 1.2 summarizes the characteristic features of transfer DNA (T-DNA)-based vectors designed to express the three biologically active genomic RNAs (gRNAs) of BMV (pB1, pB2, and pB3) when transiently expressed in *N. benthamiana* plants (Annamalai & Rao, 2005). Likewise, T-DNA constructs shown in Fig. 1.2B are designed to transiently express BMV replicase proteins 1a (p1a), 2a (p2a), and CP (pCP). A strategy for the separate assembly of each virion type of BMV is shown schematically in Fig. 1.3. Prior to designing this strategy, we considered the following three criteria: first, genome packaging in BMV is functionally coupled to replication (Annamalai & Rao, 2006; Annamalai et al., 2008), i.e., only the replication-derived progeny RNA is packaged into virions; second, BMV CP (BCP) expressed in the absence of replication is nonspecific in RNA packaging (Annamalai & Rao, 2005); third, the packaging specificity is dictated by an interaction between CP and p2a (Chaturvedi & Rao, 2014). Therefore, keeping these requirements in perspective, the strategy shown in Fig. 1.3 was designed to assemble desired virion types by infiltrating the following sets of inocula. (i) Agrotransformants of all three wild type (wt) plasmids (Fig. 1.3A) or only pCP (Fig. 1.3B) infiltrated into plants served as controls. (ii) An inoculum was formulated to assemble $B1^V$ by mixing agrotransformants pB1, p2a, and pCP (Fig. 1.3C). Following infiltration into *N. benthamiana* leaves, pB1 would result in the synthesis of a biologically active full-length B1, and its translation would yield p1a.

Agrotransformant p2a would result in the synthesis of an mRNA competent to translate p2a, but it would not be replicated since it lacks 5' and 3' noncoding regions (Fig. 1.2B). Translation of mRNA synthesized from agrotransformant pCP would provide CP subunits to direct virion assembly. A functional replicase assembled with p1a and p2a would result in the replication of B1. Since replicase-CP interaction directs the packaging of replication-derived progeny (Chaturvedi & Rao, 2014), an interaction between p2a and CP would result in the assembly of $B1^V$ (Fig. 1.3C). (iii) A similar strategy was used to assemble $B2^V$ by mixing agrotransformants p1a, B2, and pCP (Fig. 1.3D). Infiltration would result in the synthesis of biologically active B2 and its translation product, i.e., p2a complexed with transiently expressed p1a would result in the assembly of a functional replicase followed by the assembly of $B2^V$ (Fig. 1.3D). (iv) Finally, to assemble $B3+4^V$ (copackaging B3 and sgB4), plants were infiltrated with a mixture of agrotransformants containing p1a, p2a, and B3 (Fig. 1.3E). Assembly of a functional replicase would result in the replication of B3 followed by the synthesis of sgB4 for CP production, resulting in the assembly of $B3+4^V$ (Fig. 1.3E).

Characteristic properties of $B1^V$, $B2^V$, and $B3+4^V$

Sucrose density gradient purified virions from *N. benthamiana* leaves infiltrated with either control infiltrations of wt (i.e., pB1+pB2+pB3) (Fig. 1.3A) or pCP (Fig. 1.3B) or with pB1+p2a+pBCP (i.e., $B1^V$) (Fig. 1.3C), p1a+pB2+pBCP

(i.e., $B2^V$) (Fig. 1.3D), or p1a+p2a+pB3 (i.e., $B3+4^V$) (Fig. 1.3E) were subjected to negative-stain EM examination. Results shown in Fig. 1.4A indicate that virions of $B1^V$, $B2^V$, and $B3+4^V$ are indistinguishable from those of the wt control in morphology and size (i.e., the average diameter being 26 to 28 nm). However, it is interesting to note that virions of $B1^V$ appear to be fuller than those of $B2^V$ and B3+4V. It is likely that the interaction between the CP and large size of RNA1 (3.2 kb) compared to that of RNA2 (2.8 kb) or RNA3 plus -4 (2.9 kb) would result in the assembly of fuller particles. Additional experiments using cryo-EM are in progress to confirm this assumption.

The analysis of agarose gel electrophoretic mobility patterns of purified virions is an ideal approach for identifying changes, if any, in surface charge (Calhoun & Rao, 2008; Calhoun, Speir, & Rao, 2007). Therefore, $B1^V$, $B2^V$, and $B3+4^V$ were subjected to agarose gel electrophoresis along with wt virions of BMV and *Cowpea Chlorotic Mottle virus* (CCMV; a member of the genus Bromovirus) as controls. The capsid sizes of BMV and CCMV are essentially identical (Lane, 1981). However, the charge on the solvent-accessible residues of BMV specified in VIPER (http://viperdb.scripps.edu/) is +1,020 compared to -1,209 for CCMV. Consequently, CCMV and BMV migrate toward the positive and negative electrodes, respectively (Carrillo-Tripp et al., 2009). Results shown in Fig. 1.4B confirmed the relative electrophoretic mobilities of wt BMV and CCMV virions (Fig. 1.4B, compare lanes 1 and 2). The indistinguishable electrophoretic mobility profiles of wt BMV (Fig. 1.4B, lane 2) and either $B1^V$ (Fig. 1.4B, lane 3), $B2^V$ (Fig.

1.4B, lane 4), or B3+4^{V} (Fig. 1.4B, lane 5) suggest that all three virion types exhibit similar surface charges.

To confirm the genetic composition of B1^{V}, B2^{V}, and B3+4^{V}, virion RNA was isolated and subjected to a reverse transcription-PCR (RT-PCR) assay using a set of primers that are designed to specifically amplify each of the three gRNAs and a single sgRNA (see Materials and Methods). RNA isolated from wt virions was used as a control. Results shown in Fig. 1.5A confirmed that B1^{V}, B2^{V}, and B3+4^{V} encapsidated expected RNA progeny. Since the sgB4 RNA sequence is present in the 3' half of B3, an additional Northern blot assay was used to confirm the copackaging of B3+4^{V} (data not shown).

To further assess the purity of B1^{V}, B2^{V}, and B3+4^{V}, an infectivity assay was performed in *Chenopodium quinoa*. As shown in Fig. 1.5B, phenotypic local and systemic symptoms characteristic of wt BMV (Rao & Grantham, 1995) were observed only when the inoculum contained a mixture of all three virion types (i.e., B1^{V}+B2^{V}+B3+4^{V}) but not with either individual (i.e., B1^{V}, B2^{V}, or B3+4^{V}) or pairwise combinations (i.e., B1^{V}+B2^{V}, B1^{V}+B3+4^{V}, or B2^{V}+B3+4^{V}). Taken together, these results confirm that B1^{V}, B2^{V}, and B3+4^{V} are highly pure and completely free from their counterparts.

Virion stability of $B1^V$, $B2^V$, and $B3+4^V$

To test the relative thermal stability of $B1^V$, $B2^V$, and $B3+4^V$, a differential scanning fluorimetry (DSF) assay was performed as described in Materials and Methods. The hydrophobic dye used in this assay increases the intensity of the fluorescence following its binding to the accessible hydrophobic regions of the viral CP during thermal denaturation (Rayaprolu et al., 2014). Results of the DSF analysis of the temperature-dependent melting of virions of $B1^V$, $B2^V$, and $B3+4^V$ and control samples (wt BMV and lysozyme) under three buffer and pH conditions are summarized in Fig. 1.6. Thermal denaturation in water showed a clear difference between virions of $B1^V$ and $B2^V$ and those of $B3+4^V$ (Fig. 1.6A), For example, virions of $B1^V$ and $B2^V$ displayed melting of thermally unstable populations at ~50°C and ~70°C (Fig. 1.6A, left and middle). By contrast, virions of $B3+4^V$ melted only at ~70°C (Fig. 1.6A, left and middle). Analysis of the three virion types by DSF in virus suspension buffer (pH 4.5) and phosphate buffer (pH 7.2) revealed identical thermal stability profiles, the least stable being in phosphate buffer (Fig. 1.6A, right). Interestingly, a different scenario was observed for wt BMV (Fig. 1.6B). The majority of the wt BMV virions remained thermally stable in water and virus suspension buffer and displayed a small shoulder peak at ~50°C (Fig. 1.6B, left and middle). Since wt BMV represents a disproportionate mixture of three virion types (Fig. 1.1C), it is likely that the shoulder peak represents virions of $B1^V$

and $B2^V$, as shown in Fig. 1.6A. As expected, the thermal stability of lysozyme remained indistinguishable under all three buffer conditions (Fig. 1.6C).

Analysis of the capsid dynamics of $B1^V$, $B2^V$, and $B3+4^V$ by MALDI-TOF

One of the promising approaches in distinguishing crystallographically identical viral capsids involves the use of limited proteolysis followed by the identification of the cleavage products of the capsid subunits by mass spectrometry (Bothner et al., 1999). Proteolytic cleavage sites present on the exterior of the capsid will be most accessible to the enzyme and therefore will be among the first digestion fragments observed. Consequently, MALDI-TOF analysis of proteolytic cleavage products would contribute to understanding the dynamic domains within the capsid structure (Bothner et al., 1999; Speir et al., 2006).

First, the relative capsid dynamics were investigated by trypsin digestion performed at various time points to verify whether $B1^V$, $B2^V$, and $B3+4^V$ virion types display any discernible effect on the rate of digestion (see Materials and Methods). Parallel digestions were performed with virions of wt BMV (mixture of all three virion types) and BCP^V (assembled in the absence of the viral replicase and packaging cellular RNA) as controls. Trypsin cleaves peptides on the C-terminal side of lysine and arginine residues (X-K/-X and X-R/-X); furthermore, if a proline residue is on the carboxyl side of the cleavage site, the cleavage will not occur. Therefore, the BMV CP linear sequence that is 189-aa long has 22 potential trypsin

cleavage sites (Running, Ni, Kao, & Reilly, 2012). Following trypsin digestion, each virion type preparation was divided in half. One half was subjected to Western blot analysis using an anti-CP antibody to identify the cleavage peptides, while the second half was subjected to EM analysis to verify the integrity of virions. Results are summarized in Fig. 1.7A and B. Undigested CP of virions of control samples (Fig. 1.7A, left, lanes 1 and 5) as well as all three individual virion types ($B1^V$, $B2^V$, and $B3+4^V$) (Fig. 1.7A, left, lanes 2 to 4) migrated as a single intact band with the expected molecular weight (~20 kDa). Analysis of the trypsin cleavage products for each virus sample revealed interesting profiles. For virions of wt and type 3 ($B3+4^V$), trypsin digested 50% of the CP, resulting in three faster-migrating peptide fragments in addition to a single intact protein band (Fig. 1.7A, middle, lanes 1 and 4). Based on the mass spectrometry data, these fragments correspond to residues 15 to 189, 27 to 189, and 43 to 189 (data not shown). By contrast, digestion of virion types 1 and 2 and BCP with trypsin failed to yield any detectable peptide fragments on the Western blot (Fig. 1.7A, middle, lanes 2, 3, and 5) and are indistinguishable from those of undigested samples (Fig. 1.7A, left, lanes 2, 3, and 5). These profiles did not change even after the digestion time to trypsin was extended (10 and 45 min) (Fig. 1.7A, right; Table 1.1). Electron microscopic analysis of trypsin-digested virion preparations (Fig. 1.7B) confirmed the Western blot data, showing that virions of type 1 and 2 as well as BCP are structurally intact, while those of wt and type 3 are unstable and degraded rapidly.

Next, MALDI-TOF was used to identify the cleavage products present in the trypsin-digested virion samples. The deconvoluted mass spectrum obtained from the total ion chromatogram (TIC) of the undigested virions of wt, $B1^V$, $B2^V$, $B3+4^V$, and BCP^V indicate that all the virions are assembled from a single protein of 20,296 Da, which underlines their purity. A representative example of the deconvoluted mass spectrum of undigested virions is shown in Fig. 1.8A.

Analysis of the released peptides after 10, 20, 30, and 45 min clearly distinguished virions of $B1^V$ and $B2^V$ from those of $B3+4^V$: virions of $B1^V$ and $B2^V$ are grouped into class I and those of $B3+4^V$ into class II. Although early time points of the reaction are indicative of the very first sites of protease cleavage (Speir et al., 2006), the trypsin digestion pattern for $B1^V$ and $B2^V$ is similar and domain specific irrespective of time of exposure, either early (10 and 20 min) or late (30 min, 45 min, and 3 h) (Table 1.1). MALDI-TOF mass mapping identified a prominent but low-abundance fragment corresponding to the N-terminal 2 to 8 aa (Fig. 1.8B and D). The authenticity of the 2 to 8 aa fragment was confirmed when the mass spectrum between 670 to 690 m/z was analyzed (Fig. 1.8C and E). Trypsin digestion did not release any peptide beyond 2 to 8 aa (Fig. 1.8F and G). Extending the trypsin digestion time to 3 h and 18 h did not change the cleavage pattern (Table 1.1). Although highly basic, the N-proximal region is predicted to be mobile/disordered and internalized following its interaction with RNA (Lucas et al., 2002). Taken together, these data suggest that in $B1^V$ and $B2^V$, only the N-terminal

ARM region, encompassing aa 2 to 8, which is crystallographically defined as being internal to BMV, is made accessible to protease digestion.

The scenario and the rate at which virions of B3+4^{V} are digested by trypsin are observed to be qualitatively distinct from those of B1^{V} and B2^{V}. For example, Western blot analysis revealed that for virions of B3+4^{V}, the intact protein present in trypsin-digested sample was less than 50% compared to that of either untreated B3+4^{V} or trypsin-treated B1^{V} and B2^{V} samples (Fig. 1.7A). At every time point examined, including the early time points (e.g., 10 and 20 min), virions of B3+4^{V} were highly susceptible to trypsin, releasing multiple peptides. Identification of the released peptides by mass mapping revealed that the accessible trypsin cleavage sites (e.g., K65, R103, K111, and K165) (Fig.1.9; Table 1.1) were consistent with the reported surface structure of the BMV virions (Lucas et al., 2002) (see Discussion). This explains why EM shows the trypsin-treated virions of B3+4^{V} to be visibly degraded (Fig. 1.7B). These observations suggest that virions of B3+4^{V} are either dynamically distinct from those of B1^{V} and B2^{V} and/or that the two virion types are conformationally different in the exterior arrangement of the CP amino acid residues. Although peptides representing N-terminal regions (21 to 26 aa) were detected at the earliest time point (e.g., 10 min) (Fig. 1.9), their accessibility to protease coincided with other cleavage sites as well (Fig. 1.9; Table 1.1). Therefore, it is likely that these N-terminal peptides on virions of B3+4^{V} may not be the first sites of protease cleavage, since multiple simultaneous cleavages at other sites expose the otherwise internalized N-terminal region to proteolysis (see

Discussion). A similar explanation can account for the detection of peptides encompassing the N-ARM region of 2 to 8 aa after extended periods of digestion (e.g., 45 min in Fig. 1.9; Table 1.1). The rationale and biological significance for the different surface configurations of the individual virions of the tripartite BMV are discussed below.

Figures 1.7A and 1.10 summarize the Western blot analysis of trypsin digestion products and their MALDI-TOF analysis, respectively, for the virions of the wt BMV and BCP^{V} used as controls. The digestion profiles of wt BMV are identical to those of $B3+4^{V}$ (Fig. 1.7, 1.9, and 1.10). By contrast, unexpected trypsin cleavage profiles were obtained for BCP^{V} (Fig. 1.10). Although BCP^{V} virions are distinct in size and RNA packaging traits compared to those of wt BMV (Annamalai & Rao, 2005), remarkably, their sensitivity to trypsin digestion and subsequent MALDI-TOF profiles are shared with those of $B1^{V}$ and $B2^{V}$ (Fig. 1.10; Table 1.1). We speculate that some of the unassigned peaks observed in MALDI-TOF analysis (Fig. 1.8 and 1.10) may be the result of trypsin self-cleavage (http://prospector.ucsf.edu/prospector/mshome.htm). For brevity, Fig. 1.11 summarizes the location of the trypsin cleavage sites identified to be located on $B1^{V}$, $B2^{V}$, and $B3+4^{V}$ by MALDI-TOF.

DISCUSSION

Following entry to a susceptible host cell, viruses face a daunting challenge of not only surviving in the harsh cellular environment, but they must also release their genome to perform various functions in establishing an infection. A series of biochemical and biophysical studies with a range of viruses has revealed that viral capsids undergo controlled conformational transitions to alter the surface structures compatible with disassembly and release of the genome when required (Johnson, 2003; Mateu, 2013). The primary focus of our present study is to investigate whether physically indistinguishable virions of BMV— each with a different RNA content— can be distinguished in solution, as demonstrated for other RNA viruses such as members of the families Nodaviridae (Johnson, 2003; Rayaprolu et al., 2014) and Picornaviridae (Speir et al., 2006). Using agroinfiltration, we were successful in assembling, for the first time, the three virion types of BMV, $B1^V$, $B2^V$, and $B3+4^V$ separately in planta, virions which are otherwise impossible to separate in pure forms (Lane, 1981). A series of biochemical (e.g., RT-PCR) (Fig. 1.5A) and biological assays (Fig. 1.5B) established the purity of each virion type. Although the three virion types are physically and morphologically indistinguishable (Fig. 1.4A), application of thermal denaturation analysis and limited proteolysis with trypsin followed by MALDI-TOF distinguishes between two dynamical classes of the three virion types: $B1^V$ and

$B2^V$ are grouped into class I and $B3+4^V$ as class II. Below, we discuss the biological significance of this distinction.

Virions of $B1^V$ and $B2^V$ are dynamically distinct from those of $B3+4^V$

Prior to this study, separation of the three types of virions into individual components by multiple rounds of $CsCl_2$ buoyant density centrifugation (Ni et al., 2014; Vaughan et al., 2014) had resulted only in the enrichment of a given virion type rather than freeing it completely from the other two components. By contrast, the feasibility of assembling pure $B1^V$, $B2^V$, and $B3+4^V$ virion types has been demonstrated by the strategy shown in Fig. 1.3C to E).

Although EM analysis (Fig. 1.4A) and electrophoretic mobility profiles (Fig. 1.4B) suggest that virions of $B1^V$, $B2^V$, and $B3+4^V$ are physically indistinguishable and homogeneous, limited proteolysis followed by MALDI-TOF analysis proved otherwise. Based on the BMV structure model (Lucas et al., 2002), the four accessible trypsin cleavage sites (K65, R103, K111, and K165) located on the surfaces of the A, B, and C subunits of BMV CP are shown in Fig. 1.12. Arginine and lysine residues located in the highly basic N-proximal region (e.g., K 8 , R11, and R14) are least exposed (Fig. 1.12) and predicted to internalize by interacting with the packaged RNA (Lucas et al., 2002). Consequently, these are not expected to be accessible for trypsin cleavage.

Identification of the cleavage products of $B1^V$, $B2^V$, and $B3+4^V$ at various time points by mass mapping suggested the following: (i) for $B1^V$ and $B2^V$, the N-proximal ARM region encompassing aa 2 to 8 is transiently exposed on the capsid surface. Since N-terminal residues 1 to 27 are not ordered in the crystal structure (Lucas et al., 2002), their cleavage did not affect the structural integrity of the virions (Fig. 1.7B). (ii) For $B3+4^V$, amino acids K65, R103, K111, and K165 are located on the surface of the capsid and hence are readily accessible for cleavage. In BMV, the stability of noncovalent dimers, the building blocks of icosahedral viruses (Zhao, Fox, Olson, Baker, & Young, 1995; Zlotnick, Aldrich, Johnson, Ceres, & Young, 2000), is controlled by the interaction between the invading C-terminal arm and the N-terminal clamp of the adjacent CP subunits, and any mutations engineered in the C terminus disrupt virion assembly (Okinaka, Mise, Suzuki, Okuno, & Furusawa, 2001; Zhao et al., 1995). Thus, cleavage at K165 alone is sufficient to disrupt the capsid structure. This explains why $B3+4^V$ appears visibly degraded in EM (Fig. 1.7B). Detection of peptides encompassing the N-proximal 21 to 26 and 20 to 26 aa region at an early time point (10 min) suggests their externalization in $B3+4^V$ (Fig. 1.9). Alternatively, it is likely that the extensive cleavage of the capsid as early as 10 min by trypsin (Fig. 1.9) results in degradation of the capsid structure (Fig. 1.7B), which leads to externalization of the N terminus and its subsequent proteolysis.

MALDI-TOF analysis profiles of wt BMV virions are indistinguishable from those of $B3+4^V$ (Fig. 1.11). This is not surprising, since purified virion preparation

of wt BMV is a mixture of all three virion types, with B3+4^{V} constituting ~60% of the total (Fig. 1.1C). However, virions of BCP, characterized by the distinct virion phenotype packaging cellular RNA (Annamalai & Rao, 2005), remained highly resistant to trypsin (Fig. 1.7A and B) and positioned the N-proximal 2 to 8 aa peptides externally to the capsid (Fig. 1.10). Although the reasons for the unexpected dynamics are currently unclear, it is possible that the type of RNA packaged influences the observed conformational dynamics.

A couple of previous studies have attempted to analyze the dynamics of bromoviral capsids without using pure virion type as reported in this study. For example, when the dynamics of wt CCMV and a salt-stable variant of CCMV (SS-CCMV) (Speir et al., 2006) were compared, it was observed that wt CCMV particles are more sensitive to trypsin than SS-CCMV. However, the pattern of released peptides is similar for both forms of CCMV, and the reported cleavage sites were localized to the N terminus of the CP (Speir et al., 2006). In contrast to CCMV, Vaughan et al. (Vaughan et al., 2014) attempted to segregate each virion type of BMV using $CsCl_2$ centrifugation, even though BMV has been shown to be unstable in $CsCl_2$ due to its “salt-labile” nature (Hull, 1976; Kaper, 1973; Lane, 1974). However, they were only successful in getting the fractions enriched in a given virion type (i.e., not free from remaining counterparts). The results obtained using contaminated virion fractions in conjunction with a different protease (broadly specific proteinase K), coupled with the fact that B3+4^{V} constitutes ~60% of the total virion population (Fig. 1.1C) and that B1^{V} and B2^{V} are dynamically distinct

from those of B3+4^{V} (shown in this study), make the comparison of our results to those of Vaughan et al. (Vaughan et al., 2014) problematic.

Biological significance

Based on our initial results comparing the stability (Fig. 1.6) and proteolysis profiles (Fig. 1.8 and 1.10) for B1^{V} and B2^{V} on the one hand and B3+4^{V} on the other, we hypothesize that the stability and conformational fluctuations displayed by B1^{V} and B2^{V} versus that of B3+4^{V} are linked to a specific role during the establishment of infection in a given host. For example, in B1^{V} and B2^{V}, the N-proximal 2 to 8 aa region is transiently externalized, allowing the virions to retain their structural integrity following trypsin digestion (Fig. 1.7B), suggesting the scenario shown in Fig. 1.13A. It is well established that the primary phase in the infection cycle of BMV (and other RNA viruses as well) is the production of replicase proteins. BMV replication requires both p1a and p2a (Ahlquist, 1992) and occurs in ER-derived vesicles or spherules, and their induction is mediated by p1a (Bamunusinghe, Seo, & Rao, 2011; Schwartz, Chen, Lee, Janda, & Ahlquist, 2004). Therefore, following viral entry, the instability under neutral pH conditions and the observed capsid dynamics allow ribosomes to bind B1 and B2 RNA and initiate translation of p1a and p2a, respectively (Fig. 1.13A). Instability of the virions in conjunction with translation of B1 and B2 RNA leads to cotranslational disassembly of B1^{V} and B2^{V} (Fig. 1.13A).

A contrasting scenario is proposed for the virions of B3+4^{V} (Fig. 1.13B). Unlike the genomic RNAs B1 and B2, replication is favored over translation for the genomic RNA B3 for the following reason. In BMV, CP plays a multifunctional role, including the stimulation of plus-strand synthesis over that of minus strands (de Wispelaere, Sivanandam, & Rao, 2020) by interacting with replicase protein p2a (Chaturvedi & Rao, 2014; Ni & Cheng Kao, 2013). Thus, in order to synthesize CP, RNA3 must undergo replication to generate CP mRNA, i.e., sgB4. As in B1^{V} and B2^{V}, the N terminus of the CP in B3+4^{V} virions is not exclusively sensitive to trypsin digestion (Fig. 1.9 and 1.11C), suggesting that the N-ARM region is internal and not exposed outside the capsid, resulting in B3 RNA being unavailable for translation initiation. Virions of B3+4^{V} are highly sensitive to trypsin (Fig. 1.7B), resulting in complete release of their RNA. Consequently, the internalization and the interaction between the N-ARM and B3 inhibit translation and favor replication.

In conclusion, results of this study represent a starting point toward understanding the differences among the otherwise structurally indistinguishable three virion types of BMV. Our results obtained analyzing the virion stability and capsid dynamics place BMV in a new perspective and shed light in understanding the overall biology of the virus. The strategy used to assemble independent virions of BMV (Fig. 1.3) is applicable to other RNA viruses and specifically to multicomponent viruses, such as cucumber mosaic virus, that exhibit particle homogeneity similar to that of BMV. Finally, the independently assembled virion types of BMV are ideal candidates for determining the structure of each virion type

and the application of single-particle tomography (Galaz-Montoya, Flanagan, Schmid, & Ludtke, 2015; Galaz-Montoya & Ludtke, 2017) to complete the map of the conformational heterogeneity in these virion types.

MATERIALS AND METHODS

Agroplasmids used in this study

Construction and characteristic properties of agroplasmids pB1, pB2, and pB3 (Fig. 1.2A), engineered to express biologically active full-length genomic RNAs of BMV following agroinfiltration into plants, were described previously (Annamalai & Rao, 2005). Likewise, agroplasmids p1a, p2a, and pCP (Fig. 1.2B) were engineered to transiently express replicase protein 1a (p1a), replicase protein 2a (p2a), and CP, respectively, as described previously (Annamalai & Rao, 2005; Seo, Kwon, & Rao, 2012).

Virion purification, negative-stain electron microscopy, virion RNA electrophoresis, and Western blot analysis

The procedure used to purify BMV virions from agroinfiltrated leaves 4 to 6 days postinfiltration (dpi) followed by sucrose density gradient centrifugation was as described by Rao et al. (A. Rao, Duggal, Lahser, & Hall, 1994). For negative-

stain EM analysis, gradient-purified virions were spread on glow-discharged grids followed by negative staining with 2% uranyl acetate prior to examination with a Tecnai F20 transmission electron microscope operated at 200 KeV (The Core Microscopy Facility, The Scripps Research Institute, La Jolla, CA). EM images were collected using Leginon program. Virions of BCP were imaged at UC-Riverside (UCR) using a Tecnai 12 operated at 120 KeV, and images were recorded digitally. For electrophoretic mobility analysis, purified virions were loaded in a 1% agarose gel, prepared, and electrophoresed in BMV suspension buffer at 7 V/cm for 2 to 2.5 h at 4°C. For RNA analysis, virion RNA was electrophoresed in 1.2% agarose gels under denaturing conditions as described previously (Annamalai & Rao, 2005). Following ethidium bromide staining, quantitation of each RNA was performed using Image J software (Schneider, Rasband, & Eliceiri, 2012). Western blot analysis of undigested and trypsin-digested virion samples using anti-CP antibodies was performed as described previously (Annamalai & Rao, 2005).

Differential scanning fluorimetry

DSF was performed essentially as described previously (Rayaprolu et al., 2014). Desired virus and control (lysozyme) samples were resuspended either in Nanopure sterile water (pH 7.1), in virus suspension buffer (50 mM sodium acetate, 8 mM magnesium acetate, pH 4.5), or in 100 mM phosphate buffer (pH

7.2). The experiment was performed three times independently using three replicates for each sample. DSF data were analyzed and plotted as described by Rayaprolu et al. (Rayaprolu et al., 2014).

MALDI-TOF

For MALDI-TOF analysis, a desired purified virion preparation was diluted to 1 mg/ml in 25 mM Tris-HCl, 1 mM EDTA buffer. A 30 µl sample (i.e., 30 µg of the virus) was digested with a 1:100 (wt/wt) ratio of trypsin (Pierce Trypsin protease, mass spectrometry grade; Thermo Fisher Scientific) to virus for various time points at 25°C (Bothner et al., 1998; Bothner et al., 1999). Twenty microliters of water was added to 10 µl of the digested sample, and approximately 0.5 µl of each digested or undigested (control) sample was analyzed on an AB Sciex TOF/TOF 5800 MALDI MS with -cyano-4-hydroxycinnamic acid matrix. The instrument was calibrated with standards, and the test samples were analyzed with external calibration. The accuracy is approximately 0.05 Da. The MALDI-TOF data were analyzed with AB Sciex Data Explorer, and baseline was corrected with peak width of 32, flexibility of 0.5, and degree of 0.1. For noise removal, the standard deviation was set at 2. To determine the peak detection criteria, percent centroid was taken as 50, signal/noise (S/N) threshold was 3, and the noise window width m/z was 250. The threshold after S/N recalculation was set at 20. The peptide

fragments were assigned based on the UCSF Protein Prospector's MS-Digest function (Running et al., 2012).

RT-PCR

RNA was isolated from purified virions and subjected to RT-PCR using an RT-PCR kit (NEB) and the following set of primers. A 1,700-nt fragment of B1 RNA located between the 3' tRNA-like structure (TLS) and a portion of rep-1a open reading frame (ORF) was amplified with a reverse primer (5'-^{3234}TGGTCTCTTTTAGAGATTTAC^{3014}-3') and forward primer (5'-^{1534}CTGAAGAGGACTTATTC^{1543}-3'). Likewise, a 1,700- nt fragment of B2 RNA located between the 3' TLS and a portion of rep-2a ORF was amplified with a reverse primer (5'-^{2865}TGGTCTCTTTTAGAGATTTAC^{2846}-3') and a forward primer (5'-^{1149}CTATGGATGTCATGACT^{1165}-3'). A 650-nt fragment of MP ORF of B3 RNA located between nucleotide (nt) 92 and 1007 was amplified using a reverse primer (5'-^{92}ATGTCTAACATAGTTTCTC^{110}-3') and a forward primer (5'-^{752}CAGTCTGTCAAATGGCAT^{760}-3'). Similarly, a 650-nt fragment of CP ORF of B3/sgB4 RNA located between the 3' TLS and a portion of the CP ORF was amplified with a reverse primer (5'-^{2117}TGGTCTCTTTTAGAGATTTAC^{1997}-3') and a forward primer (5'-^{1451}CATGAGTATCACTCTGC^{1435}-3'). The resulting PCR products were analyzed by electrophoresis in a 1% agarose gel.

ACKNOWLEDGEMENTS

We thank William Gelbart, Charles Knobler, Christian Beren, and Rees Garmann for helpful discussions during this work, Sonali Chaturvedi for help with illustrations, and Venkatesh Sivanandam for help with RNA gel analysis. We also thank Matthew Dickson at Center for Advanced Microscopy and Microanalysis facility at UC-Riverside (UCR) for helping with the imaging of BCP virions, Jie Zhou at Analytical Chemistry Instrumentation Facility at UCR for helping with MALDI-TOF analysis, Mathew Collin at Institute for Integrative Genome Biology at UCR, and Rajesh Yadav for guidance with analysis of DSF data.

This research was supported by grants from the UC Multicampus Research Program Initiative (MRI-17-454873) and AES/RSAP.

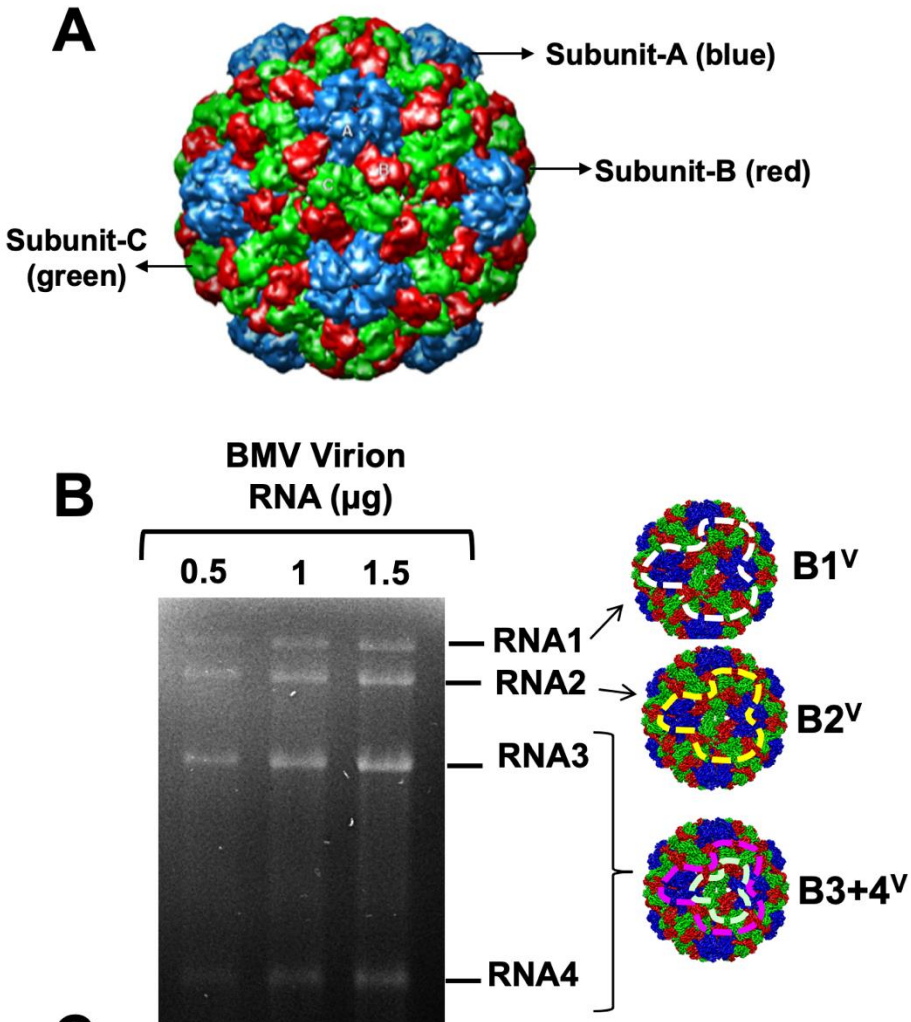

C

Virion Type	% Population
B1	10
B2	30
B3+4	60

Figure 1.1 Quantitative analysis of the three types of BMV virions. (A) Structure of a BMV virion showing the arrangement of subunits A, B, and C. (B) RNA was isolated from wt purified virion preparation, denatured with formamide/formaldehyde, and subjected to 1.2% agarose gel electrophoresis as described previously. After staining with ethidium bromide, the amount of RNA molecules present in each band was estimated using ImageJ software (Schneider et al., 2012). Three lanes, each containing a different total mass of RNA (0.5, 1, or 1.5 μg), were analyzed. (C) The intensity of each RNA band shown in panel B was determined using ImageJ (Schneider et al., 2012) and was used to determine the mole ratios of the viral RNAs isolated from virions. These mole ratios were then used to determine the fraction of each virion type.

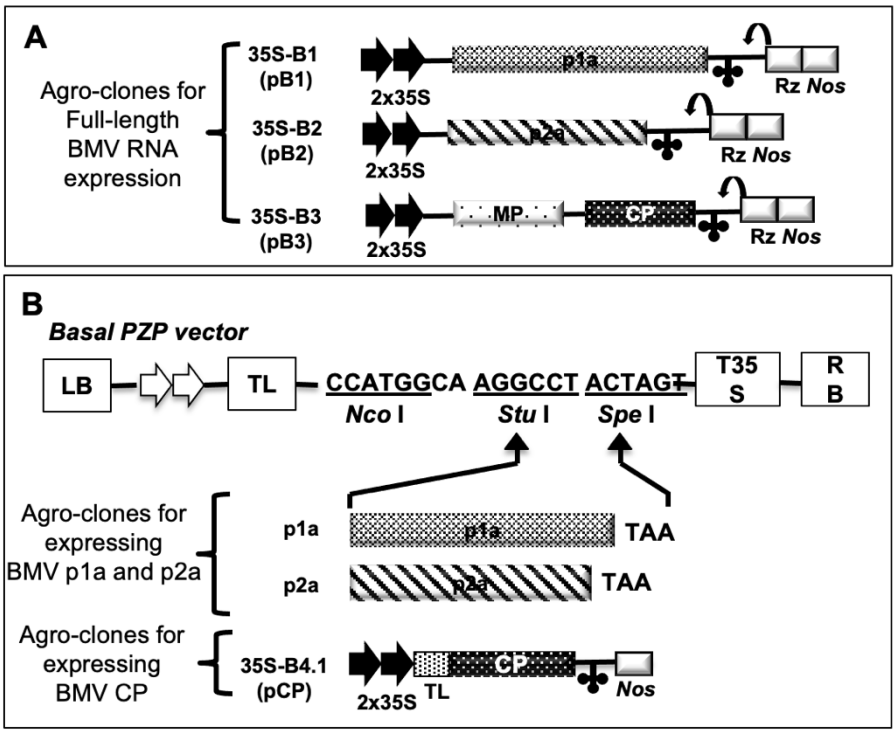

Figure 1.2 Characteristic features of agroplasmids used in this study. (A) Characteristics of agroplasmids harboring BMV genomic RNAs used for transient expression in plants. The 35S-B1 (pB1), 35S-B2 (pB2), and 35S-B3 (pB3) constructs contain full-length cDNA copies of BMV genomic RNA1 (B1), -2 (B2), and -3 (B3), respectively. Single lines and open boxes represent noncoding and coding regions, respectively. Monocistronic B1 encoding replicase protein 1a (p1a), and monocistronic B2 encoding replicase protein 2a (p2a) are indicated. In B3, the locations of the movement protein (MP) and coat protein (CP) genes are shown. At the 3' end of each construct, the clover leaf-like conformation represents a tRNA-like motif conserved among all three BMV genomic RNAs. Two black arrows at the 5' ends represent the double 35-S. A bent arrow indicates the predicted self-cleavage site by the ribozyme. The location of the *Nos* terminator is also indicated. (B) Agroconstructs for transient expression of p1a, p2a, and CP (pCP). Open reading frames (ORFs) of BMV p1a, p2a, and CP were fused in-frame to each pair of binary vectors using *Stu*I and *Spe*I sites. Each binary vector contained, in sequential order, a left border of T-DNA (LB), a double 35S promoter (35SX2), a tobacco etch virus (TEV) translation enhancer leader sequence (TL), multiple cloning sites, a 35S terminator (T35S), and a right border of T-DNA (RB). The construction and characteristic features of pCP are as described previously (Annamalai & Rao, 2005).

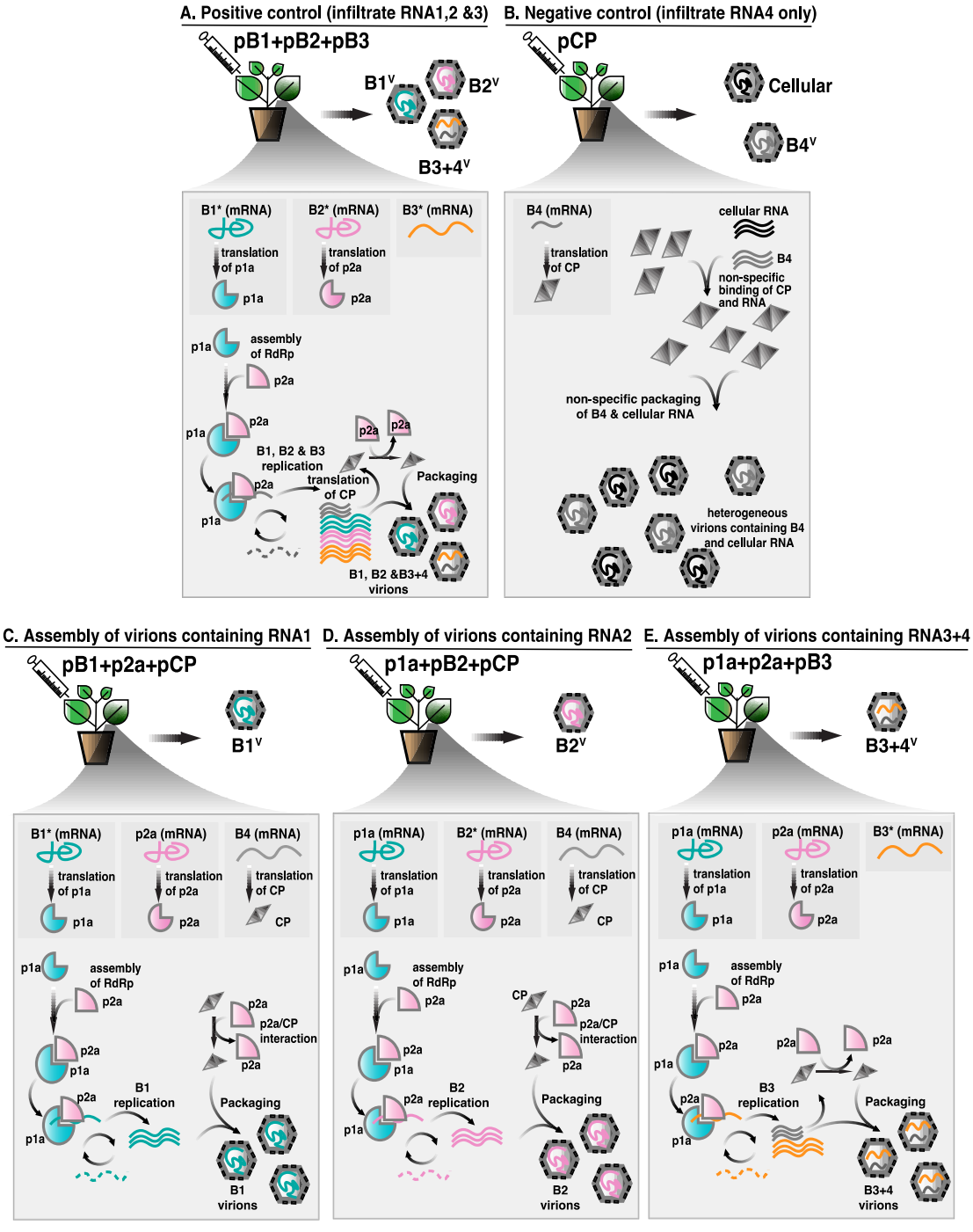
A. Positive control (infiltrate RNA1,2 &3)
pB1+pB2+pB3
B1V
B2V
B3+4V
B1* (mRNA)
translation of p1a
p1a
B2* (mRNA)
translation of p2a
p2a
B3* (mRNA)
assembly of RdRp
B1, B2 & B3 replication
translation of CP
Packaging
B1, B2 &B3+4 virions
B. Negative control (infiltrate RNA4 only)
pCP
Cellular
B4V
B4 (mRNA)
translation of CP
cellular RNA
B4
non-specific binding of CP and RNA
non-specific packaging of B4 & cellular RNA
heterogeneous virions containing B4 and cellular RNA
C. Assembly of virions containing RNA1
pB1+p2a+pCP
B1V
p2a (mRNA)
CP
p2a/CP interaction
B1 replication
B1 virions
D. Assembly of virions containing RNA2
p1a+pB2+pCP
B2V
B2 replication
B2 virions
E. Assembly of virions containing RNA3+4
p1a+p2a+pB3
B3+4V
B3* (mRNA)
B3 replication
B3+4 virions

Figure 1.3 Schematic representation of the strategy used for autonomous assembly of the three virions of BMV *in vivo*. (A) (Positive control) Infiltration of the inoculum containing a mixture of pB1+pB2+pB3 would induce wt BMV infection resulting in the assembly of mixture of all three virions. (B) (Negative control) Infiltration of the inoculum containing pCP would result in the expression of CP mRNA followed by the translation wt CP and nonspecific assembly of virions containing CP mRNA and cellular RNA, as demonstrated previously (Annamalai & Rao, 2005). (C) Assembly of virions packaging RNA1 ($B1^V$). A mixture of inoculum containing agrotransformants B1+p2a+pCP (see Fig. 1.2 for details) is infiltrated into *N. benthamiana* leaves. Transcription of pB1 results in the synthesis of a biologically active full-length genomic RNA1 whose translation gives functional replicase protein p1a; similarly, agrotransformant p2a results in an mRNA competent to give replicase p2a but not competent to be replicated, because it lacks the requisite 5' and 3' noncoding regions. Finally, translation of the mRNA transcribed from agrotransformant pCP gives the CP subunits for directing virion assembly. As a result, a functional replicase complex is assembled from proteins p1a and p2a that ensures the replication of B1 RNA followed by its packaging into virions by the transiently expressed CP subunits. (D) Assembly of virions packaging RNA2 ($B2^V$). The inoculum shown in this panel is identical to the one shown in panel C, except that pB1 and p2a are replaced by p1a and pB2, respectively. Agroinfiltration of this inoculum results in the assembly of virions containing B2 RNA. (E) Assembly of virions packaging RNA3 and -4 ($B3+4^V$). The inoculum shown in this panel is formulated to assemble virions packaging B3 RNA and sgB4 by mixing agrotransformants of p1a, p2a, and pB3. Transiently expressed proteins p1a and p2a then direct replication of B3 followed by the synthesis of sgB4 for CP production.

A

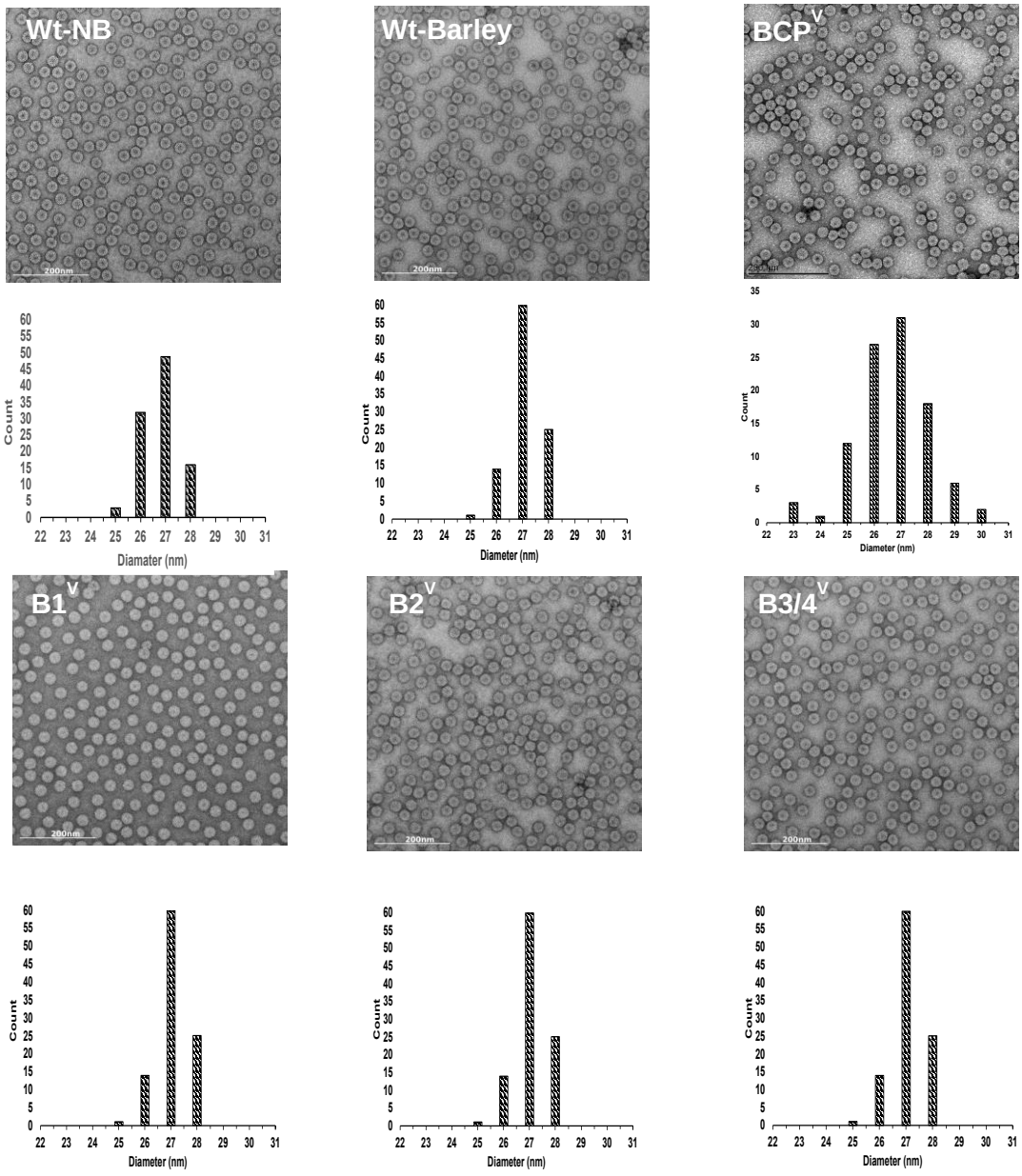
Wt-NB
Wt-Barley
BCP V
B1 V
B2 V
B3/4 V
200nm
Count
Diameter (nm)
Diamater (nm)

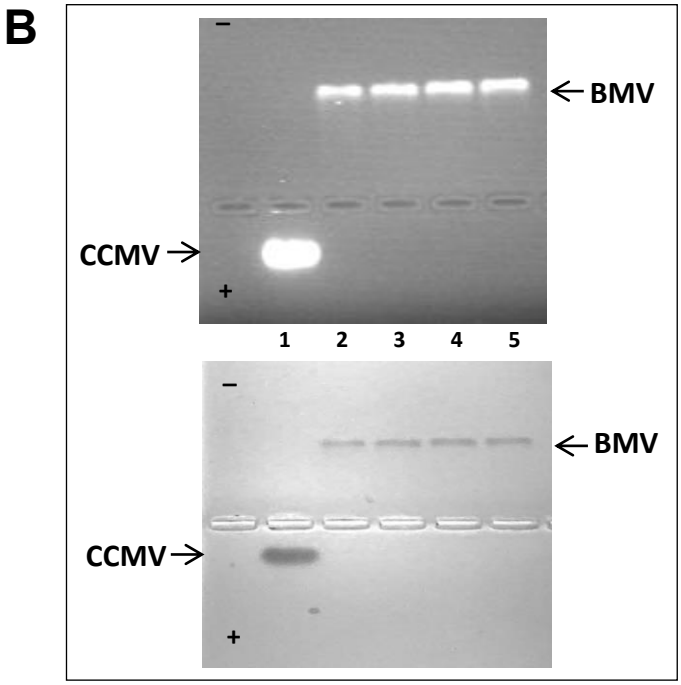

Figure 1.4 Physical characterization of $B1^V$, $B2^V$, and $B3+4^V$. (A) Negative-stain electron micrographs of density gradient-purified virions of either wt BMV from mechanically inoculated *N. benthamiana* or barley plants or autonomously assembled virions of $B1^V$, $B2^V$, $B3+4^V$, and BCP^V via agroinfiltration. Graphic representations shown below each image show a histogram of the virion sizes obtained by measuring at least 100 virions/sample. (B) Virion electrophoresis. Density gradient-purified virions of CCMV (lane 1), BMV (lane 2), $B1^V$ (lane 3), $B2^V$ (lane 4), and $B3+4^V$ (lane 5) were subjected to agarose gel analysis as described in Materials and Methods. Gel shown at the top was stained with ethidium bromide to detect RNA and then restained with Coomassie blue to detect protein (bottom panel). BMV and CCMV virions migrating toward negative and positive, respectively, are indicated.

A

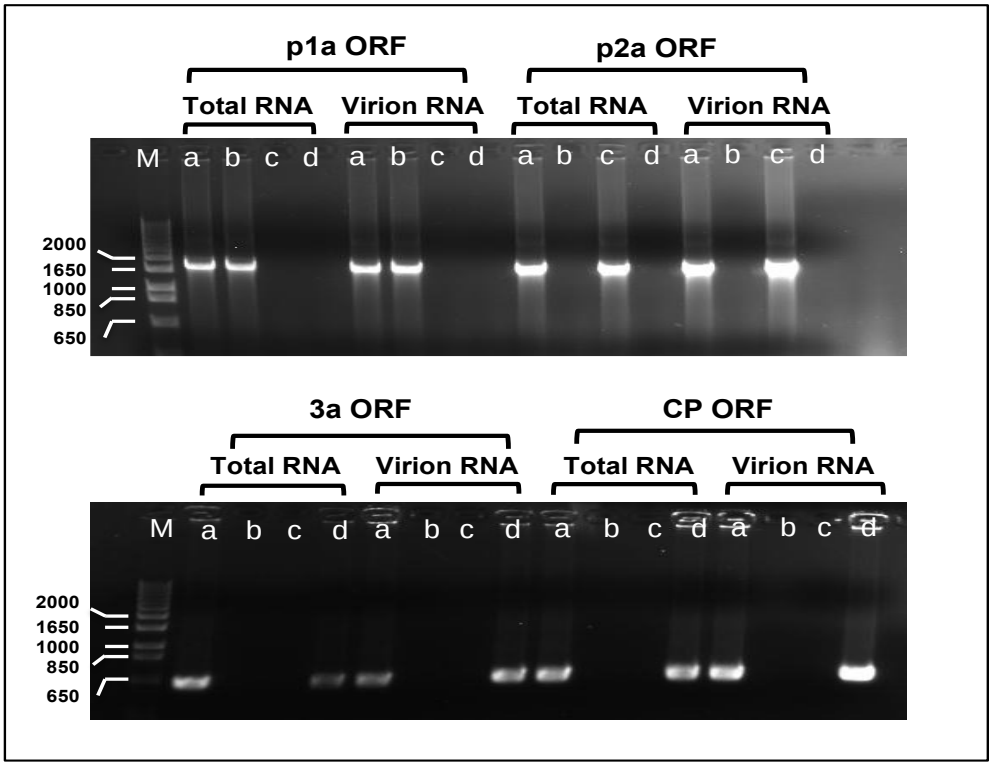

B

Infectivity of wild type, $B1^V$, $B2^V$ and $B3+4^V$

Inoculum	Infectivity in *C. quinoa*[a]	
	Local	Systemic
Wild Type[b]	+	+
$B1^V$	-	-
$B2^V$	-	-
$B3+4^V$	-	-
$B1^V+B2^V$	-	-
$B1^V+B3+4^V$	-	-
$B2^V+B3+4^V$	-	-
$B1^V+B2^V+B3+4^V$	+	+

[A] Infectivity assays in *C. quinoa* was tested as described under Materials and Methods.

+ and – respectively, represent the presence and absence of symptoms characteristic of BMV.

[b] Wild type represents a purified virion preparation from infected barley plants containing all three virions.

Figure 1.5 Genome content and infectivity of $B1^V$, $B2^V$, and $B3+4^V$. (A) RT-PCR analysis. Agarose gel analysis of RT-PCR products amplified from total RNA and virion RNA of wt BMV (a), $B1^V$ (b), $B2^V$ (c), and $B3+4^V$ (d) using a set of primers designed to specifically amplify the regions encompassing either p1a ORF, p2a ORF, 3a ORF, or CP ORF as described in Materials and Methods. M, marker lane. (B) Infectivity assays. *C. quinoa* leaves were mechanically inoculated with either wt BMV or agrotransformants of $B1^V$, $B2^V$, or $B3+4^V$ in the indicated combinations. Presence (+) or absence (-) of local and systemic infection characteristic of BMV was monitored and recorded over a period of 2 weeks.

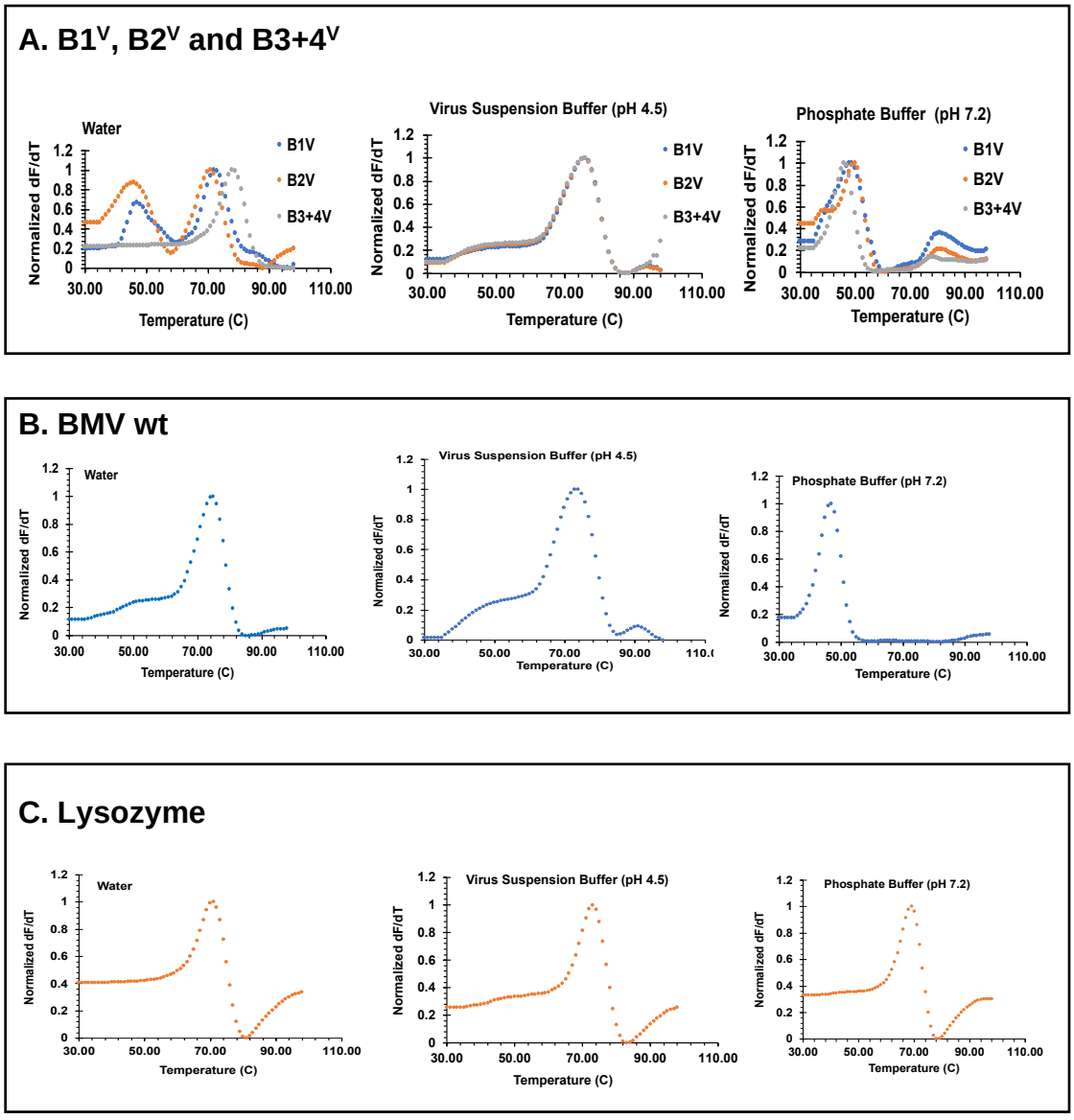

Figure 1.6 Stability analysis of the three BMV virion types using differential scanning fluorimetry (DSF). DSF measurements of derivative of fluorescence intensity as a function of temperature for each virion type normalized so that the maximum of the derivative is set to 1 (y axis) during heating of $B1^V$, $B2^V$, and $B3+4^V$ (A), wt BMV (control) (B), and lysozyme (control) (C) at various temperatures (x axis) under indicated conditions. Although virions of wt BMV and $B1^V$, $B2^V$, and $B3+4^V$ displayed identical temperature dependence (~70°C) for melting in all three solutions, a portion of virions of $B1^V$ and $B2^V$ melted at lower temperatures (see "Virion stability of $B1^V$, $B2^V$, and $B3+4^V$" for details). Lysozyme used as a positive control showed identical melting characteristics (~60°C) under all three solution conditions.

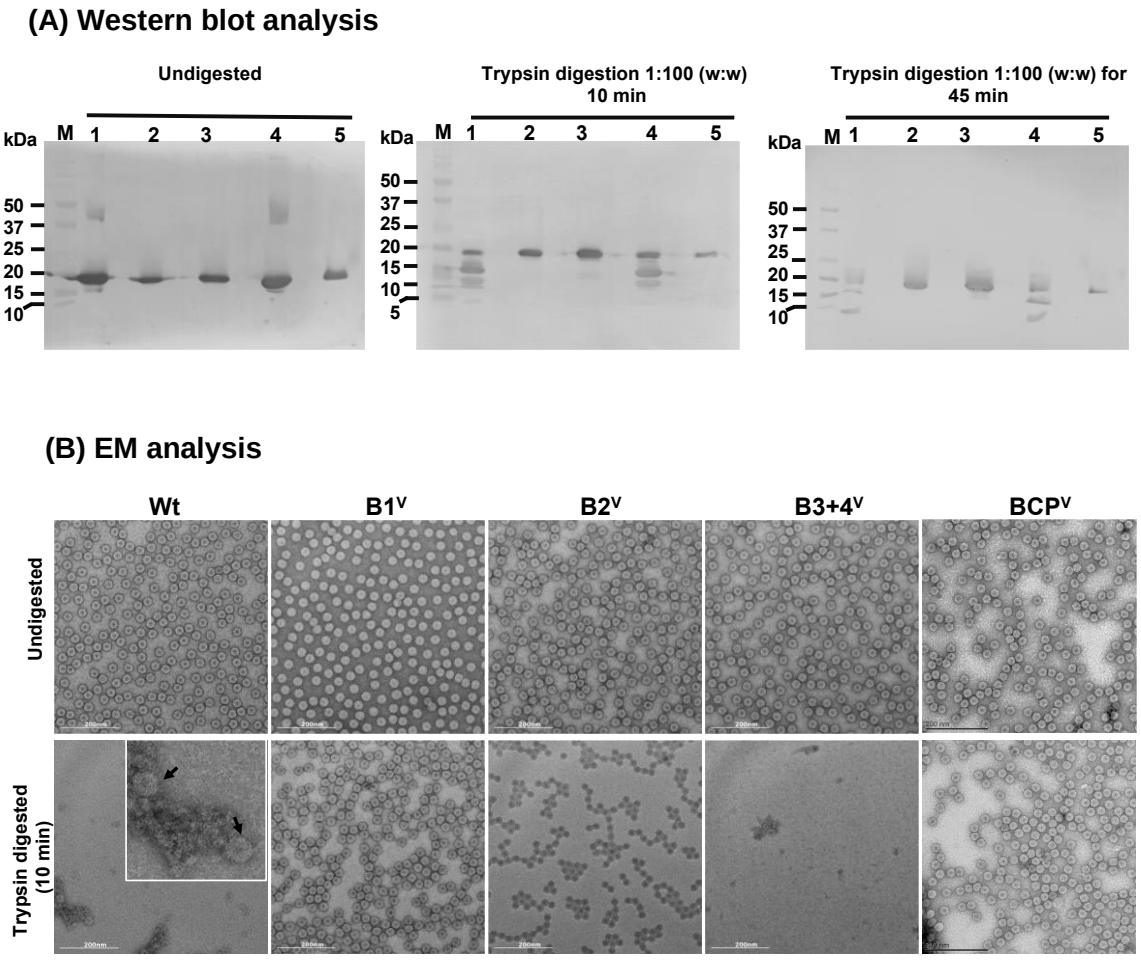

Figure 1.7 Proteolysis of $B1^V$, $B2^V$, and $B3+4^V$ monitored by Western blotting and negative-stain EM analysis. (A) Western blot for wt BMV (lane 1), $B1^V$ (lane 2), $B2^V$ (lane 3), $B3+4^V$ (lane 4), and BCP^V (lane 5). Prior to Western blot analysis, each virion preparation was either undigested (left) or digested with trypsin for 10 min (middle) or 45 min (right). (B) Negative-stain electron micrographs show the integrity of the undigested and trypsin-digested virion preparations of the indicated samples. (Inset) Arrows indicate intact virions of trypsin-resistant $B1^V$ and/or $B2^V$.

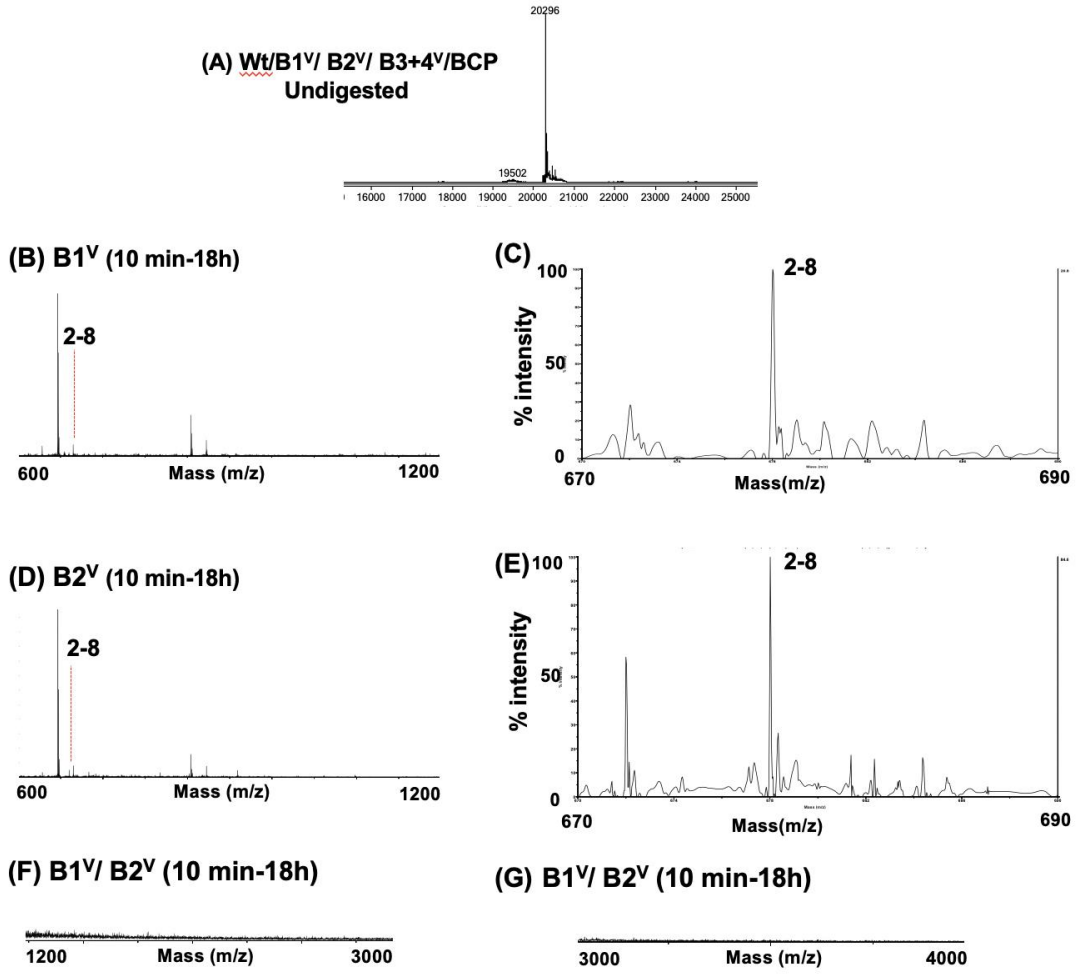

Figure 1.8 MALDI-TOF analysis of undigested and trypsin-digested virions. (A) Mass spectrometry of undigested virions of wt, $B1^V$, $B2^V$, $B3+4^V$, and BCP^V yielded a single peak with a value of 20,296 Da. MALDI-TOF analysis of peptides released from $B1^V$ (B, F and G) and $B2^V$ (D, F and G) following digestion with trypsin at the indicated time points. (C and E) Authenticity (intensity nearing 100%) of a peptide corresponding to 2 to 8 aa of the N-ARM in $B1^V$ and $B2^V$ when the mass spectrum between 670 to 690 m/z was analyzed. Peaks are labeled with corresponding polypeptide fragments of indicated amino acids residues. Table 1.1 summarizes masses and identifies the corresponding amino acid residues.

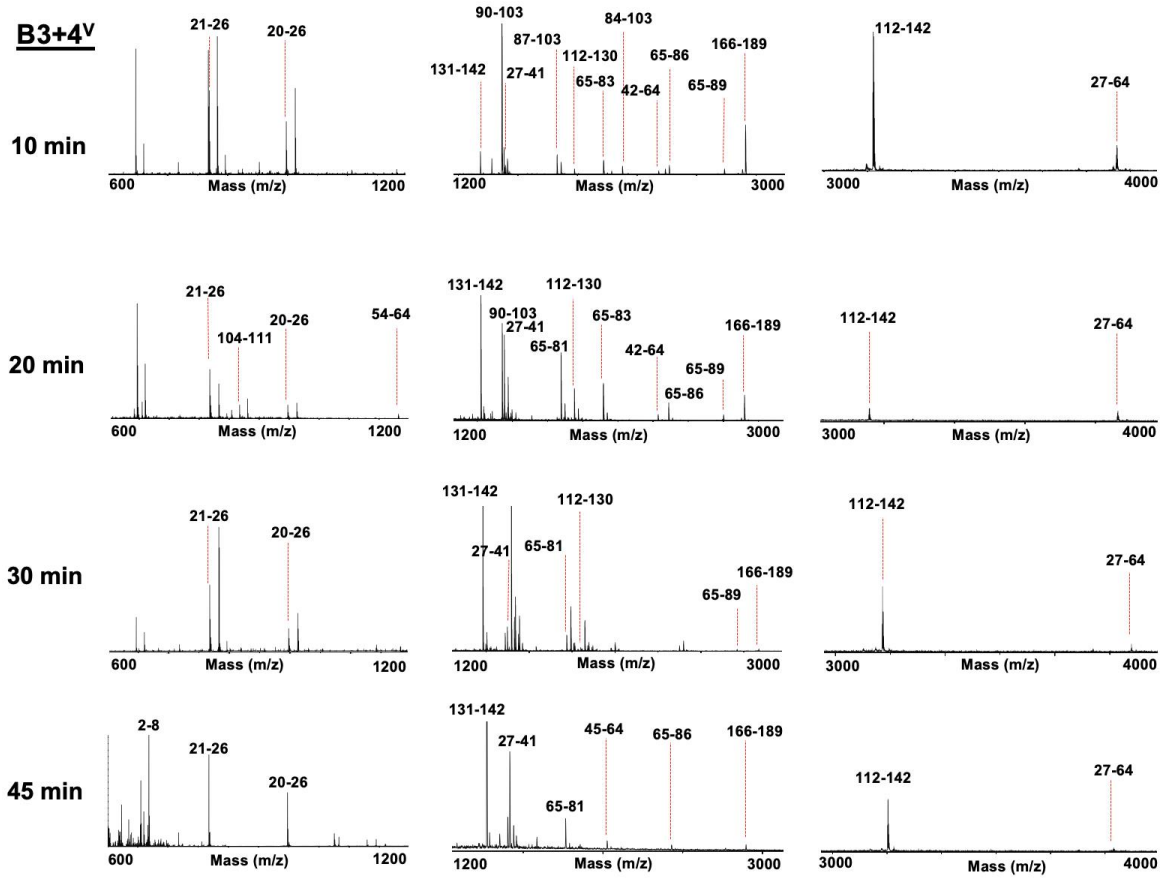

Figure 1.9 MALDI-TOF analysis of peptides released from B3+4^{V} following trypsin digestion at the indicated time points. Peaks are labeled with corresponding polypeptide fragments of indicated amino acids residues. Table 1.1 summarizes masses and identifies the corresponding amino acid residues.

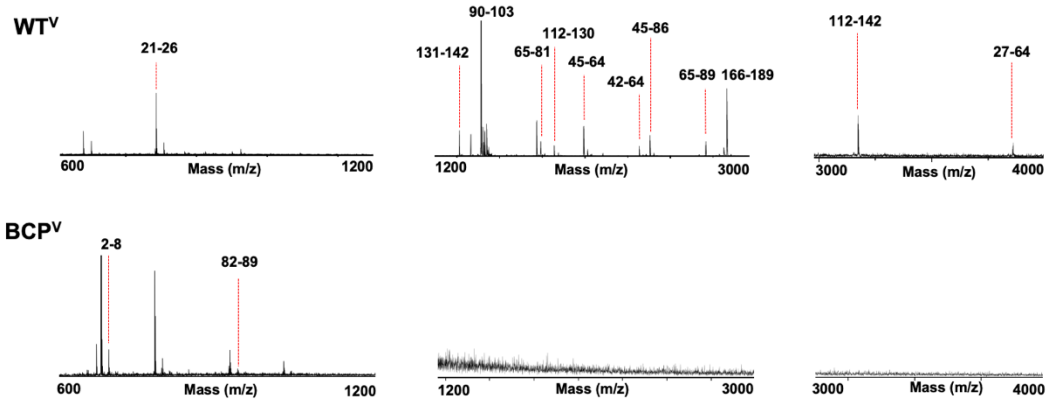

Figure 1.10 MALDI-TOF analysis of peptides released from virions of wt BMV and BCP^V following trypsin digestion at 10 min. Peaks are labeled with corresponding polypeptide fragments of indicated amino acids residues. Table 1.1 summarizes masses and identifies the corresponding amino acid residues.

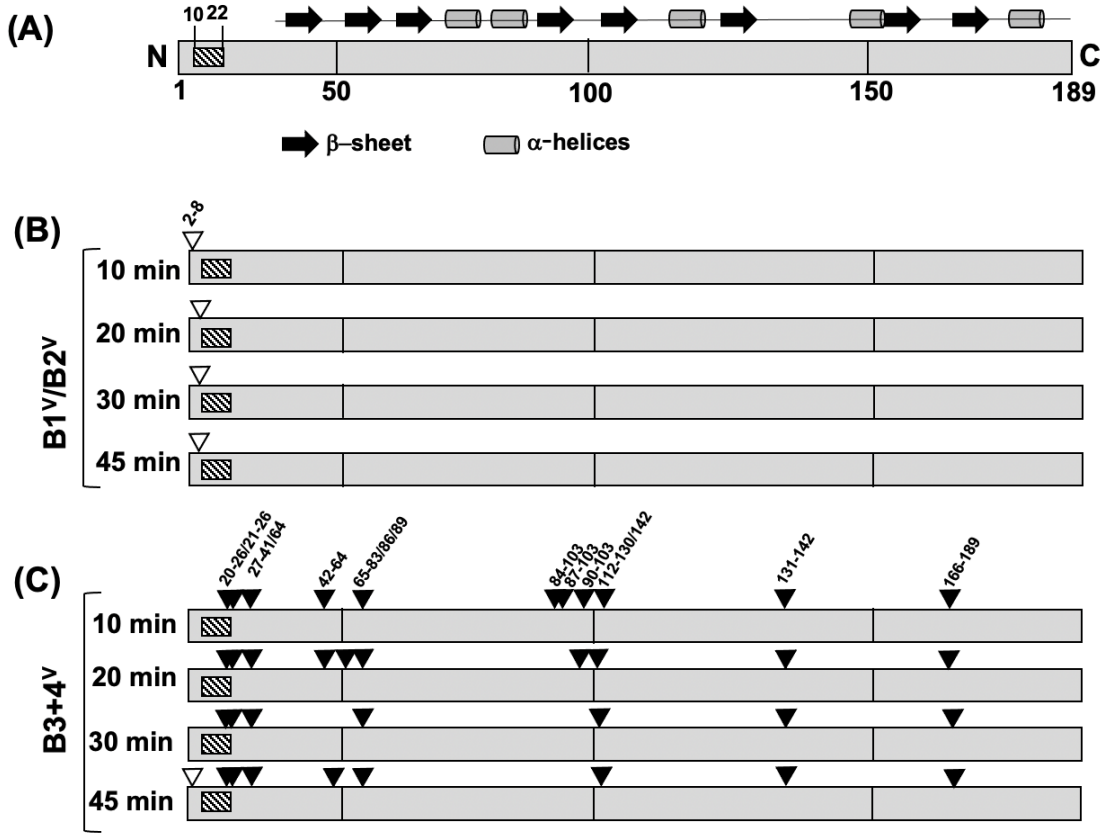

Figure 1.11 Summary of proteolytic cleavage sites mapped to the virions of $B1^V$, $B2^V$, and $B3+4^V$. (A) Schematic representation of linear representation of the 189 aa of the BMV CP subunit. Location of the arginine-rich motif (ARM) at aa 10 to 22 in the N-proximal region is indicated as a stippled box. (B) Empty arrowheads represent the trypsin-accessible sites located in the N-ARM regions of $B1^V$ and $B2^V$ (B) and $B3+4^V$ (C), whereas filled arrowheads indicate the trypsin-accessible sites present at other locations on the CP.

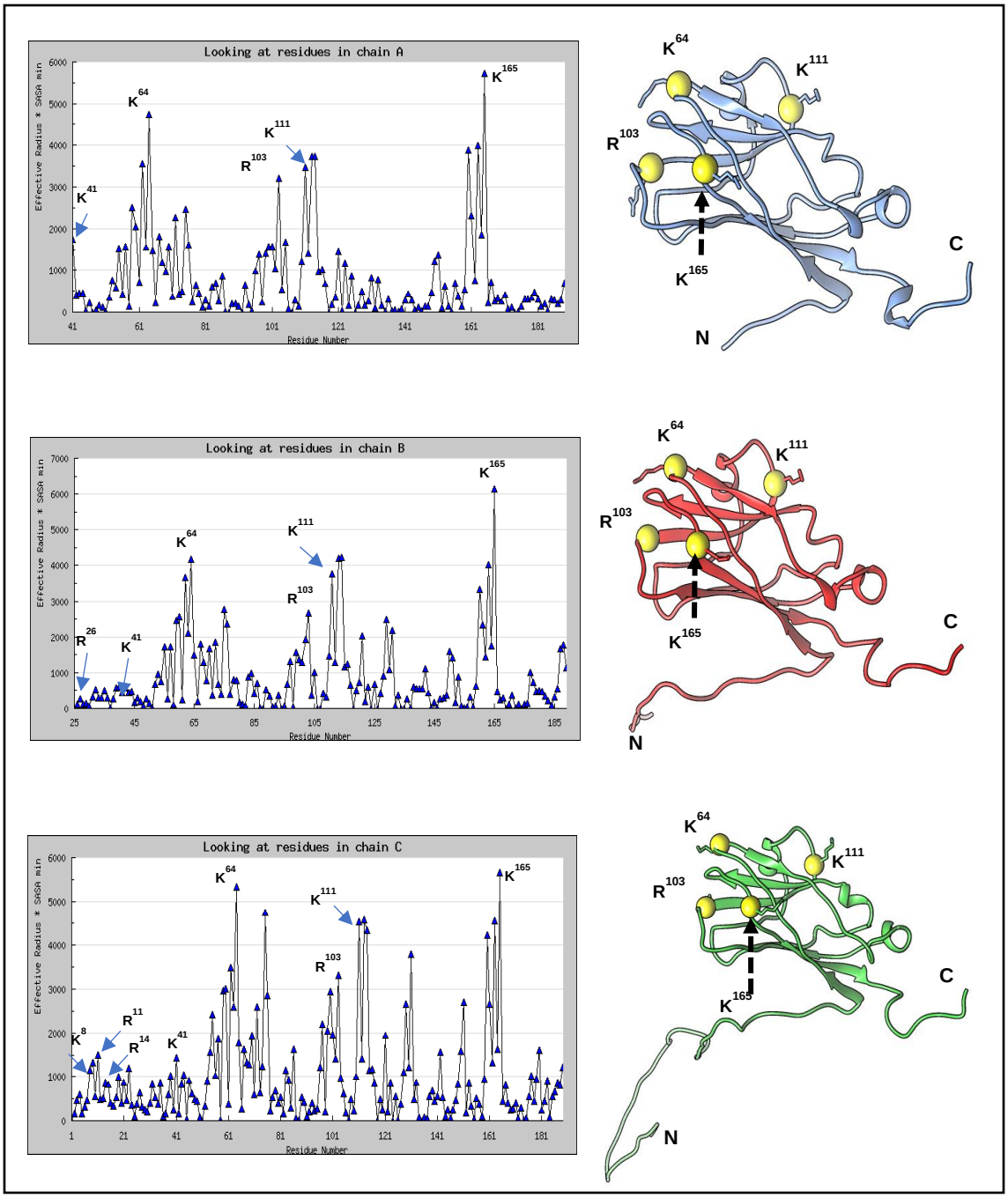

Figure 1.12 Location of the amino acid sites accessible for trypsin digestion on the A, B, and C subunits of the BMV CP (http://viperdb.scripps.edu/). Location of trypsin sites on A, B, and C subunits of BMV CP.

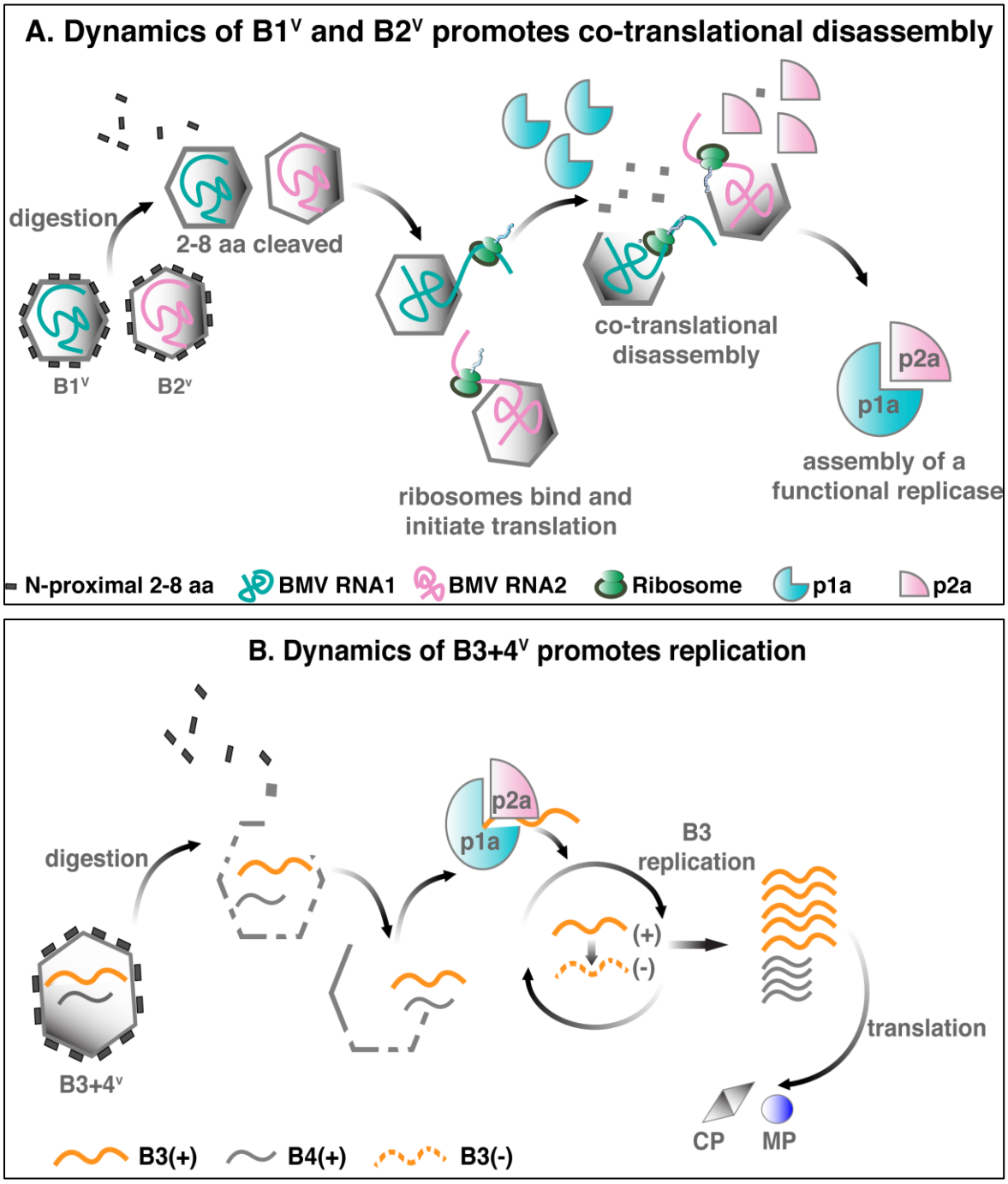
A. Dynamics of B1ᵛ and B2ᵛ promotes co-translational disassembly
digestion
2-8 aa cleaved
B1ᵛ
B2ᵛ
ribosomes bind and initiate translation
co-translational disassembly
p2a
p1a
assembly of a functional replicase
N-proximal 2-8 aa
BMV RNA1
BMV RNA2
Ribosome
p1a
p2a
B. Dynamics of B3+4ᵛ promotes replication
digestion
B3+4ᵛ
p2a
p1a
B3 replication
(+)
(-)
translation
CP
MP
B3(+)
B4(+)
B3(-)

Figure 1.13 A schematic model showing a role for the externalization (in $B1^V$ and $B2^V$) and internalization (in $B3+4^V$) of the CP-N-proximal region in translation and replication, respectively. BMV replication requires both p1a and p2a (Ahlquist, 1992) and occurs in ER-derived vesicles or spherules whose formation is mediated by p1a (Bamunusinghe et al., 2011; Schwartz et al., 2004). Therefore, following virus entry, B1 and B2 RNAs must be available to the translational machinery, and this is facilitated by fluctuation of the N terminus outside the capsid, as shown for B1 and B2 virions (Fig. 1.11A), which carries with it the 5' RNA end needed for ribosomal binding followed by cotranslational disassembly. In contrast, the $B3+4^V$ (Fig. 1.11B) virions make their RNA available to replication by the replicase complex, resulting in the synthesis of sgRNA4 from replication-derived minus-strand B3 progeny (Miller et al., 1985) for translation of the CP that stimulates plus-sense RNA synthesis over that of minus-sense RNA (de Wispelaere et al., 2020). See "Biological significance" for details.

Table 1: Kinetics of trypsin cleavage sites located on $B1^V$, $B2^V$ and $B3+4^V$

			$B1^V$	$B2^V$	$B3+4^V$					
Residues	Sequence	m/z	10 min-18hr	10 min-18hr	10 min	20 min	30 min	45 min	3 hr	18 hr
2-8	STSGTGK	679.3257	+	+	-	-	-	+	+	-
20-26	RNRWTAR	959.5282	-	-	+	+	+	+	-	-
21-26	NRWTAR	803.4271	-	-	+	+	+	+	+	+
27-41	VQPVIVEPLAAGQGK	1505.8686	-	-	+	+	+	+	-	-
27-64	VQPVIVEPLAAGQGKAIKAIAGYSISKWEASSDAITAK	3868.1219	-	-	+	+	+	+	-	-
42-64	AIKAIAGYSISKWEASSDAITAK	2381.2711	-	-	+	+	-	-	-	-
45-64	AIAGYSISKWEASSDAITAK	2069.055	-	-	-	-	-	+	-	-
54-64	WEASSDAITAK	1178.5688	-	-	-	+	-	-	-	-
65-81	ATNAMSITLPHELSSEK	1828.9109	-	-	-	+	+	+	-	+
65-83	ATNAMSITLPHELSSEKNK	2071.0488	-	-	+	+	-	-	-	-
65-86	ATNAMSITLPHELSSEKNKELK	2441.2705	-	-	+	+	-	+	-	-
65-89	ATNAMSITLPHELSSEKNKELKVGR	2753.4614	-	-	+	+	+	-	-	-
84-103	ELKVGRVLLWLGLLPSVAGR	2176.3329	-	-	+	-	-	-	-	-
84-105	ELKVGRVLLWLGLLPSVAGRIK	2417.5119	-	-	-	-	-	-	+	-
87-103	VGRVLLWLGLLPSVAGR	1806.1112	-	-	+	-	-	-	-	-
90-103	VLLWLGLLPSVAGR	1493.9202	-	-	+	+	-	-	+	+
104-111	IKACVAEK	861.4863	-	-	-	+	-	-	-	-
106-111	ACVAEK	620.3072	-	-	-	-	-	-	+	-
112-130	QAQAEAAFQVALAVADSSK	1904.9712	-	-	+	+	+	-	+	-
112-142	QAQAEAAFQVALAVADSSKEVVAAMYTDAFR	3258.61	-	-	+	+	+	+	-	-
131-142	EVVAAMYTDAFR	1372.6566	-	-	+	+	+	+	+	+
166-189	AVVVHLEVEHVRPTFDDFFTPVYR	2872.4781	-	-	+	+	+	+	+	+

Table 1.1 Kinetics of trypsin cleavage sites located on $B1^V$, $B2^V$, and $B3+4^V$.

REFERENCES

Ahlquist, P. (1992). Bromovirus RNA replication and transcription. *Curr Opin Genet Dev, 2*(1), 71-76. doi:10.1016/s0959-437x(05)80325-9

Annamalai, P., & Rao, A. L. (2005). Replication-independent expression of genome components and capsid protein of brome mosaic virus in planta: a functional role for viral replicase in RNA packaging. *Virology, 338*(1), 96-111. doi:10.1016/j.virol.2005.05.013

Annamalai, P., & Rao, A. L. (2006). Packaging of brome mosaic virus subgenomic RNA is functionally coupled to replication-dependent transcription and translation of coat protein. *J Virol, 80*(20), 10096-10108. doi:10.1128/JVI.01186-06

Annamalai, P., Rofail, F., Demason, D. A., & Rao, A. L. (2008). Replication-coupled packaging mechanism in positive-strand RNA viruses: synchronized coexpression of functional multigenome RNA components of an animal and a plant virus in Nicotiana benthamiana cells by agroinfiltration. *J Virol, 82*(3), 1484-1495. doi:10.1128/JVI.01540-07

Bamunusinghe, D., Chaturvedi, S., Seo, J. K., & Rao, A. L. (2013). Mutations in the capsid protein of Brome mosaic virus affecting encapsidation eliminate vesicle induction in planta: implications for virus cell-to-cell spread. *J Virol, 87*(16), 8982-8992. doi:10.1128/JVI.01253-13

Bamunusinghe, D., Seo, J. K., & Rao, A. L. (2011). Subcellular localization and rearrangement of endoplasmic reticulum by Brome mosaic virus capsid protein. *J Virol, 85*(6), 2953-2963. doi:10.1128/JVI.02020-10

Bothner, B., Dong, X. F., Bibbs, L., Johnson, J. E., & Siuzdak, G. (1998). Evidence of viral capsid dynamics using limited proteolysis and mass spectrometry. *J Biol Chem, 273*(2), 673-676. doi:10.1074/jbc.273.2.673

Bothner, B., Schneemann, A., Marshall, D., Reddy, V., Johnson, J. E., & Siuzdak, G. (1999). Crystallographically identical virus capsids display different properties in solution. *Nat Struct Biol, 6*(2), 114-116. doi:10.1038/5799

Calhoun, S. L., & Rao, A. L. (2008). Functional analysis of brome mosaic virus coat protein RNA-interacting domains. *Arch Virol, 153*(2), 231-245. doi:10.1007/s00705-007-1085-z

Calhoun, S. L., Speir, J. A., & Rao, A. L. (2007). In vivo particle polymorphism results from deletion of a N-terminal peptide molecular switch in brome mosaic virus capsid protein. *Virology, 364*(2), 407-421. doi:10.1016/j.virol.2007.03.034

Carrillo-Tripp, M., Shepherd, C. M., Borelli, I. A., Venkataraman, S., Lander, G., Natarajan, P., . . . Reddy, V. S. (2009). VIPERdb2: an enhanced and web API enabled relational database for structural virology. *Nucleic Acids Res, 37*(Database issue), D436-442. doi:10.1093/nar/gkn840

Chaturvedi, S., & Rao, A. L. N. (2014). Live cell imaging of interactions between replicase and capsid protein of Brome mosaic virus using Bimolecular Fluorescence Complementation: implications for replication and genome packaging. *Virology, 464-465*, 67-75. doi:10.1016/j.virol.2014.06.030

de Wispelaere, M., Sivanandam, V., & Rao, A. L. N. (2020). Regulation of Positive-Strand Accumulation by Capsid Protein During Brome Mosaic Virus Infection *in planta*. *Phytopathology, 110*(1), 228-236. doi:10.1094/PHYTO-07-19-0236-FI

Galaz-Montoya, J. G., Flanagan, J., Schmid, M. F., & Ludtke, S. J. (2015). Single particle tomography in EMAN2. *J Struct Biol, 190*(3), 279-290. doi:10.1016/j.jsb.2015.04.016

Galaz-Montoya, J. G., & Ludtke, S. J. (2017). The advent of structural biology. *Biophys Rep, 3*(1), 17-35. doi:10.1007/s41048-017-0040-0

Hull, R. (1976). The behavior of salt-labile plant viruses in gradients of cesium sulphate. *Virology, 75*(1), 18-25. doi:10.1016/0042-6822(76)90003-9

Johnson, J. E. (2003). Virus particle dynamics. *Adv Protein Chem, 64*, 197-218. doi:10.1016/s0065-3233(03)01005-2

Kao, C. C., & Sivakumaran, K. (2000). Brome mosaic virus, good for an RNA virologist's basic needs. *Mol Plant Pathol, 1*(2), 91-97. doi:10.1046/j.1364-3703.2000.00017.x

Kaper, J. M. (1973). Arrangement and identification of simple isometric viruses according to their dominating stabilizing interactions. *Virology, 55*(1), 299-304. doi:10.1016/s0042-6822(73)81035-9

Lane, L. C. (1974). The bromoviruses. *Adv Virus Res, 19*, 151-220. doi:10.1016/s0065-3527(08)60660-0

Lane, L. C. (1981). Bromoviruses. In *Hand book of plant virus infections and comparative diagnosis* (pp. 333-376): Elsevier Biomedical Press.

Lucas, R. W., Larson, S. B., & McPherson, A. (2002). The crystallographic structure of brome mosaic virus. *J Mol Biol, 317*(1), 95-108. doi:10.1006/jmbi.2001.5389

Mateu, M. G. (2013). Assembly, stability and dynamics of virus capsids. *Arch Biochem Biophys, 531*(1-2), 65-79. doi:10.1016/j.abb.2012.10.015

Miller, W. A., Dreher, T. W., & Hall, T. C. (1985). Synthesis of brome mosaic virus subgenomic RNA in vitro by internal initiation on (-)-sense genomic RNA. *Nature, 313*(5997), 68-70. doi:10.1038/313068a0

Ni, P., & Cheng Kao, C. (2013). Non-encapsidation activities of the capsid proteins of positive-strand RNA viruses. *Virology, 446*(1-2), 123-132. doi:10.1016/j.virol.2013.07.023

Ni, P., Vaughan, R. C., Tragesser, B., Hoover, H., & Kao, C. C. (2014). The plant host can affect the encapsidation of brome mosaic virus (BMV) RNA: BMV virions are surprisingly heterogeneous. *J Mol Biol, 426*(5), 1061-1076. doi:10.1016/j.jmb.2013.09.007

Okinaka, Y., Mise, K., Suzuki, E., Okuno, T., & Furusawa, I. (2001). The C terminus of brome mosaic virus coat protein controls viral cell-to-cell and long-distance movement. *J Virol, 75*(11), 5385-5390. doi:10.1128/JVI.75.11.5385-5390.2001

Rao, A., Duggal, R., Lahser, F., & Hall, T. (1994). Analysis of RNA replication in plant viruses. In A. KW (Ed.), *Methods in Molecular Genetics: Molecular Virology Techniques* (Vol. 4, pp. 216-236): Academic Press, San Diego, CA.

Rao, A. L. (2006). Genome packaging by spherical plant RNA viruses. *Annu Rev Phytopathol, 44*, 61-87. doi:10.1146/annurev.phyto.44.070505.143334

Rao, A. L., Chaturvedi, S., & Garmann, R. F. (2014). Integration of replication and assembly of infectious virions in plant RNA viruses. *Curr Opin Virol, 9*, 61-66. doi:10.1016/j.coviro.2014.09.008

Rao, A. L., & Cheng Kao, C. (2015). The brome mosaic virus 3' untranslated sequence regulates RNA replication, recombination, and virion assembly. *Virus Res, 206*, 46-52. doi:10.1016/j.virusres.2015.02.007

Rao, A. L., & Grantham, G. L. (1995). Biological significance of the seven amino-terminal basic residues of brome mosaic virus coat protein. *Virology, 211*(1), 42-52. doi:10.1006/viro.1995.1377

Rayaprolu, V., Kruse, S., Kant, R., Movahed, N., Brooke, D., & Bothner, B. (2014). Fluorometric Estimation of Viral Thermal Stability. *Bio Protoc, 4*(15). doi:10.21769/bioprotoc.1199

Running, W. E., Ni, P., Kao, C. C., & Reilly, J. P. (2012). Chemical reactivity of brome mosaic virus capsid protein. *J Mol Biol, 423*(1), 79-95. doi:10.1016/j.jmb.2012.06.031

Schmitz, I., & Rao, A. L. (1996). Molecular studies on bromovirus capsid protein. I. Characterization of cell-to-cell movement-defective RNA3 variants of brome mosaic virus. *Virology, 226*(2), 281-293. doi:10.1006/viro.1996.0656

Schneider, C. A., Rasband, W. S., & Eliceiri, K. W. (2012). NIH Image to ImageJ: 25 years of image analysis. *Nat Methods, 9*(7), 671-675. doi:10.1038/nmeth.2089

Schwartz, M., Chen, J., Lee, W. M., Janda, M., & Ahlquist, P. (2004). Alternate, virus-induced membrane rearrangements support positive-strand RNA virus genome replication. *Proc Natl Acad Sci U S A, 101*(31), 11263-11268. doi:10.1073/pnas.0404157101

Seo, J. K., Kwon, S. J., & Rao, A. L. (2012). A physical interaction between viral replicase and capsid protein is required for genome-packaging specificity in an RNA virus. *J Virol, 86*(11), 6210-6221. doi:10.1128/JVI.07184-11

Speir, J. A., Bothner, B., Qu, C., Willits, D. A., Young, M. J., & Johnson, J. E. (2006). Enhanced local symmetry interactions globally stabilize a mutant virus capsid that maintains infectivity and capsid dynamics. *J Virol, 80*(7), 3582-3591. doi:10.1128/JVI.80.7.3582-3591.2006

Vaughan, R., Tragesser, B., Ni, P., Ma, X., Dragnea, B., & Kao, C. C. (2014). The tripartite virions of the brome mosaic virus have distinct physical properties that affect the timing of the infection process. *J Virol, 88*(11), 6483-6491. doi:10.1128/JVI.00377-14

Zhao, X., Fox, J. M., Olson, N. H., Baker, T. S., & Young, M. J. (1995). In vitro assembly of cowpea chlorotic mottle virus from coat protein expressed in Escherichia coli and in vitro-transcribed viral cDNA. *Virology, 207*(2), 486-494. doi:10.1006/viro.1995.1108

Zlotnick, A., Aldrich, R., Johnson, J. M., Ceres, P., & Young, M. J. (2000). Mechanism of capsid assembly for an icosahedral plant virus. *Virology, 277*(2), 450-456. doi:10.1006/viro.2000.0619

CHAPTER 2

Comparative Capsid Dynamics Among the Three Virions of Cowpea Chlorotic Mottle Virus and Brome Mosaic Virus

ABSTRACT

Viral capsids are conformationally dynamic assemblies fluctuating from inside to the outside of the particle. These fluctuations or the protein subunits' dynamism manifest the breathing of the particles and play an essential role in the infectivity. *Cowpea chlorotic mottle virus* (CCMV) is an ssRNA plant virus belonging to the family *Bromoviridae* and closely resembles the *Brome mosaic virus* (BMV) in its packaging scheme and replication characteristics. The replication-derived RNA progeny of CCMV is packaged by a single capsid protein (CP) into three types of morphologically indistinguishable icosahedral virions. Type 1 ($C1^V$) and type 2 ($C2^V$) virions package the largest two genomic RNAs, RNA1 and RNA2, respectively, while type 3 ($C3+4^V$) virions co-package genomic RNA3 (C3) and its subgenomic RNA4 (sgRNA4). A robust *Agrobacterium*-mediated transient expression system was applied to assemble each virion type of CCMV separately *in planta* in this study. Experimental approaches demonstrated that the virion types are identical in their size, morphology, and electrophoretic mobility. Subsequently, differential scanning fluorimetry and protease-based peptide mass mapping experiments were used to analyze the stability and the conformational dynamics of the individual virion types and wild-type CCMV virions isolated from natural host cowpea and asymptomatic experimental host *Nicotiana benthamiana*. As demonstrated previously in the case of BMV RNA1 and 2 containing virions, a large percentage of $C1^V$ and $C2^V$ retained their capsid structural integrity upon

trypsin digestion while releasing peptides corresponding to the amino acids in the N-proximal region of CP. In contrast, C3+4^{V} capsids were unstable with trypsin, releasing several peptides encompassing various trypsin cleavage sites on the capsid surface. These results highlight the qualitatively different dynamics for the three types of virions in CCMV and further suggest that the different RNA genes in the multipartite plant RNA viruses in Bromoviridae may have differential translational efficiency and timing.

INTRODUCTION

Viral capsids are dynamic structures made of multiple copies of one or a few types of capsid protein (CP) subunits. The assembly of viral capsids is promoted and directed by the interaction between the CP subunits and the viral nucleic acid in both sequence-specific and non-specific manners and the assistance of other scaffolding proteins (Mateu, 2013). Once mature, the primary function of a viral capsid is encapsidation or enclosing the viral genome, which demands it to be stable enough to withstand the physicochemical environmental conditions until a susceptible host cell is encountered. However, viral capsids also have important roles like receptor binding, cellular entry, navigating the intracellular environment, and releasing the viral genome that requires flexibility. To meet these two contesting requirements, viral capsids undergo a reversible reorganization of biologically relevant surface peptides critical for their infectivity (Doerschuk, Gong, Xu, Domitrovic, & Johnson, 2016). Most of the plant viruses lack an envelope. Therefore, the CP plays an essential role as a coordinator to establish viral infection by being a part of the replicase complex or suppressing plant immune responses (Kao, Ni, Hema, Huang, & Dragnea, 2011).

Tripartite plant RNA viruses like the members of the family *Bromoviridae* have a single strand, positive-sense RNA genome that is divided among three genomic RNAs. The replication-derived progeny RNA is packaged in three homogeneous or four heterogeneous virion particles (Fig. 2.1C). *Cowpea chlorotic*

mottle virus (CCMV), a member of the *Bromoviridae* family closely related to *Brome mosaic virus* (BMV), contains a single-stranded, positive-sense RNA genome divided into three unique RNA molecules encapsidated separately in three individual virions. The largest two monocistronic genomic RNAs, RNA1 (C1, 3171 nt) and RNA2 (C2, 2774 nt), encoding nonstructural replicase proteins 1a (methyltransferase/helicase-like) and 2a (RNA-dependent RNA polymerase) respectively, get packaged separately into two virion types, $C1^V$ and $C2^V$. The dicistronic genomic RNA3 (C3) encodes a nonstructural movement protein (MP) at its 5' and a structural CP at its 3' end. CP is translated from a replication-derived subgenomic RNA4 made by an internal initiation mechanism from a minus-strand RNA3. Genomic RNA3 (2173 nt) and subgenomic RNA4 (sgRNA4) are co-packaged into a third virion type, $C3+4^V$ (Fig. 2.1D). (Lane, 1974). Unlike the BMV CP, CCMV CP does not require a virus-derived 3' tRNA-like structure (TLS) *in cis* or *trans* for packaging of RNA. Additionally, CCMV RNA3 does not require a bipartite packaging signal for effective packaging into virions, otherwise a strict requirement for BMV RNA3 (Annamalai & Rao, 2005a).

The capsid of CCMV consists of 180 identical subunits of a ~20kDa, 190 amino acid CP forming icosahedral virions with a diameter of 28 nm and T=3 quasi-symmetry (Fig. 2.1B) (Dasgupta & Kaesberg, 1982; Speir, Munshi, Baker, & Johnson, 1993; Speir, Munshi, Wang, Baker, & Johnson, 1995). Residues 1-26, including predominantly basic arginine and lysine residues, are not visible in the electron density map. These residues are internal and interact with the RNA inside

the viral capsid. Different numbers of observable residues are present in A subunits (residues 42-190), in comparison with B and C subunits (residues 27-190), which reflect their differences in containing a different proportion of polypeptides that confirm icosahedral symmetry (Fig. 2.1A) (Speir et al., 1995). The N-terminal Arginine Rich Motif (N-ARM) in wild-type CCMV CP is highly dynamic and sensitive to trypsin protease, indicating that it can transiently extend on the virion surface (Speir et al., 2006). Deletion mutants of CCMV CP lacking the N-ARM assemble into polymorphic virions (Annamalai, Apte, Wilkens, & Rao, 2005). Interestingly, the requirement of CP in cell-to-cell trafficking of monocot- vs. dicot-adapted members of genus *Bromovirus* was found to be distinct (Weber & Bujarski, 2015). Biologically active RNA3 of BMV and CCMV where CP was substituted with a reporter gene showed that, unlike BMV, epidermal cell-to-cell movement of CCMV could occur without a functional CP (Rao, 1997). However, neither BMV CP nor CCMV CP was found to harbor host-specific determinants for systemic spread when chimeric RNA3 expressing heterologous CP from both viruses were studied (Osman, Grantham, & Rao, 1997). Another study outlined a critical difference between the requirements of amino acid residues 41-47 from the N-ARM in BMV vs. CCMV. A deletion mutant of BMV CP lacking amino acid residues 41-47 from the N-ARM resulted in the assembly of polymorphic virions *in vivo,* which were noninfectious. Significantly, the CP subunits from these virions were incompetent for *in vitro* assembly. Interestingly enough, the same mutation

did not affect the assembly and infectivity of CCMV virions (Calhoun, Speir, & Rao, 2007).

CCMV virions are stabilized through protein-RNA interaction, where the positively charged interior of the viral capsid strongly interacts with the negatively charged RNA (Culver et al., 2015). Therefore, these virions are unstable under conditions of even mild physical denaturants like ultracentrifugation or pH and ionic strength changes. Nevertheless, CCMV is one of the best-suited viruses for assembly studies as the tertiary structure of its CP subunit remains stable during the disassembly process. It was shown that when purified using atypical mild procedures, CCMV can form crystals capable of diffracting X-rays to a resolution of 3.2 Å (Speir et al., 1993).

In vitro assembly mechanism has been well studied in CCMV for over the last 25 years. CCMV was the first icosahedral virus to be successfully assembled *in vitro* from purified CP subunits and RNA into infectious virions (Bancroft & Hiebert, 1967). The wild-type CCMV is stable at pH 5.0. When pH is increased to 7.0 and the ionic strength and divalent cation concentration of the solution are decreased, the virions undergo swelling resulting in an average increase in particle size by ~10%. However, the RNA-protein ratio in these virions remains the same as wild-type (Bancroft, Hills, & Markham, 1967). This transition is reversible if the pH is decreased to 5.0, or if the concentration of Mg^{+2} or Ca^{+2} is increased to 0.05 M (D. W. Adolph & Butler, 1977; K. W. Adolph & Butler, 1974). The native virions dissociate inro CP dimers and RNA-protein complexes at an increased ionic

strength and a pH higher than 7.0. Subsequently, a mutant was isolated harboring single lysine (K)-to-arginine (R) mutation in the residue 42 of CCMV CP that did not dissociate at high pH and ionic strength, retaining 70% infectivity compared to the wild-type. The phenotype was termed as salt-stable (SS) (Fox, Zhao, Speir, & Young, 1996). Speir et al. (2006) compared the capsid dynamics of closed and swollen forms of wild-type CCMV (WT-CCMV) and a salt stable mutant of CCMV (SS-CCMV). Surprisingly, although a swollen state is expected to expose more trypsin cleavage sites, it was observed that SS-CCMV was less susceptible to trypsin protease treatment than WT-CCMV. MALDI-TOF analysis showed that cleavage of the tryptic peptide regions is localized in the N-terminus of the CP, and the virions remained intact when examined under an electron microscope (Speir et al., 2006).

Despite a wealth of data available from the structural studies of the different CCMV virion conformations, the three virion types of CCMV remain physically inseparable by routinely using separation techniques like sucrose density gradient centrifugation as virion types of CCMV are physically homogeneous in morphology and size. Therefore, the reported crystallographic structure of CCMV virions is an average of the three virion types (Speir et al., 1995). Consequently, it is unknown whether the three virion types containing different RNA genes are structurally identical and how local and global conformational changes contribute to the dynamic nature of these viral capsids, further modulating functions of biological importance. We recently developed an *Agrobacterium*-mediated transient

expression (agroinfiltration) system that is amenable for dissecting RNA replication and packaging events in BMV. This robust system helped us assemble individual virions on BMV autonomously in an experimental host *Nicotiana benthamiana*, in which BMV spreads systemically. We had further characterized each virion type of BMV for physical morphology and electrophoretic mobility profiles that revealed that all three virion types are remarkably indistinguishable. However, examination of the viral surface structure using matrix-assisted laser desorption ionization-time of flight (MALDI-TOF) mass spectrometry, an approach that can identify viral proteolysis products to examine the viral surface structure, revealed that virions of type 1 and 2 are dynamically distinct from those of type 3 (Chakravarty, Reddy, & Rao, 2020).

This study used a similar agroinfiltration-based system to assemble individual virions of CCMV, a *Bromovirus* closely related to BMV, autonomously in *N. benthamiana.* Both viruses spread systemically in *N. benthamiana* without developing any symptom phenotypes. Also, BMV and CCMV CP share high sequence homology (~70% identical sequence) (Fig. 2.1E). However, CCMV is a dicot-adapted virus vs. BMV, which infects monocots in the natural environment. Previous studies showed that the degree of sensitivity to trypsin in $B1^V$, $B2^V$, and $B3+4^V$ assembled in an experimental dicot host *N. benthamiana* (Chakravarty et al., 2020), is distinct from those produced in natural host monocot plants (Ni, Vaughan, Tragesser, Hoover, & Kao, 2014). Therefore, an important goal of the current study was to analyze the comparative stability and capsid dynamics of WT

CCMV virions assembled in natural host cowpea (*Vigna unguiculata*) vs. those produced in experimental host *N. benthamiana.* The results showed a significant difference in the stability and susceptibility to trypsin protease in cowpea vs. *N. benthamiana*-assembled WT CCMV virions highlighting that host plants can profoundly influence capsid dynamics. Subsequently, we characterized the individual virion types' physical morphology and electrophoretic mobility using negative-stain electron microscopy (EM) and agarose gel electrophoresis. Each of the virion types in CCMV, $C1^V$, $C2^V$, and $C3+4^V$ is indistinguishable in size and morphology. However, examining the exposed surface residues on the individual virions using proteolysis followed by MALDI-TOF revealed a large percentage of $C1^V$ and $C2^V$ retained their capsid structural integrity upon trypsin digestion while releasing peptides corresponding to the amino acids in the N-proximal region of CP. In contrast, $C3+4^V$ capsids were unstable with trypsin, releasing several peptides encompassing various trypsin cleavage sites along the capsid surface. These results parallel the qualitatively different capsid dynamics for the three types of virions in BMV and suggest that the individual virions in bromoviruses containing different RNA genes may have important biological significance.

RESULTS

Throughout this study, virion types $C1^V$, $C2^V$, and $C3+4^V$ represent individual virions packaging genomic RNA1, RNA2, and RNA3 plus -4. Wild type (WT) represents a mixture of three virions of CCMV, each containing RNA1, RNA2, and RNA3 plus -4 purified from infected cowpea or *N. benthamiana* plants.

Determining the quantitative distribution of virion types in WT CCMV

To estimate the percent distribution of virion types in CCMV, RNA was isolated from purified WT virions assembled in cowpea and subjected to denaturing agarose gel electrophoresis. Following ethidium bromide staining, the percent distribution of each of the four RNAs was estimated using ImageJ analysis. The results show that the virion types accumulated disproportionately, with the most prevalent species (~54%) being virion type 3 that co-packaged RNA3 and 4. The virion type 1 packaging RNA1 and virion type 2 packaging RNA2 contributed to the rest of the population (~46%, (Fig. 2.1F). A similar proportion is observed in BMV virions accumulation in *N. benthamiana,* where virion type 3+4 made up ~60% of the total population. In comparison, type 1 and 2 contributed to the remaining ~40% (Chakravarty et al., 2020).

Strategy for in vivo assembly of three independent virion types of CCMV

Figure 2.2A summarizes the characteristic features of transfer DNA (T-DNA)-based vectors designed to express the three biologically active genomic RNAs (gRNAs) of CCMV (pC1, pC2, and pC3) when transiently expressed in *N. benthamiana* plants. Likewise, T-DNA constructs shown in Fig. 2.2B are designed to transiently express CCMV replicase proteins 1a (C1a), 2a (C2a), and CP (pCCP). A strategy for the separate assembly of each virion type of CCMV is shown schematically in Fig. 2.3. Before designing this strategy, we considered the following three criteria: first, genome packaging in bromoviruses is functionally coupled to replication (P. Annamalai & A. L. Rao, 2006; Annamalai, Rofail, Demason, & Rao, 2008), i.e., only the replication-derived progeny RNA is packaged into virions; second, CP in BMV, a related bromovirus, expressed in the absence of replication is non-specific in RNA packaging (Annamalai & Rao, 2005b); third, the packaging specificity is dictated by an interaction between BMV CP and replicase protein 2a (Chaturvedi & Rao, 2014). Therefore, keeping these requirements and the similarity between replication strategies observed in BMV and CCMV in perspective, the strategy shown in Fig. 2.3 was designed to assemble desired virion types by infiltrating the following sets of inocula. (i) Agrotransformants of all three plasmids expressing full-length RNA (Fig. 2.3A) or only pCCP (Fig. 2.3B) infiltrated into plants served as controls. (ii) An inoculum was formulated to assemble $C1^{V}$ by mixing agrotransformants pC1, pC2a, and

pCCP (Fig. 2.3C). Following infiltration into *N. benthamiana* leaves, pC1 would synthesize a biologically active full-length C1, and its translation would yield C1a. Agrotransformant pC2a would produce an mRNA competent to translate C2a, but it would not be replicated since it lacks 5' and 3' noncoding regions (Fig. 2.2B). Translation of mRNA synthesized from agrotransformant pCCP would provide CP subunits to direct virion assembly. A functional replicase assembled with C1a and C2a would result in the replication of C1. Since replicase-CP interaction leads to the packaging of replication-derived progeny, an interaction between C2a and CCP would result in the assembly of $C1^V$ (Fig. 2.3C). (iii) A similar strategy was used to assemble $C2^V$ by mixing agrotransformants pC1a, pC2, and pCCP (Fig. 2.3D). Infiltration would result in the synthesis of biologically active C2 and its translation product, i.e., C2a complexed with transiently expressed C1a would result in the assembly of a functional replicase followed by the assembly of $C2^V$ (Fig. 2.3D). (iv) Finally, to assemble $C3+4^V$ (co-packaging C3 and sgC4), plants were infiltrated with a mixture of agrotransformants containing pC1a, pC2a, and C3 (Fig. 2.3E). Assembly of a functional replicase would result in the replication of C3 followed by the synthesis of sgC4 for CP production, resulting in the assembly of $C3+4^V$ (Fig. 2.3E).

Total protein was extracted from each of the plants infiltrated with the specified mixture of the inoculum (Fig. 2.3A-E), and the presence of the ~20 kDa CCMV CP was confirmed in each of the samples using Coomassie brilliant blue R-250 staining (Fig. 2.4A) and Western blot (Fig. 2.4B).

Characteristic properties of $C1^V$, $C2^V$, and $C3+4^V$

Purified virions from *N. benthamiana* leaves infiltrated with either control infiltrations of WT (i.e., pC1+pC2+pC3) (Fig. 2.3A) or with pC1+pC2a+pCCP (i.e., $C1^V$) (Fig. 2.3C), pC1a+pC2+pCCP (i.e., $C2^V$) (Fig. 2.3D), or pC1a+pC2a+pC3 (i.e., $C3+4^V$) (Fig. 2.3E) were subjected to negative-stain EM examination. Results shown in Fig. 2.5A indicate that virions of $C1^V$, $C2^V$, and $C3+4^V$ are indistinguishable from those of the WT control in morphology and size (i.e., the average diameter being 28 nm).

The analysis of 1% agarose gel electrophoretic mobility patterns of purified virions is ideal for identifying any changes in the surface charge (Calhoun & Rao, 2008; Calhoun et al., 2007). Therefore, $C1^V$, $C2^V$, and $C3+4^V$ purified from *N. benthamiana* leaves were subjected to agarose gel electrophoresis along with WT virions of CCMV and BMV as controls. The capsid sizes of CCMV and BMV are essentially identical (Fig. 2.1E). However, the charge on the solvent-accessible residues of CCMV specified in VIPER (http://viperdb.scripps.edu/) is -1,209 compared to +1,020 for BMV. Consequently, CCMV and BMV migrate toward the positive and negative electrodes, respectively (Carrillo-Tripp et al., 2009). Results shown in Fig. 2.5B confirmed the relative electrophoretic mobilities of WT BMV and CCMV virions (Fig. 2.5B, compare lanes 1 and 2). The indistinguishable electrophoretic mobility profiles of WT CCMV (Fig. 2.5B, lane 2) and either $C1^V$

(Fig. 2.5B, lane 3), $C2^V$ (Fig. 2.5B, lane 4), or $C3+4^V$ (Fig. 2.5B, lane 5) suggest that all three virion types exhibit similar surface charges.

To confirm the genetic composition of $C1^V$, $C2^V$, and $C3+4^V$, virion RNA was isolated and subjected to a reverse transcription-PCR (RT-PCR) assay using a set of primers designed to specifically amplify each of the three genomic RNAs and a single sgRNA (see Materials and Methods). RNA isolated from WT virions was used as a control. Results shown in Fig. 2.6A confirmed that $C1^V$, $C2^V$, and $C3+4^V$ encapsidated expected RNA progeny.

To further assess the purity of $C1^V$, $C2^V$, and $C3+4^V$, an infectivity assay was performed in *N. benthamiana*. As shown in Fig. 2.6B, systemic accumulation of WT CCMV was confirmed using Western Blot only when the inoculum contained a mixture of all three virion types (i.e., $C1^V+C2^V+C3+4^V$) but not with either individual (i.e., $C1^V$, $C2^V$, or $C3+4^V$) or pairwise combinations (i.e., $C1^V+C2^V$, $C1^V+C3+4^V$, or $C2^V+C3+4^V$). These results confirm that $C1^V$, $C2^V$, and $C3+4^V$ are highly pure and completely free from their counterparts.

Virion stability of $C1^V$, $C2^V$, and $C3+4^V$

To test the relative thermal stability of $C1^V$, $C2^V$, and $C3+4^V$, a differential scanning fluorimetry (DSF) assay was performed as described in Materials and Methods. The hydrophobic dye SYPRO orange used in this assay binds to the hydrophobic regions of the unfolding viral CP during thermal denaturation. The

fluorescence intensity increases following its binding to more accessible areas (Rayaprolu et al., 2014). The DSF analysis of the temperature-dependent melting of virions of $C1^V$, $C2^V$, and $C3+4^V$ and control samples (WT CCMV assembled in cowpea and *N. benthamiana* and lysozyme) under two buffer and pH conditions are summarized in Fig. 2.7. Thermal denaturation in virus suspension buffer (pH 4.5) showed near-identical thermal stability in virions of $C1^V$ and $C2^V$ and those of $C3+4^V$ (Fig. 2.7A), All three virion types displayed melting at ~70°C (Fig. 2.7A), with the peaks seen in $C1^V$ and $C2^V$ had a shoulder peak at ~50°C which is absent in case of $C3+4^V$. By contrast, in phosphate buffer (pH 7.2), all three virion types displayed melting of thermally unstable populations at ~50°C and ~85°C. Under this condition, $C3+4^V$ melted mostly at ~50°C, with a less pronounced peak present at ~85°C when compared with $C1^V$ and $C2^V$ (Fig. 2.7B). Interestingly, WT CCMV (WT CCMV-cowpea) assembled in cowpea showed a slightly different thermal stability in virus suspension buffer (pH 4.5) when compared to WT CCMV assembled in *N. benthamiana* (WT CCMV-NB) (Fig. 2.7C). The WT CCMV-cowpea showed melting at ~65°C, whereas WT CCMV-NB displayed melting at ~69°C. Additionally, WT CCMV-NB showed a small shoulder peak at ~50°C, which resembled the one seen in $C1^V$ and $C2^V$ under similar pH conditions. This shoulder peak was absent in WT CCMV-cowpea (Fig. 2.7C). In phosphate buffer (pH 7.2), both WT CCMV-cowpea and WT CCMV-NB displayed melting of thermally unstable populations at ~50°C and ~70°C. At this pH, WT CCMV-cowpea dissolved mostly at ~50°C, with a less pronounced peak present at ~70°C when

compared with WT CCMV-NB (Fig. 2.7D). Interestingly, WT CCMV-cowpea closely resembled the denaturation profile of C3+4^{V}, whereas WT CCMV-NB resembled that of C1^{V} and C2^{V}. This observation aligns with our previous observation of C3+4^{V} being the predominant virion population in WT CCMV-cowpea. Similarly, we can expect C1^{V} and C2^{V} to make the dominant virion population in WT CCMV-NB as a given host can alter the composition of the three virion types (Verduin, 1978). As expected, the thermal stability of lysozyme remained indistinguishable under both buffer conditions (Fig. 2.7E & F).

Analysis of the capsid dynamics of C1^{V}, C2^{V}, and C3+4^{V} by trypsin proteolysis followed by MALDI-TOF

Crystallographically identical viral capsids can be easily distinguished using limited proteolysis, followed by identifying the cleavage products of the capsid subunits by mass spectrometry (Bothner et al., 1999). Proteolytic cleavage sites present on the capsid exterior will be the first residues accessible to the enzyme and among the first digestion products observed. Accordingly, MALDI-TOF analysis of proteolytic cleavage products would contribute to understanding the dynamic nature of the capsid structure (Bothner, Dong, Bibbs, Johnson, & Siuzdak, 1998; Speir et al., 2006).

First, the differential capsid dynamics were investigated by trypsin digestion performed at various time points (10 min, 30 min, 45 min, 3 hr, and 18 hr) to verify

whether WT CCMV-cowpea and WT CCMV-NB display any discernible effect on the rate of digestion (see Materials and Methods). Parallel digestions were performed with $C1^V$, $C2^V$, $C3+4^V$, and CCP^V assembled in *N. benthamiana*. Trypsin cleaves peptides on the C-terminal side of lysine and arginine residues (X-K/-X and X-R/-X); furthermore, if a proline residue is on the carboxyl side of the cleavage site, the cleavage will not occur. Therefore, the CCMV CP linear sequence is 190-aa long and has 20 potential trypsin cleavage sites (https://prospector.ucsf.edu/prospector/mshome.htm). Following trypsin digestion, each virion type preparation was divided in half. One half was subjected to Western blot analysis using an anti-CP antibody to identify the cleavage peptides. In contrast, the second half was subjected to EM analysis to verify the integrity of virions. Results are summarized in Fig. 2.8A and B. Undigested CP of virions of control samples of both WT CCMV-cowpea and WT CCMV-NB (Fig. 2.8A, top panel, left blot, lanes 1 and 5) as well as all three individual virion types ($C1^V$, $C2^V$, $C3+4^V$, CCP^V) (Fig. 2.8A, bottom panel, left blot, lanes 1 to 4) migrated as a single intact band with the expected molecular weight (~20 kDa). In the case of WT, CCMV-cowpea monomers and dimers of CP are detected in the Western blot. WT CCMV-NB predominantly showed accumulation of CP monomers, with dimers being at a presumably low concentration beyond the level of detection (Fig. 2.8A).

Analysis of the trypsin cleavage products for each virus sample revealed exciting profiles. For virions of WT CCMV-cowpea and type 3 ($C3+4^V$), trypsin digested >50% of the CP, resulting in several faster-migrating peptide fragments

in addition to a single intact protein band (Fig. 2.8A, top panel, left blot; lanes 2-4, right blot; lanes 1 and 2, bottom panel, left blot; lane 7, middle blot; lanes 3 and 7, right blot; lanes 3 and 7). By contrast, digestion of virion types, WT CCMV-NB, $C1^V$ and $C2^V$ and CCP^V with trypsin failed to yield any significant peptide fragments on the Western blot beyond a negligible amount of cleavage (Fig. 2.8A, top panel, left blot; lanes 6-8, right blot; lanes 3 and 4, bottom panel, left blot; lanes 5, 6, and 8, middle blot; lanes 1, 2, 4, 5, 6 and 8, right blot; lanes 1, 2, 4, 5, 6 and 8) and were indistinguishable from those of undigested samples to a large extent (Fig. 2.8A, top panel, left blot, lanes 1 and 5, bottom panel, left blot, lanes 1 to 4). These profiles did not change even after the digestion time to trypsin was extended from 10 min to 18 hr (Fig. 2.8A, Table 2.1). Electron microscopic analysis of trypsin-digested virion preparations (Fig. 2.8B) confirmed the Western blot data, showing that most virions of WT CCMV-NB, type 1 and 2 (Fig. 2.8B), as well as CCP (data not shown), are structurally intact. In contrast, WT CCMV-cowpea and type 3 are unstable and visibly rapidly compared to the undigested samples.

Subsequently, MALDI-TOF was used to identify the cleavage products present in the trypsin-digested virion samples. The deconvoluted mass spectrum obtained from the total ion chromatogram (TIC) of the undigested WT CCMV-cowpea, WT CCMV-NB, $C1^V$, $C2^V$, $C3+4^V$, and CCP^V indicates that all the virions are assembled from a single protein of 20 kDa, which underlines their purity. A representative example of the deconvoluted mass spectrum of undigested virions is shown in Fig. 2.9A.

Analysis of the released peptides at early time points (10 min) distinguished virions of $C1^V$ and $C2^V$ from those of $C3+4^V$. After 10 min of trypsin digestion, $C1^V$ and $C2^V$ virions appeared highly resistant to trypsin protease in Western blot, and the same was observed in MALDI results. These virions only released 2-20 aa from the N-ARM region (Fig 2.10B, 2.12, 2.13). Although highly basic, the N-proximal region is predicted to be mobile/disordered and internalized following its interaction with RNA (Speir et al., 1995). Since N-terminal residues 1 to 26 are not ordered in the crystal structure, their cleavage did not affect the structural integrity of most of the $C1^V$ and $C2^V$ virions, as seen in Fig. 2.8. However, a small percentage of $C1^V$ and $C2^V$ release peptide fragments corresponding to aa 24-42, 83-87, and 85-90. Subsequently, after 45 mins and 3 hr of trypsin digestion, $C1^V$ and $C2^V$ release several other aa fragments corresponding to other cleavage sites on the virion surface, including K65 (Fig 2.10B, 2.12, 2.13). These fragments are present at a low % intensity and presumably released from a subset of $C1^V$ and $C2^V$ virions with regions like 24-42, 83-87, and 85-90 exposed and accessible to trypsin at an early time point. However, >95% of $C1^V$ and $C2^V$ virions remain highly resistant to trypsin (Fig. 2.8). As a result, it was predicted that these fragments are coming from <5% of these virions and, therefore, very low in abundance.

In contrast, the rate at which virions of $C3+4^V$ are digested by trypsin is observed to be qualitatively distinct from those of $C1^V$ and $C2^V$. For example, Western blot analysis revealed that for virions of $C3+4^V$, the intact protein present in the trypsin-digested sample was approximately 50% compared to that of either

untreated C3+4^{V} or trypsin-treated C1^{V} and C2^{V} samples (Fig. 2.8). At every time point examined, including the early time points (e.g., 10 min) and late time points (30 min, 45 min, 3 hr, and 18 hr), virions of C3+4^{V} were highly susceptible to trypsin, releasing multiple peptides. Mass mapping identification of the released peptides revealed that the accessible trypsin cleavage sites (e.g., K45, K54, K65, K87, K106, and K131) (Fig. 2.9; Table 2.1) were consistent with the reported surface structure of the CCMV virions. These observations suggest that virions of C3+4^{V} have qualitatively distinct capsid dynamics from those of C1^{V} and C2^{V} and that the two virion types have a different conformational arrangement of the CP amino acid residues in the virion exterior. Although peptides representing N-terminal regions, 2 to 26 aa, were detected at the earliest time point (e.g., 10 min) (Fig. 2.10 and 2.14), their accessibility to protease coincided with other cleavage sites as well (Fig. 2.9; Table 1.1). Therefore, it is likely that these N-terminal peptides on virions of C3+4^{V} may not be the first sites of protease cleavage since multiple simultaneous cleavages at other sites expose the otherwise internalized N-terminal region to proteolysis.

Figures 2.8 and 2.11 summarize the Western blot analysis of trypsin digestion products and their MALDI-TOF analysis, respectively, for the virions of WT CCMV-cowpea, WT CCMV-NB, and CCP^{V} used as controls. The MALDI-TOF profile of WT CCMV-cowpea and WT CCMV-NB is identical to C3+4^{V} (Fig. 2.8, 2.11, and 2.14). By contrast, unexpected trypsin cleavage profiles were obtained for CCP^{V} (Fig. 2.11). Although CCP^{V} virions are distinct in size and RNA packaging

traits compared to WT CCMV, their sensitivity to trypsin digestion and subsequent MALDI-TOF profiles are shared with $C1^V$ and $C2^V$ (Fig. 2.10, 2.11; Table 2.1).

We speculate that some of the unassigned peaks observed in MALDI-TOF analysis (Fig. 2.10, 2.11, 2.12, 2.13, 2.14) may result from trypsin self-cleavage (http://prospector.ucsf.edu/prospector/mshome.htm). For brevity, Table 2.1 summarizes the location of the trypsin cleavage sites identified to be located on $C1^V$, $C2^V$, and $C3+4^V$ by MALDI-TOF.

DISCUSSION

The primary focus of this study is to investigate whether physically indistinguishable virions of CCMV, each with a different RNA content, can be distinguished in solution. Using agroinfiltration, we were successful in assembling, for the first time, the three virion types of CCMV, $C1^V$, $C2^V$, and $C3+4^V$, separately *in planta* (Fig. 2.3), virions which are otherwise impossible to separate in pure forms. A series of biochemical (e.g., RT-PCR) and biological assays established the purity of each virion type (Fig. 2.6). Although the three virion types are physically and morphologically indistinguishable (Fig. 2.5), application of thermal denaturation assay and limited proteolysis with trypsin followed by MALDI-TOF distinguishes between two dynamical classes of the three virion types: $C1^V$ and $C2^V$ are grouped as class I and $C3+4^V$ as class II (Fig. 2.8-14, Table 2.1).

Virions of $C1^V$ and $C2^V$ are dynamically distinct from those of $C3+4^V$

Based on the CCMV structure, the accessible trypsin cleavage sites (K42, K65, K87, and K106) are located on the surfaces of the A, B, and C subunits of CCMV CP are shown in Fig. 2.9. Identification of the cleavage products of $C1^V$, $C2^V$, and $C3+4^V$ at various time points by mass mapping suggested the following: a) for $C1^V$ and $C2^V$, the N-ARM region is transiently exposed on the capsid surface as those are the first cleavage products recovered after digesting the virions for 10

min with trypsin (Table 2.1). Since the residues 1-26 are not ordered in the crystal structure, their cleavage did not affect >95% of the virions (Fig. 2.8). These virions do not have external residues like K65 transiently exposed on their surface and appear highly resistant to trypsin cleavage even during extended periods of trypsin digestion (up to 18 hr, Fig 2.8). Residues like R82, K84, K131, and K143 are least exposed and are not expected to be accessible for trypsin cleavage (Fig. 2.9). However, a subset of $C1^V$ and $C2^V$ release fragments like 83-87 aa and 85-90 aa at the earliest digestion time point (Fig. 2.12 and 2.13). Given the low abundance of these fragments and the detention of >95% intact virions upon digestion in western blot and EM, we predict these unstable virions to make a negligible proportion (<5%) of total $C1^V$ and $C2^V$ virions. This small subset of $C1^V$ and $C2^V$ gets further digested as digestion time is prolonged and releases several other fragments encompassing other exposed residues on the capsid surface. These digestion products are below the detection limit of Western blot (Fig. 2.8) and can only be detected using sensitive techniques such as MALDI-TOF. b) For $C3+4^V$, amino acids K42, K65, K87, and K106 are located on the surface of the capsid and hence are readily accessible for cleavage. The stability of CP dimers, the building blocks of icosahedral virus capsids, is controlled by the interaction between the invading C-terminal arm and the N-terminal clamp of the adjacent CP subunits, and any mutations engineered in the C terminus disrupt virion assembly (Okinaka, Mise, Suzuki, Okuno, & Furusawa, 2001; Zlotnick, Aldrich, Johnson, Ceres, & Young, 2000). Thus, any cleavage at C-terminal in positions like K143 can disrupt

the capsid structure. This explains the visibly degraded C3+4^{V} in Western blot after briefest exposure to trypsin for 10 min (Fig. 2.8). Unlike previously described in BMV (Chakravarty et al., 2020), the C3+4^{V} virions have peptides from their N-ARM detected in the early time points. One possibility is that C3+4^{V} virions have their N-ARM transiently exposed on the surface of the capsid. Alternatively, these N-ARM peptides may not be the first sites of trypsin cleavage since multiple simultaneous cleavages at other sites expose the otherwise internalized N-terminal region to proteolysis.

MALDI-TOF fragmentation profile of WT CCMV-cowpea virions is indistinguishable from those of C3+4^{V} (Fig. 2.8, 2.11). This is plausible since purified virion preparation of WT CCMV-cowpea is a mixture of all three virion types, with C3+4^{V} constituting ~54% of the total (Fig. 2.1F). WT CCMV-NB also resembles the MALDI-TOF fragmentation profile of C3+4^{V} (Fig. 2.11). However, the thermal denaturation profile and trypsin digestion pattern of WT CCMV-NB resembles C1^{V} and C2^{V} (Fig. 2.7, 2.8). Therefore it would be interesting to investigate if the host can influence the proportion of different virion types of CCMV in cowpea and *N. benthamiana,* as shown previously in the case of cowpea and *Chenopodium hybridum* (Verduin, 1978). CCP^{V} remained highly resistant to trypsin (Fig. 2.8 and 2.11) and positioned the N-ARM peptides externally to the capsid along with a few other residues exposed on the capsid surface. The type of RNA that gets packaged in CCP^{V} may influence the observed conformational dynamics.

A previous study analyzed the dynamics of WT CCMV and a salt-stable variant of CCMV (SS-CCMV). It was observed that WT CCMV particles are more sensitive to trypsin than SS-CCMV. However, the pattern of released peptides is similar for both forms of CCMV, and the reported cleavage sites were localized to the N-terminus of the CP, resulting in virions retraining their structural integrity even after 8 hours of trypsin cleavage (Speir et al., 2006). As Speir et al. 2006 used the WT-CCMV, a mixture of all three types of CCMV virions and a trypsin concentration of 1:1,000 (wt/wt), a comparison of our results to them is problematic. These details may also explain the lack of fragments encompassing regions other than N-ARM in the study mentioned earlier that we recovered in our experiments using individual virion types.

The capsid dynamics of individual virion types in BMV and CCMV are near identical with a few differences

Our previous data showed that stability and conformational dynamics displayed by BMV RNA1 (B1) and 2 (B2) containing virions vs. that of RNA3+4 containing virions are distinct. In these two virion types, the N-proximal 2-8 aa region is transiently externalized, allowing the virions to retain their structural integrity following trypsin digestion. Also, the instability under neutral pH conditions and the observed capsid dynamics may enable ribosomes to bind B1 and B2 RNA and initiate translation of p1a and p2a, respectively. We hypothesized that

instability of the virions in conjunction with the translation of B1 and B2 RNA leads to co-translational disassembly of BMV RNA1 and 2 containing virions (Chakravarty et al., 2020). On the other hand, unlike the genomic RNAs B1 and B2, replication is favored over translation for the genomic RNA3 (B3). RNA3 must undergo replication to generate CP mRNA. The N terminus of the CP in BMV RNA 3+4 containing virions is not accessible for trypsin digestion, suggesting that the N-ARM region is internal and not exposed outside the capsid, resulting in B3 RNA being unavailable for translation initiation. B3+4 containing virions are highly sensitive to trypsin resulting in complete release of their RNA. Consequently, the internalization and the interaction between the N-ARM and B3 inhibit translation and support replication (Chakravarty et al., 2020).

Capsid proteins of the genetically related BMV and CCMV exhibit ~70% sequence homology and are 189 and 190 amino acids in length respectively. These two viruses are readily distinguished by the symptom phenotypes they induce in their natural hosts cowpea and barley respectively. For example, cowpea plants are susceptible to CCMV but not to BMV, whereas barley is susceptible to BMV but not to CCMV. This study demonstrated that CCMV RNA1 and 2 containing virions showed near-identical stability and capsid dynamics as their BMV counterparts, so do the CCMV RNA3+4 containing virions. Therefore, our results indicate that individual virion types in bromoviruses may use identical capsid dynamics as a strategy to facilitate efficient replication. Therefore, this phenomenon may be an adaptation to a specific host as both viruses systemically

infect *N. benthamiana* (Chakravarty & Rao, 2021) but does not cause any symptoms.

At the same time, BMV is a monocot-adapted virus vs. CCMV, a dicot-adapted virus. Interestingly, in *C. quinoa*, a shared experimental host, BMV induces chlorotic local lesions followed by systemic mottling, whereas CCMV induces local necrotic lesions without systemic spread. Our study highlighted a few differences in stability and dynamics between the BMV and CCMV virions. In comparison to BMV, CCMV differs by thermal stability. The three BMV virion types show identical thermal stability at neutral pH vs. CCMV virions which are divided into two classes. The majority of C3+4^{V} melt at ~50°C, whereas C1^{V} and C2^{V} show one more thermally unstable population at ~85°C in addition to the one at ~50°C at a neutral pH. CCMV differs in proteolysis profile also. EM results of trypsin digested virions show that most WT-CCMV virions assembled in *N. benthamiana* remain intact whereas, most of the WT BMV virions assembled in the same host lose their structural integrity. CCMV differs slightly in MALDI results from BMV. A small percentage of C1^{V} and C2^{V} virions transiently expose residues encompassing 83-87 and 85-90 in addition to releasing N-ARM peptides. This is absent in B1^{V} and B2^{V} virions. However, the integrity of C1^{V} and C2^{V} virions did not seem to get affected. These slight differences may account for adaptation to different host plants.

Our data adds a new perspective and sheds light on understanding the general biology of bromoviruses. Finally, the strategy used to assemble first the

independent virions of BMV (Chakravarty et al., 2020), and now CCMV applies to other RNA viruses and specifically to multicomponent viruses, such as cucumber mosaic virus, that exhibit particle homogeneity similar to BMV and CCMV.

MATERIALS AND METHODS

Agroplasmids used in this study

Plasmids pCass-RzC1, pCass-RzC2, and pCass-RzC3 contain full-length cDNA clones corresponding to CCMV genomic RNAs1 (C1, accession number M65139.1), 2 (C2, accession number M28817.1), and 3 (C3, accession number M28818.1), respectively were constructed for this study. To facilitate the construction of pCass-RzC1, a 3174 bp PCR product encompassing a full-length cDNA sequence corresponding to the CCMV genomic RNA1 was amplified using a forward primer (5' AGGGGTACCGTAATCCACGAGAGCGAGG 3'; *Kpn*I site is underlined) and a reverse primer (5' AGCTCTAGATGGTCTCCTTAGAGATCACCT; *Xba*I site is underlined). The resulting product was digested with *Kpn*I and *Xba*I and was ligated into a similarly treated pCass-Rz, a binary vector derived from pCass2 (Annamalai & Rao, 2005b). To facilitate the construction of pCass-RzC2, a 2771 bp PCR product encompassing a full-length cDNA sequence corresponding to the CCMV genomic

RNA2 was amplified using a forward primer (5' AGGGGTACCGTAATCCACGAGAGCGAGG 3'; *Kpn*I site is underlined) and a reverse primer (5' AGCTCTAGATGGTCTCCTTAGAGATCACCT; *Xba*I site is underlined). The resulting product was digested with *Kpn*I and *Xba*I and was ligated into a similarly treated pCass-Rz vector. To facilitate the construction of pCass-RzC3, a 2205 bp PCR product encompassing a full-length cDNA sequence corresponding to the CCMV genomic RNA3 was amplified using a forward primer (5' AGGGGTACCGTAATCTTTACCAAACAACTTTCA 3'; *Kpn*I site is underlined) and a reverse primer (5' AGCTCTAGATGGTCTCCTTAGAGATCACCT; *Xba*I site is underlined). The resulting product was digested with *Kpn*I and *Xba*I and was ligated into a similarly treated pCass-Rz vector. Each resulting plasmids 35S-C1, 35S-C2, and 35S-C3 (for expression of genomic RNA) contains a double 35S promoter, cDNA complementary to respective full-length CCMV RNAs, a 68-nt fragment encompassing the ribozyme (Rz) sequence of a satellite RNA of tobacco ringspot virus, and *Nos* terminator in sequential order. Likewise, agroplasmids PZPC1a, PZPC2a, and PZPCCP were engineered to transiently express CCMV replicase protein 1a (C1a), replicase protein 2a (C2a), and capsid protein (CP), respectively. PZPC1a was constructed by amplifying a 2879 bp PCR product encompassing cDNA sequence corresponding to the CCMV genomic RNA1 open reading frame using a forward primer (5' ATGGCAAGTTCTTTAGATCTTTTG 3') and a reverse primer (5' GGACTAGTTAAGATATACTTCTAAATATTAAATCACCT 3'; *Spe*I site is underlined). The resulting product was digested with *Spe*I and was

ligated into a *Stu*I and *Spe*I treated PZP vector. PZPC2a was constructed by amplifying a 2426 bp PCR product encompassing cDNA sequence corresponding to the CCMV genomic RNA2 open reading frame using a forward primer (5' ATGTCTAAGTTCATTCCAGAAGGT 3') and a reverse primer (5' GGACTAGTTATTTAGAAAGGGTCTTACGCA 3'; *Spe*I site is underlined). The resulting product was digested with *Spe*I and was ligated into a *Stu*I and *Spe*I treated PZP vector. PZPCCP was constructed by amplifying a 573 bp PCR product encompassing cDNA sequence corresponding to the CCMV CP open reading frame using a forward primer (5' ATGTCTACAGTCGGAACAGGGAAGT 3') and a reverse primer (5' GGACTAGTCTAATACACCGGAGTGAAAGAG 3'; *Spe*I site is underlined). The resulting product was digested with *Spe*I and was ligated into a *Stu*I and *Spe*I treated PZP vector.

Agroinfiltration, total protein extraction, virion purification, negative-stain electron microscopy, virion RNA electrophoresis, and Western blot analysis

All agroplasmids used in this study were transformed into *Agrobacterium* strain GV3101. The transformed *Agrobacterium* cells containing the desired transformant were infiltrated into the abaxial surface of wild-type *N. benthamiana* leaves described previously (P. Annamalai & A. L. N. Rao, 2006). After 4 days post infiltration (dpi), agroinfiltrated local and systemic leaves were ground in liquid nitrogen. Total protein was extracted in 3 volumes of extraction buffer (20mM Tris-

Cl; pH 7.5, 1mM EDTA; pH 8.0, 5mM DTT). The leaf slurry was centrifuged at 14,000 rpm for 5 minutes, and the supernatant was used for downstream analysis of total proteins using SDS-PAGE and Western blot. The procedure used to purify CCMV virions from 4 dpi agroinfiltrated leaves of *N. benthamiana* or cowpea (*Vigna unguiculata*) followed by sucrose density gradient centrifugation was as described previously (Annamalai & Rao, 2005a). For negative-stain EM analysis, virions were imaged using a Tecnai 12 operated at 120 KeV, and images were recorded digitally. For electrophoretic mobility analysis, purified virions were loaded in a 1% agarose gel and electrophoresed in virus suspension buffer (50 mM sodium acetate, 8 mM magnesium acetate, pH 4.5) at 7 V/cm for 2.5 hours at 4°C. For RNA analysis, virion RNA was electrophoresed in 1.2% agarose gels under denaturing conditions as described previously (Annamalai & Rao, 2005b). Following ethidium bromide staining, quantification of each RNA was performed using ImageJ software. Western blot analysis of undigested and trypsin-digested virion samples using anti-CP antibodies was performed as described previously (Annamalai & Rao, 2005b).

Differential scanning fluorimetry

DSF was performed as described previously (Rayaprolu et al., 2014). Desired virion samples and control (lysozyme) samples were resuspended either in virus suspension buffer (50 mM sodium acetate, 8 mM magnesium acetate, pH

4.5) or in 100 mM phosphate buffer (pH 7.2). The experiment was performed three times independently, using three replicates for each sample. DSF data were analyzed and plotted as described previously (Chakravarty et al., 2020; Rayaprolu et al., 2014).

MALDI-TOF

For MALDI-TOF, analysis was performed as described previously (Chakravarty et al., 2020). A desired purified virion preparation was diluted to 1 mg/ml in 25 mM Tris-HCl, 1 mM EDTA buffer. A 30 µl sample (i.e., 30 µg of the desired virion preparation) was digested with a 1:100 (wt/wt) ratio of trypsin (Pierce Trypsin protease, mass spectrometry grade; Thermo Fisher Scientific) to virus for various time points at 25°C (Bothner et al., 1999). 10 µl of water was added to 20 µl of the digested sample. Approximately 0.5 µl of each digested or undigested (control) sample was analyzed on an AB Sciex TOF/TOF 5800 MALDI MS with -cyano-4-hydroxycinnamic acid matrix. The instrument was calibrated with standards, and the test samples were analyzed with external calibration. The accuracy is approximately 0.05 Da. The MALDI-TOF data were analyzed with AB Sciex Data Explorer, and baseline was corrected with a peak width of 32, flexibility of 0.5, and degree of 0.1. For noise removal, the standard deviation was set at 2. To determine the peak detection criteria, the percent centroid was taken as 50, the signal/noise (S/N) threshold was 3, and the noise window width m/z was 250. The

threshold after S/N recalculation was set at 20. The peptide fragments were assigned based on the UCSF Protein Prospector's MS-Digest function.

RT-PCR

RNA was isolated from purified individual type of virions and subjected to RT-PCR using iScript™ cDNA Synthesis Kit (Bio-Rad) and Q5® High-Fidelity DNA Polymerase (NEB) and the following set of primers. A 1,805 nucleotide (nt) fragment of C1 RNA located between the 3' tRNA-like structure (TLS) and a portion of replicase 1a ORF was amplified with a forward primer (5' GCTACCTCAAGCACCGGTAA 3') and a reverse primer (5' TGGTCTCCTTAGAGATCACC 3'). Likewise, a 1,827-nt fragment of C2 RNA located between the 3' TLS and a portion of replicase 2a ORF was amplified with a forward primer (5' GGCAGAGTGATGTTGATTGG 3') and a reverse primer (5' TGGTCTCCTTAGAGATCACC 3'). A 601-nt fragment of MP ORF of C3 RNA located between nucleotides 546 and 1147 was amplified using a forward primer (5' TGTGAGGACGACAACAGTGAC 3') and a reverse primer (5' CTATCTACGTTTGATAGACATCG 3'). Similarly, a 700-nt fragment of CP ORF of C3/sgC4 RNA located between the 3' TLS and a portion of the CP ORF was amplified with a forward primer (5' GGCCAAGGCAAGGCTATTA 3') and a reverse primer (5' TGGTCTCCTTAGAGATCACC 3'). The resulting PCR products were analyzed by 1% agarose gel electrophoresis.

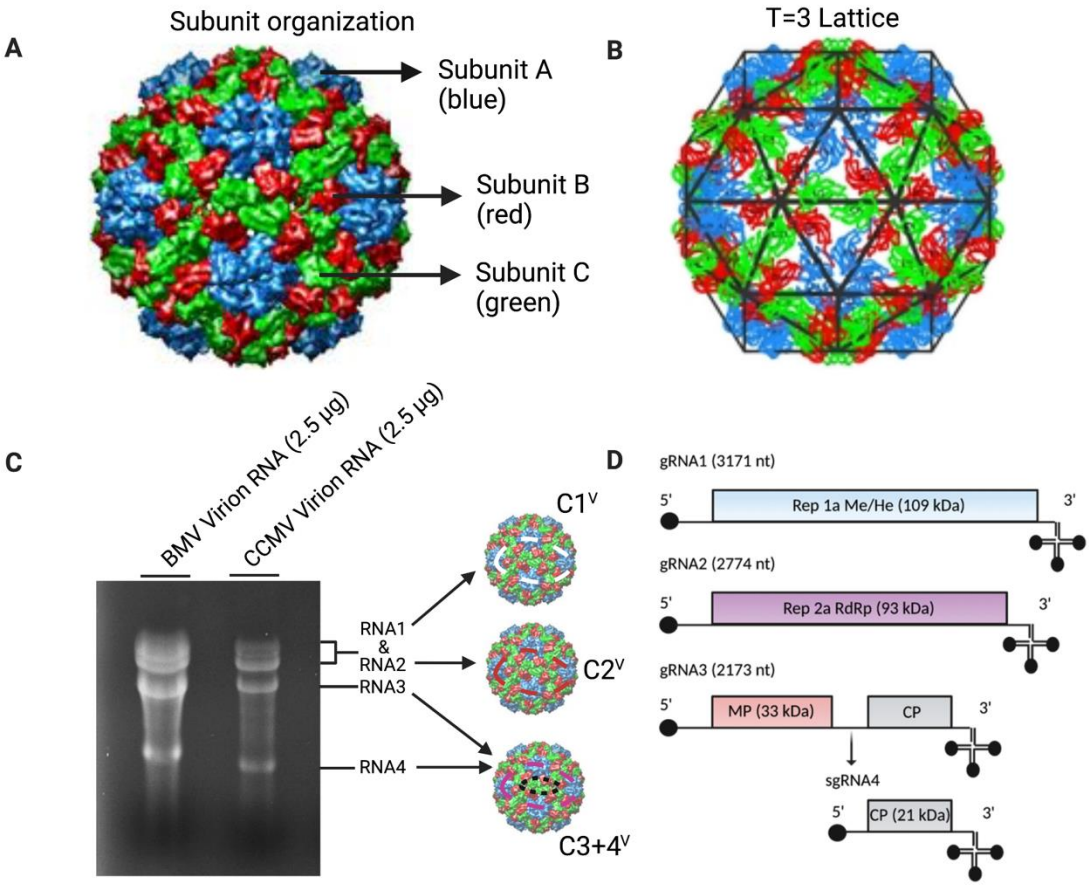

E

CLUSTAL O(1.2.4) multiple sequence alignment

```
CCMV      MSTVGTGKLTRAQRRAAARKNKRNTRVVQPVIVEPIASGQGKAIKAWTGYSVSKWTASCA  60
BMV       MSTSGTGKMTRAQRRAAARRNRWT-ARVQPVIVEPLAAGQGKAIKAIAGYSISKWEASSD  59
          *** *****:**********:*: .   ********:*:******** :***:*** **.

CCMV      AAEAKVTSAITISLPNELSSERNKQLKVGRVLLWLGLLPSVSGTVKSCVTETQTTAAASF  120
BMV       AITAKATNAMSITLPHELSSEKNKELKVGRVLLWLGLLPSVAGRIKACVAEKQAQAEAAF  119
          *  **.*.*::*:**:*****:**:*****************:* :*:**:*.*: * *:*

CCMV      QVALAVADNSKDVVAAMYPEAFKGITLEQLTADLTIYLYSSAALTEGDVIVHLEVEHVRP  180
BMV       QVALAVADSSKEVVAAMYTDAFRGATLGDLL-NLQIYLYASEAVPAKAVVVHLEVEHVRP  178
          ********.**:****** :**:* ** :*  :* ****:* *:    *:**********

CCMV      TFDDSFTPVY-   190
BMV       TFDDFFTPVYR   189
          **** *****
```

F

Virion Type	% Population
$C1^V$ & $C2^V$	~46
$C3+4^V$	~54

Figure 2.1 Structure, genome organization, and quantitative analysis of the three types of CCMV virions. (A) and (B) Structure of CCMV capsid based on the PDB entry 1CWP showing the A, B, C subunits and T=3 lattice. (C) RNA was isolated from WT purified BMV and CCMV virion preparation, denatured with formamide/formaldehyde and subjected to 1.2% agarose gel electrophoresis as described previously. (D) Genome organization of CCMV. (E) Alignment of CCMV and BMV CP sequences shows 70% sequence homology. The sequences were analyzed using Clustal Omega multiple sequence alignment tool. (F) After staining the gel from panel C with ethidium bromide, the amount of RNA molecules present in each band was estimated using ImageJ software and was used to determine the mole ratios of the viral RNAs isolated from virions. These mole ratios were then used to determine the fraction of each virion type (Schneider, Rasband, & Eliceiri, 2012).

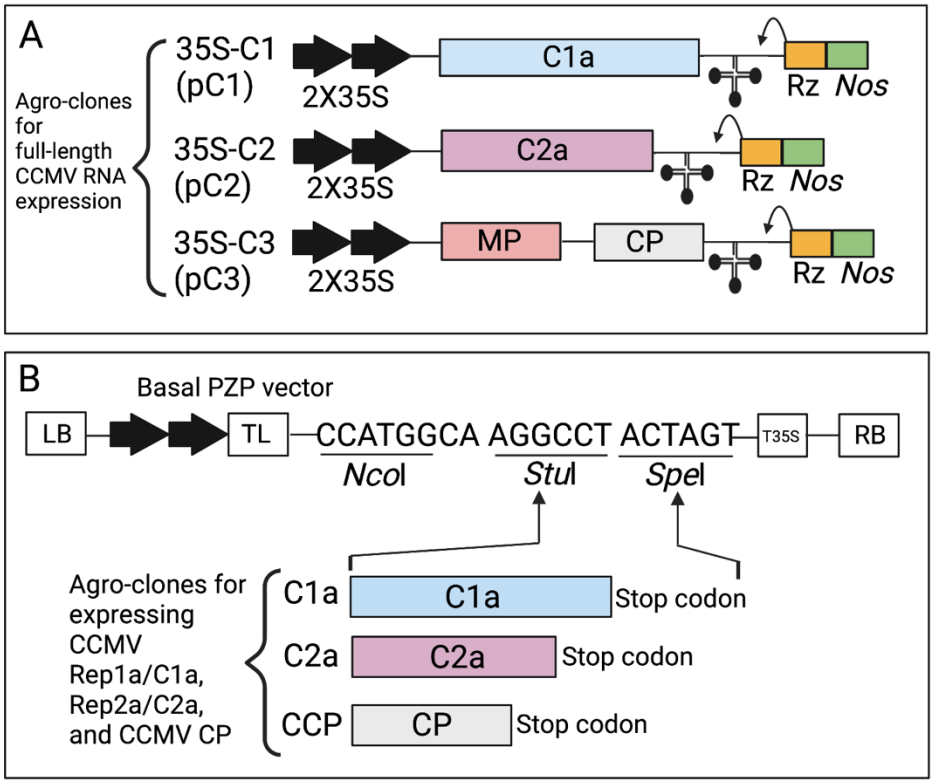

Figure 2.2 Characteristic features of agroplasmids used in this study. (A) Characteristics of agroplasmids harboring CCMV genomic RNAs used for transient expression in plants. The 35S-C1 (pC1), 35S-C2 (pC2), and 35S-C3 (pC3) constructs contain full-length cDNA copies of CCMV genomic RNA1 (C1), -2 (C2), and -3 (C3), respectively. Single lines and open boxes represent noncoding and coding regions, respectively. Monocistronic C1 encoding replicase protein 1a (C1) and monocistronic C2 encoding replicase protein 2a (C2a) are indicated. In C3, the locations of the movement protein (MP) and coat protein (CP) genes are shown. At the 3' end of each construct, the clover leaf-like conformation represents a tRNA-like motif conserved among all three CCMV genomic RNAs. Two black arrows at the 5' ends represent the double 35-S. A bent arrow indicates the predicted self-cleavage site by the ribozyme. The location of the *Nos* terminator is also indicated. (B) Agroconstructs for transient expression of C1a, C2a, and CP (pCCP). Open reading frames (ORFs) of CCMV p1a, p2a, and CP were fused in-frame to each pair of binary vectors using *Stu*I and *Spe*I sites. Each binary vector contained, in sequential order, a left border of T-DNA (LB), a double 35S promoter (35SX2), a tobacco etch virus (TEV) translation enhancer leader sequence (TL), multiple cloning sites, a 35S terminator (T35S), and a right border of T-DNA (RB).

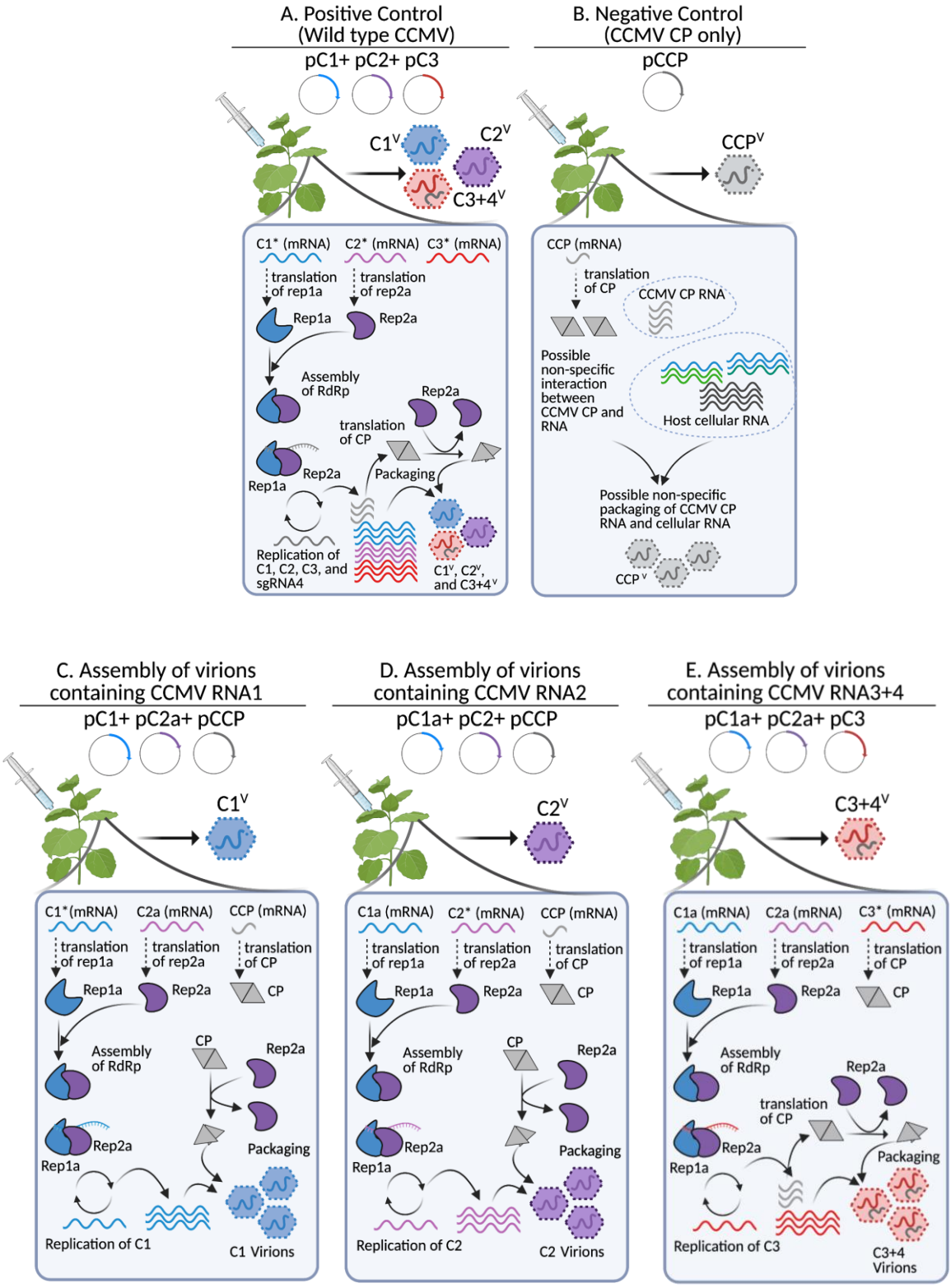
A. Positive Control
(Wild type CCMV)
pC1+ pC2+ pC3
C1V
C2V
C3+4V
C1* (mRNA)
C2* (mRNA)
C3* (mRNA)
translation of rep1a
translation of rep2a
Rep1a
Rep2a
Assembly of RdRp
Rep2a
translation of CP
Rep1a
Rep2a
Packaging
Replication of C1, C2, C3, and sgRNA4
C1V, C2V, and C3+4V
B. Negative Control
(CCMV CP only)
pCCP
CCPV
CCP (mRNA)
translation of CP
CCMV CP RNA
Possible non-specific interaction between CCMV CP and RNA
Host cellular RNA
Possible non-specific packaging of CCMV CP RNA and cellular RNA
CCPV
C. Assembly of virions containing CCMV RNA1
pC1+ pC2a+ pCCP
C1V
C1*(mRNA)
C2a (mRNA)
CCP (mRNA)
translation of rep1a
translation of rep2a
translation of CP
Rep1a
Rep2a
CP
Assembly of RdRp
CP
Rep2a
Rep2a
Rep1a
Packaging
Replication of C1
C1 Virions
D. Assembly of virions containing CCMV RNA2
pC1a+ pC2+ pCCP
C2V
C1a (mRNA)
C2* (mRNA)
CCP (mRNA)
translation of rep1a
translation of rep2a
translation of CP
Rep1a
Rep2a
CP
Assembly of RdRp
CP
Rep2a
Rep2a
Rep1a
Packaging
Replication of C2
C2 Virions
E. Assembly of virions containing CCMV RNA3+4
pC1a+ pC2a+ pC3
C3+4V
C1a (mRNA)
C2a (mRNA)
C3* (mRNA)
translation of rep1a
translation of rep2a
translation of CP
Rep1a
Rep2a
CP
Assembly of RdRp
Rep2a
translation of CP
Rep2a
Rep1a
Packaging
Replication of C3
C3+4 Virions

Figure 2.3 Schematic representation of the strategy used for autonomous assembly of the three virions of CCMV *in vivo*. (A) (Positive control) Infiltration of the inoculum containing a mixture of pC1+pC2+pC3 would induce WT CCMV infection resulting in the assembly of a mix of all three virions. (B) (Negative control) Infiltration of the inoculum containing pCCP would result in the expression of CP mRNA followed by the translation of WT CP and non-specific assembly of virions containing CP mRNA and cellular RNA. (C) Assembly of virions packaging RNA1 ($C1^V$). A mixture of inoculum containing agrotransformants pC1+pC2a+pCCP (see Fig. 2 for details) is infiltrated into *N. benthamiana* leaves. Transcription of pC1 results in the synthesis of a biologically active full-length genomic RNA1 whose translation gives functional replicase protein 1a; similarly, agrotransformant pC2a results in an mRNA competent to give replicase 2a but not competent to be replicated because it lacks the requisite 5' and 3' noncoding regions. Finally, translation of the mRNA transcribed from agrotransformant pCCP gives the CP subunits for directing virion assembly. As a result, a functional replicase complex is assembled from proteins 1a and 2a that ensures the replication of C1 RNA followed by its packaging into virions by the transiently expressed CCMV CP subunits. (D) Assembly of virions packaging RNA2 ($C2^V$). The inoculum shown in this panel is identical to the one shown in panel C, except that pC1 and pC2a are replaced by pC1a and pC2, respectively. Agroinfiltration of this inoculum results in the assembly of virions containing C2 RNA. (E) Assembly of virions packaging RNA3 and -4 ($C3+4^V$). The inoculum shown in this panel is formulated to assemble virions packaging C3 RNA and sgC4 by mixing agrotransformants of pC1a, pC2a, and pC3. Transiently expressed replicase proteins 1a and 2a then direct replication of C3 followed by the synthesis of sgC4 for CP production.

A. SDS-PAGE analysis of total protein stained with Coomassie Brilliant Blue R-250

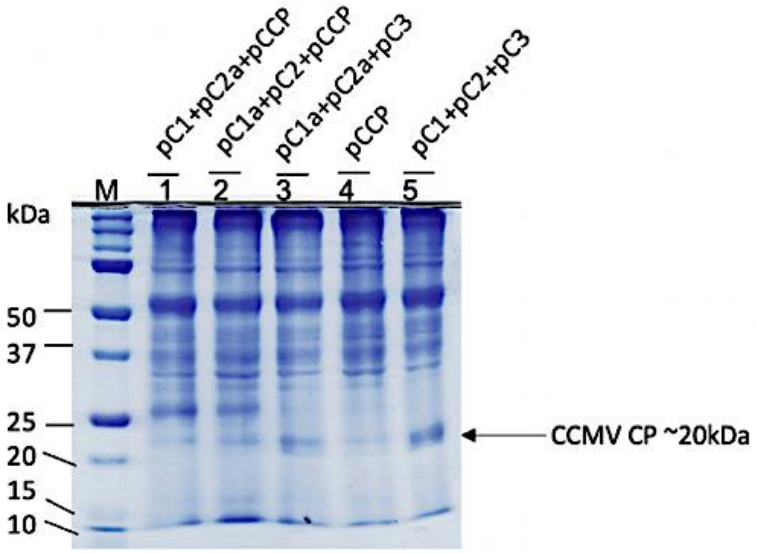

B. Western blot analysis of total protein using anti-BMV CP antibody

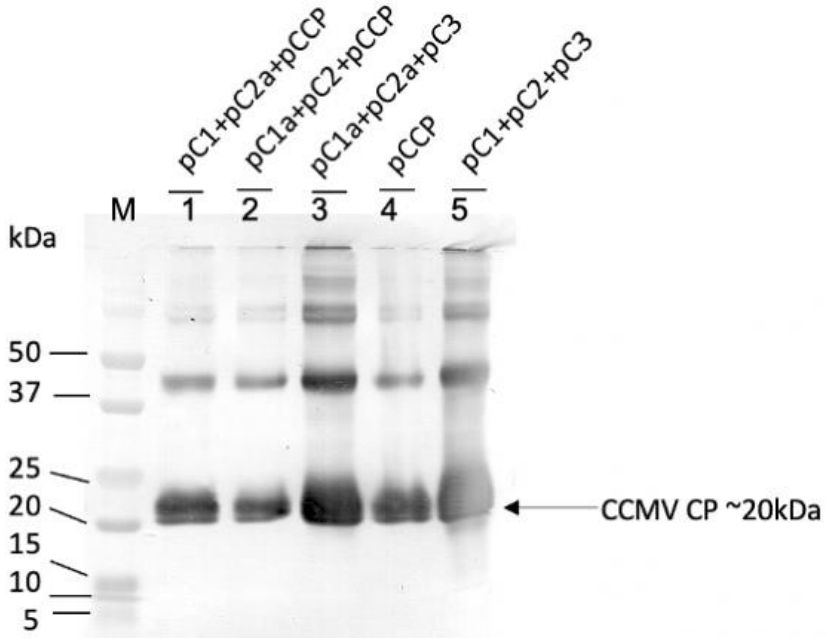

Figure 2.4 Analysis of total protein extracted from 4dpi leaves. (A) SDS-PAGE analysis of total protein extracted from the 4 dpi leaves of *N. benthamiana.* Lane 1 contains total protein from leaf infiltrated with agrotransformants pC1+pC2a+pCCP that results in assembly of $C1^V$; lane 2 contains total protein from leaf infiltrated with agrotransformants pC1a+pC2+pCCP that results in accumulation of $C2^V$; lane 3 contains total protein from leaf infiltrated with agrotransformants pC1a+pC2a+pC3 that results in assembly of $C3+4^V$; lane 4 contains total protein from leaf infiltrated with agrotransformant pCCP that results in assembly of CCP^V; lane 5 contains total protein from leaf infiltrated with agrotransformants pC1+pC2+pC3 that results in accumulation of WT CCMV virions. Each lane has 30 µg of total protein estimated by Bradford protein assay. The gel is stained with Coomassie Brilliant Blue R-250 to demonstrate the loading controls. (B) Western blot analysis of total protein extracted from the 4 dpi leaves of *N. benthamiana* using anti BMV-CP antibody. The samples are loaded in the order as mentioned above in lanes 1-5.

A

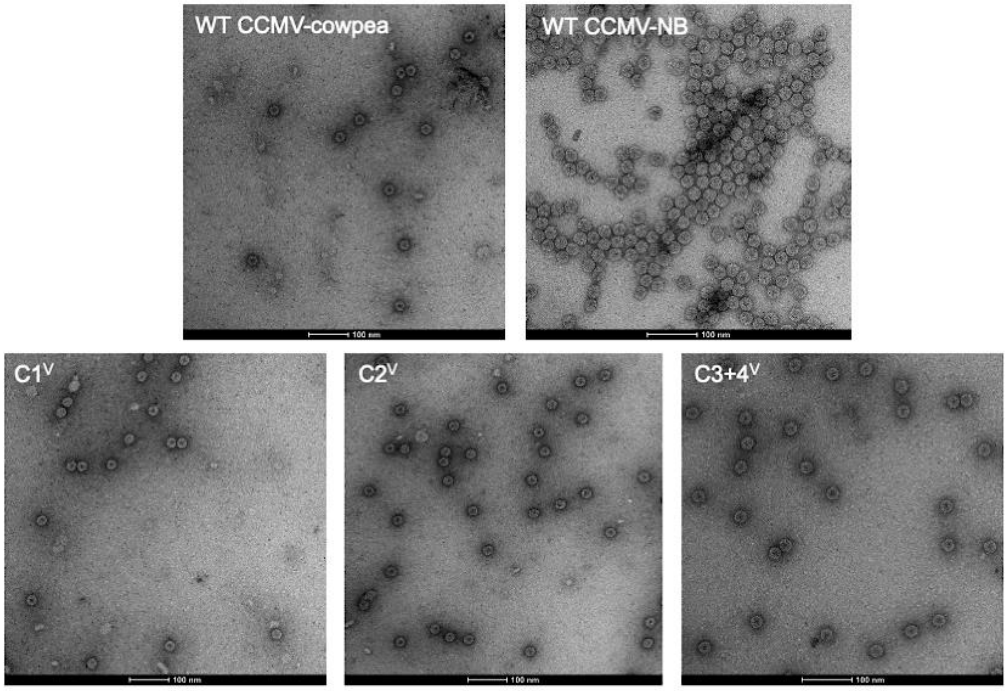

B

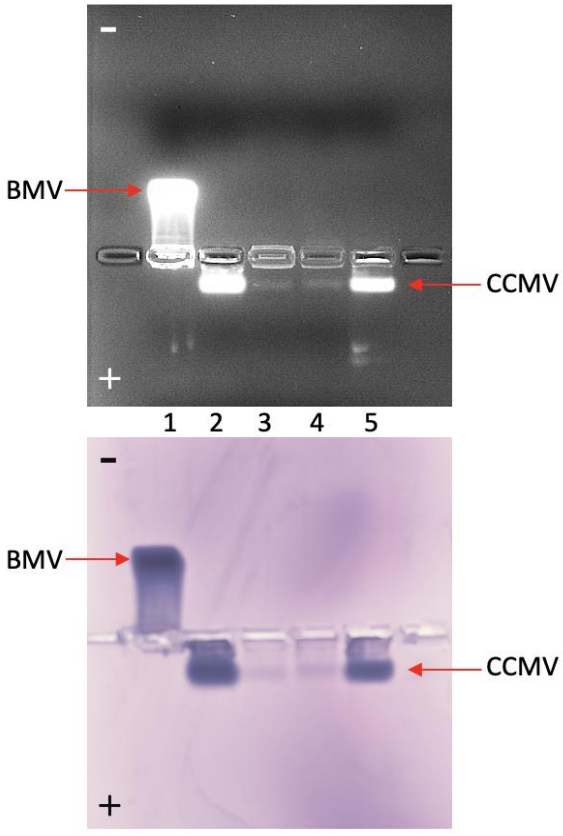

Figure 2.5 Physical characterization of $C1^V$, $C2^V$, and $C3+4^V$. (A) Negative-stain electron micrographs of density gradient-purified virions of either WT CCMV from *N. benthamiana* or cowpea plants or autonomously assembled virions of $C1^V$, $C2^V$, and $C3+4^V$ via agroinfiltration. (B) Virion electrophoresis. Density gradient-purified virions of WT BMV (lane 1), WT CCMV (lane 2), $C1^V$ (lane 3), $C2^V$ (lane 4), and $C3+4^V$ (lane 5) were subjected to agarose gel analysis as described in Materials and Methods. The gel shown at the top panel was stained with ethidium bromide to detect RNA and then restained with Coomassie blue to detect protein (bottom panel). BMV and CCMV virions migrating toward negative and positive, respectively, are indicated.

A

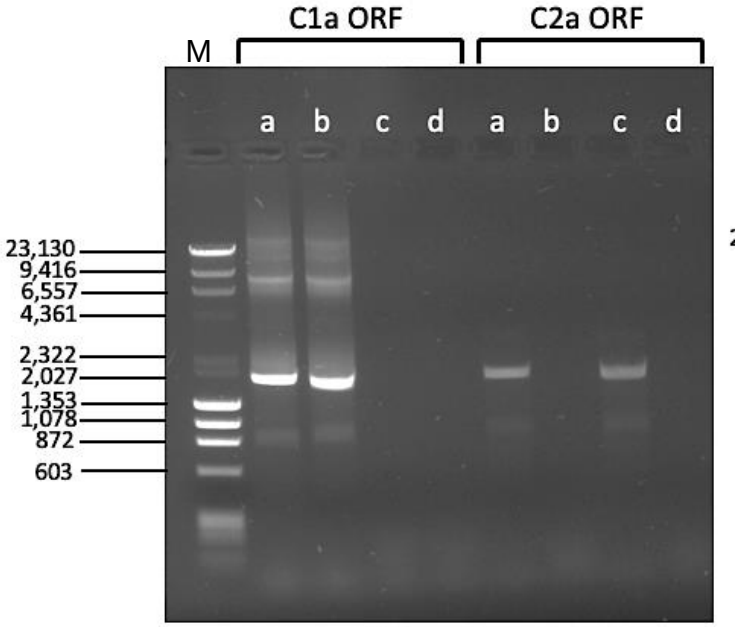

a: WT, b: $C1^V$, c: $C2^V$, d: $C3+4^V$

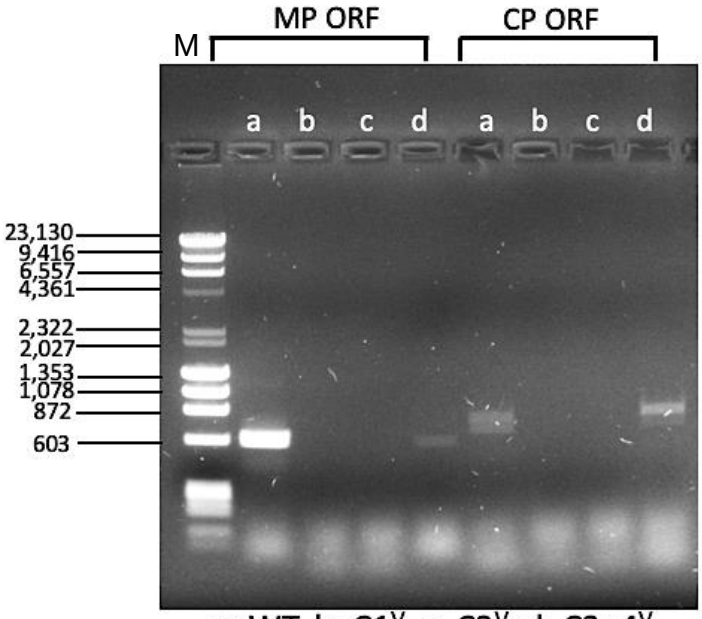

a: WT, b: $C1^V$, c: $C2^V$, d: $C3+4^V$

B. Infectivity of WT CCMV and C1^{V}, C2^{V}, C3+4^{V} virions

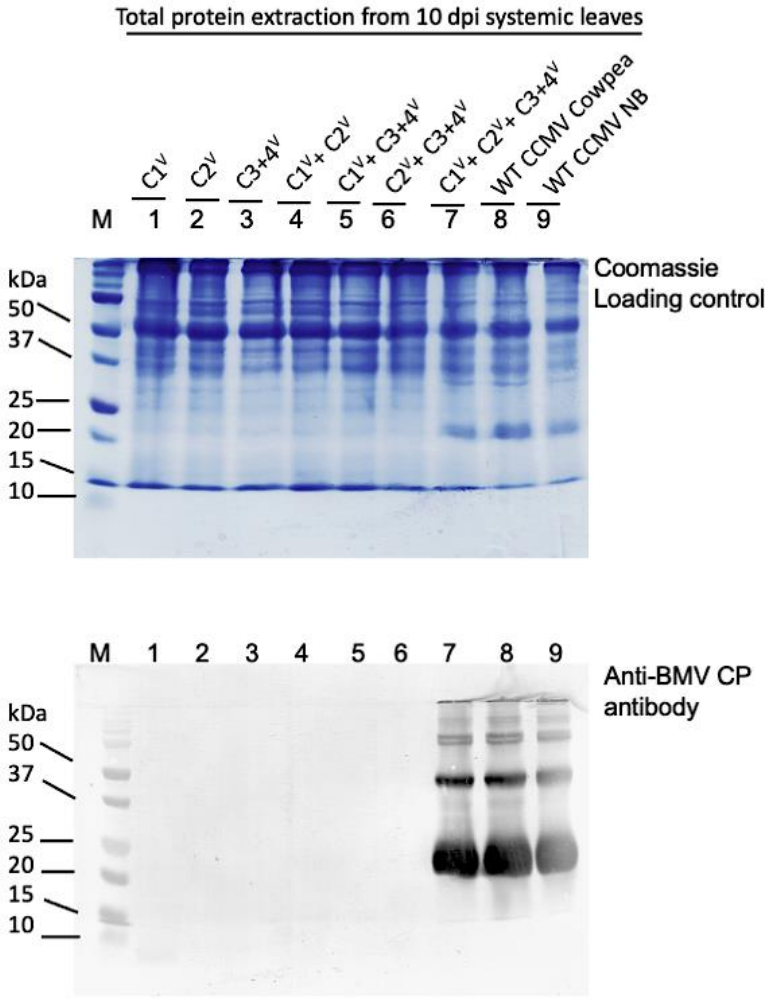

Figure 2.6 Genome content and infectivity of C1^{V}, C2^{V}, and C3+4^{V}. (A) RT-PCR analysis. Agarose gel analysis of RT-PCR products amplified from virion RNA of WT CCMV (a), C1^{V} (b), C2^{V} (c), and C3+4^{V} (d) using a set of primers designed to specifically amplify the regions encompassing either C1a ORF, C2a ORF (top panel), 3a ORF, or CP ORF (bottom panel) as described in Materials and Methods. M, marker lane. (B) Infectivity assay. *N. benthamiana* leaves were mechanically inoculated with either WT CCMV or purified virions of C1^{V}, C2^{V}, and C3+4^{V} in the indicated combinations. 10 dpi systemic leaves were harvested. Systemic accumulation of WT CCMV was confirmed using Coomassie Brilliant Blue R-250 staining (top panel) in either WT CCMV inoculated plants or plants that received all three purified virions. Western blot analysis using the anti-CP antibody of total protein extracted from the same leaves is indicated in the bottom panel. The samples are loaded in the order as mentioned above in lanes 1-9.

C1^{V}, C2^{V,}, and C3+4^{V}

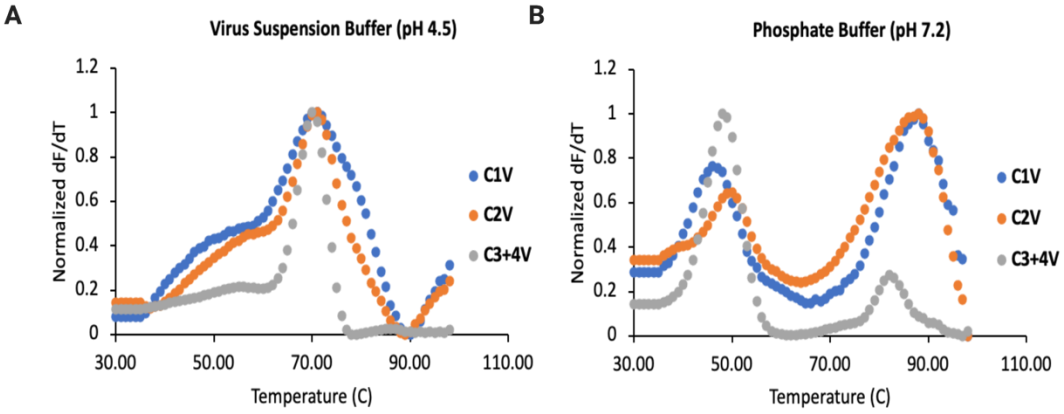

WT CCMV

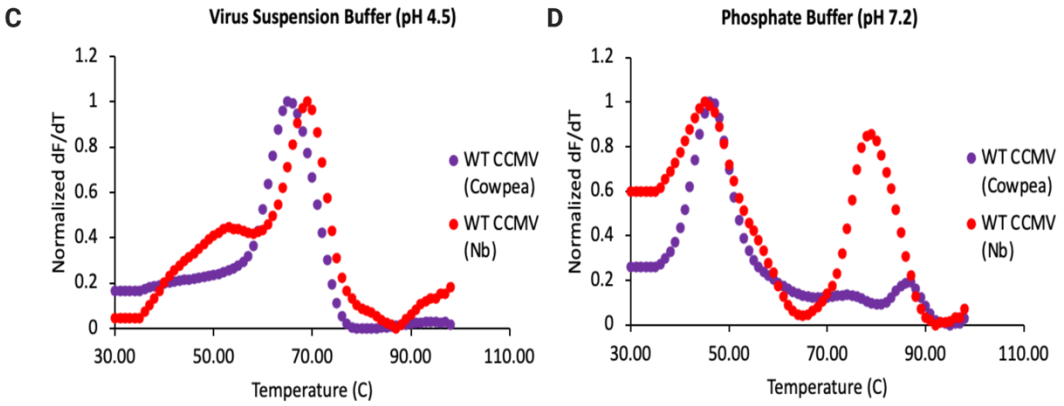

Lysozyme

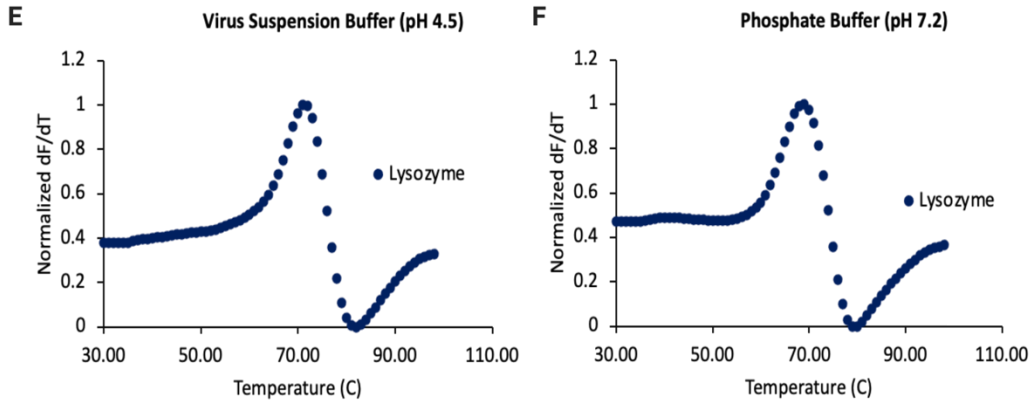

Figure 2.7 Stability analysis of the three CCMV virion types using differential scanning fluorimetry (DSF). DSF measurements of derivative of fluorescence intensity as a function of temperature for each virion type normalized so that the maximum of the derivative is set to 1 (y-axis) during heating of $C1^V$, $C2^V$, and $C3+4^V$ (A and B), WT CCMV purified from cowpea and *N. benthamiana* (control) (C and D), and lysozyme (control) (E and F) at various temperatures (x-axis) under indicated conditions. Although virions of WT CCMV and $C1^V$, $C2^V$, and $C3+4^V$ displayed identical temperature dependence (~70°C) for melting under buffer conditions of both pH 4.5 and pH 7.2, a portion of virions of $C1^V$, $C2^V$, and $C3+4^V$ melted at lower temperatures (see "Virion stability of $C1^V$, $C2^V$, and $C3+4^V$" for details) at pH 7.2. Lysozyme used as positive control showed identical melting characteristics (~60°C) under both pH conditions.

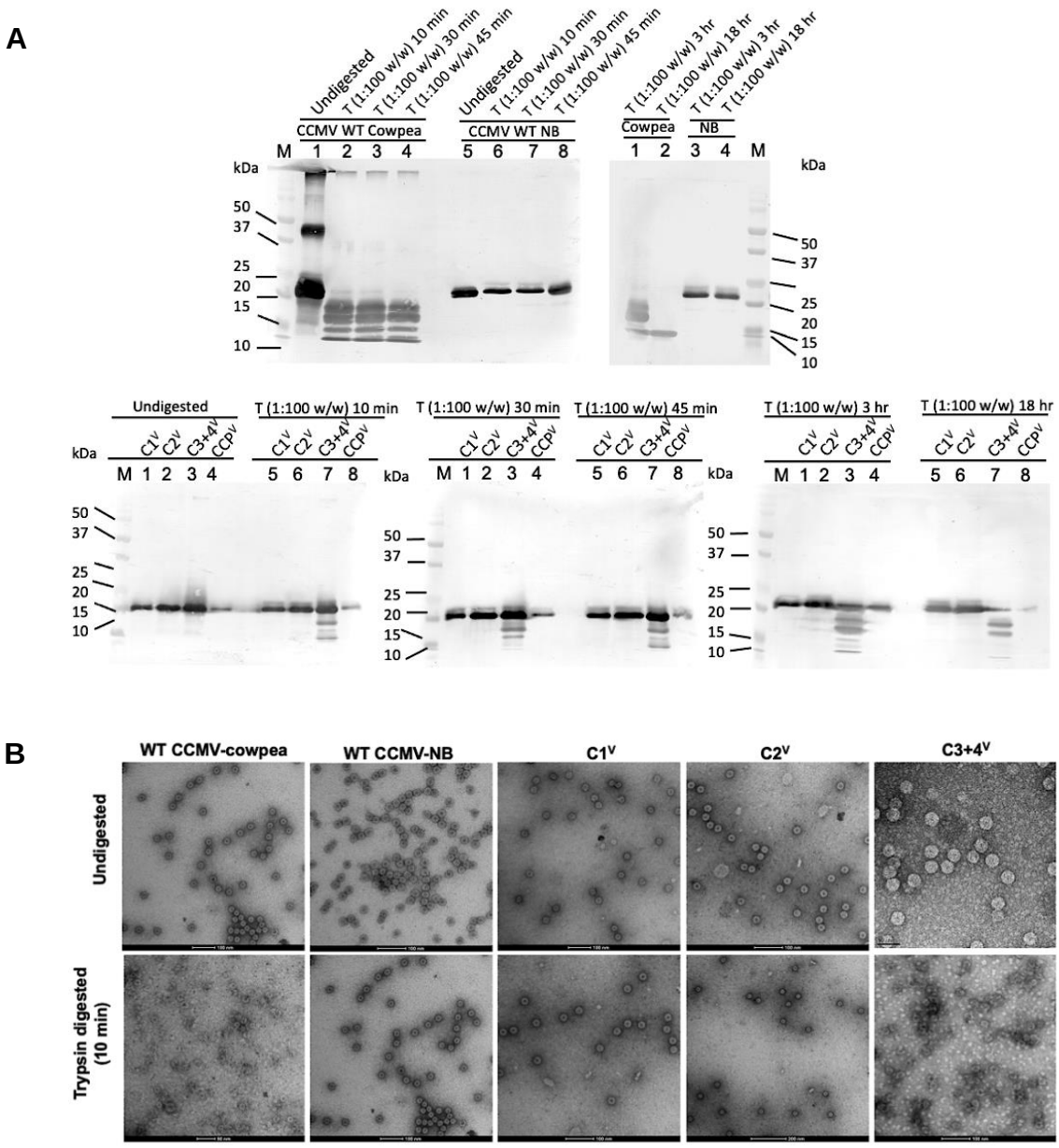

Figure 2.8 Proteolysis of WT CCMV-cowpea, WT CCMV-NB, $C1^V$, $C2^V$, $C3+4^V$, CCP^V monitored by Western blotting and negative-stain EM analysis. (A) Western blot for WT CCMV-cowpea, WT CCMV-NB, $C1^V$, $C2^V$, $C3+4^V$, CCP^V. Before Western blot analysis, each virion preparation was either undigested or digested with trypsin for 10 min, 30 min, 45 min, 3hr, or 18 hr. (B) Negative-stain electron micrographs show the integrity of the undigested and trypsin-digested virion preparations of the indicated samples.

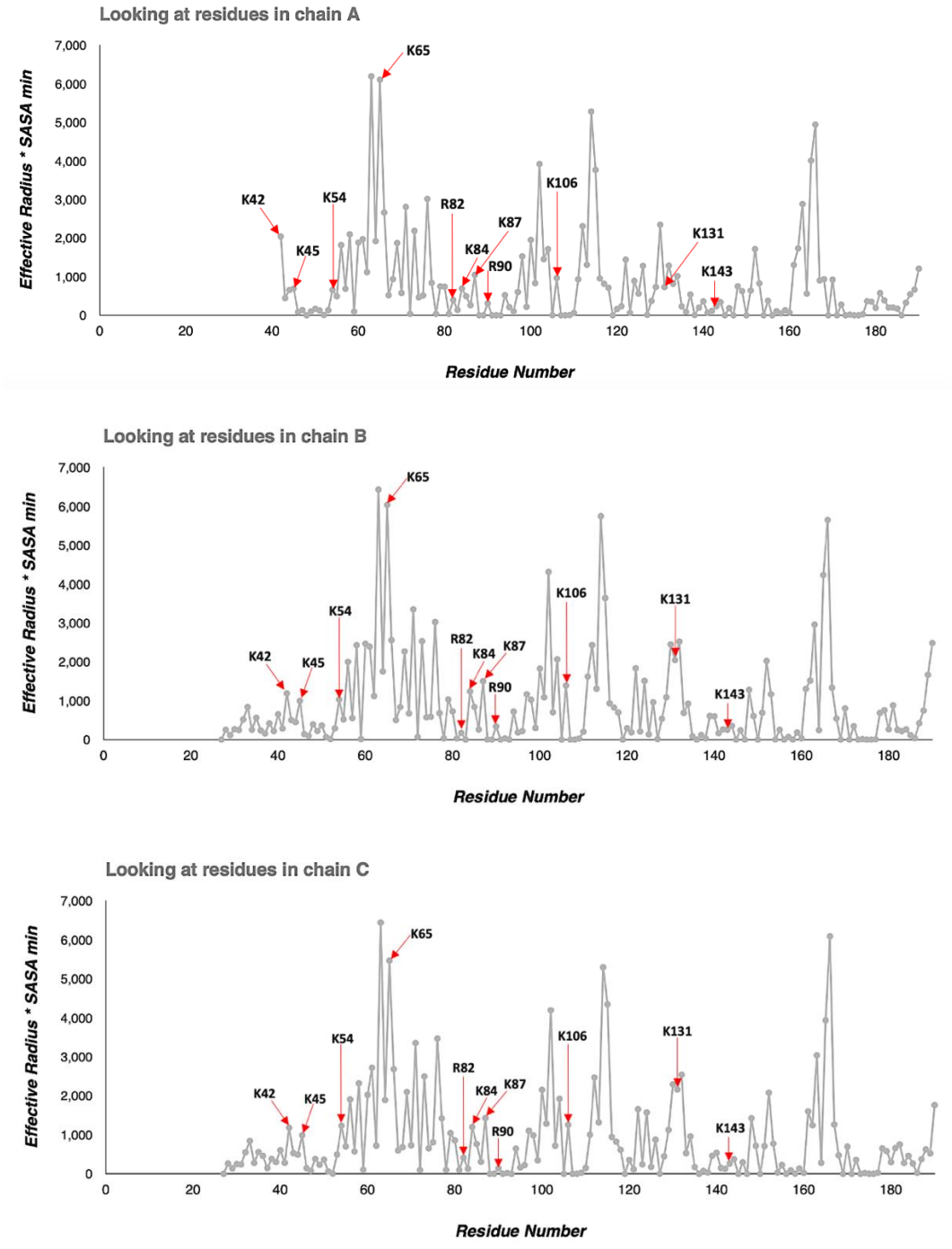

Figure 2.9 Location of the amino acid sites accessible for trypsin digestion on the A, B, and C subunits of the CCMV CP (http://viperdb.scripps.edu/).

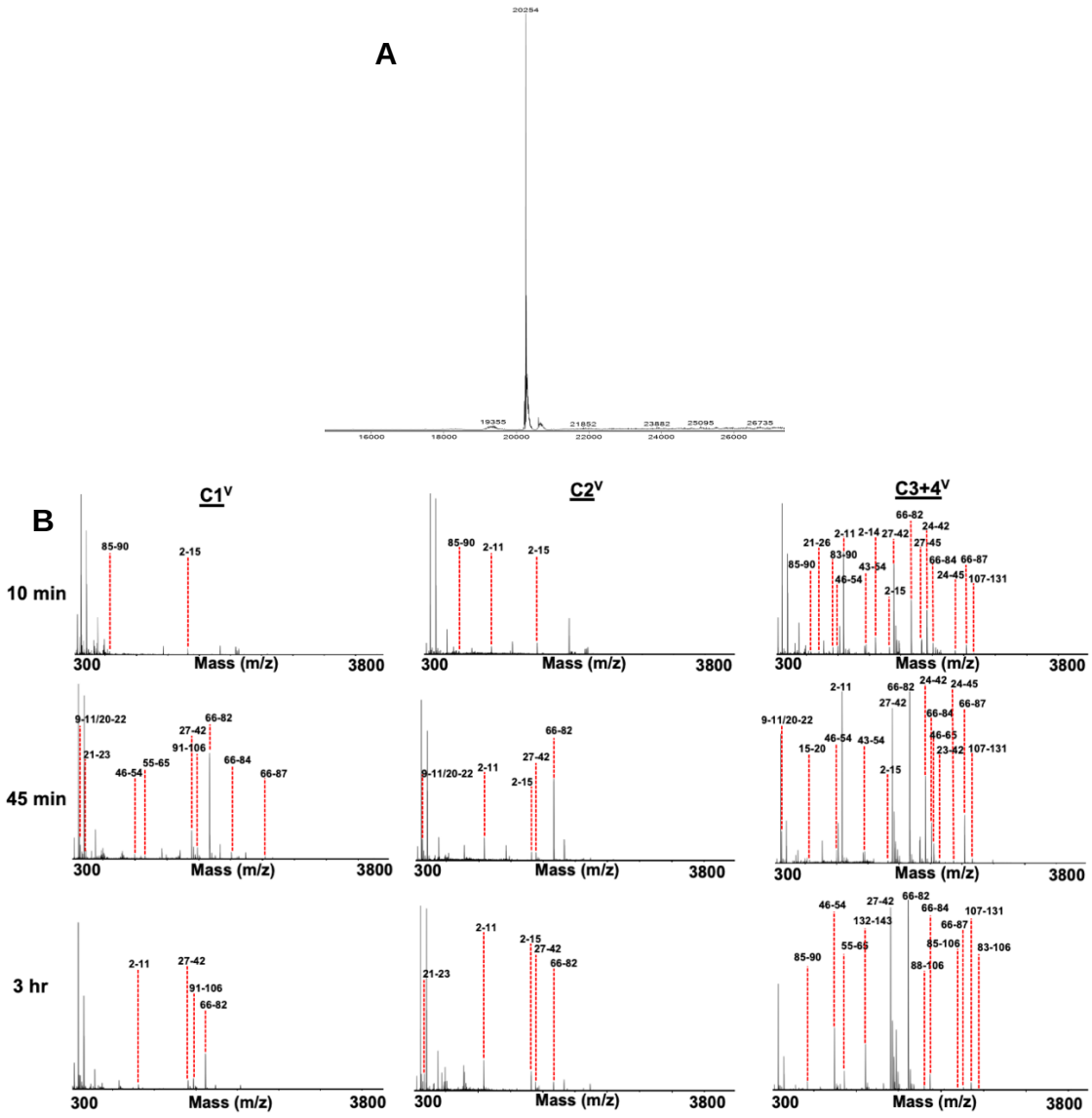

Figure 2.10 MALDI-TOF analysis of undigested and trypsin-digested virions. (A) Mass spectrometry of undigested virions of WT-CCMV-CP, WT-CCMV-NB, $C1^V$, $C2^V$, $C3+4^V$, and CCP^V yielded a single peak with a value of 20,254 Da. (B) MALDI-TOF analysis of peptides released from $C1^V$, $C2^V$, and $C3+4^V$ following digestion with trypsin at the indicated time points. Peaks are labeled with corresponding polypeptide fragments of predicted amino acid residues. Table 2.1 summarizes masses and identifies the corresponding amino acid residues.

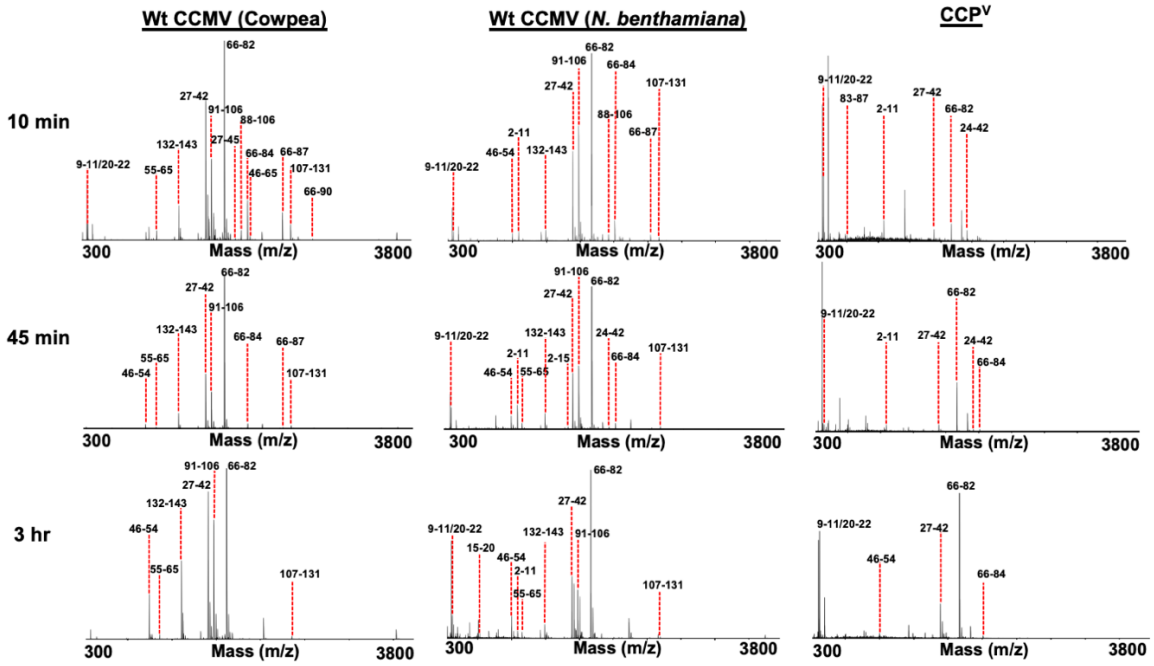

Figure 2.11 MALDI-TOF analysis of peptides released from WT-CCMV-CP, WT-CCMV-NB, and CCP^{V} following trypsin digestion at the indicated time points. Peaks are labeled with corresponding polypeptide fragments of predicted amino acid residues. Table 2.1 summarizes masses and identifies the corresponding amino acid residues.

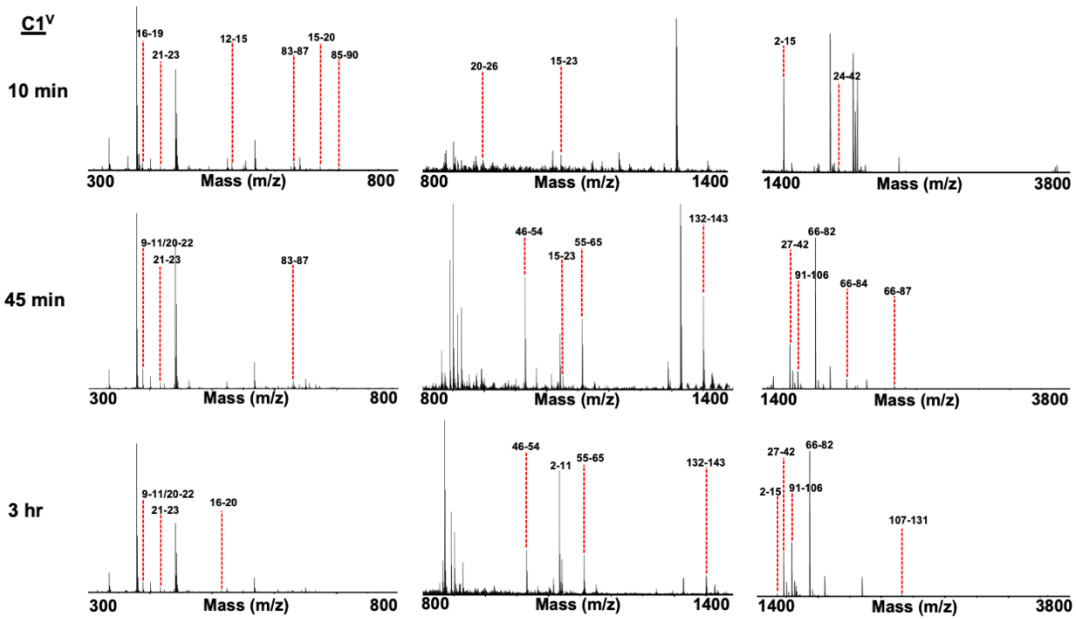

Figure 2.12 MALDI-TOF analysis of peptides released from $C1^V$ following trypsin digestion at the indicated time points. Peaks are labeled with corresponding polypeptide fragments of predicted amino acid residues. Table 2.1 summarizes masses and identifies the corresponding amino acid residues.

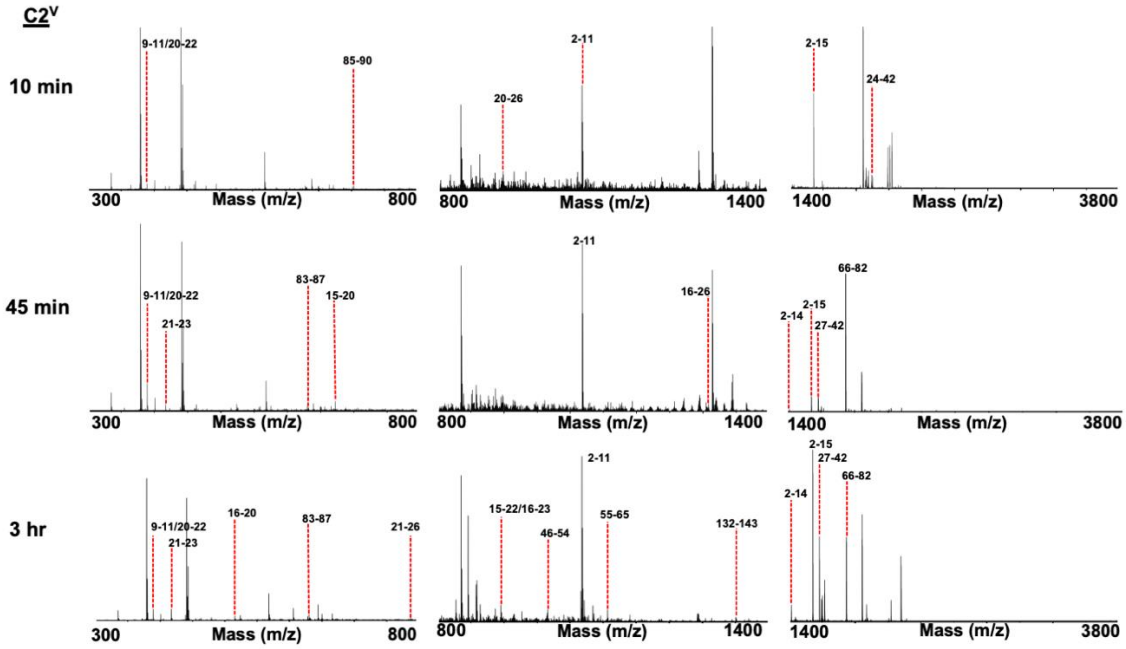

Figure 2.13 MALDI-TOF analysis of peptides released from $C2^V$ following trypsin digestion at the indicated time points. Peaks are labeled with corresponding polypeptide fragments of predicted amino acid residues. Table 2.1 summarizes masses and identifies the corresponding amino acid residues.

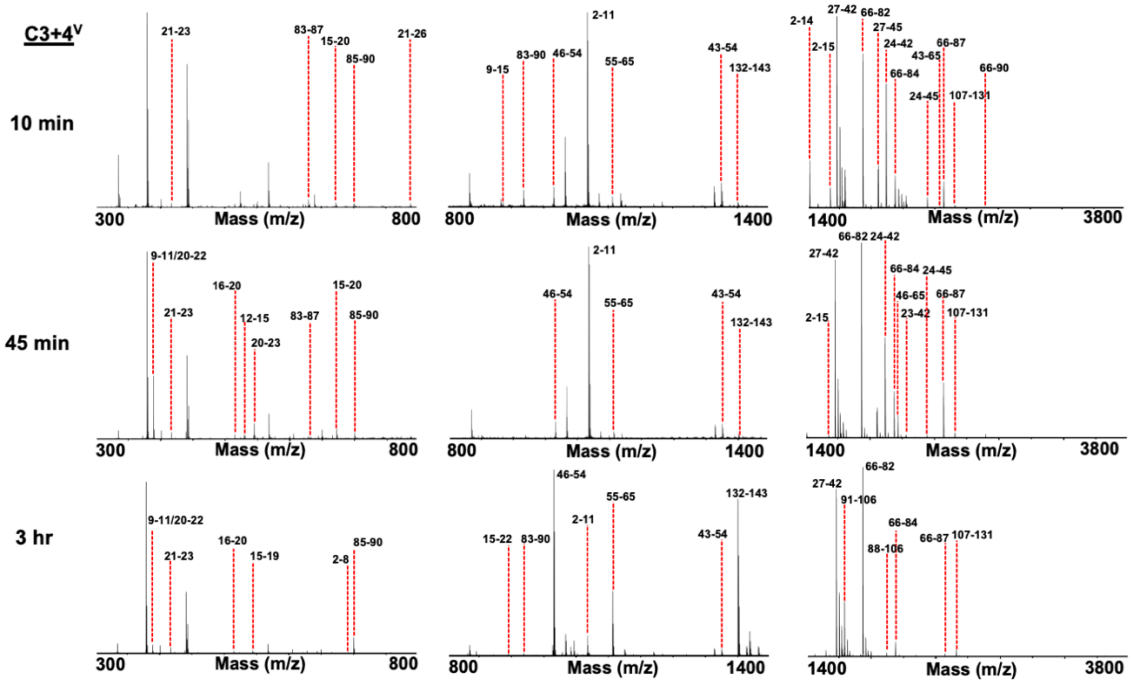

Figure 2.14 MALDI-TOF analysis of peptides released from C3+4^{V} following trypsin digestion at the indicated time points. Peaks are labeled with corresponding polypeptide fragments of predicted amino acid residues. Table 2.1 summarizes masses and identifies the corresponding amino acid residues.

Table 2.1 Kinetics of trypsin cleavage sites located on $C1^V$, $C2^V$, and $C3+4^V$

			Time to cleavage									
			$C1^V$			$C2^V$			$C3+4^V$			
Residues	Sequence	m/z	10 min	45 min	3 hr	10 min	45 min	3 hr	10 min	45 min	3 hr	
2-11	STVGTGKLTR	1061.5949	-	-	+	+	+	+	+	+	+	
2-14	STVGTGKLTRAQR	1416.7918	-	-	-	-	+	+	+	-	-	
2-15	STVGTGKLTRAQRR	1572.8929	+	-	-	+	+	+	+	+	-	
9-15	LTRAQRR	900.5486	-	-	-	-	-	-	+	-	-	
15-20	RAAARK	672.4264	+	-	-	-	+	-	+	+	-	
15-23	RAAARKNKR	1070.6654	+	+	+	-	-	-	-	-	-	
21-23	NKR	417.2568	+	+	+	-	+	+	+	+	+	
21-26	NKRNTR	788.4486	-	-	-	-	-	+	+	-	-	
24-42	NTRVVQPVIVEPIASGQGK	1992.1237	+	-	-	+	-	-	+	+	-	
24-45	NTRVVQPVIVEPIASGQGKAIK	2304.3398	-	-	-	-	-	-	+	+	-	
27-42	VVQPVIVEPIASGQGK	1620.9319	-	+	+	-	+	+	+	+	+	
27-45	VVQPVIVEPIASGQGKAIK	1933.1481	-	-	-	-	-	-	+	-	-	
43-54	AIKAWTGYSVSK	1310.7103	-	-	-	-	-	-	+	+	+	
43-65	AIKAWTGYSVSKWTASCAAAEAK	2400.2016	-	-	-	-	-	-	+	-	-	
46-54	AWTGYSVSK	998.4942	-	+	+	-	-	+	+	+	+	
55-65	WTASCAAAEAK	1108.5092	-	+	+	-	-	+	+	+	+	
66-82	VTSAITISLPNELSSER	1816.9651	-	+	+	-	+	+	+	+	+	
66-84	VTSAITISLPNELSSERNK	2059.1030	-	+	+	-	-	-	+	+	+	
66-87	VTSAITISLPNELSSERNKQLK	2428.3406	-	+	+	-	-	-	+	+	+	
66-90	VTSAITISLPNELSSERNKQLKVGR	2740.5316	-	-	-	-	-	-	+	-	-	
83-87	NKQLK	630.3933	+	+	-	-	+	+	+	+	-	
83-90	NKQLKVGR	942.5843	-	-	-	-	-	-	+	-	+	
85-90	QLKVGR	700.4464	+	-	-	+	-	-	+	+	+	
88-106	VGRVLLWLGLLPSVSGTVK	1994.2161	-	-	-	-	-	-	-	-	+	
91-106	VLLWLGLLPSVSGTVK	1682.0251	-	+	+	-	-	-	-	-	+	
107-131	SCVTETQTTAAASFQVALAVADNSK	2513.2188	-	-	+	-	-	-	+	+	+	
132-143	DVVAAMYPEAFK	1340.6555	-	+	+	-	-	+	+	+	+	

Table 2.1 Kinetics of trypsin cleavage sites located on $C1^V$, $C2^V$, and $C3+4^V$. The fragments released during early time points by $C1^V$, $C2^V$ are highlighted in yellow, and those released by $C3+4^V$ are highlighted in blue.

REFERENCES

Adolph, D. W., & Butler, P. J. (1977). Studies on the assembly of a spherical plant virus. III. Reassembly of infectious virus under mold conditions. *J Mol Biol, 109*(2), 345-357. doi:10.1016/s0022-2836(77)80038-7

Adolph, K. W., & Butler, P. J. (1974). Studies on the assembly of a spherical plant virus. I. States of aggregation of the isolated protein. *J Mol Biol, 88*(2), 327-341. doi:10.1016/0022-2836(74)90485-9

Annamalai, P., Apte, S., Wilkens, S., & Rao, A. L. (2005). Deletion of highly conserved arginine-rich RNA binding motif in cowpea chlorotic mottle virus capsid protein results in virion structural alterations and RNA packaging constraints. *J Virol, 79*(6), 3277-3288. doi:10.1128/JVI.79.6.3277-3288.2005

Annamalai, P., & Rao, A. L. (2005a). Dispensability of 3' tRNA-like sequence for packaging cowpea chlorotic mottle virus genomic RNAs. *Virology, 332*(2), 650-658. doi:10.1016/j.virol.2004.12.009

Annamalai, P., & Rao, A. L. (2005b). Replication-independent expression of genome components and capsid protein of brome mosaic virus in planta: a functional role for viral replicase in RNA packaging. *Virology, 338*(1), 96-111. doi:10.1016/j.virol.2005.05.013

Annamalai, P., & Rao, A. L. (2006). Packaging of brome mosaic virus subgenomic RNA is functionally coupled to replication-dependent transcription and translation of coat protein. *J Virol, 80*(20), 10096-10108. doi:10.1128/JVI.01186-06

Annamalai, P., & Rao, A. L. N. (2006). Delivery and expression of functional viral RNA genomes in planta by agroinfiltration. *Curr Protoc Microbiol, Chapter 16*, 16B.12.11-16B.12.15. doi:10.1002/9780471729259.mc16b02s01

Annamalai, P., Rofail, F., Demason, D. A., & Rao, A. L. (2008). Replication-coupled packaging mechanism in positive-strand RNA viruses: synchronized coexpression of functional multigenome RNA components of an animal and a plant virus in Nicotiana benthamiana cells by agroinfiltration. *J Virol, 82*(3), 1484-1495. doi:10.1128/JVI.01540-07

Bancroft, J. B., & Hiebert, E. (1967). Formation of an infectious nucleoprotein from protein and nucleic acid isolated from a small spherical virus. *Virology, 32*(2), 354-356. doi:10.1016/0042-6822(67)90284-x

Bancroft, J. B., Hills, G. J., & Markham, R. (1967). A study of the self-assembly process in a small spherical virus. Formation of organized structures from protein subunits in vitro. *Virology, 31*(2), 354-379. doi:10.1016/0042-6822(67)90180-8

Bothner, B., Dong, X. F., Bibbs, L., Johnson, J. E., & Siuzdak, G. (1998). Evidence of viral capsid dynamics using limited proteolysis and mass spectrometry. *J Biol Chem, 273*(2), 673-676. doi:10.1074/jbc.273.2.673

Bothner, B., Schneemann, A., Marshall, D., Reddy, V., Johnson, J. E., & Siuzdak, G. (1999). Crystallographically identical virus capsids display different properties in solution. *Nat Struct Biol, 6*(2), 114-116. doi:10.1038/5799

Calhoun, S. L., & Rao, A. L. (2008). Functional analysis of brome mosaic virus coat protein RNA-interacting domains. *Arch Virol, 153*(2), 231-245. doi:10.1007/s00705-007-1085-z

Calhoun, S. L., Speir, J. A., & Rao, A. L. (2007). In vivo particle polymorphism results from deletion of a N-terminal peptide molecular switch in brome mosaic virus capsid protein. *Virology, 364*(2), 407-421. doi:10.1016/j.virol.2007.03.034

Carrillo-Tripp, M., Shepherd, C. M., Borelli, I. A., Venkataraman, S., Lander, G., Natarajan, P., . . . Reddy, V. S. (2009). VIPERdb2: an enhanced and web API enabled relational database for structural virology. *Nucleic Acids Res, 37*(Database issue), D436-442. doi:10.1093/nar/gkn840

Chakravarty, A., & Rao, A. L. (2021). The interplay between capsid dynamics and pathogenesis in tripartite bromoviruses. *Curr Opin Virol, 47*, 45-51. doi:10.1016/j.coviro.2020.12.005

Chakravarty, A., Reddy, V. S., & Rao, A. L. N. (2020). Unravelling the Stability and Capsid Dynamics of the Three Virions of Brome Mosaic Virus Assembled Autonomously. *J Virol, 94*(8). doi:10.1128/JVI.01794-19

Chaturvedi, S., & Rao, A. L. N. (2014). Live cell imaging of interactions between replicase and capsid protein of Brome mosaic virus using Bimolecular Fluorescence Complementation: implications for replication and genome packaging. *Virology, 464-465*, 67-75. doi:10.1016/j.virol.2014.06.030

Culver, J. N., Brown, A. D., Zang, F., Gnerlich, M., Gerasopoulos, K., & Ghodssi, R. (2015). Plant virus directed fabrication of nanoscale materials and devices. *Virology, 479-480*, 200-212. doi:10.1016/j.virol.2015.03.008

Dasgupta, R., & Kaesberg, P. (1982). Complete nucleotide sequences of the coat protein messenger RNAs of brome mosaic virus and cowpea chlorotic mottle virus. *Nucleic Acids Res, 10*(2), 703-713. doi:10.1093/nar/10.2.703

Doerschuk, P. C., Gong, Y., Xu, N., Domitrovic, T., & Johnson, J. E. (2016). Virus particle dynamics derived from CryoEM studies. *Curr Opin Virol, 18*, 57-63. doi:10.1016/j.coviro.2016.02.011

Fox, J. M., Zhao, X., Speir, J. A., & Young, M. J. (1996). Analysis of a salt stable mutant of cowpea chlorotic mottle virus. *Virology, 222*(1), 115-122. doi:10.1006/viro.1996.0402

Kao, C. C., Ni, P., Hema, M., Huang, X., & Dragnea, B. (2011). The coat protein leads the way: an update on basic and applied studies with the Brome mosaic virus coat protein. *Mol Plant Pathol, 12*(4), 403-412. doi:10.1111/j.1364-3703.2010.00678.x

Lane, L. C. (1974). The bromoviruses. *Adv Virus Res, 19*, 151-220. doi:10.1016/s0065-3527(08)60660-0

Mateu, M. G. (2013). Assembly, stability and dynamics of virus capsids. *Arch Biochem Biophys, 531*(1-2), 65-79. doi:10.1016/j.abb.2012.10.015

Ni, P., Vaughan, R. C., Tragesser, B., Hoover, H., & Kao, C. C. (2014). The plant host can affect the encapsidation of brome mosaic virus (BMV) RNA: BMV virions are surprisingly heterogeneous. *J Mol Biol, 426*(5), 1061-1076. doi:10.1016/j.jmb.2013.09.007

Okinaka, Y., Mise, K., Suzuki, E., Okuno, T., & Furusawa, I. (2001). The C terminus of brome mosaic virus coat protein controls viral cell-to-cell and long-distance movement. *J Virol, 75*(11), 5385-5390. doi:10.1128/JVI.75.11.5385-5390.2001

Osman, F., Grantham, G. L., & Rao, A. L. (1997). Molecular studies on bromovirus capsid protein. IV. Coat protein exchanges between brome mosaic and cowpea chlorotic mottle viruses exhibit neutral effects in heterologous hosts. *Virology, 238*(2), 452-459. doi:10.1006/viro.1997.8849

Rao, A. L. (1997). Molecular studies on bromovirus capsid protein. III. Analysis of cell-to-cell movement competence of coat protein defective variants of

cowpea chlorotic mottle virus. *Virology, 232*(2), 385-395. doi:10.1006/viro.1997.8579

Rayaprolu, V., Kruse, S., Kant, R., Movahed, N., Brooke, D., & Bothner, B. (2014). Fluorometric Estimation of Viral Thermal Stability. *Bio Protoc, 4*(15). doi:10.21769/bioprotoc.1199

Schneider, C. A., Rasband, W. S., & Eliceiri, K. W. (2012). NIH Image to ImageJ: 25 years of image analysis. *Nat Methods, 9*(7), 671-675. doi:10.1038/nmeth.2089

Speir, J. A., Bothner, B., Qu, C., Willits, D. A., Young, M. J., & Johnson, J. E. (2006). Enhanced local symmetry interactions globally stabilize a mutant virus capsid that maintains infectivity and capsid dynamics. *J Virol, 80*(7), 3582-3591. doi:10.1128/JVI.80.7.3582-3591.2006

Speir, J. A., Munshi, S., Baker, T. S., & Johnson, J. E. (1993). Preliminary X-ray data analysis of crystalline cowpea chlorotic mottle virus. *Virology, 193*(1), 234-241. doi:10.1006/viro.1993.1119

Speir, J. A., Munshi, S., Wang, G., Baker, T. S., & Johnson, J. E. (1995). Structures of the native and swollen forms of cowpea chlorotic mottle virus determined by X-ray crystallography and cryo-electron microscopy. *Structure, 3*(1), 63-78. doi:10.1016/s0969-2126(01)00135-6

Verduin, B. J. M. (1978). Reversible Change in the Nucleoprotein Composition of Bromoviruses after Multiplication in Chenopodium hybridum L. *Journal of General Virology, 38*(3), 571-575. doi:https://doi.org/10.1099/0022-1317-38-3-571

Weber, P. H., & Bujarski, J. J. (2015). Multiple functions of capsid proteins in (+) stranded RNA viruses during plant-virus interactions. *Virus Res, 196*, 140-149. doi:10.1016/j.virusres.2014.11.014

Zlotnick, A., Aldrich, R., Johnson, J. M., Ceres, P., & Young, M. J. (2000). Mechanism of capsid assembly for an icosahedral plant virus. *Virology, 277*(2), 450-456. doi:10.1006/viro.2000.0619

CHAPTER 3

Comparative Dynamics of BMV and CCMV Capsids Assembled in the Presence of Heterologous Replicase

ABSTRACT

In *Brome mosaic virus* (BMV) and *Cowpea chlorotic mottle virus* (CCMV), a heterologous combination of RNA1 and RNA2 encoding for viral replicase proteins 1a and 2a does not support viral RNA replication. However, exchanging heterologous RNA3 into either genome produced viable chimeric viruses. In BMV and other viruses, it has been conclusively shown that the interaction of replicase with capsid protein (CP) dictates packaging specificity. Therefore, to test our hypothesis that the replicase-CP interaction controls capsid dynamics, we assembled chimeric RNA3 and subgenomic RNA4 containing virions of BMV and CCMV in the presence of heterologous replicase. Our results demonstrated a significant difference in thermal stability and susceptibility to trypsin protease between BMV and CCMV RNA3+4 containing virions assembled with heterologous replicase compared with those assembled in the presence of homologous replicase. The virions assembled in the presence of heterologous replicase have higher thermal stability than their equivalents assembled in the presence of homologous replicase. Additionally, the heterologous combination of replicase and CP resulted in virions that are highly resistant to trypsin and release fewer species of peptides upon digestion with trypsin than those assembled with homologous replicase. This observation highlights a potentially different arrangement of amino acids exposed on the capsid exterior in virions assembled with heterologous replicase influencing the capsid dynamics in these virions.

INTRODUCTION

Viral genomes undergo evolutionary events like recombination and reassortment to obtain genetic materials that are not native. When segmented viruses (same or closely related) exchange one or more complete genome segments, the process is called reassortment. Several cases of reassortment have been observed in the member viruses of the family *Bromoviridae*. All three genomic RNAs are interchangeable amongst different *Cucumber mosaic virus* (CMV) strains (Jacquemond, 2012). However, several studies investigating interspecies reassortment found that only RNA3 but neither RNA1 nor RNA2 are replaceable within bromoviruses and cucumoviruses. (Allison, Janda, & Ahlquist, 1988; Rao & Francki, 1981; Suzuki, Yoshida, Yoshinuma, & Hibi, 2003). In *Brome mosaic virus* (BMV) and *Cowpea chlorotic mottle virus* (CCMV), viral RNA replication was not detected in barley protoplast with heterologous RNA1 and RNA2 encoding trans-acting viral replicase proteins 1a and 2a. However, the substitution of the heterologous RNA3 into either genome produced viable chimera viruses. Interestingly, the hybrid viruses failed to cause infection in the natural hosts of BMV and CCMV, barley and California blackeye respectively (Dinant, Janda, Kroner, & Ahlquist, 1993). Another study demonstrated that the combination of *Peanut stunt virus* (PSV) RNA1 and CMV RNA2, both cucumoviruses, resulted in the physical interaction between two heterologous replicases and replication of three genomic RNAs. However, this interaction was not sufficient to synthesize subgenomic RNA4 (Suzuki et al., 2003).

In the absence of replication, packaging in BMV was nonspecific since transiently expressed CP subunits efficiently packaged ubiquitous cellular RNA (P. Annamalai & A. L. Rao, 2006). It has also been conclusively shown that the physical interaction between replicase with capsid protein (CP), more specifically replicase protein 2a, dictates RNA packaging specificity in BMV (Chaturvedi & Rao, 2014). Previous studies have also demonstrated that differential RNA content regulates the stability of CP subunits and ultimately capsid dynamics in otherwise morphologically indistinguishable virions (Bothner et al., 1999). Additionally, recent studies in our lab showed that each virion types in BMV containing either genomic RNA1 ($B1^V$), genomic RNA1 ($B2^V$), or genomic RNA3 and subgenomic RNA4 ($B3+4^V$) have differential capsid dynamics that may have important biological implications in the viral replication cycle.

Based on these collective pieces of evidence, we hypothesized that the replicase-CP interaction might have a regulatory role in controlling capsid dynamics in bromoviruses, and chimeric virions assembled in the presence of heterologous replicase may have different capsid dynamics and stability as compared to those assembled in the presence of homologous replicase. A previous agroinfiltration-based study had assembled individual RNA3+4 containing virions of BMV in *Nicotiana benthamiana* plants (Chakravarty, Reddy, & Rao, 2020). Since it is not plausible to assemble pure RNA1 and RNA2 containing virions in the presence of heterologous replicase as BMV 1a and CCMV 2a are not compatible and vice versa, this study used an agroinfiltration-based

method to assemble chimeric RNA3+4 containing virions of BMV and CCMV exploiting the inherent compatibility of replicase and capsid proteins. Since the BMV and CCMV CPs show strong homology (~70%) at the amino acid level, the contribution of otherwise conserved amino-acid sequences to capsid dynamics can be explored using the following set of experiments (Fig. 3.1).

i) To assemble virions co-packaging CCMV RNA 3+4 in the presence of heterologous BMV replicase, we will infiltrate plants with agroconstructs of replicase protein 1a ORF (p1a) and 2a ORF (p2a) of BMV and full-length construct of CCMV RNA3 (C3). This inoculum will result in the synthesis of CCMV RNA3 and its sgRNA4 followed by the translation of CCMV CP and assembly of virions co- packaging CCMV RNA3 and sgRNA 4 in the presence of BMV replicase.

ii) To assemble virions co-packaging BMV RNA3+4 in the presence of heterologous CCMV replicase, we infiltrated plants with agroconstructs of replicase protein 1a ORF (C1a) and 2a ORF of CCMV (C2a) and full-length construct of BMV RNA3 (B3). This inoculum will produce BMV RNA3 and its sgRNA4, followed by the translation of BMV CP and the assembly of virions co-packaging BMV RNA3 and sgRNA4 in the presence of CCMV replicase.

iii) Plants infiltrated with a mixture of agroconstructs to assemble RNA3+4 containing virions in the presence of the homologous replicase protein would serve as controls (p1a+ p2a+ B3 and C1a+ C2a+ C3).

iv) Plants infiltrated with a mixture of agroconstructs to assemble all three genomic RNA containing virions of either BMV (B1, B2, B3) or CCMV (C1, C2, C3) in the presence of homologous (B1+ B2+ B3 and C1+ C2+ C3) or heterologous replicase (C1+ C2+ B3 and B1+ B2+ C3) will serve as controls, to elucidate how the presence of full-length RNAs encoding heterologous replicase influence the overall dynamic nature of virions.

We characterized the physical morphology and the electrophoretic mobility profile of the assembled virions using negative-stain electron microscopy (EM) and agarose gel electrophoresis. The BMV and CCMV RNA3+4 containing virions assembled with the heterologous replicase-CP interaction are morphologically identical and showed identical electrophoretic mobility with the wild type (WT) BMV and CCMV, respectively. However, this study showed a significant difference in thermal stability between RNA3+4 containing virions of BMV and CCMV assembled with either homologous or heterologous replicase. The virions assembled using heterologous replicase demonstrate higher thermal stability than those with similar RNA content but assembled with homologous replicase.

Interestingly, the virions assembled due to heterologous replicase-CP interaction are dynamically distinct from their counterparts assembled with homologous replicase. The former group of virions retained their capsid structural integrity upon trypsin digestion compared with the latter, suggesting a different arrangement of exposed surface residues when examined using proteolysis

followed by matrix-assisted laser desorption ionization-time flight (MALDI-TOF) mass spectrometry. Taking these pieces of evidence together, our results indicate that the specificity of replicase-CP interaction may have a significant implication in the dynamics of *Bromovirus* capsids.

RESULTS

Throughout this study, B1+ B2+ B3 represents WT BMV virions containing a mixture of $B1^V$, $B2^V$, and $B3+4^V$, C1+ C2+ B3 represents virions assembled with full-length CCMV RNA1 and 2 expressed in the presence of BMV RNA3, resulting in all three RNAs being replicated and packaged in BMV CP. The p1a+ p2a+ B3 represents BMV RNA3+4 containing virions assembled in the presence of homologous BMV 1a/2a replicase. The C1a+ C2a+ B3 represents BMV RNA3+4 containing virions assembled in the presence of heterologous CCMV 1a/2a replicase.

Likewise, C1+ C2+ C3 represents WT CCMV virions containing a mixture of $C1^V$, $C2^V$, and $C3+4^V$, B1+ B2+ C3 represents virions assembled with full-length BMV RNA1 and 2 expressed in the presence of CCMV RNA3, resulting in all three RNAs being replicated and packaged in CCMV CP. The C1a+ C2a+ C3 represents CCMV RNA3+4 containing virions assembled in the presence of homologous CCMV replicase. The p1a+ p2a+ C3 represents CCMV RNA3+4 containing virions assembled in the presence of BMV 1a/2a replicase. All the virion preparations, as mentioned earlier, are assembled in *N. benthamiana* plants.

Strategy for in vivo assembly of three independent virion types of CCMV

Figure 3.1A summarizes the characteristic features of transfer DNA (T-DNA)-based vectors designed to express the three biologically active genomic

RNAs (gRNAs) of BMV (pB1, pB2, pB3) or CCMV (pC1, pC2, and pC3) when transiently expressed in *N. benthamiana* plants. Likewise, T-DNA constructs shown in Fig. 3.1A are designed to transiently express BMV replicase proteins 1a (p1a), 2a (p2a), and CP (pBCP) and CCMV replicase proteins 1a (C1a), 2a (C2a), and CP (pCCP). A strategy for the separate assembly of chimeric RNA3+4 containing virions and appropriate controls is shown schematically in Fig. 3.1B-F. (i) Agrotransformants of all three plasmids expressing full-length RNA of BMV or CCMV (Fig. 3.1B) infiltrated into plants served as controls. (ii) The combination of agrotransformants indicated in Fig. 3.1C and Fig. 3.1D infiltrated into plants assembled into individual virion types in BMV and CCMV. The resultant virions indicated in Fig. 3.1C and Fig. 3.1D have qualitatively different capsid dynamics (Chakravarty et al., 2020). (iii) The combination of agrotransformants indicated in Fig. 3.1E infiltrated into plants assembled into either BMV RNA1, BMV RNA2, and CCMV RNA3+4 containing virions encapsidated in CCMV CP or CCMV RNA1, CCMV RNA2, and BMV RNA3+4 containing virions encapsidated in BMV CP. (iv) An inoculum was formulated to assemble CCMV RNA3+4 containing virions in the presence of heterologous BMV replicase by mixing agrotransformants p1a, p2a, and pC3 (Fig. 3.1F). The following infiltration into *N. benthamiana* leaves, p1a would synthesize an mRNA competent to translate BMV replicase 1a. Agrotransformant p2a would produce an mRNA competent to translate BMV replicase 2a, but both RNAs would not be replicated since they lack 5' and 3' noncoding regions (Fig. 3.1A). Assembly of a BMV functional replicase would

result in the replication of C3 followed by the synthesis of sgC4 for CP production, resulting in the assembly of CCMV RNA3+4 containing virions in the presence of BMV replicase. (v) Another inoculum was formulated to assemble BMV RNA3+4 containing virions in the presence of heterologous CCMV replicase by mixing agrotransformants C1a, C2a, and pB3 (Fig. 3.1F). The following infiltration into *N. benthamiana* leaves, C1a would synthesize an mRNA competent to translate CCMV replicase 1a. Agrotransformant C2a would produce an mRNA competent to translate CCMV replicase 2a, but both RNAs would not be replicated since they lack 5' and 3' noncoding regions (Fig. 3.1A). Assembly of a CCMV functional replicase would result in the replication of B3 followed by the synthesis of sgB4 for CP production, resulting in the assembly of BMV RNA3+4 containing virions in the presence of CCMV replicase.

Total protein was extracted from each of the plants infiltrated with the specified mixture of the inoculum (Fig. 3.2), and the presence of the BMV or CCMV CCMV CP was confirmed in each of the samples using Western blot.

Electrophoretic mobility analysis of BMV and CCMV capsids assembled in the presence of heterologous replicase

The analysis of 1% agarose gel electrophoretic mobility patterns of purified virions is ideal for identifying any changes in the surface charge (Calhoun & Rao, 2008; Calhoun, Speir, & Rao, 2007). Therefore, BMV and CCMV virions assembled in the presence of homologous and heterologous replicase, purified

from *N. benthamiana* leaves, were subjected to agarose gel electrophoresis along with WT virions of BMV and CCMV as controls. The capsid sizes of CCMV and BMV are essentially identical. However, the charge on the solvent-accessible residues of CCMV specified in VIPER (http://viperdb.scripps.edu/) is -1,209 compared to +1,020 for BMV. Consequently, CCMV and BMV migrate toward the positive and negative electrodes, respectively (Carrillo-Tripp et al., 2009). Results shown in Fig. 3.3A confirmed the relative electrophoretic mobilities of WT BMV (Fig. 3.3A, lane 1) and WT CCMV virions (Fig. 3.3A, lane 5). The indistinguishable electrophoretic mobility profiles of WT BMV (Fig. 3.3A, lane 1) and that of either BMV RNA3+4 containing virions, assembled with BMV 1a/2a replicase (p1a+p2a+B3; B3+4^{V}) (Fig. 3.3A, lane 3), or in the presence of full-length RNAs encoding heterologous CCMV 1a/2a replicase C1+C2+B3 (Fig. 3.3A, lane 6), or BMV RNA3+4 containing virions assembled in the presence of ORFs encoding CCMV 1a/2a replicase (C1a+C2a+B3) (Fig. 3.3A, lane 8) suggest that all of these virion types exhibit similar surface charges. The CCMV RNA3+4 containing virions assembled with either homologous replicase (C1a+C2a+C3; C3+4^{V}) (Fig. 3.3A, lane 7), or in the presence of full-length RNAs encoding BMV 1a/2a replicase B1+B2+C3 (Fig. 3.3A, lane 2), or CCMV RNA3+4 containing virions assembled the presence of ORFs encoding heterologous BMV 1a/2a replicase (p1a+p2a+C3) (Fig. 3.3A, lane 4) showed identical electrophoretic mobility with that of WT CCMV suggesting that all these virion types exhibit identical surface charges.

To confirm the genetic composition of BMV and CCMV virions assembled in the presence of native or heterologous replicase, virion RNA was isolated from each of the virion preparations and subjected to a reverse transcription-PCR (RT-PCR) assay using a set of primers designed to specifically amplify either BMV RNA3 or CCMV RNA3 (see Materials and Methods). RNA isolated from WT virions was used as a control. Results shown in Fig. 3.3B confirmed that BMV and CCMV assembled in the presence of either homologous or heterologous replicase encapsidated expected RNA progeny.

Comparative thermal stability of BMV and CCMV virions assembled in the presence of either homologous or heterologous replicase

To test the relative thermal stability of the virion types mentioned in Fig. 3.3, a differential scanning fluorimetry (DSF) assay was performed as described in Materials and Methods (Fig. 3.4). The hydrophobic dye SYPRO orange used in this assay binds to the hydrophobic regions of the unfolding viral CP during thermal denaturation. The fluorescence intensity increases following its binding to more accessible areas (Rayaprolu et al., 2014). The DSF analysis of the temperature-dependent melting of virions of BMV and CCMV virions assembled in the presence of homologous and heterologous replicase and control samples (WT BMV and WT CCMV) under two buffer and pH conditions are summarized in Fig. 3.4A-H. Thermal denaturation profiles of WT BMV (B1+ B2+ B3) (Fig. 3.4A) and B3+4^{V} (p1a+ p2a+ B3) (Fig. 3.4C) in virus suspension buffer (pH 4.5) are identical with a

melting peak at ~70°C. Similarly, WT CCMV (C1+ C2+ C3) (Fig. 3.4E) and C3+4^{V} (C1a+ C2a+ C3) (Fig. 3.4G) in virus suspension buffer (pH 4.5) showed near-identical thermal stability with a melting peak at ~70°C in addition to a shoulder peak at ~50°C in the case of WT CCMV. However, virions assembled in the presence of either full-length RNAs or ORFs encoding heterologous replicase showed aberrant thermal denaturation profiles in virus suspension buffer (pH 4.5). The thermal stability of B1+ B2+ B3 is similar to C1+ C2+ B3 (Fig. 3.4A). However, when compared the denaturation profile of C1+ C2+ C3 with B1+ B2+ C3, the latter showed at least three thermally unstable populations compared to WT CCMV (Fig. 3.4E).

As a combination of different RNA-containing virions makes it challenging to analyze the dynamics of each virion type correctly, we analyzed the denaturation profile of BMV RNA3+4 containing virions assembled in the presence of either homologous BMV 1a/2a replicase or heterologous CCMV 1a/2a replicase (Fig. 3.4C). The virions containing BMV RNA3+4 replicated by homologous replicase and encapsidated in BMV CP showed a melting peak at ~76°C, whereas the BMV RNA3+4 expressed in the presence of CCMV replicase ORF and replicated by the same showed a melting peak at ~80°C (Fig. 3.4C). In CCMV, the virions containing CCMV RNA3+4 replicated by homologous replicase and encapsidated in CCMV CP showed a melting peak at ~70°C. Although the CCMV RNA3+4 expressed in the presence of BMV replicase ORF and replicated by the same showed a similar melting peak at ~70°C, the peak was much broader and indicated towards the

presence of heterogeneous virion populations that are different in their thermal stability (Fig. 3.4G).

We parallelly analyzed the thermal stability of all virion types discussed above in phosphate buffer (pH 7.2) to investigate how heterologous replicase-CP interaction modulates capsid dynamics in an environment that closely mimics the pH of living cells. WT BMV (B1+ B2+ B3) (Fig. 3.4B) and B3+4^{V} (p1a+ p2a+ B3) (Fig. 3.4D) in phosphate buffer (pH 7.2) showed near-identical thermal stability. However, in the presence of full-length RNA of heterologous replicase (C1+ C2+ B3), virions showed two thermally unstable populations, one at ~50°C and the other one at ~80°C, as compared to predominantly one population in WT BMV (B1+ B2+ B3), melting at ~50°C (Fig. 3.4B). Similarly, in the presence of heterologous replicase encoding ORFs of CCMV, BMV RNA3+4 containing virions (C1a+ C2a+ B3) show two thermally unstable populations melting at ~60°C and ~88°C respectively, when compared to BMV RNA3+4 containing virions assembled in the presence of homologous replicase encoding mRNA (p1a+ p2a+ B3) melting entirely at ~50°C (Fig. 3.4D). In the case of WT CCMV (C1+ C2+ C3), virions melt at ~45°C and ~80°C as two thermally unstable populations (Fig. 3.4F). In B1+ B2+ C3, the peaks move to ~60°C and ~90°C, respectively (Fig. 3.4F). Finally, in the presence of heterologous replicase encoding ORFs of BMV, CCMV RNA3+4 containing virions (p1a+ p2a+ C3) denatured at a much higher temperature of ~85°C, whereas CCMV RNA3+4 containing virions assembled in the presence of homologous replicase encoding mRNA (C1a+ C2a+ C3) melted

entirely at ~50°C (Fig. 3.4H). As expected, the thermal stability of lysozyme remained indistinguishable under both buffer conditions (data not shown).

Comparative capsid dynamics in BMV and CCMV virions assembled in the presence of either homologous or heterologous replicase

The results from the previous sections of this chapter show that the BMV and CCMV virions assembled in the presence of either homologous or heterologous replicase are morphologically identical and share equivalent surface charge with WT BMV and CCMV. Therefore, we applied limited proteolysis with trypsin, followed by identifying the cleavage products of the capsid subunits by mass spectrometry to distinguish between these morphologically identical capsids (Bothner et al., 1999). Subsequently, MALDI-TOF analysis of proteolytic cleavage products would contribute to understanding the capsid dynamics (Speir et al., 2006).

First, the differential capsid dynamics were investigated by trypsin digestion performed for 10 min to verify whether the virions indicated in Fig 3.5A display any observable effect on the rate of digestion (see Materials and Methods). The exposed lysine and arginine residues on the capsid exterior will be the first residues accessible to the enzyme and among the first digestion products observed. A previous study on individual virion types of BMV showed that the earliest time points of trypsin digestion could accurately predict the exposed residues on the capsid surface as prolonged digestion causes multiple

simultaneous cleavages at other sites otherwise internalized gradually get exposed (Chakravarty et al., 2020). Therefore, we digested the BMV and CCMV virions assembled in the presence of either homologous or heterologous replicase for 10 min. Following trypsin digestion, each virion type preparation was divided in half. One-half was subjected to Western blot analysis using an anti-CP antibody to identify the cleavage peptides. In contrast, the second half was subjected to EM analysis to verify the integrity of virions. Results are summarized in Fig. 3.5A and B. The BMV CP linear sequence is 189-aa long and has 22 potential trypsin cleavage sites, whereas the CCMV CP linear sequence is 190-aa long and has 20 potential trypsin cleavage sites. Undigested CP of virions of control samples of WT BMV (B1+ B2+ B3) and B3+4^{V} (p1a+ p2a+ B3) (Fig. 3.5A, left blot, lanes 1 and 3), as well as those assembled with CCMV 1a/2a replicase, C1+ C2+ B3 and C1a+ C2a+ B3 (Fig. 3.5A, left blot, lanes 2 and 4), migrated as a single intact band with the expected molecular weight (~20 kDa). Similarly, Undigested CP of virions of control samples of WT CCMV (C1+ C2+ C3) and C3+4^{V} (C1a+ C2a+ C3) (Fig. 3.5A, left blot, lanes 5 and 7), as well as those assembled with BMV 1a/2a replicase, B1+ B2+ C3 and p1a+ p2a+ C3 (Fig. 3.5A, left blot, lanes 6 and 8), migrated as a single intact band with the expected molecular weight (~20 kDa). The single amino acid difference in the length of BMV and CCMV is evident, with BMV CP migrating slightly faster than CCMV CP.

Analysis of the trypsin cleavage products for each virus sample revealed that, as reported previously (Chakravarty et al., 2020), trypsin digested >50% of

the CP in WT BMV and B3+4^{V} (Fig. 3.5A, right blot, lanes 1 and 3), compared to undigested samples (Fig. 3.5A, left blot, lanes 1 and 3). As reported in chapter 2 of this thesis, trypsin digestion of WT CCMV assembled in *N. benthamiana* failed to yield any significant peptide fragments on the Western blot beyond a negligible amount of cleavage (Fig. 3.5A, right blot, lane 5). However, a large amount of C3+4^{V} CP gets digested after 10 min of trypsin treatment (Fig. 3.5A, right blot, lane 7). Interestingly, both BMV virion types, C1+ C2+ B3 and C1a+ C2a+ B3, assembled with heterologous CCMV replicase, remained highly resistant to trypsin digestion (Fig. 3.5A, right blot, lane 2 and 4). Similarly, both CCMV virion types, B1+ B2+ C3 and p1a+ p2a+ C3, assembled with heterologous BMV replicase, did not release detectable fragments upon trypsin digestion (Fig. 3.5A, right blot, lane 6 and 8). Electron microscopic analysis of trypsin-digested virion preparations (Fig. 3.5B) confirmed the Western blot data, showing that most virions of BMV and CCMV assembled with heterologous replicase remained structurally intact upon trypsin digestion. The B3+4^{V} virions were readily digested upon trypsin digestion as reported previously (Chakravarty et al., 2020), so did most of the C3+4^{V} virions (Fig. 3.5C).

Subsequently, MALDI-TOF was used to identify the cleavage products released due to trypsin digestion. The deconvoluted mass spectrum obtained from the total ion chromatogram (TIC) of each virion type indicated that all the virions are assembled from a single protein of 20 kDa, which underlines their purity (data not shown). Analysis of the released peptides at early time points (10 min)

distinguished BMV and CCMV virions assembled with homologous replicase-CP interaction from those assembled with heterologous interaction. In agreement with the previous report (Chakravarty et al., 2020), the K65, R103, K111, and K165 residues were exposed on the surface of B3+4^{V} virions assembled with homologous BMV replicase (Fig. 3.6A, bottom panel). In these virions, the N-terminal arginine-rich motif (N-ARM) is internalized; therefore, peptides encompassing this region are not detected in early time points. MALDI profile of trypsin-digested WT BMV closely resembles that of B3+4^{V} (Fig. 3.6A, top and bottom panel), as RNA3+4 containing virions are the predominant type (~60%) in WT, a mixture of three virion types containing three genomic RNAs.

In comparison, the C1+ C2+ B3 (Fig. 3.6B, top panel) or C1a+ C2a+ B3 (Fig. 3.6B, bottom panel) virions assembled with heterologous CCMV replicase did not release peptides encompassing previously reported surface residues (K65, K111, and K165) indicating these residues are internalized in those virions and not accessible to trypsin cleavage. Also, the heterologous virions expose their N-ARM on the capsid surface, as evidenced by the cleavage products recovered. However, as these residues are not a part of the structure, any disruption encompassing those does not impact the overall structural integrity of the virions assembled with heterologous replicase. Table 3.3 summarizes the location of the trypsin cleavage sites identified to be located on BMV virions assembled in the presence of either homologous (WT BMV and B3+4^{V}) or heterologous replicase (C1+ C2+ B3 and C1a+ C2a+ B3).

In the case of CCMV, the MALDI profile of trypsin-digested WT virions closely resembles that of C3+4^{V}, as reported previously in this thesis (Fig. 3.7A). The fragment profile of trypsin digested B1+ B2+ C3 virions (Fig. 3.7B, top panel) resembled WT CCMV (Fig. 3.7A, top panel). However, the low abundance of released fragments indicates those originate from a relatively small subset of virions. The p1a+ p2a+ C3 virions (Fig. 3.7B, bottom panel), assembled with heterologous BMV replicase, release very few fragments compared to C3+4^{V}, and release of these low abundance fragments does not compromise the structural integrity in most of these virions (Table 3.4).

DISCUSSION

The primary focus of this study is to investigate the role of homologous vs. heterologous replicase-CP interaction in controlling the capsid dynamics of BMV and CCMV virions. Using agroinfiltration, we were successful in assembling BMV and CCMV RNA3+4 containing virions using either full-length RNA or ORF encoding homologous and heterologous replicase (Fig. 3.1). The resultant virions share identical surface charges with respective wild types (Fig. 3.3A). An RT-PCR assay established that each virion type encapsidated the desired RNAs (either BMV RNA3) or (CCMV RNA3) (Fig. 3.3B). Interestingly, the virions assembled with heterologous replicase showed atypical and increased thermal stability than those assembled with homologous replicase (Fig. 3.4).

According to the reported BMV crystal structure, residues K65, R103, K111, and K165 residues were exposed on the surface of virions (Lucas, Larson, & McPherson, 2002). Also, based on the CCMV structure, the accessible trypsin cleavage sites (K42, K65, K87, and K106) are located on the surfaces of the A, B, and C subunits of CCMV CP (Speir, Munshi, Wang, Baker, & Johnson, 1995). Identification of the cleavage products of BMV virions assembled with homologous vs. heterologous replicase after 10 min of trypsin digestion by mass mapping suggested the following: The B3+4^{V} has the reported residues exposed on the capsid exterior. However, when BMV RNA3 is replicated by CCMV 1a/2a replicase and gets packaged in the BMV CP, the resultant virions show a distinct dynamics

of capsid with K65, K111, and K165, the three out of four residues internalized and not accessible to trypsin that was reported to be on the capsid surface in WT BMV. Any cleavage at K165 alone is sufficient to disrupt the BMV capsid structure (Zlotnick, Aldrich, Johnson, Ceres, & Young, 2000), explaining why these virions retain their structural integrity even if a small percentage of them released a peptide encompassing R103.

On the other hand, the effect of BMV 1a/2a replicase was investigated on capsid dynamics of CCMV RNA3+4 containing virions. Interestingly, CCMV RNA3 packaging is independent of movement protein (MP) ORF or CP ORF or 3' t-RNA like structure (TLS) (Annamalai & Rao, 2005a). *In vitro* assembly studies in CCMV also supported this observation by noting CP dimers attach to and fold the RNA genome in a sequence-independent and CP quaternary-structure-dependent fashion (Johnson, Willits, Young, & Zlotnick, 2004). BMV, a monocot-adapted virus, uses a bipartite packaging signal made up of a 3' TLS and a packaging element on MP ORF (Choi & Rao, 2003). We observed that the C3+4^{V} has the reported residues (K42, K65, K87, and K106) are exposed on the capsid exterior and gets readily digested upon trypsin treatment. However, when CCMV RNA3 is replicated by BMV 1a/2a replicase and gets packaged in the CCMV CP, the virions show resistance to trypsin, indicating the predicted exposed residues may not be exposed on the surface as we observed in BMV. The fragmentation profile of CCMV RNA3+4 virions assembled in the presence of BMV replicase demonstrate peptides released from N-ARM, including those covering K42, K65, and K106 but

not K87. These fragments were present in relatively low abundance, and most virions were intact, as seen in Western blot and EM. Taken together, our results suggest that heterologous replicase-CP interaction plays an essential role in altering the stability and capsid dynamics of BMV and CCMV RNA3+4 containing virions.

MATERIALS AND METHODS

Agroplasmids used in this study

Construction and characteristic properties of agroplasmids pB1, pB2, and pB3 (Fig. 3.1A), engineered to express biologically active full-length genomic RNAs of BMV following agroinfiltration into plants, were described previously (Annamalai & Rao, 2005b). Likewise, agroplasmids p1a, p2a, and pCP (Fig. 3.1A) were engineered to transiently express replicase protein 1a (p1a), replicase protein 2a (p2a), and CP, respectively, as described previously (Annamalai & Rao, 2005b; Seo, Kwon, & Rao, 2012). The CCMV full-length genomic RNAs C1, C2, and C3, were amplified using the primers as mentioned in Table 3.1. The amplified PCR products were digested with *Kpn*I and *Xba*I and were ligated into a similarly treated pCass-Rz. The CCMV 1a, 2a, and CP open reading frames (ORFs) were amplified using the primers as mentioned in Table 3.1. The resultant PCR products were digested with *Spe*I and were ligated into a *Stu*I and *Spe*I treated PZP vector.

Primers	Sequence
CCMV R1-5E-*Kpn*I-Fw	5' AGGGGTACCGTAATCCACGAGAGCGAGG 3'
CCMV-R2-5E-*Kpn*I-Fw	5' AGGGGTACCGTAATCCACGAGAGCGAGG 3'

CCMV-R3-5E-*Kpn*I-Fw	5' AGGGGTACCGTAATCTTTACCAAACAACTTTCA 3'
CCMV-RNAs-3E-*Xba*I-Rv	5' AGCTCTAGATGGTCTCCTTAGAGATCACCT
CCMV-1a-5E-Fw	5' ATGGCAAGTTCTTTAGATCTTTTG 3'
CCMV-1a-3E-*Spe*I-Rv	5' GGACTAGTTAAGATATACTTCTAAATATTAAATCACCT 3'
CCMV-2a-5E-Fw	5' ATGTCTAAGTTCATTCCAGAAGGT 3'
CCMV-2a-3E-*Spe*I-Rv	5' GGACTAGTTATTTAGAAAGGGTCTTACGCA 3'
CCMV-CP-5E-Fw	5' ATGTCTACAGTCGGAACAGGGAAGT 3'
CCMV-CP-3E-*Spe*I-Rv	5' GGACTAGTCTAATACACCGGAGTGAAAGAG 3'

Table 3.1 List of primers used to amplify CCMV full-length and ORF clones

Agroinfiltration, total protein extraction, virion purification, negative-stain electron microscopy, and Western blot analysis

All agroplasmids used in this study were transformed into *Agrobacterium* strain GV3101. The transformed *Agrobacterium* cells containing the desired transformant (Fig. 3.1B, C, D, E, F) were infiltrated into the abaxial surface of wild-type *Nicotiana benthamiana* leaves described previously (P. Annamalai & A. L. N. Rao, 2006). After 4 days post infiltration (dpi), agroinfiltrated local and systemic leaves were ground in liquid nitrogen. Total protein was extracted in 3 volumes of extraction buffer (20mM Tris-Cl; pH 7.5, 1mM EDTA; pH 8.0, 5mM DTT). The leaf slurry was centrifuged at 14,000 rpm for 5 minutes, and the supernatant was used for downstream analysis of total proteins using SDS-PAGE and Western blot. The procedure used to purify heterologous virions from 4 dpi agroinfiltrated leaves of *N. benthamiana* followed by sucrose density gradient centrifugation as described previously (Annamalai & Rao, 2005a). For negative-stain EM analysis, virions were imaged using a Tecnai 12 operated at 120 KeV, and images were recorded digitally. For electrophoretic mobility analysis, purified virions were loaded in a 1% agarose gel and electrophoresed in virus suspension buffer (50 mM sodium acetate, 8 mM magnesium acetate, pH 4.5) at 7 V/cm for 2.5 hours at 4°C. Western blot analysis of undigested and trypsin-digested virion samples using anti-CP antibodies was performed as described previously (Annamalai & Rao, 2005b).

Differential scanning fluorimetry

DSF was performed as described previously (Rayaprolu et al., 2014). Desired virion samples and control (lysozyme) samples were resuspended either in virus suspension buffer (50 mM sodium acetate, 8 mM magnesium acetate, pH 4.5) or in 100 mM phosphate buffer (pH 7.2). The experiment was performed three times independently, using three replicates for each sample. DSF data were analyzed and plotted as described previously (Chakravarty et al., 2020; Rayaprolu et al., 2014).

MALDI-TOF

For MALDI-TOF, analysis was performed as described previously (Chakravarty et al., 2020). A desired purified virion preparation was diluted to 1 mg/ml in 25 mM Tris-HCl, 1 mM EDTA buffer. A 30 µl sample (i.e., 30 µg of the desired virion preparation) was digested with a 1:100 (wt/wt) ratio of trypsin (Pierce Trypsin protease, mass spectrometry grade; Thermo Fisher Scientific) to the virus for various time points at 25°C (Bothner et al., 1999). 10 µl of water was added to 20 µl of the digested sample. Approximately 0.5 µl of each digested or undigested (control) sample was analyzed on an AB Sciex TOF/TOF 5800 MALDI MS with -cyano-4-hydroxycinnamic acid matrix. The instrument was calibrated with standards, and the test samples were analyzed with external calibration. The

accuracy is approximately 0.05 Da. The MALDI-TOF data were analyzed with AB Sciex Data Explorer, and baseline was corrected with a peak width of 32, flexibility of 0.5, and degree of 0.1. For noise removal, the standard deviation was set at 2. To determine the peak detection criteria, the percent centroid was taken as 50, the signal/noise (S/N) threshold was 3, and the noise window width m/z was 250. The threshold after S/N recalculation was set at 20. The peptide fragments were assigned based on the UCSF Protein Prospector's MS-Digest function.

RT-PCR

RNA was isolated from a purified individual preparation of virions and subjected to RT-PCR using iScript™ cDNA Synthesis Kit (Bio-Rad) and Q5® High-Fidelity DNA Polymerase (NEB). Each cDNA was amplified by the following two sets of primers listed in Table 4.2. The resulting PCR products were analyzed by 1% agarose gel electrophoresis.

Primers	Sequence
BMV RNA3 Fw	5’ TCCCTTCAGTGGTTCCTCAC 3’
BMV RNA3 Rev	5' CTGTACGGTACCCGCATTCT 3'
CCMV RNA3 Fw	5’ TGGACACATCGGTTTTTGAA 3’
CCMV RNA3 Rev	5’ GGTACAAAGCAGCGACAACA 3’

Table 3.2 List of primers used to amplify BMV RNA3 or CCMV RNA3

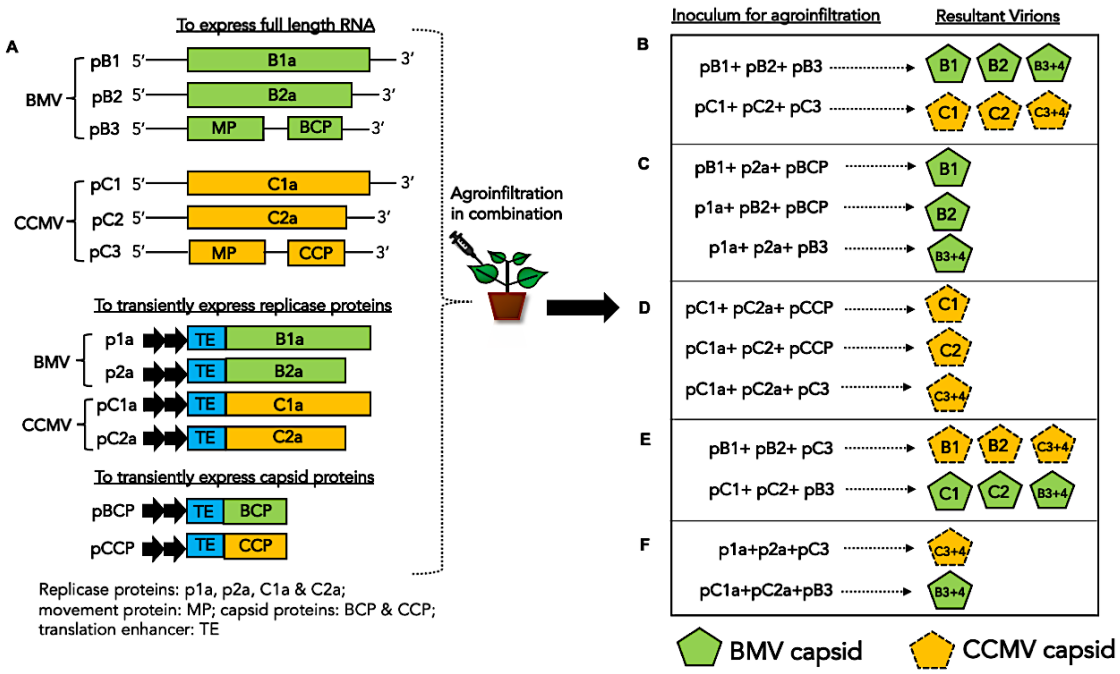

Figure 3.1 Characteristic features of agroplasmids used in this study. (A) Characteristics of agroplasmids harboring BMV genomic RNAs and CCMV genomic RNAs used for transient expression in plants. The 35S-B1 (pB1), 35S-B2 (pB2), and 35S-B3 (pB3) constructs contain full-length cDNA copies of BMV genomic RNA1 (B1), -2 (B2), and -3 (B3), respectively. The 35S-C1 (pC1), 35S-C2 (pC2), and 35S-C3 (pC3) constructs contain full-length cDNA copies of CCMV genomic RNA1 (C1), -2 (C2), and -3 (C3), respectively. Single lines and open boxes represent noncoding and coding regions, respectively. Two black arrows at the 5' ends represent the double 35-S. Open reading frames (ORFs) of BMV p1a, p2a, CP, and CCMV C1a, C2a, and CP were fused in-frame to each pair of PZP binary vectors using *Stu*I and *Spe*I sites (Annamalai & Rao, 2005b; Seo et al., 2012). Schematic representation of the strategy used for autonomous assembly of (B) BMV WT and CCMV WT; (C) $B1^{V}$, $B2^{V}$, and $B3+4^{V}$ (Chakravarty et al., 2020); (D) $C1^{V}$, $C2^{V}$, and $C3+4^{V}$; (E) BMV RNA1, BMV RNA2, and CCMV RNA3+4 containing virions encapsidated in CCMV CP or CCMV RNA1, CCMV RNA2, and BMV RNA3+4 containing virions encapsidated in BMV CP; (F) CCMV RNA3+4 containing virions assembled in the presence of heterologous BMV replicase ORF and BMV RNA3+4 containing virions assembled in the presence of heterologous CCMV replicase ORF.

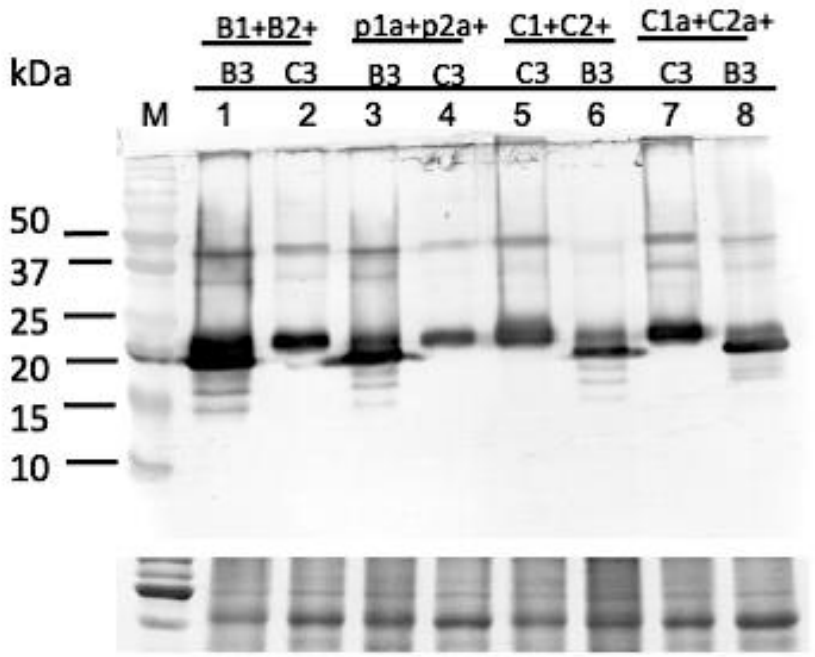

Figure 3.2 Analysis of total protein extracted from 4dpi leaves. (Top panel) Western blot analysis of total protein extracted from the 4 dpi leaves of *N. benthamiana* using an anti-CP antibody. Lane 1 contains total protein from leaf infiltrated with agrotransformants B1+ B2+ B3; lane 2 contains total protein from leaf infiltrated with agrotransformants B1+ B2+ C3; lane 3 contains total protein from leaf infiltrated with agrotransformants p1a+ p2a+ B3; lane 4 contains total protein from leaf infiltrated with agrotransformants p1a+ p2a+ C3; lane 5 contains total protein from leaf infiltrated with agrotransformants C1+ C2+ C3; lane 6 contains total protein from leaf infiltrated with agrotransformants C1+ C2+ B3; lane 7 contains total protein from leaf infiltrated with agrotransformants The C1a+ C2a+ C3; lane 8 contains total protein from leaf infiltrated with agrotransformants C1a+ C2a+ B3. Each lane has 30 µg of total protein estimated by Bradford protein assay. (Bottom panel) For samples used in the Western blot, the gel is stained with Coomassie Brilliant Blue R-250 to demonstrate the loading controls. The samples are loaded in the order as mentioned above in lanes 1-8.

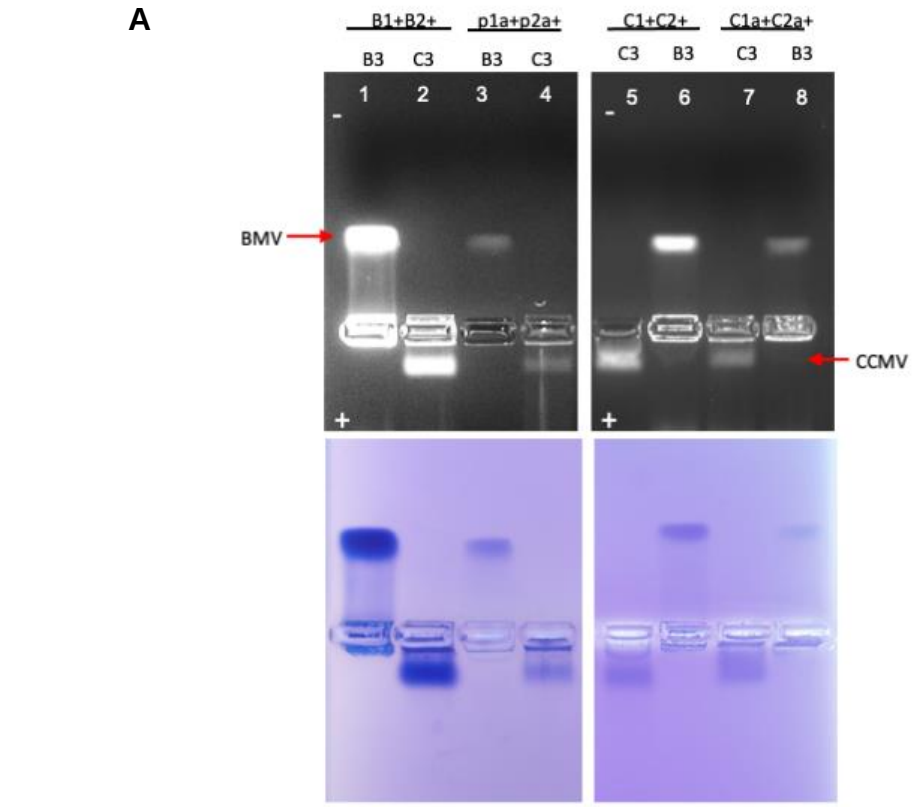
A
B1+B2+
p1a+p2a+
C1+C2+
C1a+C2a+
B3
C3
B3
C3
C3
B3
C3
B3
1
2
3
4
5
6
7
8
-
+
BMV
CCMV

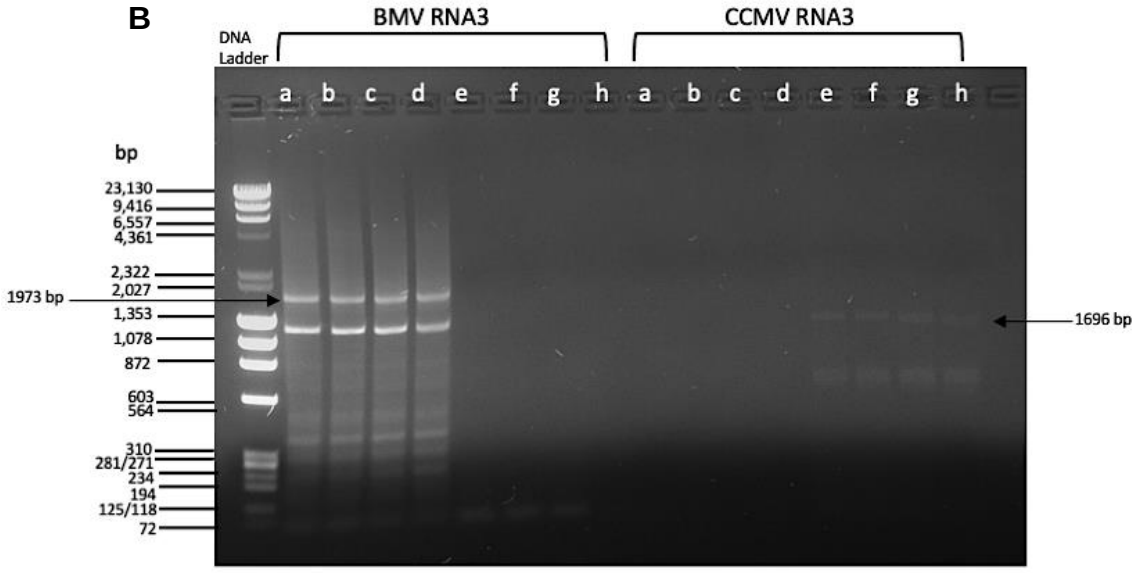
B
BMV RNA3
CCMV RNA3
DNA Ladder
a b c d e f g h a b c d e f g h
bp
23,130
9,416
6,557
4,361
2,322
2,027
1,353
1,078
872
603
564
310
281/271
234
194
125/118
72
1973 bp
1696 bp

Figure 3.3 Electrophoretic mobility and Genome content of BMV and CCMV virions assembled in the presence of either homologous or heterologous replicase. (A) Virion electrophoresis. Density gradient-purified virions of WT BMV (lane 1), B1+ B2+ C3 (lane 2), p1a+ p2a+ B3/ B3+4^{V} (lane 3), p1a+ p2a+ C3 (lane 4), WT CCMV (lane 5), C1+ C2+ B3 (lane 6), C1a+ C2a+ C3/ C3+4^{V} (lane 7), C1a+C2a+ B3 (lane 8), were subjected to agarose gel analysis as described in Materials and Methods. The gel shown at the top panel was stained with ethidium bromide to detect RNA and then re-stained with Coomassie blue to detect protein (bottom panel). BMV and CCMV virions migrating toward negative and positive, respectively, are indicated. (B) RT-PCR analysis. Agarose gel analysis of RT-PCR products amplified from virion RNA of WT BMV (a), C1+ C2+ B3 (b), p1a+ p2a+ B3/ B3+4^{V} (c), C1a+C2a+ B3 (d), WT CCMV (e), B1+ B2+ C3 (f), C1a+ C2a+ C3/ C3+4^{V} (g), and p1a+ p2a+ C3 (h) using a set of primers designed to specifically amplify the regions encompassing either BMV RNA3 or CCMV RNA3 as described in Materials and Methods.

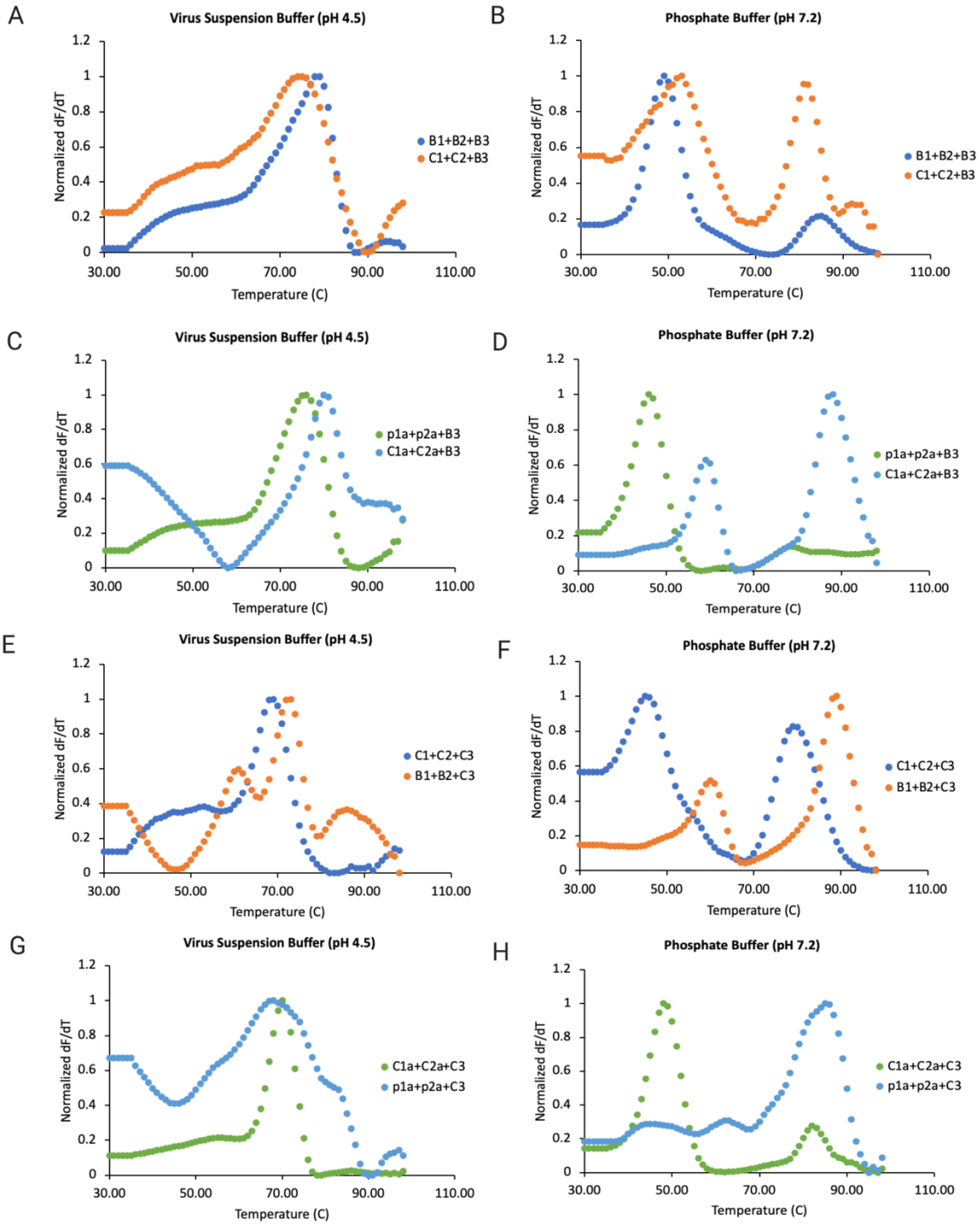
A
Virus Suspension Buffer (pH 4.5)
Normalized dF/dT
Temperature (C)
B1+B2+B3
C1+C2+B3
B
Phosphate Buffer (pH 7.2)
Normalized dF/dT
Temperature (C)
B1+B2+B3
C1+C2+B3
C
Virus Suspension Buffer (pH 4.5)
Normalized dF/dT
Temperature (C)
p1a+p2a+B3
C1a+C2a+B3
D
Phosphate Buffer (pH 7.2)
Normalized dF/dT
Temperature (C)
p1a+p2a+B3
C1a+C2a+B3
E
Virus Suspension Buffer (pH 4.5)
Normalized dF/dT
Temperature (C)
C1+C2+C3
B1+B2+C3
F
Phosphate Buffer (pH 7.2)
Normalized dF/dT
Temperature (C)
C1+C2+C3
B1+B2+C3
G
Virus Suspension Buffer (pH 4.5)
Normalized dF/dT
Temperature (C)
C1a+C2a+C3
p1a+p2a+C3
H
Phosphate Buffer (pH 7.2)
Normalized dF/dT
Temperature (C)
C1a+C2a+C3
p1a+p2a+C3

Figure 3.4 Stability analysis of the BMV and CCMV virions assembled in the presence of either homologous or heterologous replicase using differential scanning fluorimetry (DSF). DSF measurements of derivative of fluorescence intensity as a function of temperature for each virion type normalized so that the maximum of the derivative is set to 1 (y-axis) during heating of the virions indicated (A-H) at various temperatures (x-axis) under indicated conditions. The WT BMV and B3+4^{V} and WT CCMV and C3+4^{V} displayed identical temperature dependence for melting under buffer conditions of both pH 4.5 and pH 7.2. The virions assembled in the presence of either full-length RNAs or ORFs encoding heterologous replicase show unusual and increased thermal stability at pH 4.5 and 7.2 compared to those assembled as a result of interaction between homologous replicase and CP (see "Comparative thermal stability of BMV and CCMV virions assembled in the presence of either homologous or heterologous replicas" for details).

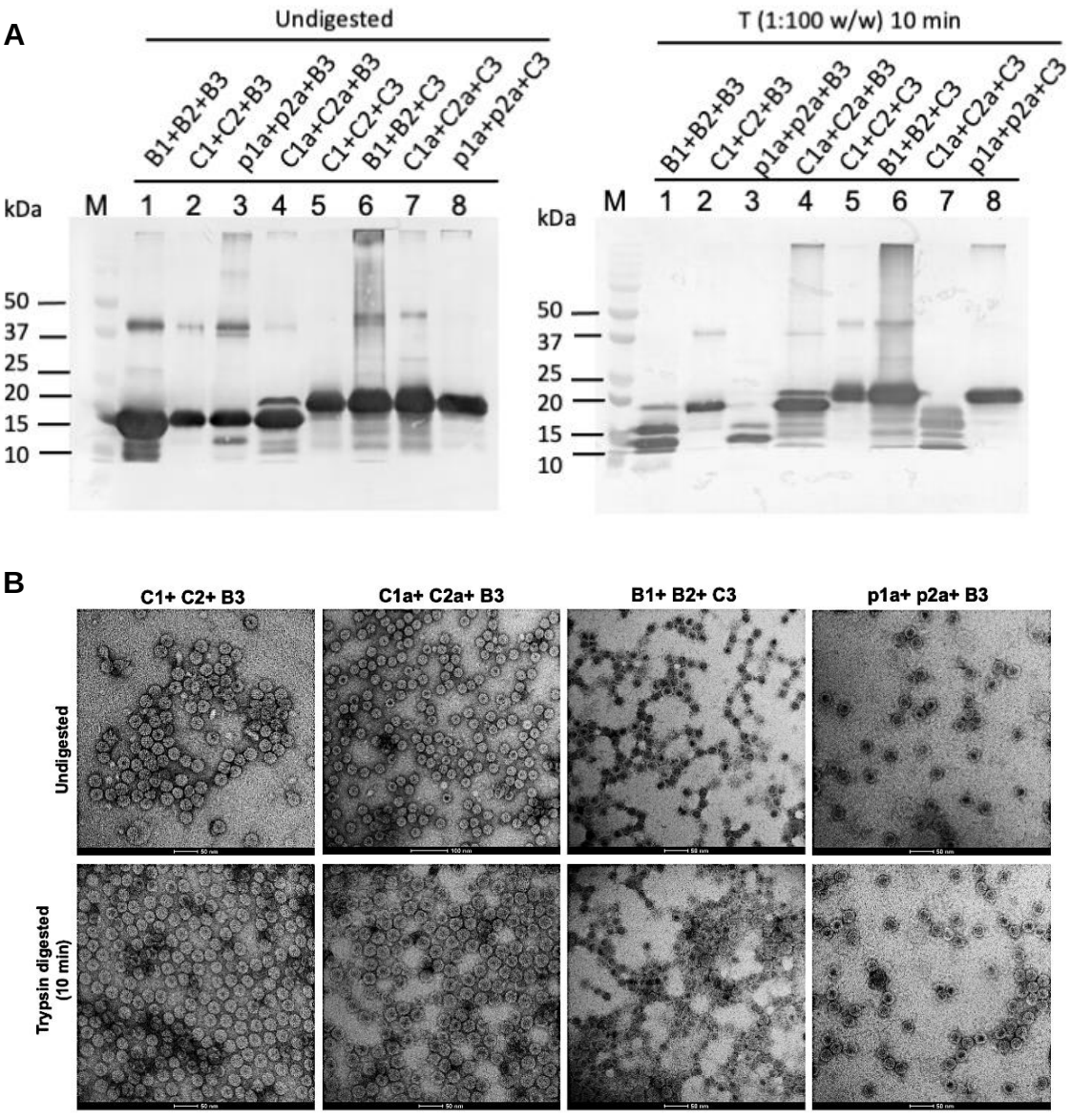
A
Undigested
T (1:100 w/w) 10 min
B1+B2+B3
C1+C2+B3
p1a+p2a+B3
C1a+C2a+B3
C1+C2+C3
B1+B2+C3
C1a+C2a+C3
p1a+p2a+C3
kDa
M
1 2 3 4 5 6 7 8
50
37
25
20
15
10
B
C1+ C2+ B3
C1a+ C2a+ B3
B1+ B2+ C3
p1a+ p2a+ B3
Undigested
Trypsin digested (10 min)

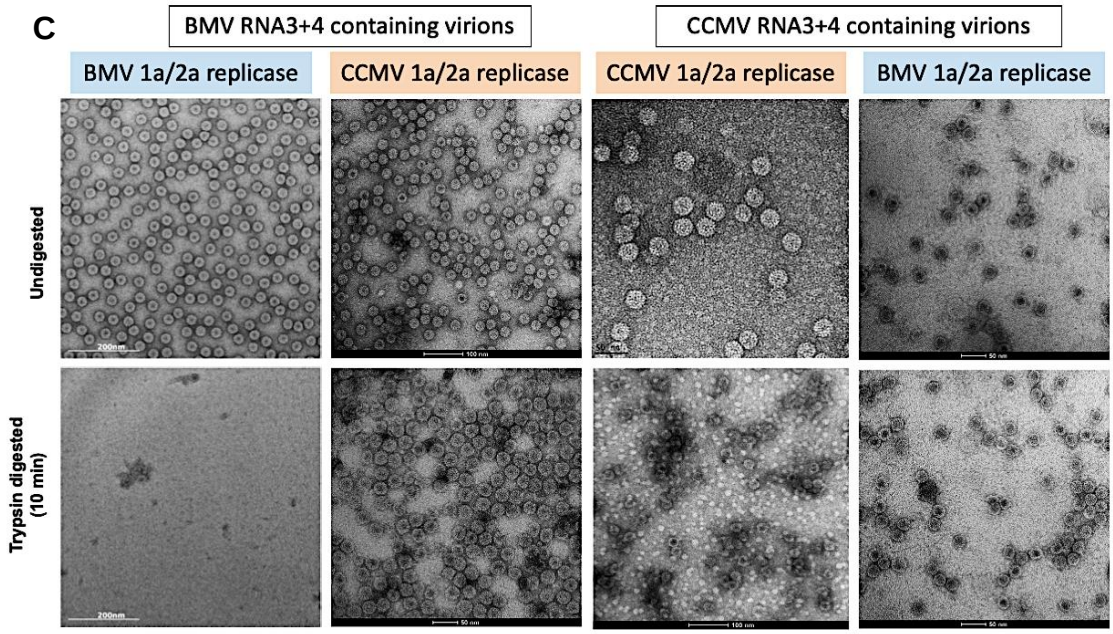

Figure 3.5 Proteolysis of BMV and CCMV virions assembled in the presence of either homologous or heterologous replicase monitored by Western blotting and negative-stain EM analysis. (A) Western blot for WT BMV, C1+ C2+ B3, B3+4^{V}, C1a+ C2a+ B3, WT CCMV, B1+ B2+ C3, C3+4^{V}, p1a+ p2a+ C3. Before Western blot analysis, each virion preparation was either undigested or digested with trypsin for 10 min. (B) Negative-stain electron micrographs show the integrity of the undigested and trypsin-digested virion preparations of the indicated samples. (C) Negative-stain electron micrographs show the integrity of the undigested and trypsin-digested virion preparations of BMV RNA3+4 containing virions and CCMV RNA3+4 containing virions assembled with either BMV 1a/2a or CCMV 1a/2a replicase.

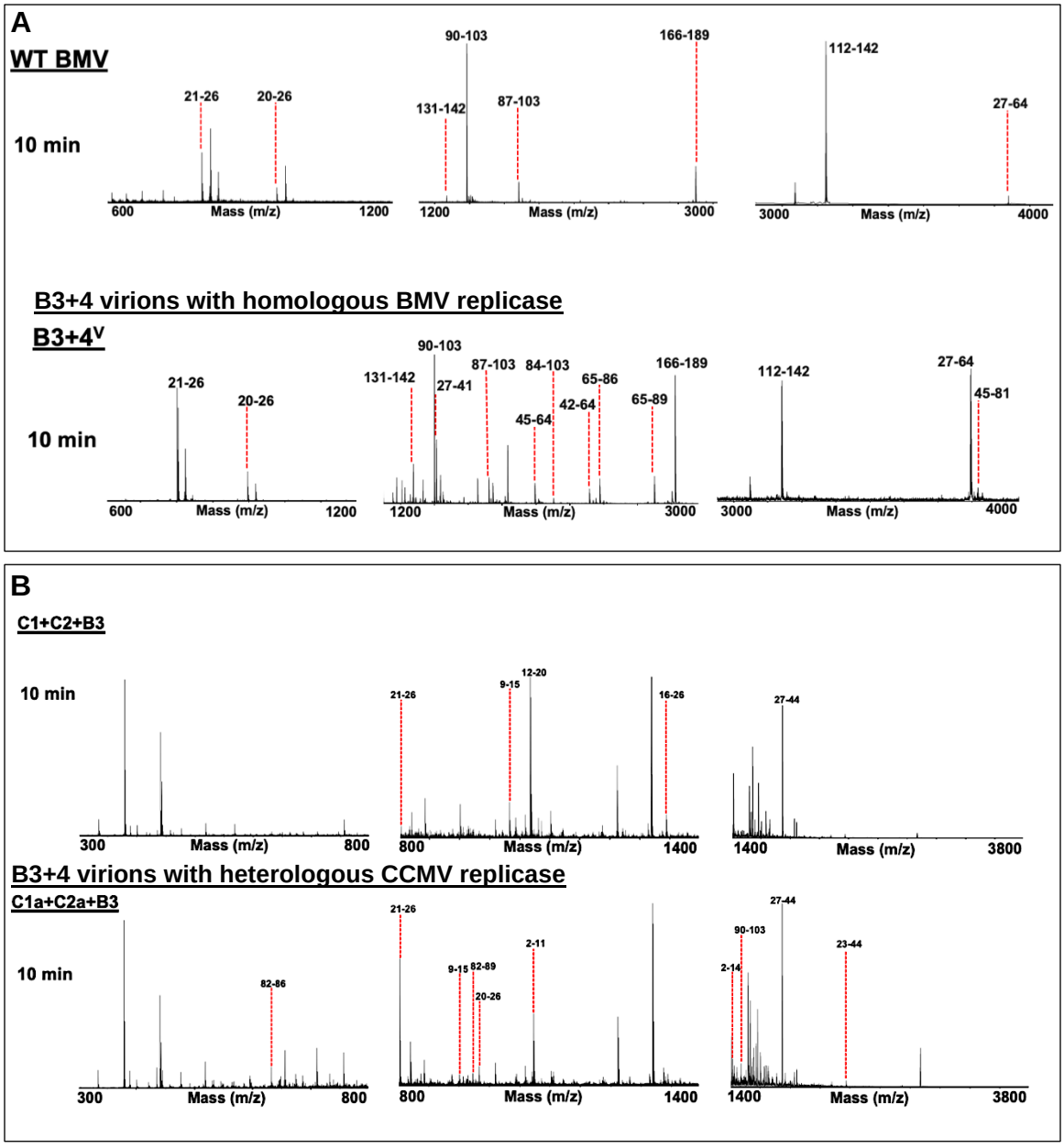

Figure 3.6 MALDI-TOF analysis of trypsin-digested virions. (A) MALDI-TOF analysis of peptides released from WT BMV and B3+4^{V} (virions assembled due to homologous replicase-CP interaction) following digestion with trypsin at 10 min. (B) MALDI-TOF analysis of peptides released from C1+ C2+ B3 and C1a+ C2a+ B3 (virions assembled due to heterologous replicase-CP interaction) following digestion with trypsin at 10 min. Peaks are labeled with corresponding polypeptide fragments of predicted amino acid residues. Table 3.3 summarizes masses and identifies the corresponding amino acid residues.

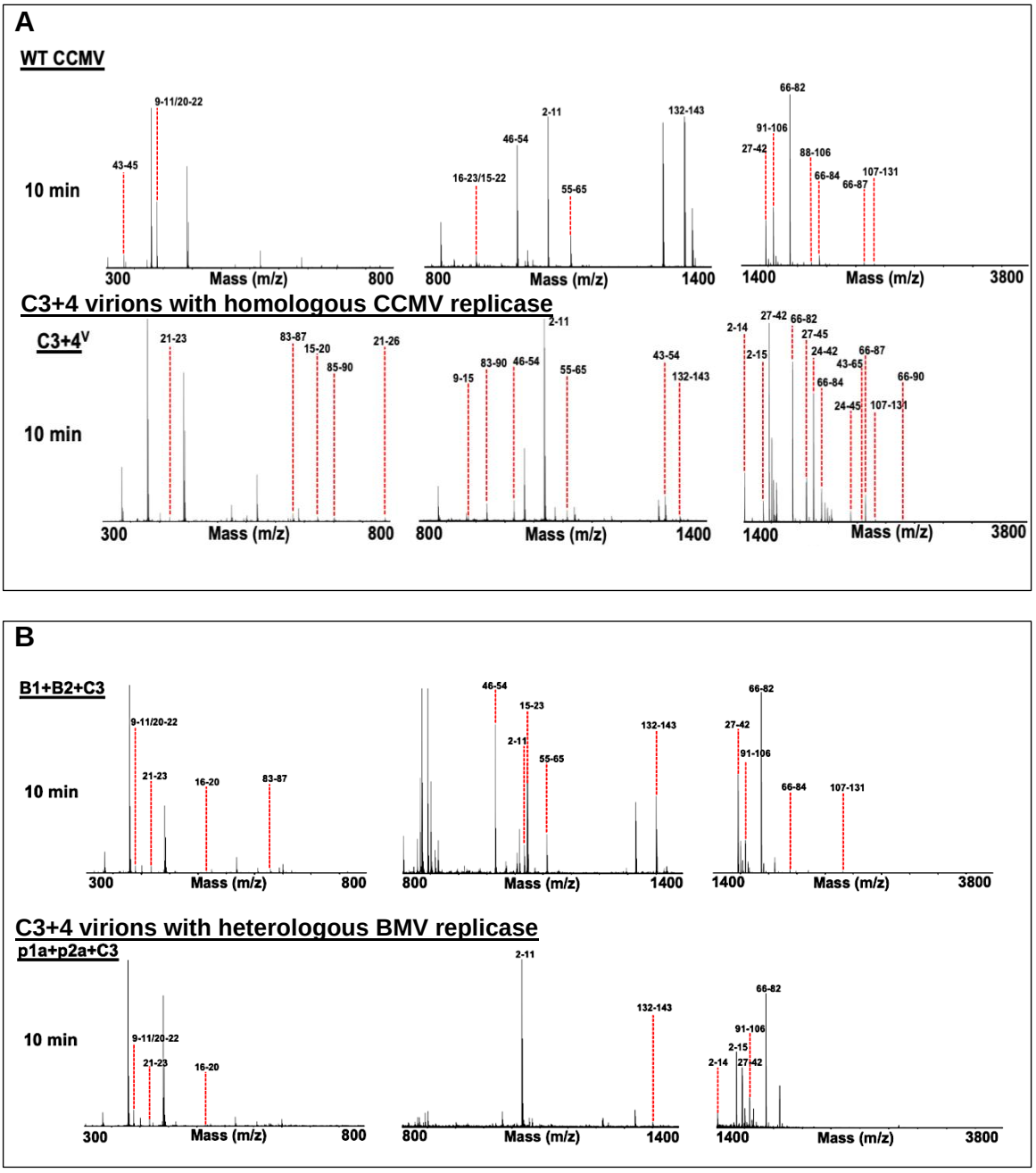

Figure 3.7 MALDI-TOF analysis of trypsin-digested virions. (A) MALDI-TOF analysis of peptides released from WT CCMV and C3+4^{V} (virions assembled due to homologous replicase-CP interaction) following digestion with trypsin at 10 min. (B) MALDI-TOF analysis of peptides released from B1+ B2+ C3 and p1a+ p2a+ C3 (virions assembled due to heterologous replicase-CP interaction) following digestion with trypsin at 10 min. Peaks are labeled with corresponding polypeptide fragments of predicted amino acid residues. Table 3.4 summarizes masses and identifies the corresponding amino acid residues.

Table 3.3 Kinetics of trypsin cleavage sites located on BMV virions assembled in the presence of either homologous or heterologous replicase

Predicted tryptic peptides of BMV CP and their masses			WT BMV	C1+C2+B3	B3+4^{V}	C1a+C2a+B3
Residues	Sequence	m/z	Time to cleavage: 10 min			
2-11	STSGTGKMTR	1067.515	-	-	-	+
2-14	STSGTGKMTRAQR	1422.7118	-	-	-	+
9-15	MTRAQRR	918.505	-	+	-	+
12-20	AQRRAAARR	1055.6293	-	+	-	-
16-26	AAARRNRWTAR	1328.7407	-	+	-	-
20-26	RNRWTAR	959.5282	+	-	+	+
21-26	NRWTAR	803.4271	+	+	+	+
23-44	WTARVQPVIVEPLAAGQGKAIK	2332.35	-	-	-	+
27-41	VQPVIVEPLAAGQGK	1505.8686	-	-	+	
27-44	VQPVIVEPLAAGQGKAIK	1818.0847	-	+	-	+
27-64	VQPVIVEPLAAGQGKAIKAIAGYSISKWEASSDAITAK	3868.1219	+	-	+	-
42-64	AIKAIAGYSISKWEASSDAITAK	2381.2711	-	-	+	-
45-64	AIAGYSISKWEASSDAITAK	2069.055	-	-	+	-
45-81	AIAGYSISKWEASSDAITAKATNAMSITLPHELSSEK	3878.9481	-	-	+	-
65-86	ATNAMSITLPHELSSEKNKELK	2441.2705	-	-	+	-
65-89	ATNAMSITLPHELSSEKNKELKVGR	2753.4614	-	-	+	-
82-86	NKELK	631.3774	-	-	-	+
82-89	NKELKVGR	943.5683	-	-	-	+
84-103	ELKVGRVLLWLGLLPSVAGR	2176.3329	-	-	+	-
87-103	VGRVLLWLGLLPSVAGR	1806.1112	+	-	+	-
90-103	VLLWLGLLPSVAGR	1493.9202	+	-	+	+
112-142	QAQAEAAFQVALAVADSSKEVVAAMYTDAFR	3258.61	+	-	+	-
131-142	EVVAAMYTDAFR	1372.6566	+	-	+	-
166-189	AVVVHLEVEHVRPTFDDFFTPVYR	2872.4781	+	-	+	-

Table 3.3 Kinetics of trypsin cleavage sites located on BMV virions assembled in the presence of either homologous (WT BMV and B3+4^{V}) or heterologous replicase (C1+ C2+ B3 and C1a+ C2a+ B3). The peptides fragments recovered for each virion type are indicated with "+."

Table 3.4 Kinetics of trypsin cleavage sites located on CCMV virions assembled in the presence of either homologous or heterologous replicase

Predicted tryptic peptides of CCMV CP and their masses			WT CCMV	B1+B2+C3	C3+4^{V}	p1a+p2a+C3
Residues	Sequence	m/z	Time to cleavage: 10 min			
2-11	STVGTGKLTR	1061.5949	+	+	+	+
2-14	STVGTGKLTRAQR	1416.7918	-	-	+	+
2-15	STVGTGKLTRAQRR	1572.8929	-	-	+	+
9-11	LTR	389.2507	+	+	-	+
9-15	LTRAQRR	900.5486	-	-	+	-
15-20	RAAARK	672.4264	-	-	+	-
16-20	AAARK	516.3253	-	+	-	+
16-23	AAARKNKR	914.5643	+	-	-	-
21-23	NKR	417.2568	-	+	+	+
21-26	NKRNTR	788.4486	-	-	+	-
24-42	NTRVVQPVIVEPIASGQGK	1992.1237	-	-	+	-
24-45	NTRVVQPVIVEPIASGQGKAIK	2304.3398	-	-	+	-
27-42	VVQPVIVEPIASGQGK	1620.9319	+	+	+	+
27-45	VVQPVIVEPIASGQGKAIK	1933.1481	-	-	+	-
43-45	AIK	331.2340	+	-	-	-
43-54	AIKAWTGYSVSK	1310.7103	-	-	+	-
43-65	AIKAWTGYSVSKWTASCAAAEAK	2400.2016	-	-	+	-
46-54	AWTGYSVSK	998.4942	+	+	+	-
55-65	WTASCAAAEAK	1108.5092	+	+	+	-
66-82	VTSAITISLPNELSSER	1816.9651	+	+	+	+
66-84	VTSAITISLPNELSSERNK	2059.1030	+	+	+	-
66-87	VTSAITISLPNELSSERNKQLK	2428.3406	+	-	+	-
66-90	VTSAITISLPNELSSERNKQLKVGR	2740.5316	-	-	+	-
83-87	NKQLK	630.3933	-	+	+	-
83-90	NKQLKVGR	942.5843	-	-	+	-
85-90	QLKVGR	700.4464	-	-	+	-
88-106	VGRVLLWLGLLPSVSGTVK	1994.2161	+	-	-	-
91-106	VLLWLGLLPSVSGTVK	1682.0251	+	+	-	+
107-131	SCVTETQTTAAASFQVALAVADNSK	2513.2188	+	+	+	-
132-143	DVVAAMYPEAFK	1340.6555	+	+	+	+

Table 3.4 Kinetics of trypsin cleavage sites located on CCMV virions assembled in the presence of either homologous (WT CCMV and C3+4^{V}) or heterologous replicase (B1+ B2+ C3 and p1a+ p2a+ C3). The peptides fragments recovered for each virion type are indicated with "+."

REFERENCES

Allison, R. F., Janda, M., & Ahlquist, P. (1988). Infectious in vitro transcripts from cowpea chlorotic mottle virus cDNA clones and exchange of individual RNA components with brome mosaic virus. *J Virol, 62*(10), 3581-3588.

Annamalai, P., & Rao, A. L. (2005a). Dispensability of 3' tRNA-like sequence for packaging cowpea chlorotic mottle virus genomic RNAs. *Virology, 332*(2), 650-658. doi:10.1016/j.virol.2004.12.009

Annamalai, P., & Rao, A. L. (2005b). Replication-independent expression of genome components and capsid protein of brome mosaic virus in planta: a functional role for viral replicase in RNA packaging. *Virology, 338*(1), 96-111. doi:10.1016/j.virol.2005.05.013

Annamalai, P., & Rao, A. L. (2006). Packaging of brome mosaic virus subgenomic RNA is functionally coupled to replication-dependent transcription and translation of coat protein. *J Virol, 80*(20), 10096-10108. doi:10.1128/JVI.01186-06

Annamalai, P., & Rao, A. L. N. (2006). Delivery and expression of functional viral RNA genomes in planta by agroinfiltration. *Curr Protoc Microbiol, Chapter 16*, 16B.12.11-16B.12.15. doi:10.1002/9780471729259.mc16b02s01

Bothner, B., Schneemann, A., Marshall, D., Reddy, V., Johnson, J. E., & Siuzdak, G. (1999). Crystallographically identical virus capsids display different properties in solution. *Nat Struct Biol, 6*(2), 114-116. doi:10.1038/5799

Calhoun, S. L., & Rao, A. L. (2008). Functional analysis of brome mosaic virus coat protein RNA-interacting domains. *Arch Virol, 153*(2), 231-245. doi:10.1007/s00705-007-1085-z

Calhoun, S. L., Speir, J. A., & Rao, A. L. (2007). In vivo particle polymorphism results from deletion of a N-terminal peptide molecular switch in brome mosaic virus capsid protein. *Virology, 364*(2), 407-421. doi:10.1016/j.virol.2007.03.034

Carrillo-Tripp, M., Shepherd, C. M., Borelli, I. A., Venkataraman, S., Lander, G., Natarajan, P., . . . Reddy, V. S. (2009). VIPERdb2: an enhanced and web API enabled relational database for structural virology. *Nucleic Acids Res, 37*(Database issue), D436-442. doi:10.1093/nar/gkn840

Chakravarty, A., Reddy, V. S., & Rao, A. L. N. (2020). Unravelling the Stability and Capsid Dynamics of the Three Virions of Brome Mosaic Virus Assembled Autonomously. *J Virol, 94*(8). doi:10.1128/JVI.01794-19

Chaturvedi, S., & Rao, A. L. N. (2014). Live cell imaging of interactions between replicase and capsid protein of Brome mosaic virus using Bimolecular Fluorescence Complementation: implications for replication and genome packaging. *Virology, 464-465*, 67-75. doi:10.1016/j.virol.2014.06.030

Choi, Y. G., & Rao, A. L. (2003). Packaging of brome mosaic virus RNA3 is mediated through a bipartite signal. *J Virol, 77*(18), 9750-9757. doi:10.1128/jvi.77.18.9750-9757.2003

Dinant, S., Janda, M., Kroner, P. A., & Ahlquist, P. (1993). Bromovirus RNA replication and transcription require compatibility between the polymerase- and helicase-like viral RNA synthesis proteins. *J Virol, 67*(12), 7181-7189.

Jacquemond, M. (2012). Cucumber mosaic virus. *Adv Virus Res, 84*, 439-504. doi:10.1016/B978-0-12-394314-9.00013-0

Johnson, J. M., Willits, D. A., Young, M. J., & Zlotnick, A. (2004). Interaction with capsid protein alters RNA structure and the pathway for in vitro assembly of cowpea chlorotic mottle virus. *J Mol Biol, 335*(2), 455-464. doi:10.1016/j.jmb.2003.10.059

Lucas, R. W., Larson, S. B., & McPherson, A. (2002). The crystallographic structure of brome mosaic virus. *J Mol Biol, 317*(1), 95-108. doi:10.1006/jmbi.2001.5389

Rao, A. L., & Francki, R. I. (1981). Comparative studies on tomato aspermy and cucumber mosaic viruses. VI. Partial compatibility of genome segments from the two viruses. *Virology, 114*(2), 573-575. doi:10.1016/0042-6822(81)90238-5

Rayaprolu, V., Kruse, S., Kant, R., Movahed, N., Brooke, D., & Bothner, B. (2014). Fluorometric Estimation of Viral Thermal Stability. *Bio Protoc, 4*(15). doi:10.21769/bioprotoc.1199

Seo, J. K., Kwon, S. J., & Rao, A. L. (2012). A physical interaction between viral replicase and capsid protein is required for genome-packaging specificity in an RNA virus. *J Virol, 86*(11), 6210-6221. doi:10.1128/JVI.07184-11

Speir, J. A., Bothner, B., Qu, C., Willits, D. A., Young, M. J., & Johnson, J. E. (2006). Enhanced local symmetry interactions globally stabilize a mutant

virus capsid that maintains infectivity and capsid dynamics. *J Virol, 80*(7), 3582-3591. doi:10.1128/JVI.80.7.3582-3591.2006

Speir, J. A., Munshi, S., Wang, G., Baker, T. S., & Johnson, J. E. (1995). Structures of the native and swollen forms of cowpea chlorotic mottle virus determined by X-ray crystallography and cryo-electron microscopy. *Structure, 3*(1), 63-78. doi:10.1016/s0969-2126(01)00135-6

Suzuki, M., Yoshida, M., Yoshinuma, T., & Hibi, T. (2003). Interaction of replicase components between Cucumber mosaic virus and Peanut stunt virus. *J Gen Virol, 84*(Pt 7), 1931-1939. doi:10.1099/vir.0.19070-0

Zlotnick, A., Aldrich, R., Johnson, J. M., Ceres, P., & Young, M. J. (2000). Mechanism of capsid assembly for an icosahedral plant virus. *Virology, 277*(2), 450-456. doi:10.1006/viro.2000.0619

CHAPTER 4

Biological Significance for Co-packaging of a Genetically Redundant Subgenomic RNA4 in Brome Mosaic Virus

ABSTRACT

In the *Brome mosaic virus* (BMV), replication-derived but genetically redundant subgenomic RNA4 (mRNA for capsid protein synthesis) is co-packaged with genomic RNA3 into a single virion. The rationale for this co-packaging mechanism is not fully understood. This study used an *Agrobacterium*-mediated transient expression system to assemble individual virion sets containing either RNA3 ($B3^V$) or RNA3+4 ($B3+4^V$). Virion preparations of $B3^V$ and $B3+4^V$ appeared indistinguishable either in shape/size (by negative-stain electron microscopic analysis) or in buoyant density (by sucrose density gradient centrifugation) or thermal stability (by differential scanning fluorimetry). However, protease-based experiments of each virion preparation followed by Western blot analysis and Transmission electron microscopy (TEM) revealed noticeable differences between the two-virion sets. Virions of $B3+4^V$ treated with trypsin for 10, 20, 45 min, and 3 hr readily digested as evidenced by the Western blot analysis. Transmission electron micrographs (TEM) of negatively stained preparations confirmed that $B3+4^V$ virions are entirely degraded. Profiles of matrix-assisted laser desorption/ionization (MALDI) time-of-flight (TOF) mass spectrometry analysis identified the release of multiple peptides encompassing the entire capsid protein. In contrast, virions of $B3^V$ remained resistant to trypsin at all digestion time points and appeared as a stable single intact band when analyzed by the Western blot and remain as intact virions under TEM. However, MALDI-TOF analysis of the

released peptides revealed a profile identical to that of B3+4^{V}, suggesting that only a minor percentage of B3^{V} virions are susceptible to trypsin digestion. Taken together, our results accentuate that the virions of B3^{V} are dynamically distinct by exhibiting differential surface conformation than those of B3+4^{V}. To analyze the role of subgenomic RNA packaging in pathogenesis, we compared the local cell-to-cell spread of BMV in the case of B3^{V} and B3+4^{V} when we complemented both virion sets with B1^{V} and B2^{V} using agroinfiltration to assemble respective sets of virions. The CP was detected in non-infiltrated cells away from the cells infiltrated with agroconstructs designed to produce B1^{V}+ B2^{V}+ B3+4^{V} in all three time points (4, 6, and 10 days) case of WT. In contrast, CP was detected in non-infiltrated cells only until 4 days in the case of B1^{V}+ B2^{V}+ B3^{V}, indicating that the absence of sgRNA4 packaging regulates cell-to-cell movement.

INTRODUCTION

Several positive-strand RNA viruses belonging to the Alphavirus superfamily, like *Tobacco mosaic virus* (TMV), *Brome mosaic virus* (BMV), and *Sindbis virus* (SINV), express their downstream genes, specifically the capsid protein gene via replication-derived subgenomic mRNAs (sgRNAs). In some viruses, sgRNA may also get packaged in infectious virions. Three different mechanisms can account for the synthesis of sgRNAs. The first mechanism involves the initiation of sgRNA synthesis on a negative-strand RNA template. In this process, the functional viral replicase copies the positive-strand genomic RNA into a negative-strand of the exact length, which serves as a template for synthesizing progeny genomic RNAs and sgRNAs. The negative-strand RNA contains at least two different promoters. The promoter for genomic RNA synthesis is present at or near the 3' end, whereas one or more subgenomic RNA promoters are present internally. The viral polymerase recognizes one of these subgenomic promoters and initiates transcription to synthesize a sgRNA. This mechanism, called internal initiation, was first described in BMV (Wierzchoslawski, Dzianott, & Bujarski, 2004). In a second mechanism to make sgRNA, the viral polymerase terminates prematurely at a specific "stop" signal instead of copying the positive-strand into a full-length negative-strand. This mechanism results in a shortened negative-stand of sgRNA, which then works as a template for synthesizing positive-strand sgRNA. This method is called premature termination, and various

RNA viruses like *Closteroviruses* and *Nodaviruses* use it. The third mechanism of sgRNA synthesis uses discontinuous RNA synthesis while making the negative-strand template for sgRNA. The resultant nested set of sgRNAs can vary in size, but they are 3' co-terminal with the genomic RNA. Also, except for the smallest sgRNAs, they may contain more than more open reading frames (ORFs), but only the 5' ORF is translated in each case. This method is called discontinuous transcription, and many members of the family *Coronaviridae* use it (Sztuba-Solińska, Stollar, & Bujarski, 2011).

Most sgRNAs get translated into structural proteins or pathogenesis-related proteins by host translation machinery. However, these RNAs may have other roles than functioning as mRNAs. Such roles include regulating the balance between replication and translation or supporting genome rearrangements by RNA-RNA recombination (Sztuba-Solińska et al., 2011). The sgRNAs share several common characteristics. a) The sgRNAs are shorter than their cognate genomic RNAs, b) they are produced in the infected cells but do not hinder the expected likelihood of events during viral replication, c) the sgRNA sequences are usually co-terminal with 3' of the genomic RNA, but in some cases, they are co-terminal with the 5' end. Some viruses even make sgRNAs that contain a 5' co-terminal sequence fused to a 3' co-terminal sequence, d) a sgRNA typically contains only one ORF. If it contains one than one ORF, the 5' ORF is usually translated (Yang, Hussain, Wang, Ke, & Guo, 2009).

The family *Bromoviridae* (Bujarski et al., 2019) consists of six genera, namely *Alfamovirus*, *Anulavirus*, *Bromovirus, Cucumovirus, Ilarvirus,* and *Oleavirus.* The coat protein (CP) requirement to initiate the replication divides these six genera into two groups. The first group includes *CP-dependent* viruses like *Alfalfa mosaic virus* (AMV) in genus *Alfamovirus* and *Tobacco streak virus* (TSV) in genus *Ilarvirus* requiring either sgRNA or few molecules of CP to initiate infection. The second group includes *CP-independent* viruses like BMV in genus *Bromovirus* and *Cucumber mosaic virus* (CMV) in genus *Cucumovirus* that do not require either sgRNA or CP to initiate infection (Fig. 4.1).

CP-dependent viruses like AMV and TSV package their replication-derived sgRNA into a separate virion. Purified virions of AMV (Fig. 4.1) contain four classes of differently sized particles. Based on their sedimentation profile, they are referred to as bottom (B), middle (M), top b (Tb), and top a (Ta) components. Each B, M, and Tb particle contains one RNA molecule of genomic RNA-1, 2, and 3, respectively (Fig. 4.1). The Ta virions package two molecules of the sgRNA-4. In AMV, CP must have a discrete binding near the 3' end of viral genomic RNAs to correctly recognize RNA by the viral polymerase (Bol, 2005). On the other hand, CP-independent viruses like BMV and CMV package their genomic RNAs 1 and 2 in two distinct virions and co-package genomic RNA3 and sgRNA4 into a third virion. Although the three virion types are homogeneous in size and morphology, they are distinct in their stability and capsid dynamics (Chakravarty, Reddy, & Rao,

2020). As these viruses do not require a sgRNA to initiate infection, it remains unclear why they still co-package it with their genomic RNA3 in infectious virions.

BMV, a prototype of the family *Bromoviridae,* is one of the best-studied tripartite plant RNA viruses concerning genome replication, packaging, and virus assembly (A. L. Rao, Chaturvedi, & Garmann, 2014). The 3.4°A-resolution crystallographic structure of BMV showed that 180 subunits of a single 20 kDa CP packages the three genomic RNAs and the one sgRNA into three types of T=3 icosahedral symmetric virions morphologically indistinguishable by electron microscopy (Lucas, Larson, & McPherson, 2002). The largest two monocistronic genomic RNAs, RNA1 (3.2 kilobases [kb]) and RNA2 (2.8 kb), encoding nonstructural replicase proteins 1a (methyltransferase/helicase-like) and 2a (RNA-dependent RNA polymerase), respectively, get packaged separately into two virion types, $B1^V$ and $B2^V$. The dicistronic genomic RNA3 encodes a nonstructural movement protein (MP) at its 5' and a structural CP at its 3' end. CP is translated from a replication-derived sgRNA4 made by an internal initiation mechanism from a minus-strand RNA3. Genomic RNA3 (2.1 kb) and sgRNA4 (0.8 kb) are co-packaged into a third virion type, $B3+4^V$ (A. L. Rao, 2006).

A previous study investigating the role of the basic residues in the N-terminal arginine-rich RNA-binding motif (N-ARM) of CP demonstrated a single mutation in the amino acid positions 10, 13, and 14 of N-ARM that replaces arginine (R) with a proline (P) residue, induced local necrotic lesions, and the resultant virions failed to move systemically in *Chenopodium quinoa* plants (Choi

& Rao, 2000). In contrast, WT CP resulted in chlorotic local lesions and systemic spread. These proline variants of CP were competent in packaging viral RNA as induction of local lesions by BMV requires the synthesis of CP that is encapsidation-competent (Choi & Rao, 2000; A. L. Rao & Grantham, 1995, 1996; Schmitz & Rao, 1996). However, analysis of packaged RNA revealed that the mutant CP was specifically defective in packaging sgRNA4 both *in vivo* and *in vitro*. Exchanging the proline residue at positions 10, 13, and 14 for another basic residue like lysine rescued the sgRNA4 packaging phenotype (Choi & Rao, 2000). BMV moves between plant cells only in assembled form (Schmitz & Rao, 1996). Also, packaged RNA content has been shown to regulate protein stability in a virus assembly (Bothner et al., 1999; Chakravarty et al., 2020). Nevertheless, most in *vivo* studies performed previously mapped the biologically functional domains of CP (Schmitz & Rao, 1996). Moreover, these studies compared the packaging and symptom phenotype of WT BMV (a mixture of $B1^V$, $B2^V$, and $B3+4^V$) with a mixture of $B1^V$, $B2^V$, and only RNA3 containing virions ($B3^V$). Therefore, it remains obscure how the packaging of sgRNA influences individual capsid dynamics of $B3+4^V$ and $B3^V$.

This study established an agroinfiltration-based system to assemble only $B3^V$ in *Nicotiana benthamiana* using the R10P BMV CP mutant described previously (Choi & Rao, 2000). We then compared the stability (by differential scanning fluorimetry) and capsid dynamics (by limited proteolysis followed by peptide mass-mapping) of the purified $B3^V$ virions with the purified $B3+4^V$ virions

or WT BMV virions. The Western blot followed by Transmission electron microscopy (TEM) analysis of undigested versus trypsin digested samples between the two-virion sets revealed virions of $B3^V$ remained resistant to trypsin at various digestion times whereas virions of $B3+4^V$ treated with trypsin readily digested. However, the matrix-assisted laser desorption/ionization (MALDI) time-of-flight (TOF) mass spectrometry profile of trypsin digested $B3^V$ revealed a profile identical to that of $B3+4^V$, suggesting that only a minor percentage of $B3^V$ virions are susceptible to trypsin digestion. Subsequently, we performed a time-course analysis to compare the expression of BMV CP in the case of $B3^V$ versus $B3+4^V$ expressing local leaves when both virion sets are complemented with $B1^V$ and $B2^V$. The expression of CP was detected in the cluster of cells (sink) away from the infiltrated cells (source) for three time points (4, 6, and 10 days) in the case of WT ($B1^V$+$B2^V$+ $B3+4^V$). However, when $B3^V$ virions are incompetent in packaging sgRNA4 (($B1^V$+$B2^V$+ $B3^V$), the CP was detected in the sink cells only until 4 days and not beyond that. Taken together, our results show that the dynamics of virions packaging only B3 ($B3^V$) is distinct from that of virions co-packaging B3 and sgRNA4 ($B3+4^V$). Also, the differing dynamics exhibited by $B3^V$ and $B3+4^V$ may have important ramifications in pathogenesis.

RESULTS

Throughout this study, virion types $B1^V$, $B2^V$, $B3^V$, and $B3+4^V$ represent individual virions packaging genomic RNA1, RNA2, RNA3 only, and RNA3 plus -4. Wild type (WT) represents a mixture of three virions of BMV, each containing RNA1, RNA2, and RNA3 plus -4 purified from infected *N. benthamiana* plants.

Strategy for in vivo assembly of RNA3+4 containing and only RNA3 containing virion types of BMV

Figure 4.2A summarizes the characteristic features of transfer DNA (T-DNA)-based vectors designed to express the three biologically active genomic RNAs (gRNAs) of BMV (pB1, pB2, and pB3) when transiently expressed in *N. benthamiana* plants. B3/P10 is a B3 variant clone harboring a proline mutation in place of an arginine residue in position 10 of N-ARM. The resultant CP variant expressed by B3/P10 assembles into virions packaging RNA1, 2, and 3 but is defective in packaging sgRNA4. Likewise, T-DNA constructs shown in Fig. 4.2B are designed to transiently express BMV replicase proteins 1a (p1a) and 2a (p2a). A strategy for the separate assembly of only RNA3 containing and RNA3+4 containing virion types of BMV is shown schematically in Fig. 4.3. Before designing this strategy, we considered the following three criteria: first, genome packaging in bromoviruses is functionally coupled to replication (P. Annamalai & A. L. Rao,

2006; Annamalai, Rofail, Demason, & Rao, 2008), i.e., only the replication-derived progeny RNA is packaged into virions; second, CP in BMV, a related bromovirus, expressed in the absence of replication is non-specific in RNA packaging (Annamalai & Rao, 2005); third, the packaging specificity is dictated by an interaction between BMV CP and replicase protein 2a (Chaturvedi & Rao, 2014). Therefore, keeping these requirements in perspective, the strategy shown in Fig. 4.3 was designed to assemble desired virion types by infiltrating the following sets of inocula. (i) Agrotransformants of all three plasmids expressing full-length RNA (Fig. 4.3A) infiltrated into plants served as controls. (ii) An inoculum was formulated to assemble B3+4^{V} (co-packaging B3 and sgB4) by mixing agrotransformants p1a, p2a, and pB3 (Fig. 4.3B). The following infiltration into *N. benthamiana* leaves, p1a, would result in an mRNA competent to translate 1a. Infiltration of agrotransformant p2a would produce an mRNA competent to translate 2a, but both mRNAs would not be replicated since it lacks 5' and 3' noncoding regions (Fig. 4.2B). The transiently expressed p1a complexed with p2a would assemble into a functional replicase resulting in the replication of B3 followed by the synthesis of sgC4 for CP production, ultimately leading to the assembly of B3+4^{V} (Fig. 4.3B). (iii) An inoculum was formulated to assemble B3^{V} (packaging only B3) by mixing agrotransformants p1a, p2a, and pB3/P10 (Fig. 4.3C). Assembly of a functional replicase would result in the replication of B3/P10 followed by the synthesis of sgB4 for CP production. The resultant virions package only RNA3, as the P10

mutation disrupts the crucial interaction of N-ARM with sgRNA4 inhibiting the packaging of sgRAN4.

Characteristic properties of B3+4^{V} and B3^{V}

Purified virions from *N. benthamiana* leaves infiltrated with either control infiltrations of WT (i.e., pB1+pB2+pB3) (Fig. 4.3A) or with p1a+p2a+pB3 (i.e., B3+4^{V}) (Fig. 4.3B), or p1a+p2a+pB3/P10 (i.e., B3^{V}) (Fig. 4.3C) were subjected to negative-stain EM examination. Results shown in Fig. 4.5B, top panel indicate that virions of B3+4^{V} and B3^{V} are indistinguishable from those of the WT control (a mixture of B1^{V}, B2^{V}, and B3+4^{V}) in morphology and size (i.e., the average diameter being 28 nm).

A subsequent Northern blot experiment confirmed that WT, B3+4^{V}, B3^{V} encapsidated expected RNA progeny (data not shown).

Virion stability of B3+4^{V} and B3^{V}

To test the relative thermal stability of B3+4^{V} and B3^{V}, a differential scanning fluorimetry (DSF) assay was performed as described in Materials and Methods. The hydrophobic dye SYPRO orange used in this assay binds to the hydrophobic regions of the unfolding viral CP during thermal denaturation. The fluorescence intensity increases following its binding to more accessible areas (Rayaprolu et al.,

2014). The DSF analysis of the temperature-dependent melting of virions of B3+4^{V}, B3^{V}, and control samples (WT BMV assembled in *N. benthamiana* and lysozyme) under three buffer and pH conditions are summarized in Fig. 4.4. Thermal denaturation in virus suspension buffer (pH 4.5) showed near-identical thermal stability in virions of B3+4^{V}, B3^{V}, and WT (Fig. 4.4, top panel, left) with all three virion types displayed melting at ~70°C (Fig. 4.4, top panel, left). However, B3^{V} showed a broader melting peak than B3+4^{V} and WT BMV, showing B3^{V} started to melt at a slightly lower temperature than B3+4^{V} and WT BMV. By contrast, in phosphate buffer (pH 7.2), all three virion types displayed thermally unstable populations at ~50°C and ~70°C. Under this condition, all three virion types predominantly melted at ~50°C, with a minimal peak present at ~70°C (Fig. 4.4, top panel, middle). Thermal denaturation in water (pH 7.1) showed a similar trend of thermal stability in virions of B3+4^{V}, B3^{V}, and WT (Fig. 4.4, top panel, right). The virions of B3^{V} and WT melted at ~70°C in water, whereas in this condition, B3+4^{V} melted at a slightly higher temperature of ~75°C, as demonstrated previously (Chakravarty et al., 2020). As expected, the thermal stability of lysozyme remained indistinguishable under all three buffer conditions ((Fig. 4.4, bottom panel).

Analysis of the capsid dynamics of B3+4^{V} and B3^{V} by trypsin proteolysis followed by MALDI-TOF

Viral capsids having identical crystallographic structures can be easily distinguished using limited proteolysis followed by mass spectrometry to identify the released cleavage products of the capsid subunits (Bothner et al., 1999). Proteolytic cleavage sites present on the capsid surface will be the first residues accessible to the protease and among the first digestion products released. Accordingly, MALDI-TOF analysis of proteolytic cleavage products would contribute to understanding the dynamic nature of the capsid structure.

The differential capsid dynamics of B3+4^{V} and B3^{V} were investigated by trypsin digestion performed at various time points (10 min, 20 min, 45 min, and 3 hr) to verify whether these two virion types display any discernible effect on the rate of digestion (see Materials and Methods). Parallel digestions were performed with WT virions (a mixture of B1^{V}, B2^{V}, and B3+4^{V}) assembled in *N. benthamiana* as control. Trypsin cleaves peptides on the C-terminal side of lysine and arginine residues (X-K/-X and X-R/-X); furthermore, if a proline residue is on the carboxyl side of the cleavage site, the cleavage will not occur. Therefore, the BMV CP linear sequence is 189-amino acids (aa) long and has 22 potential trypsin cleavage sites as determined by UCSF Protein Prospector Tool.

Following trypsin digestion, each virion type preparation was divided in half. One-half was subjected to Western blot analysis using an anti-CP antibody to

identify the cleavage peptides. In contrast, the second half was subjected to EM analysis to verify the integrity of virions. Results are summarized in Fig. 4.5A, and B. Undigested CP of virions of B3+4^{V} and B3^{V,} as well as a control sample of WT BMV (Fig. 4.5A, top, WT BMV: lane 1, B3+4^{V}: lane 1, B3^{V}: lane 1), migrated as a single intact band with the expected molecular weight (~20 kDa). In all three undigested samples, monomers and dimers of CP are detected in the Western blot.

Analysis of the trypsin cleavage products for each virus sample revealed exciting profiles. Virions of B3+4^{V} treated with trypsin get readily digested as early as 10 mins, evidenced by the Western blot analysis (Fig. 4.5A, top, B3+4^{V}: lanes 2-5). In contrast, virions of B3^{V} remained highly resistant to trypsin at different digestion times and appeared as a stable single intact band when analyzed by the Western blot (Fig. 4.5A, top, B3^{V}: lanes 2-5). As expected, the digestion profile of WT BMV reflected the digestion pattern as seen in B3+4^{V} (Fig. 4.5A, top, WT BMV: lanes 2-5) as the type 3 virions are the predominant virion type in WT BMV, which is a mixture of B1^{V}, B2^{V}, and B3+4^{V} (Chakravarty et al., 2020). Using ImageJ, we compared the intensity of the CP band in undigested vs. digested samples for B3+4^{V} and B3^{V} virion sets. For virions of B3+4^{V} as well as in WT BMV control, trypsin digested ~68% of the CP, resulting in several faster-migrating peptide fragments in addition to a single intact protein band. Whereas in B3^{V}, ~87% CP of B3^{V} virions remains highly resistant to trypsin. These profiles did not change even after the digestion time to trypsin was extended from 10 min to 3 hr (Fig. 4.5A, top).

Transmission electron micrographs (TEM) of negatively stained preparations of undigested and trypsin-digested virions (Fig. 4.5B) confirmed the Western blot data. Undigested virions of B3+4^{V}, B3^{V}, and WT BMV are identical in morphology and size (i.e., the average diameter being 28 nm). Trypsin digested B3+4^{V} virions appear entirely degraded after 10 mins of treatment, whereas trypsin treated B3^{V} remains intact under TEM after the same treatment time. The WT BMV control appeared significantly degraded under TEM after 10 mins of trypsin treatment with a few intact virions presumably containing RNA1 and RNA2 (Chakravarty et al., 2020).

Subsequently, MALDI-TOF was used to identify the cleavage products present in the trypsin-digested virion samples of B3+4^{V}, B3^{V}, and WT BMV. The deconvoluted mass spectrum obtained from the total ion chromatogram (TIC) of the undigested samples of B3+4^{V}, B3^{V}, and WT BMV indicates that all the virions are assembled from a single protein of 20 kDa, which underlines their purity. A representative example of the deconvoluted mass spectrum of undigested virions is shown in Fig. 4.6A.

Identification of the cleavage products of B3+4^{V} and B3^{V} at various time points by mass mapping suggested the following: (i) amino acids K65, R103, K111, and K165, predicted to be located on the surface of the BMV crystal structure (Lucas et al., 2002), are located on the surface of the B3+4^{V} capsid and hence are readily accessible for cleavage (Fig. 4.6B). In BMV, the noncovalent CP dimers are the building blocks of icosahedral viruses (Zlotnick, Aldrich, Johnson, Ceres,

& Young, 2000). The stability of these dimers is controlled by the interaction between the invading C-terminal arm and the N-terminal clamp of the adjacent CP subunits, and any mutations engineered in the C terminus disrupt virion assembly (Zhao, Fox, Olson, Baker, & Young, 1995). Thus, cleavage at K165 alone is sufficient to disrupt the capsid structure. This explains why B3+4^{V} appears visibly degraded in EM (Fig. 4.5). (ii) The trypsin digested B3^{V} appeared as a stable single intact band when analyzed by the Western blot and remains intact under TEM. However, MALDI-TOF analysis of the released peptides revealed a profile identical to that of B3+4^{V}, suggesting that only a small percentage of B3^{V} virions are susceptible to trypsin digestion and a vast majority of the B3^{V} retained their structural integrity upon trypsin treatment (Fig. 4.7). The fragments released during trypsin treatment of B3^{V} did not affect the overall assembly. Interestingly, trypsin digestion of B3+4^{V} releases a peptide encompassing aa 131-142 in all time points, which is not recovered in B3^{V} in any of the time points. Therefore, this residue could be of potential importance in retaining structural integrity. (iii) MALDI-TOF analysis profiles of WT BMV virions are indistinguishable from those of B3+4^{V} (Fig. 1.11). This is not surprising since purified virion preparation of WT BMV is a mixture of all three virion types, with B3+4^{V} constituting ~60% of the total (Fig. 4.8) (Chakravarty et al., 2020).

Influence of sgRNA4 packaging in virus spread

In *C. quinoa,* the induction and spread of lesions make it challenging to determine a clear distinction between inoculated and uninoculated areas on a leaf, whereas, in *N. benthamiana,* BMV does not induce any visible symptoms. Therefore, using *N. benthamiana,* we can investigate the cell-to-cell movement of virion types from source to sink areas in local leaves. Interesting results were obtained when the spread of viral progeny from infiltrated cells of *N. benthamiana* to adjacent cells was analyzed in either WT BMV or pB1+pB2+pB3/P10. In the case of WT BMV, a mixture of agrotransformants of pB1+pB2+pB3 was infiltrated in the source area as indicated in Fig. 4.9A. Following infiltration, the expression of BMV CP was detected in the source and sink regions in WT after 4 days. The expression continued after 6 and 10 days in both the source and the sink (Fig. 4.9B).

However, in the case of pB1+pB2+pB3/P10 infiltration, the expression of CP was detected in the source and sink area only until 4 days. The relative expression of CP in the B3/10 infiltrated source was much lower than that of the WT infiltrated source. Additionally, after 4 days, the CP was detected only in the source area but not in the sink area in the case of B3/P10 (Fig. 4.9B). Therefore, differential capsid dynamics exhibited by $B3^{V}$ and $B3+4^{V}$ may have important implications in cell-to-cell spread and ultimately in viral pathogenesis.

DISCUSSION

The primary focus of this study is to investigate the importance of a genetically redundant subgenomic RNA4 packaging in BMV that does not require the presence of the sgRNA4 to initiate infection. Therefore, we first assembled the physically indistinguishable RNA3+4 and RNA3 only containing virions of BMV and investigated if those two virion types can be distinguished in solution. Using agroinfiltration, we assembled B3+4^{V} and B3^{V} separately *in planta* as described previously (Fig. 4.3) (Chakravarty et al., 2020; Choi & Rao, 2000). Although the two virion types have near-identical thermal stability (Fig. 4.4) and are physically and morphologically indistinguishable (Fig. 4.5B, top panel), application limited proteolysis showed the B3+4^{V} are highly susceptible to trypsin cleavage. In contrast, a vast majority of B3^{V} virions are remarkably resistant to degradation by trypsin. The MALDI-TOF profile of trypsin digested B3+4^{V} and B3^{V} virions are nearly similar, except the fragments released during trypsin treatment of B3^{V} are relatively low abundance and did not affect the overall assembly. A study of CCMV capsid dynamics has shown that a single mutation at K42R gives rise to salt-stable and trypsin-resistant phenotype in CCMV virions while revealing identical MALDI-TOF fragmentation patterns (Speir et al., 2006). This study observed that B3+4^{V} releases a peptide resulting from cleave at residue K130, which shows this residue is exposed at the capsid surface of B3+4^{V}, readily accessible for trypsin cleavage. However, any peptide fragment involving K130 is not recovered in trypsin-treated

$B3^V$. Therefore, this residue could be of potential importance in retaining structural integrity in $B3^V$ upon digestion.

BMV requires both movement protein and encapsidation-competent CP for cell-to-cell movement and induction of visible lesions in *C. quinoa* (A. L. Rao & Grantham, 1996). It was previously shown that B3/P10 translates into R10P CP variant, which is packaging competent for three genomic RNAs of BMV. This CP variant induced local lesions on a time scale like WT control; however, the lesions expanded with time resulting in necrotic patches in *C. quinoa* as the virus failed to move systemically even after 3 weeks after inoculation (Choi & Rao, 2000). Our results are consistent with this observation and add further details by showing BMV virions unable to package sgRNA4 does not accumulate in cells away from the initially inoculated cells beyond 4 days post infiltration. We hypothesize that translation of B3/P10 derived CP results in the assembly of virions leading to the local-cell-to-cell spread of $B1^V$ and $B2^V$ from source to sink area for a limited amount of time until 4 days detected through Western blot. We have shown that defects in sgRNA4 packaging result in altered capsid dynamics in $B3^V$ as it has a different RNA content than $B3+4^V$ (Fig. 4.5). Based on the progeny analysis, it is likely that these altered dynamics in $B3^V$ may result in suboptimal interaction with the host and inhibit cell-to-cell movement of this virion type from the source. As the sink areas may be lacking the RNA3 containing virions, these areas do not support further replication of viral progeny, failing detection of CP beyond 4 days and ultimately preventing the systemic spread of the virus. The $B3^V$ virions having an

altered capsid dynamic may fail to move locally from cell-to-cell resulting in necrotic lesion induction. To test this hypothesis mentioned further, it would be interesting to purify virions from the source and sink regions of WT (pB1+pB2+pB3) vs. pB1+pB2+pB3/P10 infiltrated leaves and analyze the RNA those virions package. Also, in the absence of sgRNA4, a possibility of delay in CP synthesis may happen. However, this possibility was discarded as the CP level was consistent in B3/P10 infiltrated sources for 10 days after infiltration compared to no CP detected in sinks after 4 days. Another possibility of sgRNA4 packaging defect could be disruption of plus-to-minus strand ratio, which a Northern blot analysis should investigate.

MATERIALS AND METHODS

Agroplasmids used in this study

Construction and characteristic properties of agroplasmids pB1, pB2, and pB3 (Fig. 4.2A), engineered to express biologically active full-length genomic RNAs of BMV following agroinfiltration into plants, were described previously (Annamalai & Rao, 2005). The pB3/P10 is a B3 variant clone harboring a proline mutation in place of an arginine residue in position 10 of N-ARM producing virions defective in packaging sgRNA4 as described previously (Choi & Rao, 2000). Likewise, agroplasmids p1a and p2a (Fig. 4.2B) were engineered to transiently express replicase protein 1a (p1a), replicase protein 2a (p2a), respectively, as described previously (Annamalai & Rao, 2005; Seo, Kwon, & Rao, 2012).

Agroinfiltration, total protein extraction, virion purification, negative-stain electron microscopy, and Western blot analysis

All agroplasmids used in this study were transformed into *Agrobacterium* strain GV3101. The transformed *Agrobacterium* cells containing the desired transformant were infiltrated into the abaxial surface of wild-type *N. benthamiana* leaves described previously (P. Annamalai & A. L. N. Rao, 2006). We used the identical procedure used to purify WT, B3+4^{V}, and B3^{V} virions from 4 dpi

agroinfiltrated leaves of *N. benthamiana* followed by sucrose density gradient centrifugation as described previously (A. Rao, Duggal, Lahser, & Hall, 1994). For negative-stain EM analysis, virions were imaged using a Tecnai 12 operated at 120 KeV, and images were recorded digitally. Western blot analysis of undigested and trypsin-digested virion samples using anti-CP antibodies was performed as described previously (Annamalai & Rao, 2005). Following Western blot, the intensity of bands was quantified in undigested versus trypsin digested samples using ImageJ software (Schneider, Rasband, & Eliceiri, 2012).

Differential scanning fluorimetry

DSF was performed as described previously (Rayaprolu et al., 2014). Desired virion samples and control (lysozyme) samples were resuspended either in Nanopure sterile water (pH 7.1), in virus suspension buffer (50 mM sodium acetate, 8 mM magnesium acetate, pH 4.5), or in 100 mM phosphate buffer (pH 7.2). The experiment was performed three times independently, using three replicates for each sample. DSF data were analyzed and plotted as described previously (Chakravarty et al., 2020; Rayaprolu et al., 2014).

MALDI-TOF

For MALDI-TOF, analysis was performed as described previously (Chakravarty et al., 2020). A desired purified virion preparation was diluted to 1 mg/ml in 25 mM Tris-HCl, 1 mM EDTA buffer. A 30 µl sample (i.e., 30 µg of the desired virion preparation) was digested with a 1:100 (wt/wt) ratio of trypsin (Pierce Trypsin protease, mass spectrometry grade; Thermo Fisher Scientific) to the virus for various time points at 25°C (Bothner et al., 1999). 10 µl of water was added to 20 µl of the digested sample. Approximately 0.5 µl of each digested or undigested (control) sample was analyzed on an AB Sciex TOF/TOF 5800 MALDI MS with -cyano-4-hydroxycinnamic acid matrix. The instrument was calibrated with standards, and the test samples were analyzed with external calibration. The accuracy is approximately 0.05 Da. The MALDI-TOF data were analyzed with AB Sciex Data Explorer, and baseline was corrected with a peak width of 32, flexibility of 0.5, and degree of 0.1. For noise removal, the standard deviation was set at 2. To determine the peak detection criteria, the percent centroid was taken as 50, the signal/noise (S/N) threshold was 3, and the noise window width m/z was 250. The threshold after S/N recalculation was set at 20. The peptide fragments were assigned based on the UCSF Protein Prospector's MS-Digest function.

Progeny analysis

The analysis of viral derivative progeny was done as described previously (Bamunusinghe, Chaturvedi, Seo, & Rao, 2013). To test the expression of viral CP in a cluster of agroinfiltrated cells (source) vs. non-infiltrated cells away from source (sink) areas, agrocultures of either WT BMV or pB1+pB2+pB3/P10 was spot infiltrated in the abaxial surface of *N. benthamiana* leaves as schematically shown in Fig. 4.9A. Leaf discs measuring about 4 mm were excised from the source and sink (approximately 20 mm from the source) at 4, 7, and 10 dpi, respectively. The leaf discs were ground in liquid nitrogen. Total protein was extracted in 3 volumes of extraction buffer (20mM Tris-Cl; pH 7.5, 1mM EDTA; pH 8.0, 5mM DTT). The leaf slurry was centrifuged at 14,000 rpm for 5 minutes, and the supernatant was used for downstream analysis of total proteins using SDS-PAGE and Western blot.

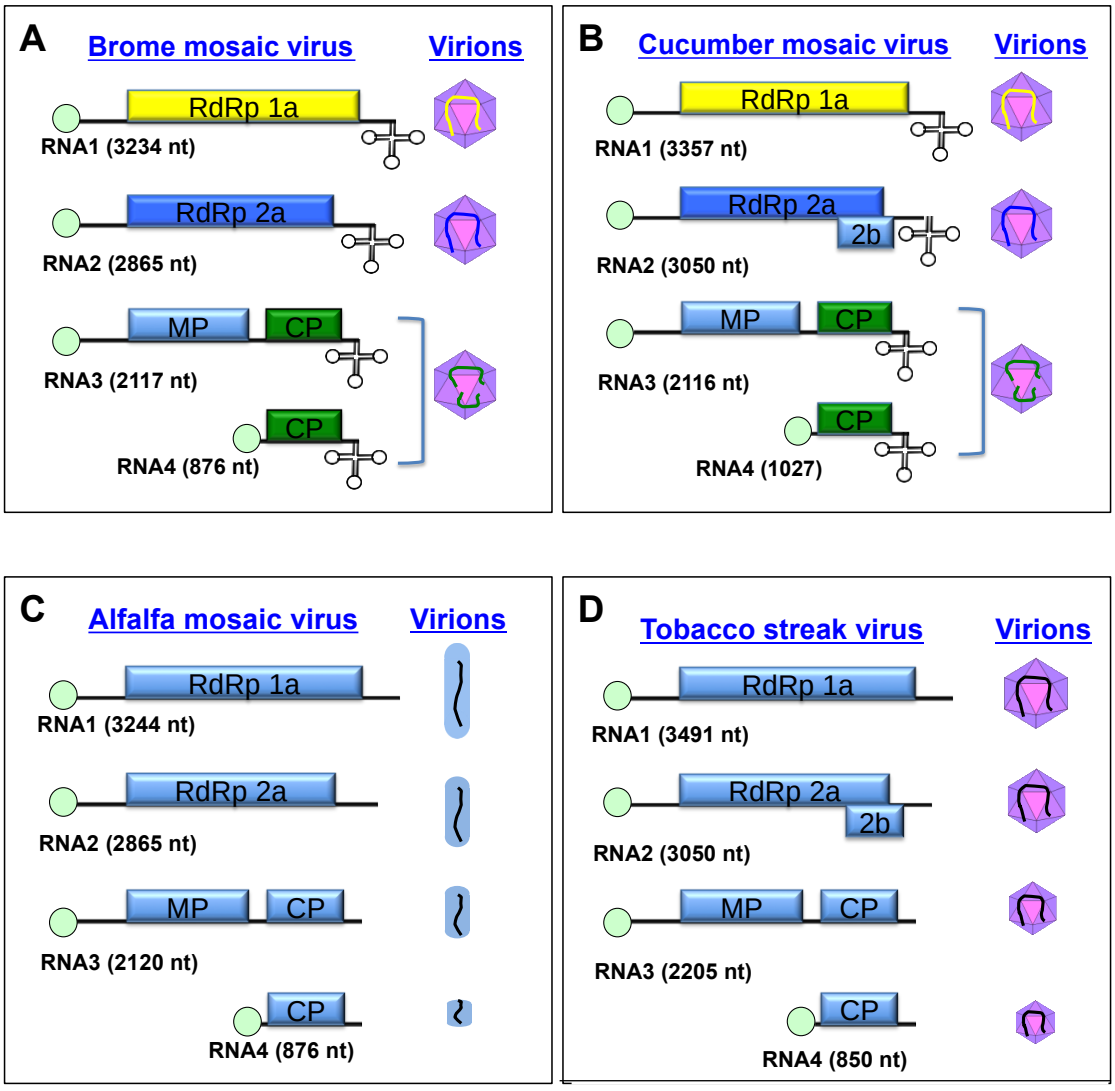

Figure 4.1 Genome organization and packaging scheme of salient members of the family *Bromoviridae*. (A) Brome mosaic virus (BMV) and (B) Cucumber mosaic virus (CMV) are CP-independent viruses that do not require sgRNA4 or CP to initiate infection but co-packages its sgRNA4 with RNA3. (C) Alfalfa mosaic virus (AMV) and (D) Tobacco steak virus (TSV) are CP-dependent viruses that require sgRNA4 or CP to initiate infection and packages its sgRNA4 in a separate virion.

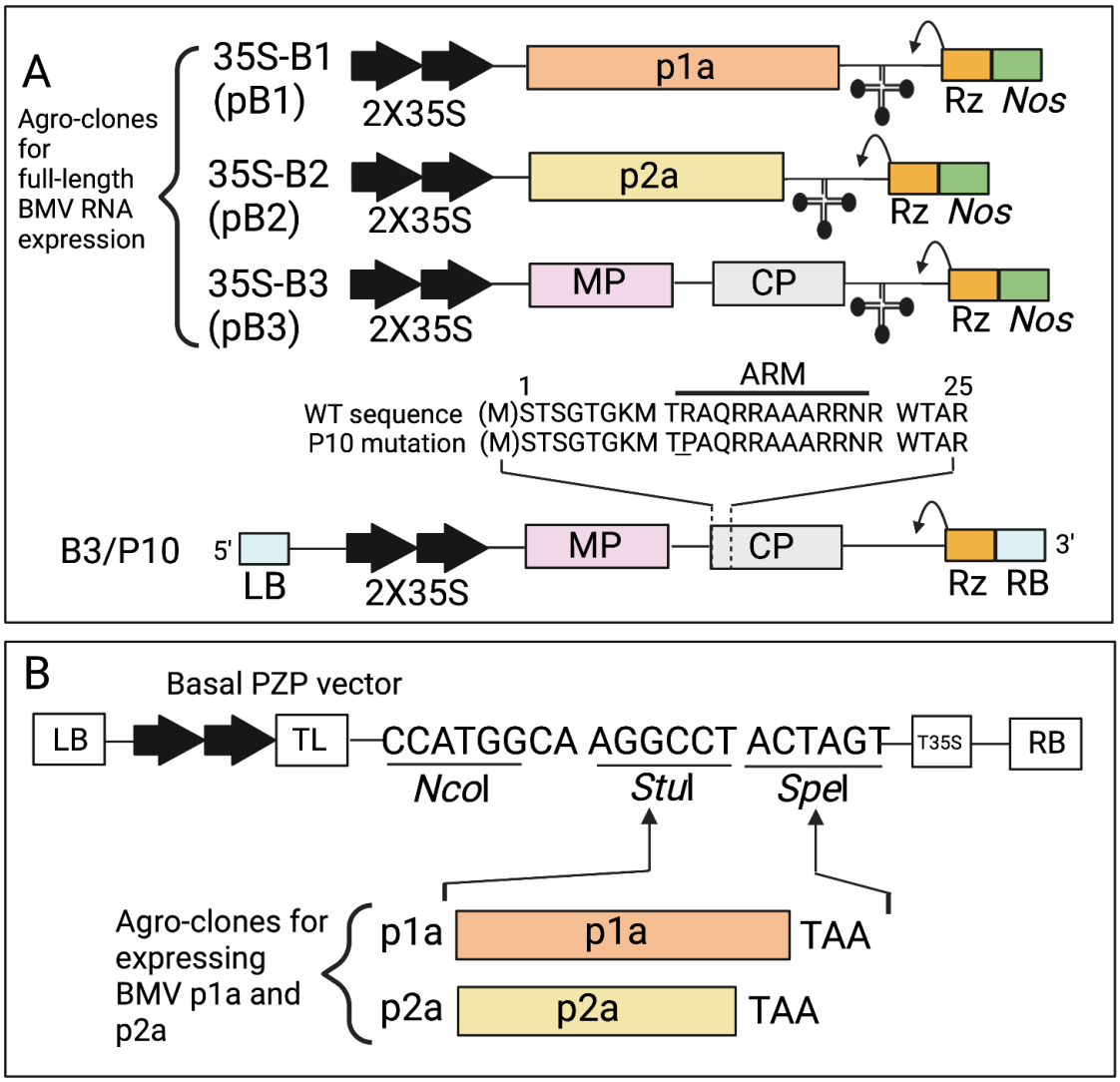

Figure 4.2 Characteristic features of agroplasmids used in this study. (A) Characteristics of agroplasmids harboring BMV genomic RNAs used for transient expression in plants. The 35S-B1 (pB1), 35S-B2 (pB2), and 35S-B3 (pB3) constructs contain full-length cDNA copies of BMV genomic RNA1 (B1), -2 (B2), and -3 (B3), respectively. B3/P10 indicates a B3 mutant construct harboring a proline mutation in place of the 10th arginine residue in N-ARM. The resultant CP variant expressed by B3/P10 assembles into virions packaging RNA1, 2, and 3 but is defective in packaging sgRNA4. Single lines and open boxes represent noncoding and coding regions, respectively. Monocistronic B1 encoding replicase protein 1a (p1a) and monocistronic B2 encoding replicase protein 2a (p2a) are indicated. In B3, the locations of the movement protein (MP) and coat protein (CP) genes are shown. At the 3' end of each construct, the clover leaf-like conformation represents a tRNA-like motif conserved among all three BMV genomic RNAs. Two black arrows at the 5' ends represent the double 35-S. A bent arrow indicates the

predicted self-cleavage site by the ribozyme. The location of the *Nos* terminator is also indicated. (B) Agroconstructs for transient expression of p1a and p2a. Open reading frames (ORFs) of BMV p1a and p2a were fused in-frame to each pair of binary vectors using *Stu*I and *Spe*I sites. Each binary vector contained, in sequential order, a left border of T-DNA (LB), a double 35S promoter (35SX2), a tobacco etch virus (TEV) translation enhancer leader sequence (TL), multiple cloning sites, a 35S terminator (T35S), and a right border of T-DNA (RB) (Annamalai & Rao, 2005; Seo et al., 2012).

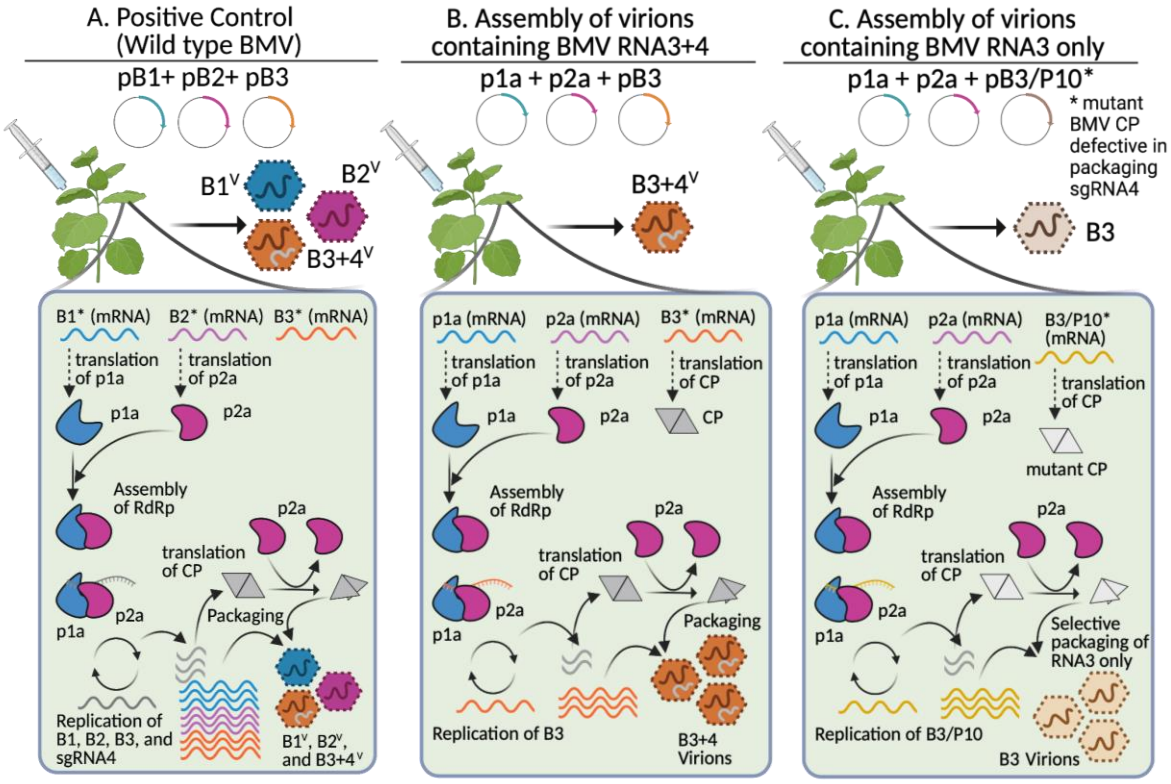

Figure 4.3 Schematic representation of the strategy used for autonomous assembly of BMV WT, B3+4^{V}, and B3^{V} *in vivo*. (A) (Positive control) Infiltration of the inoculum containing a mixture of pB1+pB2+pB3 would induce WT BMV infection resulting in the assembly of a mixture of all three virions. (B) Assembly of virions packaging RNA3+4 (B3+4^{V}). The inoculum shown in this panel is formulated to assemble virions packaging B3 RNA and sgB4 by mixing agrotransformants of p1a, p2a, and pB3 (see Fig. 4.2 for details). The inoculum is infiltrated into *N. benthamiana* leaves. Transcription of p1a results in an mRNA competent to give replicase p1a but not competent to be replicated whose translation gives functional replicase protein p1a; similarly, agrotransformant p2a results in an mRNA competent to give replicase p2a but not competent to be replicated because it lacks the requisite 5' and 3' noncoding regions. As a result, a functional replicase complex is assembled from proteins p1a and p2a, which directs replication of B3 followed by the synthesis of sgB4 for CP production. B3 RNA and sgRNA4 get packaged into virions by the CP subunits derived from the translation of sgRNA4. (C) Assembly of virions packaging RNA3 only. The inoculum shown in this panel is formulated to assemble virions packaging only B3 RNA by mixing agrotransformants of p1a, p2a, and pB3/P10 (see Fig. 4.2 for details) (Choi & Rao, 2000). The inoculum is infiltrated into *N. benthamiana* leaves. Transcription of p1a results in an mRNA competent to give replicase p1a but not

competent to be replicated whose translation gives functional replicase protein p1a; similarly, agrotransformant p2a results in an mRNA competent to give replicase p2a but not competent to be replicated because it lacks the requisite 5’ and 3’ noncoding regions. As a result, a functional replicase complex is assembled from proteins p1a and p2a, which directs replication of B3/P10 followed by the synthesis of sgB4 for CP production. The resultant virions package only RNA3, as the P10 mutation disrupts the crucial interaction of N-ARM with sgRNA4 inhibiting the packaging of sgRNA4.

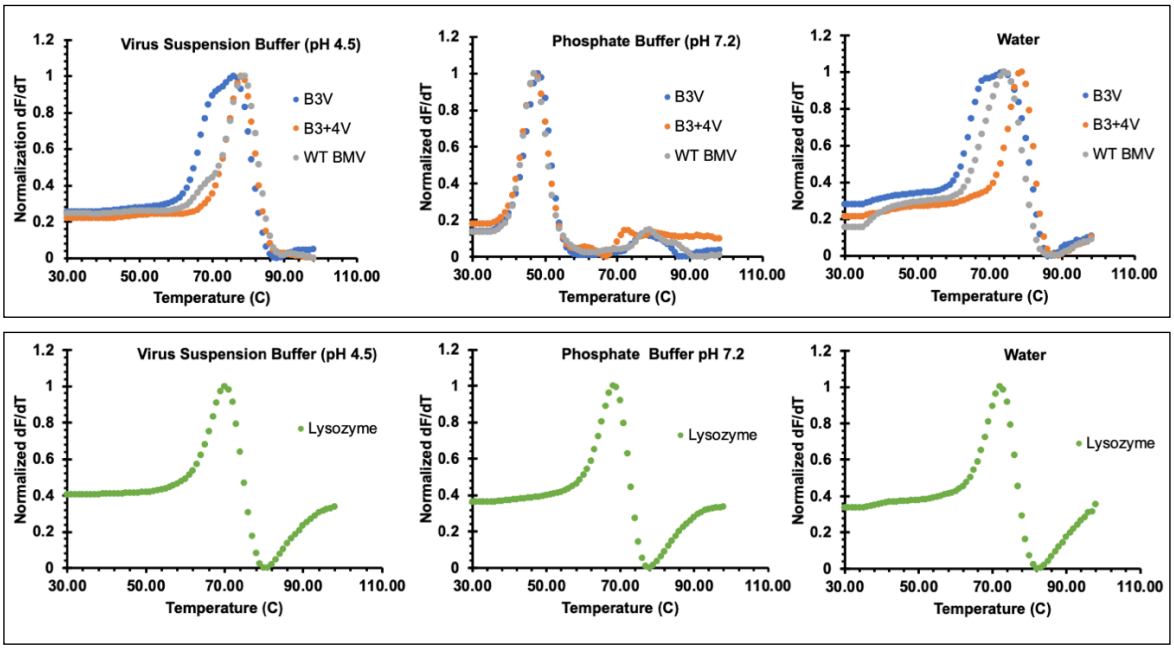

Figure 4.4 Stability analysis of the B3+4^{V}, B3^{V}, and WT BMV virions using differential scanning fluorimetry (DSF). DSF measurements of derivative of fluorescence intensity as a function of temperature for each virion type normalized so that the maximum of the derivative is set to 1 (y-axis) during heating of B3+4^{V}, B3^{V}, and WT (A) and lysozyme (control) (B) at various temperatures (x-axis) under indicated conditions. (Top panel) The virions of B3+4^{V}, B3^{V}, and WT BMV displayed near-identical temperature dependence (~70°C) for melting in the sterile water (pH 7.1) and virus suspension buffer (pH 4.5). However, B3^{V} showed a broader melting peak as compared to B3+4^{V} and WT BMV. All three virion types melted at a lower temperature (~50°C) in 100 mM phosphate buffer (pH 7.2) (see "Virion stability of B3+4^{V} and B3^{V}" for details). (Bottom panel) Lysozyme used as positive control showed identical melting characteristics (~60°C) under all three solution conditions.

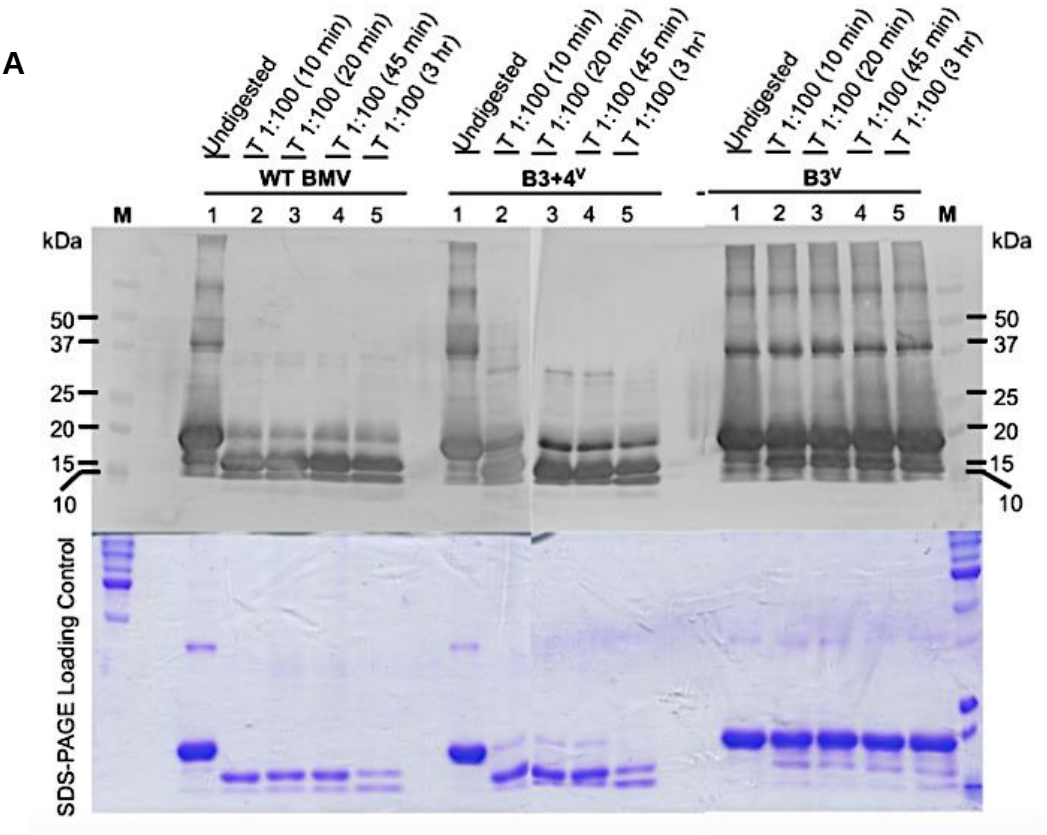
A
Undigested
T 1:100 (10 min)
T 1:100 (20 min)
T 1:100 (45 min)
T 1:100 (3 hr)
WT BMV
B3+4V
B3V
M
1 2 3 4 5
kDa
50
37
25
20
15
10
SDS-PAGE Loading Control

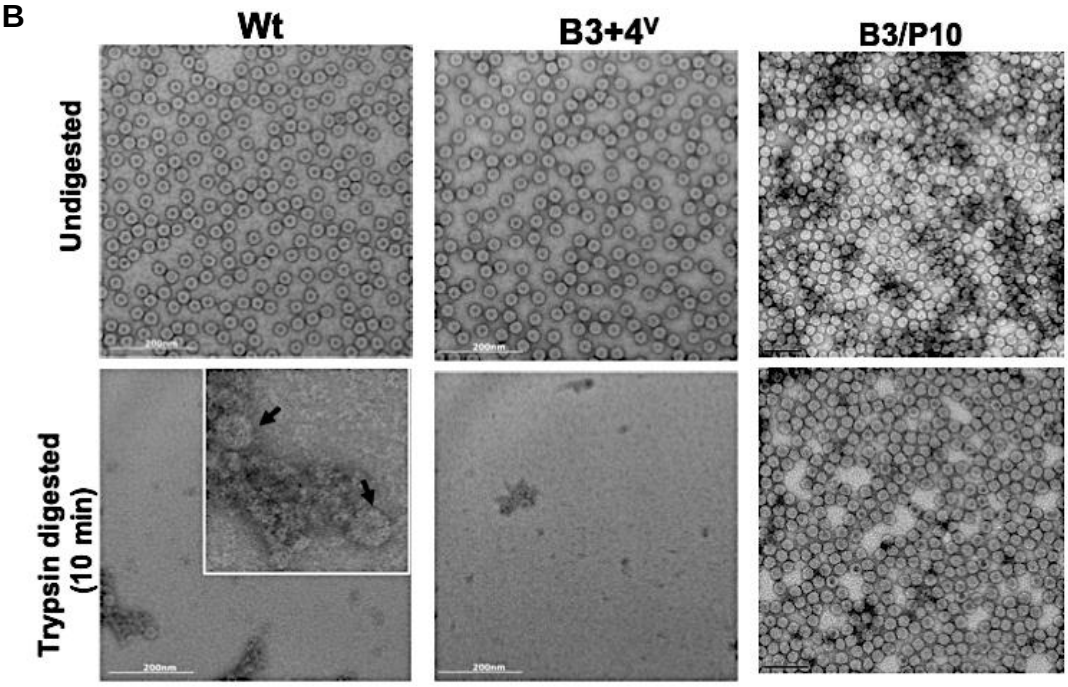
B
Wt
B3+4V
B3/P10
Undigested
Trypsin digested (10 min)
200nm

Figure 4.5 Proteolysis of B3+4^{V}, B3^{V}, and WT-BMV monitored by Western blotting and negative-stain EM analysis. (A) Western blot for B3+4^{V}, B3^{V}, and WT-BMV. Before Western blot analysis, each virion preparation was either undigested or digested with trypsin for 10 min, 20 min, 45 min, or 3hr. (B) Negative-stain electron micrographs show the integrity of the undigested and trypsin-digested virion preparations of the indicated samples.

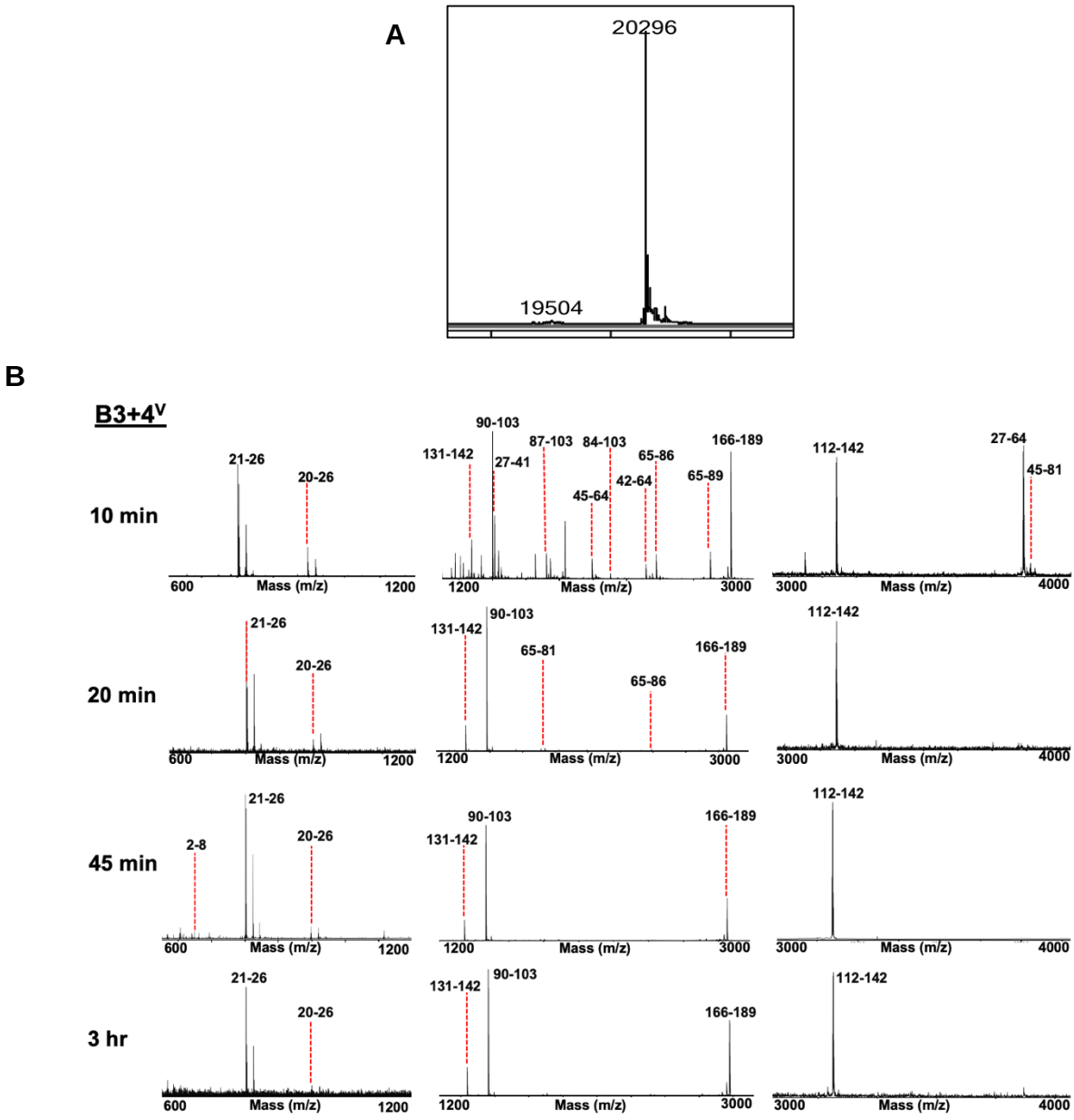

Figure 4.6 MALDI-TOF analysis of undigested and trypsin-digested virions. (A) Mass spectrometry of undigested virions of $B3^{V}$, $B3+4^{V}$, and WT-BMV yielded a single peak with a value of 20,296 Da. (B) MALDI-TOF analysis of peptides released from $B3+4^{V}$ at the indicated time points following digestion with trypsin. Peaks are labeled with corresponding polypeptide fragments of predicted amino acid residues.

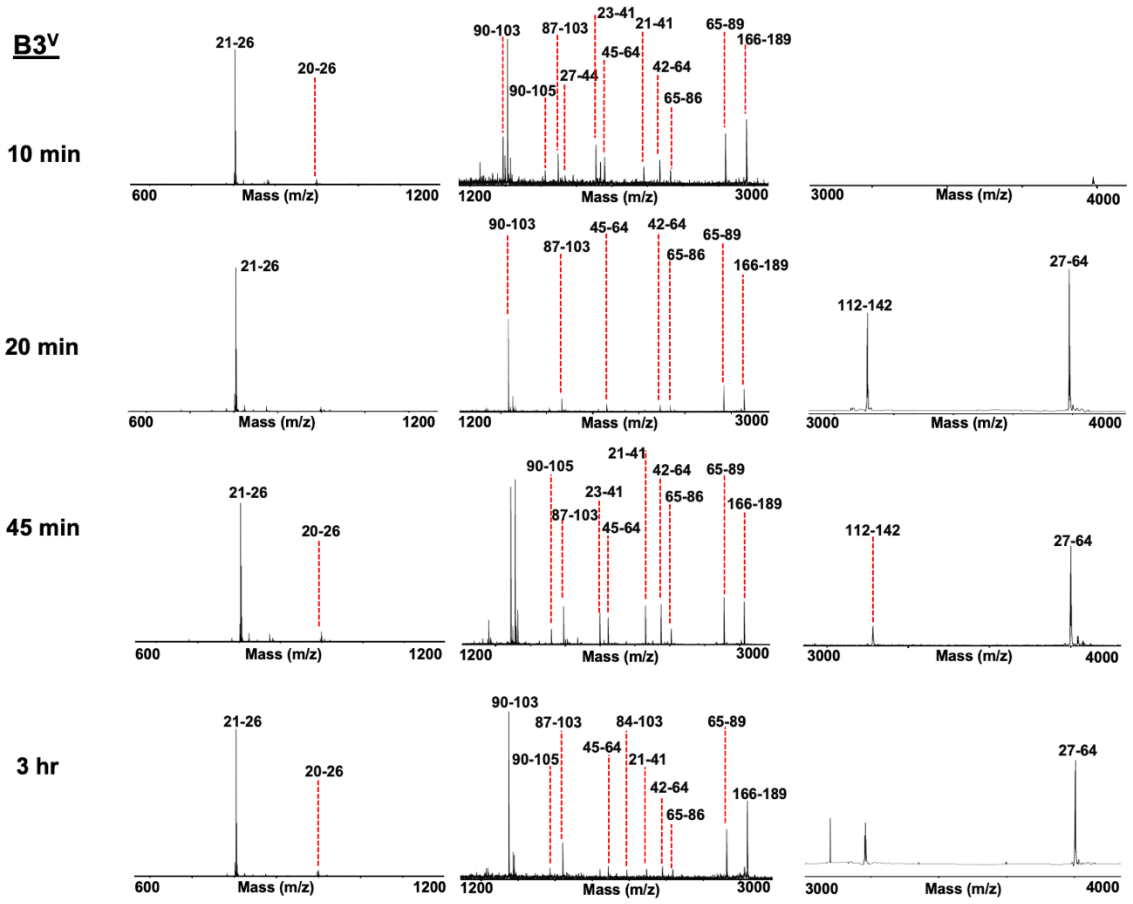

Figure 4.7 MALDI-TOF analysis of peptides released from $B3^V$ at the indicated time points following digestion with trypsin. Peaks are labeled with corresponding polypeptide fragments of predicted amino acid residues.

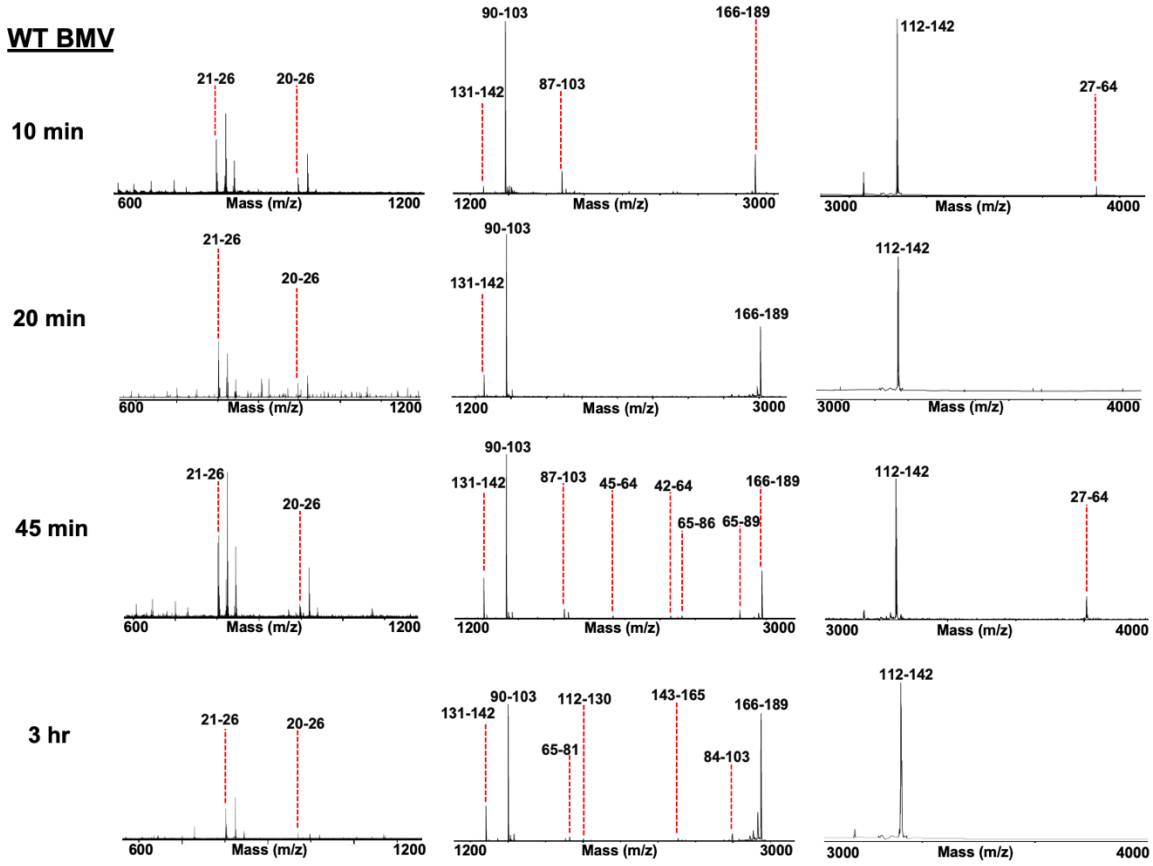

Figure 4.8 MALDI-TOF analysis of peptides released from WT BMV at the indicated time points following digestion with trypsin. Peaks are labeled with corresponding polypeptide fragments of predicted amino acid residues.

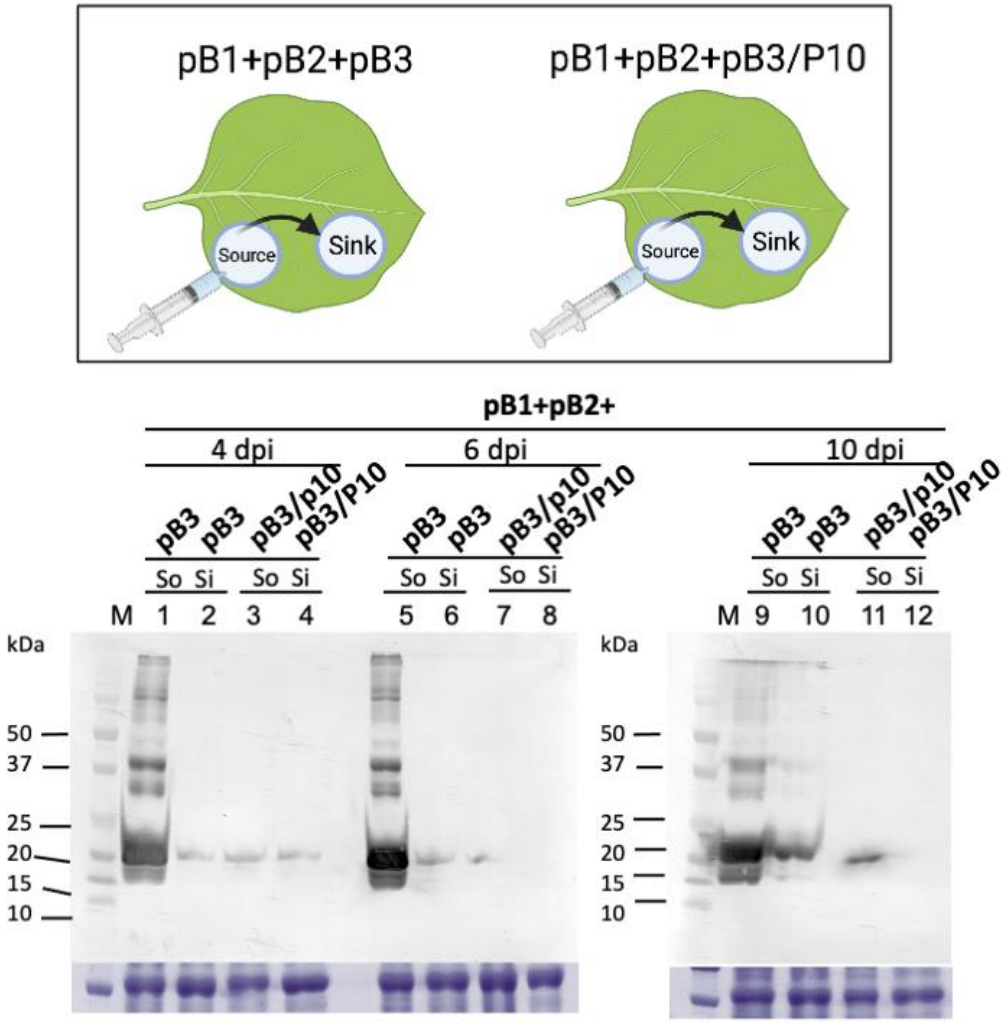

Figure 4.9 The analysis of viral derivative progeny in pB1+pB2+pB3 vs. pB1+pB2+pB3/P10 in a cluster of agroinfiltrated cells (source) vs. non-infiltrated cells away from source (sink) areas. (A) The inoculum and relative position of the source and sink leaf discs are indicated. (B) The SDS-PAGE gel stained with Coomassie Brilliant Blue R-250 to (top panel) shows the relative accumulation in source vs. sink areas when agroinfiltrated leaves expressing the indicated set of inocula are analyzed at 4, 6, and 10 dpi. (Bottom panel) The Western blot shows the relative accumulation of BMV CP when the samples are loaded in the order as mentioned above in lanes 1-12. Each lane has 30 µg of total protein estimated by Bradford protein assay.

REFERENCES

Annamalai, P., & Rao, A. L. (2005). Replication-independent expression of genome components and capsid protein of brome mosaic virus in planta: a functional role for viral replicase in RNA packaging. *Virology, 338*(1), 96-111. doi:10.1016/j.virol.2005.05.013

Annamalai, P., & Rao, A. L. (2006). Packaging of brome mosaic virus subgenomic RNA is functionally coupled to replication-dependent transcription and translation of coat protein. *J Virol, 80*(20), 10096-10108. doi:10.1128/JVI.01186-06

Annamalai, P., & Rao, A. L. N. (2006). Delivery and expression of functional viral RNA genomes in planta by agroinfiltration. *Curr Protoc Microbiol, Chapter 16*, 16B.12.11-16B.12.15. doi:10.1002/9780471729259.mc16b02s01

Annamalai, P., Rofail, F., Demason, D. A., & Rao, A. L. (2008). Replication-coupled packaging mechanism in positive-strand RNA viruses: synchronized coexpression of functional multigenome RNA components of an animal and a plant virus in Nicotiana benthamiana cells by agroinfiltration. *J Virol, 82*(3), 1484-1495. doi:10.1128/JVI.01540-07

Bamunusinghe, D., Chaturvedi, S., Seo, J. K., & Rao, A. L. (2013). Mutations in the capsid protein of Brome mosaic virus affecting encapsidation eliminate vesicle induction in planta: implications for virus cell-to-cell spread. *J Virol, 87*(16), 8982-8992. doi:10.1128/JVI.01253-13

Bol, J. F. (2005). Replication of alfamo- and ilarviruses: role of the coat protein. *Annu Rev Phytopathol, 43*, 39-62. doi:10.1146/annurev.phyto.43.101804.120505

Bothner, B., Schneemann, A., Marshall, D., Reddy, V., Johnson, J. E., & Siuzdak, G. (1999). Crystallographically identical virus capsids display different properties in solution. *Nat Struct Biol, 6*(2), 114-116. doi:10.1038/5799

Bujarski, J., Gallitelli, D., García-Arenal, F., Pallás, V., Palukaitis, P., Reddy, M. K., . . . Ictv Report Consortium. (2019). ICTV Virus Taxonomy Profile: Bromoviridae. *J Gen Virol, 100*(8), 1206-1207. doi:10.1099/jgv.0.001282

Chakravarty, A., Reddy, V. S., & Rao, A. L. N. (2020). Unravelling the Stability and Capsid Dynamics of the Three Virions of Brome Mosaic Virus Assembled Autonomously. *J Virol, 94*(8). doi:10.1128/JVI.01794-19

Chaturvedi, S., & Rao, A. L. N. (2014). Live cell imaging of interactions between replicase and capsid protein of Brome mosaic virus using Bimolecular Fluorescence Complementation: implications for replication and genome packaging. *Virology, 464-465*, 67-75. doi:10.1016/j.virol.2014.06.030

Choi, Y. G., & Rao, A. L. (2000). Molecular studies on bromovirus capsid protein. VII. Selective packaging on BMV RNA4 by specific N-terminal arginine residuals. *Virology, 275*(1), 207-217. doi:10.1006/viro.2000.0513

Lucas, R. W., Larson, S. B., & McPherson, A. (2002). The crystallographic structure of brome mosaic virus. *J Mol Biol, 317*(1), 95-108. doi:10.1006/jmbi.2001.5389

Rao, A., Duggal, R., Lahser, F., & Hall, T. (1994). Analysis of RNA replication in plant viruses. In A. KW (Ed.), *Methods in Molecular Genetics: Molecular Virology Techniques* (Vol. 4, pp. 216-236): Academic Press, San Diego, CA.

Rao, A. L. (2006). Genome packaging by spherical plant RNA viruses. *Annu Rev Phytopathol, 44*, 61-87. doi:10.1146/annurev.phyto.44.070505.143334

Rao, A. L., Chaturvedi, S., & Garmann, R. F. (2014). Integration of replication and assembly of infectious virions in plant RNA viruses. *Curr Opin Virol, 9*, 61-66. doi:10.1016/j.coviro.2014.09.008

Rao, A. L., & Grantham, G. L. (1995). Biological significance of the seven amino-terminal basic residues of brome mosaic virus coat protein. *Virology, 211*(1), 42-52. doi:10.1006/viro.1995.1377

Rao, A. L., & Grantham, G. L. (1996). Molecular studies on bromovirus capsid protein. II. Functional analysis of the amino-terminal arginine-rich motif and its role in encapsidation, movement, and pathology. *Virology, 226*(2), 294-305. doi:10.1006/viro.1996.0657

Rayaprolu, V., Kruse, S., Kant, R., Movahed, N., Brooke, D., & Bothner, B. (2014). Fluorometric Estimation of Viral Thermal Stability. *Bio Protoc, 4*(15). doi:10.21769/bioprotoc.1199

Schmitz, I., & Rao, A. L. (1996). Molecular studies on bromovirus capsid protein. I. Characterization of cell-to-cell movement-defective RNA3 variants of brome mosaic virus. *Virology, 226*(2), 281-293. doi:10.1006/viro.1996.0656

Schneider, C. A., Rasband, W. S., & Eliceiri, K. W. (2012). NIH Image to ImageJ: 25 years of image analysis. *Nat Methods, 9*(7), 671-675. doi:10.1038/nmeth.2089

Seo, J. K., Kwon, S. J., & Rao, A. L. (2012). A physical interaction between viral replicase and capsid protein is required for genome-packaging specificity in an RNA virus. *J Virol, 86*(11), 6210-6221. doi:10.1128/JVI.07184-11

Speir, J. A., Bothner, B., Qu, C., Willits, D. A., Young, M. J., & Johnson, J. E. (2006). Enhanced local symmetry interactions globally stabilize a mutant virus capsid that maintains infectivity and capsid dynamics. *J Virol, 80*(7), 3582-3591. doi:10.1128/JVI.80.7.3582-3591.2006

Sztuba-Solińska, J., Stollar, V., & Bujarski, J. J. (2011). Subgenomic messenger RNAs: mastering regulation of (+)-strand RNA virus life cycle. *Virology, 412*(2), 245-255. doi:10.1016/j.virol.2011.02.007

Wierzchoslawski, R., Dzianott, A., & Bujarski, J. (2004). Dissecting the requirement for subgenomic promoter sequences by RNA recombination of brome mosaic virus in vivo: evidence for functional separation of transcription and recombination. *J Virol, 78*(16), 8552-8564. doi:10.1128/JVI.78.16.8552-8564.2004

Yang, Y., Hussain, S., Wang, H., Ke, M., & Guo, D. (2009). Translational control of the subgenomic RNAs of severe acute respiratory syndrome coronavirus. *Virus Genes, 39*(1), 10-18. doi:10.1007/s11262-009-0357-y

Zhao, X., Fox, J. M., Olson, N. H., Baker, T. S., & Young, M. J. (1995). In vitro assembly of cowpea chlorotic mottle virus from coat protein expressed in Escherichia coli and in vitro-transcribed viral cDNA. *Virology, 207*(2), 486-494. doi:10.1006/viro.1995.1108

Zlotnick, A., Aldrich, R., Johnson, J. M., Ceres, P., & Young, M. J. (2000). Mechanism of capsid assembly for an icosahedral plant virus. *Virology, 277*(2), 450-456. doi:10.1006/viro.2000.0619

CHAPTER 5

In Vivo Assembly and Characterization of HIV-1 Gag Virus-like Particles in *Nicotiana benthamiana*

ABSTRACT

A retroviral Gag protein expression in higher eukaryotic cells has been shown to produce virus-like particles (VLPs). Previous studies have reported that the addition of nucleic acid facilitates the process of assembly *in vitro*. Prior studies involving the expression of a full-length wild-type HIV-1 p55-Gag protein in plants have indicated that the expression level of p55-Gag was low in both transient and transgenic plants. To understand the assembly of p55-Gag in plants, we engineered a plasmid amenable for the *Agrobacterium*-mediated transient expression in *Nicotiana benthamiana* plants. A high level of p55-Gag was consistently observed in plants co-expressing p19, a viral silencing suppressor. VLPs were released from infiltrated leaves by enzymatic digestion at four days post-infiltration and pelleted through 20% sucrose cushion followed by 20%-60% sucrose density gradient centrifugation. Electron microscopic examination of the VLPs showed that the wild-type p55-Gag (codon-optimized for humans) assembled into long flexuous rods up to 1 μm in length and 20 nm diameter. These VLPs were susceptible to Proteinase K but not to either DNase or RNase treatment. Analysis of RNA isolated from the VLPs revealed that they encapsidated a single DNA species of approximately 10 kb absent in healthy plants. The RT-PCR analysis confirmed that the 10kb RNA contained HIV-1 Gag-specific sequences.

IMPORTANCE

Virus-like particles (VLPs) are highly organized structures self-assembled from virus-derived structural antigens. These stable and versatile subviral particles have shown the capability to induce innate and cognate immune responses (Ludwig & Wagner, 2007). Because of their particulate structure, VLPs have a significant advantage over soluble antigens, which historically failed in vaccine trials due to weak immunogenicity or instability. VLPs are highly immunogenic as they contain antigenic determinants in multimeric units and are larger. They are also an attractive alternative to attenuated viral vaccines as they do not contain any infectious or genetic material for replication; therefore, they are safe. VLPs can efficiently activate critical immune responses to achieve potent immune stimulation and provide immunological memory.

VLPs have been produced as vaccine candidates in plants since the introduction of bio farming in 1989 when a functional monoclonal antibody was made in transgenic tobacco (Scotti et al., 2009). If the vaccines are universally used, they should be manufactured at a high yield in an inexpensive system. Plants are one of the world's most cost-effective protein producers. Plants are uniquely capable of efficient protein expression of different complexity levels and glycosylation patterns at high yields and low costs. One of the first vaccine candidates made in plants was HBsAg (Mason, Lam, & Arntzen, 1992). Recent advancement in the use of deconstructed plant vectors for whole-plant infiltration

with *Agrobacterium tumefaciens* results in very high yield of protein (Annamalai & Rao, 2005, 2006). This system for the generation of vaccines is more economical than traditional systems like eggs, yeast, bacterial, and mammalian cell culture. Green-house-based manufacturing facilities can be used for scale-up of production to meet market demands.

Despite a wealth of knowledge about the HIV-1 structural components, an effective HIV vaccine is still a global health priority. To date, several vaccine candidates have been developed based on structural (e.g., Env membrane glycoprotein and/or Gag capsid protein) or regulatory (e.g., Tat, Nef, and Pol) proteins have been developed (Johnston & Fauci, 2007; Ross, Bråve, Scarlatti, Manrique, & Buonaguro, 2010) but with no efficacy in human clinical trials (Kim, Rerks-Ngarm, Excler, & Michael, 2010). The self-assembly of HIV-1 $Pr55^{Gag}$ into VLPs provides a rationale for generating a new Gag-based VLP vaccine (Ludwig & Wagner, 2007). $Pr55^{Gag}$ derived VLPs are excellent immunogen and can elicit both humoral and strong cellular responses. However, making these VLPs in a cell-based system has not been very successful due to the low yield and size deviation from authentic virions. Therefore, it is crucial to explore the plant-based systems for cheap production of $Pr55^{Gag}$ VLPs.

INTRODUCTION

Human Immunodeficiency Virus type-1 (HIV-1) is the causal agent of AIDS, one of the most devastating infectious viral diseases in history (Freed, 2015). The virus is transmitted through certain body fluids and attacks the CD4 helper T-lymphocyte cells resulting in severely compromised immunity in infected individuals. This clinical condition makes patients highly susceptible to several potentially lethal opportunistic infections, and they may even develop a malignancy. According to estimates by WHO and UNAIDS, 36.7 million people were living with HIV at the end of 2015, and 1.1 million died of HIV-related causes. More than 1.2 million people in the United States live with HIV, and 1 in 8 of them does not know it. Therefore, HIV and AIDS remain a persistent problem for the US and countries around the world.

HIV is a member of the retrovirus family. The genome comprises two copies of non-covalently linked, un-spliced, positive-stranded RNA converted to double-stranded DNA shortly after infecting susceptible host cells. The RNA component is 9749 nucleotides long. The HIV-1 genome is comprised of nine genes. Six genes are unique to HIV, and three are common to other retroviruses (Scarlata & Carter, 2003). The main structural component of HIV-1 is Gag, one of the three gene products common to all retroviruses, is encoded by the *gag* gene, and is the sole protein required for viral particle assembly (Morikawa, Goto, & Sano, 1999). The gag is a 55 kDa protein ($Pr55^{Gag}$). The roles played by HIV-1 Gag during the virus

life cycle are numerous and complex, involving assembly and virion maturation after particle release and early post-entry steps in virus replication (Freed, 2015; Scarlata & Carter, 2003). $Pr55^{Gag}$ is produced as a 55 kDa precursor on cytosolic ribosomes (Tritel & Resh, 2000) and yields the internal structural proteins of the mature virion after being cleaved by the viral protease (Freed, 1998; Hunter, 1994; Swanstrom & Wills, 1997; Vogt, 1997; Wills & Craven, 1991). The Gag precursor contains matrix (MA-17 kDa), capsid (CA-24 kDa), nucleocapsid (NC-7 kDa), and p6 domains as well as two spacer peptides, SP1 and SP2, which separate CA from NC and NC from p6 respectively (Henderson et al., 1992; Mervis et al., 1988). The MA domain is myristylated and forms the amino-terminal domain of Gag. This domain targets Gag to the plasma membrane. CA drives Gag multimerization during assembly, and NC recruits the viral RNA genome into virions (Freed, 2015; Fuller, Wilk, Gowen, Kräusslich, & Vogt, 1997).

The gag is the autonomous molecular machine for the virus particle assembly as it provides the principal driving force for the process. Therefore, the expression of Gag protein alone is sufficient for the formation of Gag virus-like particles (VLPs), which resemble the immature form of authentic HIV (Gheysen et al., 1989). Gag protein expressed alone by transfection of expression plasmids or recombinant viruses simultaneously assemble and bud off from the cell surface (Hoshikawa et al., 1991; Jowett, Hockley, Nermut, & Jones, 1992; Smith, Srinivasakumar, Hammarskjöld, & Rekosh, 1993).

HIV-1 VLPs have been shown to assemble into spherical particles of 100 to 120 nm in mammalian cell lines. One of the earlier studies has demonstrated the release of immature Gag virus-like particles from mammalian cell lines stably expressing Gag and PR (viral encoded Protease) (Kräusslich et al., 1993). Studies have also attempted to express codon-optimized *gag* and *env* gene in stable, inducible mammalian and insect cell lines using recombinant baculoviruses (Fuller et al., 1997; Hammonds, Chen, Zhang, Lee, & Spearman, 2007). These gene products were assembled in spherical Gag-Env pseudovirions. HIV-1 Gag codon-optimized for *Saccharomyces cerevisiae* produces Gag VLPs at the plasma membrane of yeast spheroplasts (Morikawa, Goto, Yasuoka, Momose, & Matano, 2007).

In contrast to these *in vivo* analyses, the *in vitro* assembly reaction conditions were not well standardized as the *in vitro* assembled particles were much smaller than authentic HIV particles. *In vitro* assembly of Gag domains such as CA-NC in the presence of RNA was shown to give rise to long tubular structures rather than spherical structures (Campbell & Vogt, 1995). The authors proposed a model for the assembly of CA-NC and RNA into cylindrical particles *in vitro* or spherical particles *in vivo.* Two of the subsequent studies showed that both HIV-1 Gag and GagΔp6 assemble into 25-30 nm spherical particles *in vitro,* which could be corrected by adding mammalian cell lysate (Campbell & Rein, 1999) or several inositol phosphate derivatives (Campbell et al., 2001). They further argued that the N-terminal extension of HIV-1 CA-NC to include the matrix domain results in the

formation of spherical particles rather than cylindrical structures. *In vitro* assembly of wild type full-length Gag and CA-NC of HIV-1 and other retroviruses suggested Gag can alone assemble *in vitro,* but a wide variety of RNA or even short DNA oligonucleotides support the assembly reaction (Campbell & Rein, 1999; Ganser, Li, Klishko, Finch, & Sundquist, 1999; Hadravová et al., 2012; Morikawa et al., 1999). However, the role of nucleic acid in the assembly process is not clearly understood. HIV-1 MA alone was incapable of forming VLPs (Giddings, Ritter, & Mulligan, 1998). A recent study has demonstrated that Gag VLP morphology changes from sphere to cones and tubes followed by viral protease treatment. Using computer simulation, they have predicted that CA forms long open tubes in a free environment (Ning et al., 2016).

Over the past decade, plants have been used to express regulatory and structural HIV proteins as chimeric particles with little success. Only three studies have demonstrated the accumulation of HIV- 1 Gag polyprotein ($Pr55^{Gag}$) based VLPs so far in plants. A paper (Meyers et al., 2008) reported very low expression of chloroplast targeted codon-optimized Gag in *Nicotiana benthamiana* using nuclear transformation and transient expression mediated by *Agrobacterium* and TMV. Based on these results, Scotti et al., 2009 also targeted $Pr55^{Gag}$ to chloroplast through nuclear and plastid transformation methods. Both of these studies reported a lack of success to demonstrate the accumulation of $Pr55^{Gag}$ in its natural subcellular compartment, the cytoplasmic face of the plasma

membrane. Another study (Kessans, Linhart, Matoba, & Mor, 2013) developed stable transgenic lines co-expressing codon-optimized Gag and dgp41, were the first to demonstrate sufficient accumulation of full-length $Pr55^{Gag}$ in the cytoplasm. The VLPs assembled in this study were chimeric and not assembled from pure Gag. Additionally, the high expression of Gag protein in plastids caused pleiotropic effects like pigment-deficient leaves, reduced growth of transformed plants, and defective chloroplast biogenesis (Scotti et al., 2009). Hence, the current study aims to achieve a high-level accumulation of $Pr55^{Gag}$, the full-length protein in the cytosol of *N. benthamiana* leaves, and characterize the assembled VLPs as potential vaccine candidates against HIV-1.

RESULTS AND DISCUSSION

Transient expression of $Pr55^{Gag}$ in plants

Most of the studies to date have investigated the expression of codon-optimized HIV-Gag in plants (Kessans et al., 2013). Therefore, we first wanted to identify the expression levels of the native protein. However, approximately a third of the codons in the native *Gag* gene is unfavorable for expression in plants (Kessans et al., 2013). To address this caveat, we transiently expressed a full-length construct PZP-Gag^{NB} in *N. benthamiana* co-expressing p19 (Fig. 5.2A). The rationale for constructing this plasmid is to verify whether codon-optimization would affect Gag protein expression level compared to PZP-Gag^{Wt}. Western blot analysis revealed that both forms of $Pr55^{Gag}$, i.e., Gag^{Wt} and Gag^{NB} accumulated to high levels in plants as shown in Fig. 5.2B; Lane: 6, 11.

Characterization of VLPs assembled in plants expressing Gag^{Wt} and Gag^{NB}

VLPs assembled in plants were sedimented as a discrete sharp band approximately 3 mm from the top of the sucrose gradient (Fig. 5.3A). There was another diffused band below the sharp band. Both bands were collected and re-pelleted. The $Pr55^{Gag}$ was detected in the total VLP pellet (before gradient purification) and the purified VLP pellets of Gag^{Wt} and Gag^{NB}. In the case of, Gag^{Wt} two slower migrating bands of approximately 75 kDa and 80 kDa and a

faster migrating band of approximately 35 kDa are observed (Fig. 5.3B; Lane: 1,2 vs. 3,4). The two slowly migrating bands are absent in leaves expressing Gag^{NB}. We hypothesize that the 35 kDa band is a cleavage product of the full-length Gag, which is about the same size as the CA-NC fragment of the polyprotein. The 75 kDa protein could be a heterodimer of the full-length 55 kDa and the truncated form. In the second set of experiments, 300 µl fractions were collected and subjected to Western blot analysis. It was observed that the full-length $Pr55^{Gag}$ is associated with fractions corresponding to the distinct band but was absent in other fractions (Fig. 5.3C).

Morphology of VLPs assembled in plants expressing Gag^{Wt} and Gag^{NB}

The electron microscopic examination of partially purified and gradient purified preparations showed that the Gag^{Wt} assembled into two types of VLPs (Fig. 5.4B, C). The predominant ones represent long flexuous rods of approximately 850 nm-1.7 µm length, with the longest ones being almost 2.2 µm long. The average diameter of the VLPs is 14.9 nm (with a standard error of 0.3 nm). In addition to flexuous rod-like VLPs, we also observed the presence of VLPs exhibiting spherical-like structures with a diameter of approximately 80 nm, resembling those of immature HIV-1 VLPs. None of these structures were observed in an un-inoculated healthy control plant (Fig. 5.4A). The EM analysis of VLPs assembled from the expression of Gag^{NB} also revealed similar flexuous rod-

like and spherical-like structures. This preparation predominantly contained spherical-like VLPs over flexuous rod-like structures (Fig. 5.4D).

Proteinase and nuclease digestion profile of VLPs assembled in plants expressing Gag^{Wt} and Gag^{NB}

VLPs were found to be susceptible to Proteinase K but not to either DNaseI or RNaseIf treatment. The Western blot analysis (Fig. 5.5A) of untreated control and enzyme-treated VLP samples revealed the $Pr55^{Gag}$ protein band, and all the truncated bands disappeared in Proteinase K treated samples of total and purified VLPs. The HIV-Gag protein level remains unchanged in both DNaseI, and RNaseIf treated samples. This observation was confirmed by the EM analysis (Fig. 5.5B) of control and treated samples. The long flexuous rod-like and spherical-like VLPs were utterly absent in Proteinase K treated VLP samples (Fig. 5.5B: B, B') compared to their high abundance in untreated control VLPs (Fig. 5.5B: A, A'). The DNaseI or RNaseIf treatment did not seem to affect the structure of the VLPs (Fig. 5.5B: C, C', D and D').

Characterization of nucleic acid extracted from Gag^{Wt}

Previous studies have reported that nucleic acid plays an essential role in the assembly and structure of VLPs. Therefore, we hypothesized that the VLPs would contain RNA, and in the absence of HIV- 1 genomic RNA, plant cellular RNA

present locally in the same environment would functionally be substituted to promote assembly of VLPs. The concentration of total nucleic acid in VLPs was determined to be 12 µg/ ml. The native 1% agarose gel electrophoresis analysis of nucleic acid isolated from the VLPs revealed that they encapsidated a single species of nucleic acid of approximately 10kb that is absent in healthy plants (Fig. 5.6A). This observation suggested that the VLPs do not encapsidated plant cellular RNA as we had hypothesized before. An RT-PCR assay confirmed that the 10kb nucleic acid resistant to RNaseIƒ treatment contained the entire 1503 nucleotide sequence of HIV-Gag when amplified with the same set of forward and reverse primer used to clone HIV-Gag (Fig. 5.6B, C). Therefore, we argue that the plant assembled native $Pr55^{Gag}$ VLPs preferentially interacted with PZP-Gag^{Wt} DNA as the size of the PZP vector plus the Gag cDNA insert matched the size nucleic acid enclosed in the VLPs. The long 10kb nucleic acid probably also satisfies the need to stabilize long flexuous rod-like structures. However, the 10kb DNA was below the detectable limit in total nucleic acid extracted from PZP-Gag^{Wt}+p19 leaves, which we believe is due to enrichment in VLPs.

MATERIALS AND METHODS

Construction of *Agrobacterium*-based plasmids for transient expression of $Pr55^{Gag}$ in plants and Western blot

Wild type $Pr55^{Gag}$

A plasmid expressing HIV-1 Gag independently of Rev was the basis for all HIV-1 constructs used in this study (Schneider, Campbell, Nasioulas, Felber, & Pavlakis, 1997). We used PZP (10.4 kb), a plant-based protein expression vector, for this study. A cDNA fragment of 1503 nucleotides encompassing the Wild type HIV-Gag (Gag^{Wt}) protein was amplified in a PCR reaction from pRR359 plasmid (kindly provided by Prof. Alan Rein, National Cancer Institute) using a kinase treated forward primer (5'ATGGGTGCGAGAGCGTCAGTAT 3') and a reverse primer (5'GCTCTAGATTATTGTGAC GAGGAGGGGTCGTTG3'; *Xba*I site is underlined). The resulting PCR product was purified from 1% agarose gel using QIAquick gel extraction kit and was digested with *Xba*I and ligated into *Stu*I/*Spe*I (*Spe*I site is compatible with *Xba*I) digested PZP vector (Fig.2).

Codon-optimized $Pr55^{Gag}$

The Gag^{Wt} gene sequence was subjected to codon optimization for *Nicotiana benthamiana* using the Codon optimization tool from Integrated DNA

Technologies. The plant-codon optimized 1503 gBlock gene fragment synthesized by IDT (referred to as Gag^{NB}) was digested with *Xba*I and ligated into *Stu*I/*Spe*I (*Spe*I site is compatible with *Xba*I) digested PZP vector.

The resultant constructs (Gag^{Wt} and Gag^{NB}) were transformed into *E. coli* DH5α cells. Positive clones were confirmed by double-digestion with *Bam*HI and *Spe*I. Plasmid DNA from the positive clones was isolated using Invitrogen PureLink quick plasmid miniprep kit and sequenced for verification of the insert and orientation. The recombinant DNA containing the insert was transformed into *Agrobacterium* strain GV3101. Each *Agrobacterium* culture (O.D. 1.0_{600}) containing PZP-Gag^{Wt} or PZP-Gag^{NB} was co-infiltrated with PZP-p19 (a Tombusvirus silencing suppressor) into well-expanded leaves of *Nicotiana benthamiana.* The leaves were harvested at four days post-infiltration (Fig 3A).

Total protein was extracted from un-inoculated healthy leaves, PZP-Gag^{Wt}+p19 and PZP-Gag^{NB}+p19 infiltrated leaves. The Goat anti-$p24^{CA}$ antibody (kindly provided by Prof. Rein), diluted 1:10,000, was used to detect the presence of the HIV-1 Gag. Alkaline phosphatase-conjugated rabbit anti-goat IgG (Santa Cruz Biotechnology) was used as a secondary antibody, diluted at 1:5,000.

Purification of VLPs assembled in plants expressing Gag^{Wt} and Gag^{NB}

VLPs were released from 4dpi leaves by enzymatic digestion of the cell wall for virion release. Approximately 400 ml of enzyme cocktail was made in 10mM MES buffer containing 2g Cellulysin, 0.25g BSA, 0.25g Macerozyme and 0.5g Driselase (Rao, 2006). Approximately 25g of 4dpi leaves were incubated in the enzyme cocktail overnight at 28℃ with gentle shaking. Following incubation, the leaf extract was vortexed for 3 minutes to completely disrupt the cell wall material. Following low-speed centrifugation, the leaf extract was treated with a 1:1 volume of chloroform to remove chlorophyll from the remaining cellular components. Then, the VLPs were collected by centrifuging the aqueous phase through a 20% sucrose cushion (wt/volume) with an SW-28 rotor at 25,000 rpm for 3h in a Beckman L-8 M ultracentrifuge. The pellet containing VLPs was resuspended in TNE buffer (10 mM Tris-HCl, pH 7.4, 100 mM NaCl, and 1 mM EDTA). To further purify the VLPs, 0.5 ml of VLP suspension was loaded onto 20-60% sucrose gradient (wt/volume) prepared in the TNE buffer and centrifuged at 27,000 rpm for 3h an SW-41 Ti rotor.

EM analysis

Purified VLP samples were analyzed by EM using negative staining. Approximately 0.1 mg/ml of purified VLP preparation was placed onto 400-mesh carbon-Formvar grids (Ted Pella Inc., Redding, CA) for 5 min. The grids were rinsed with water, wicked dry, stained with 1-2% uranyl acetate for 5 min, and viewed at 300 kV using a Philips CM300 TEM system. Digital images were collected as a 14-bit grayscale using a Gatan 794 CCD multiscan camera and converted into 8-bit grayscale TIF files. To measure the diameter of the VLPs, the Image J program was used to analyze the EM images.

Proteinase and nuclease treatment of WT-Gag-VLPs

The VLPs were treated with either Proteinase K or DNaseI or RNaseIf (NEB) according to the manufacturer's protocol to verify the stability. The effect of these treatments was evaluated by Western blot and EM analysis.

Nucleic acid extraction from Gag^{Wt}

Purified VLPs assembled with Gag^{Wt} were treated with proteinase K followed by phenol: chloroform extraction. The total nucleic acid was then precipitated using 3M sodium acetate/ ethanol and visualized with native 1% agarose gel electrophoresis. The concentration of the nucleic acid was determined using a spectrophotometer.

The total nucleic acid was extracted from the healthy leaf, and Gag^{Wt}+ p19 inoculated leaves with 1:1 phenol: chloroform as control. The VLP nucleic acid and the controls were treated with RNaseIf for 1 hour at 37℃ to determine whether the VLPs encapsidate RNA or DNA. An RT-PCR assay was carried out with the VLP nucleic acid and the controls with the same forward and reverse primer set used to clone HIV-Gag.

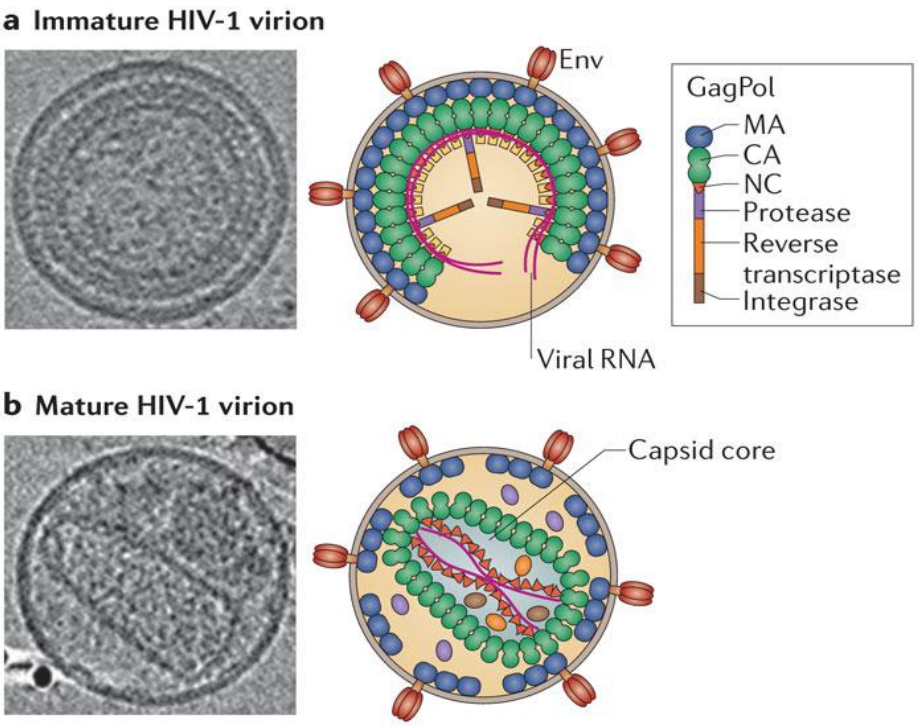

Figure 5.1 Schematic representation of immature and infectious HIV-1 virions and components of Gag polyprotein (Adopted from Freed, 2015).

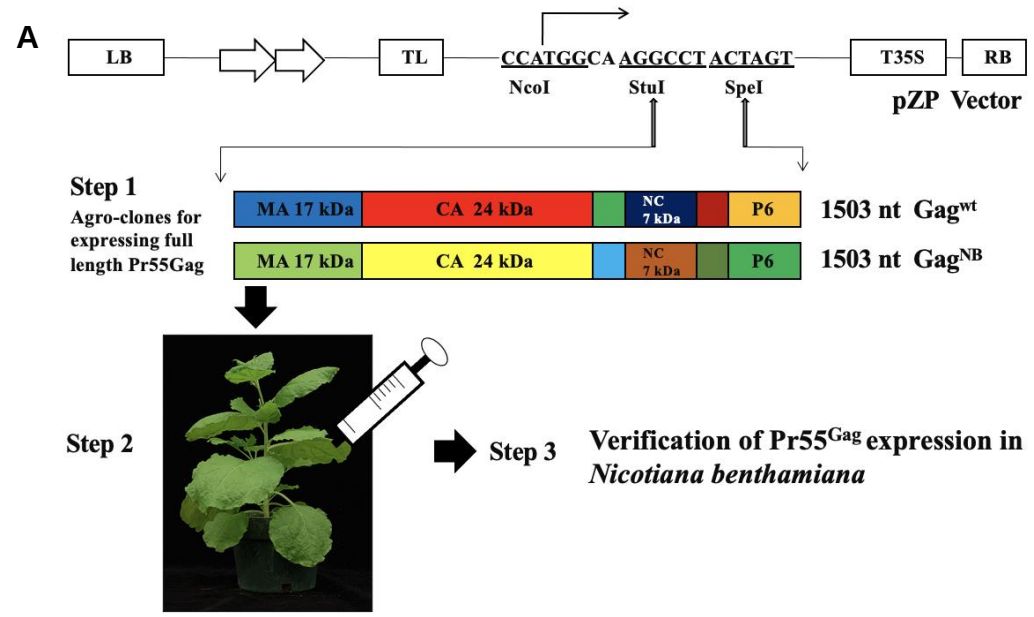

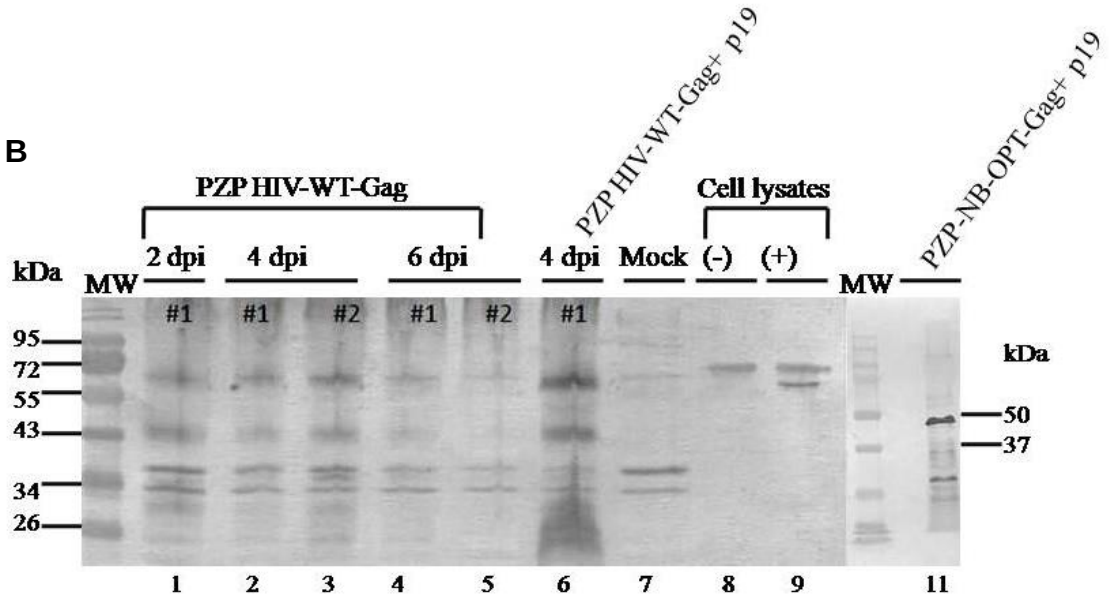

Lane 1-5: Leaves infiltrated with PZP-HIV-WT-Gag at indicated days post infiltration (dpi)
Lane 6: Leaves infiltrated with PZP-HIV-WT-Gag +p19 (suppressor of RNA silencing) at 4 dpi
Lane 7: Healthy leaf extract
Lane 8: Cell lysate negative control from Alan Rein Lab
Lane 9: Cell lysate positive control from Alan Rein Lab
Lane 11: Leaves infiltrated with PZP-HIV-NB-Opt-Gag +p19
#1 & #2 denote sample numbers

Figure 5.2 Strategy to engineer PZP vector for expressing $Pr55^{Gag}$ and analysis of $Pr55^{Gag}$ expression in *N. benthamiana* (A) Diagrammatic representation of the strategy used to express full-length HIV-Gag protein *Nicotiana benthamiana*. (B) Western blot of HIV-Gag protein expressed in plants; Lane 6 indicates high-level WT native Gag protein (55 kDa) in leaves co-infiltrated with PZP-HIV-WT-Gag+p19 compared to plants only infiltrated with PZP-Gag (Lane 1-5). Lane 11 indicates high-level expression of NB optimized Gag protein (55 kDa) in leaves co-infiltrated with PZP NB-Opt-Gag+p19.

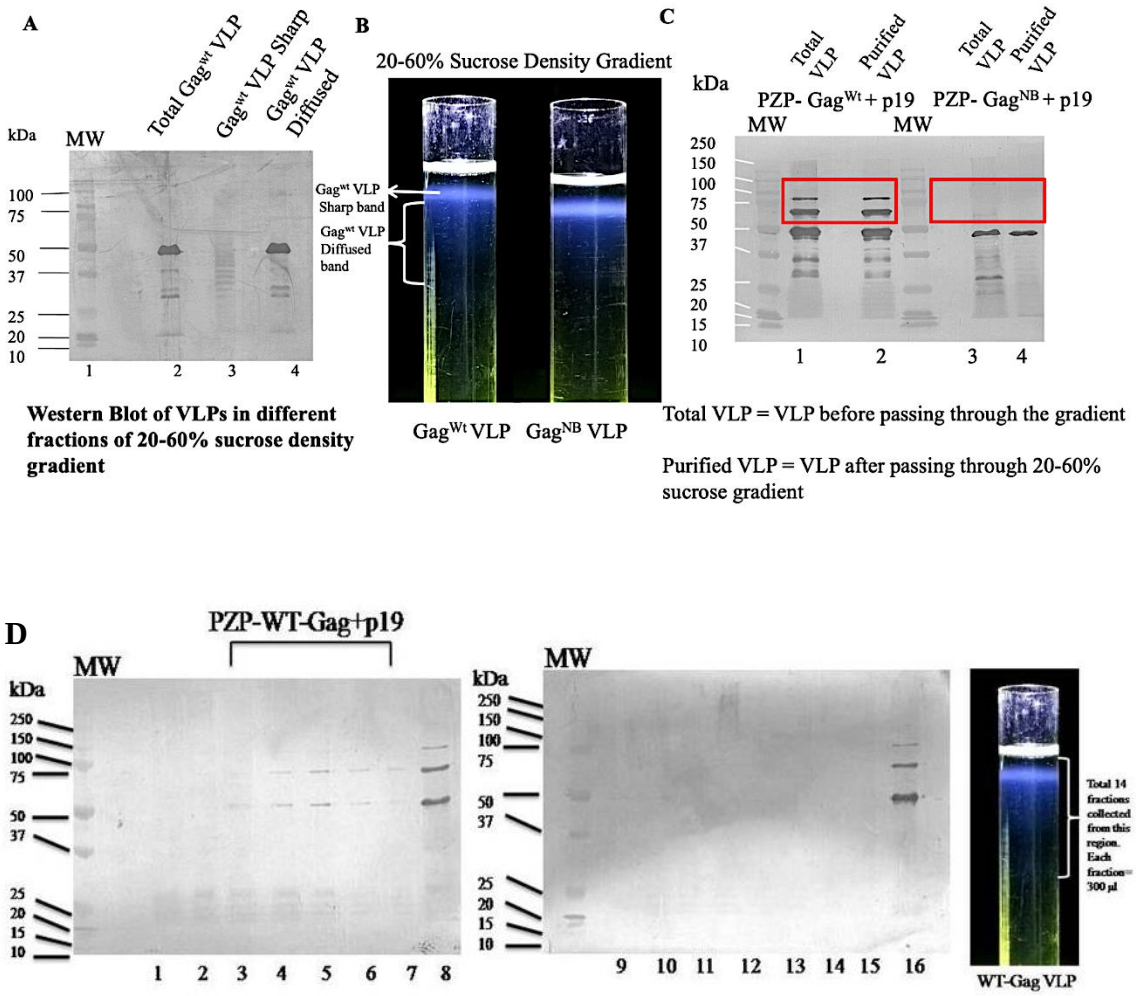

Figure 5.3 (A, B) Characteristic migration pattern of WT HIV-Gag VLPs on 20-60% sucrose density gradient. (C) Western blot of total and gradient purified Gag VLPs. (D) Western blot analysis of a total of 14 fractions collected from the density gradient of WT-Gag VLPs. Lanes 8 and 16 indicate positive control.

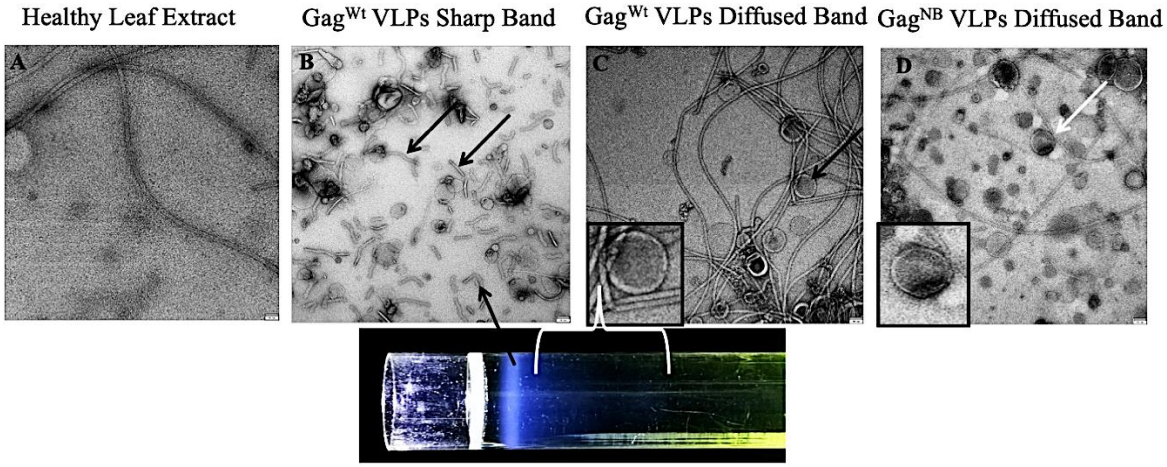

Figure 5.4 EM analysis of HIV-1 VLPs assembled in *N. benthamiana.* (A) Control un-inoculated healthy leaf; (B, C, D) Long flexuous and short rod-like structures (indicated by black arrow) and spherical immature HIV-1 virion-like structures assembled in plants infiltrated with PZP-WT-Gag+p19 and PZP-NB-Gag+p19.

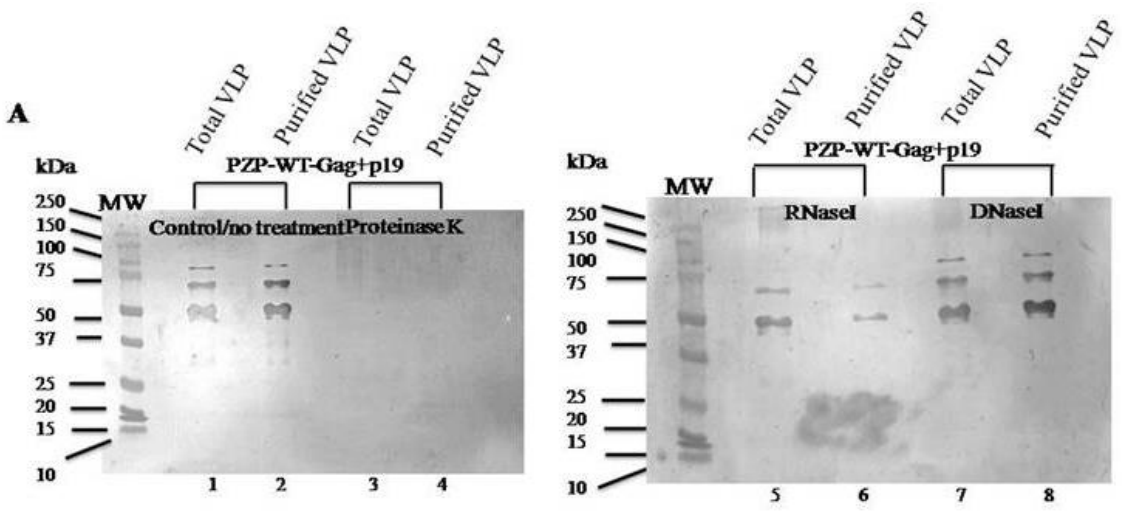
A
Total VLP
Purified VLP
Total VLP
Purified VLP
PZP-WT-Gag+p19
kDa
MW
Control/no treatment
Proteinase K
250
150
100
75
50
37
25
20
15
10
1
2
3
4
RNaseI
DNaseI
5
6
7
8

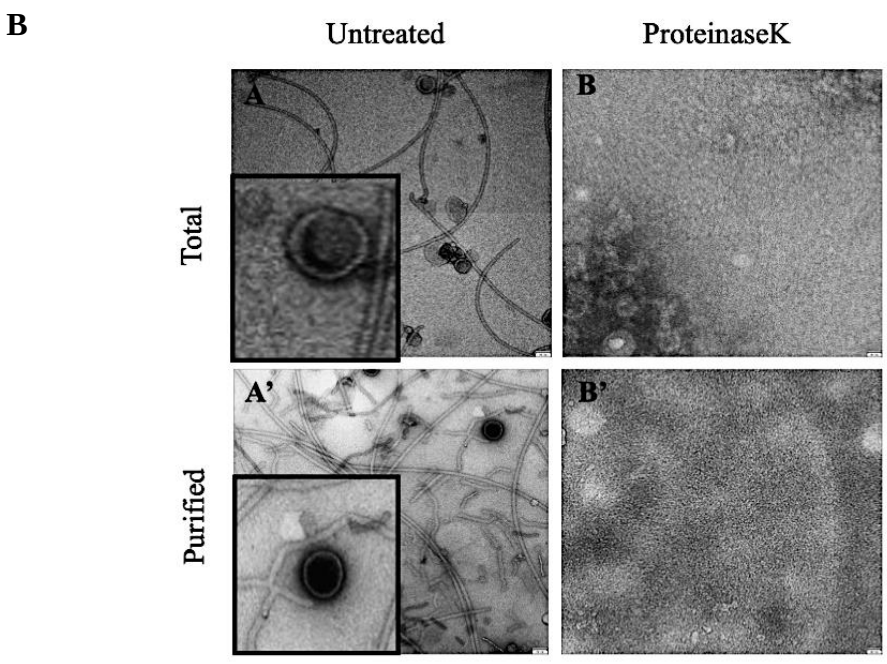
B
Untreated
ProteinaseK
Total
Purified
A
B
A'
B'

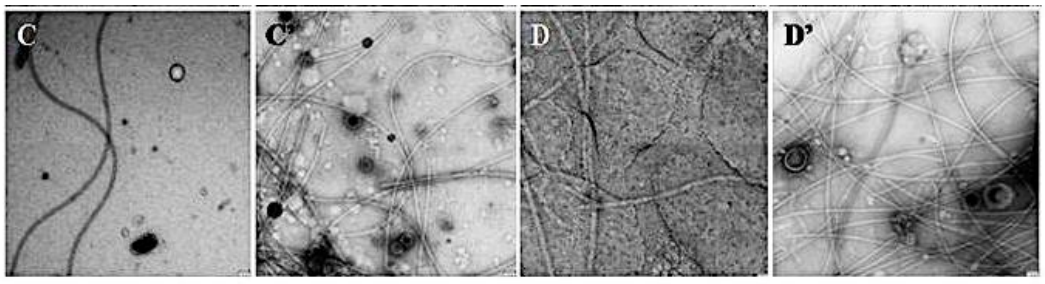
C
C'
D
D'

Figure 5.5 (A) Western blot analysis of Nuclease and Proteinase K treated VLP samples. The protein gets completely denatured in proteinase-treated samples compared to untreated samples (Left Blot); the protein level does not change after nuclease treatment (Right Blot). (B) Negative stain EM analysis of Nuclease and Proteinase K treated VLP samples. A: Total VLP, untreated; A': Purified VLP, untreated; B: Total VLP, Proteinase K; B': Purified VLP, Proteinase K; C: Total VLP, RNaseI; C': Purified VLP, RNaseI; D: Total VLP, DNaseI; D': Purified VLP, DNaseI.

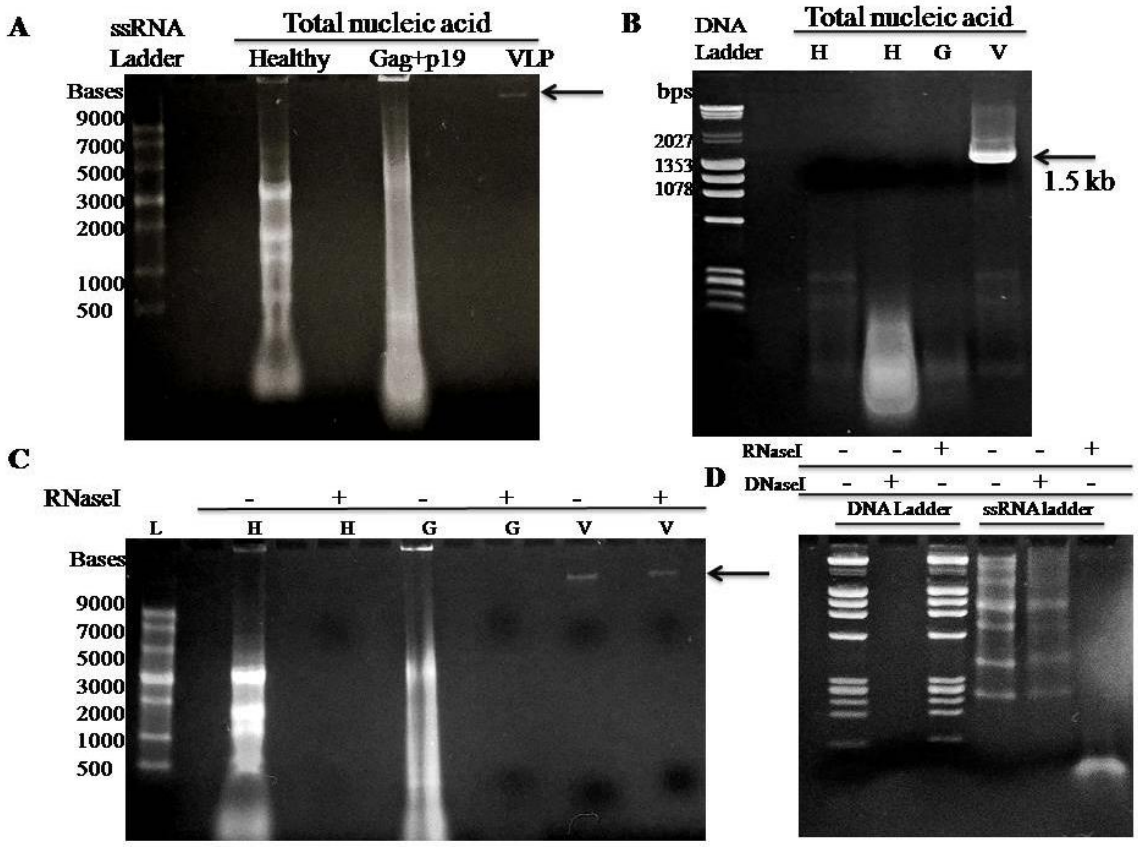

Figure 5.6 Analysis of the WT-Gag VLP content. (A) The total nucleic acid extraction from the healthy leaves, WT-Gag+ p19, infiltrated leaves, WT-Gag VLPs. The VLPs enclose a single nucleic acid species of approximately 10 kb. (B) The nucleic acid enclosed in VLP contains the entire Gag-specific sequence. (C) The nucleic acid enclosed in VLP is resistant to RNaseI (H: Healthy, G: WT-Gag+ p19, V: WT-VLP). (D) Specificity of DNaseI and RNaseI used in the present study.

REFERENCES

Annamalai, P., & Rao, A. L. (2005). Replication-independent expression of genome components and capsid protein of brome mosaic virus in planta: a functional role for viral replicase in RNA packaging. *Virology, 338*(1), 96-111. doi:10.1016/j.virol.2005.05.013

Annamalai, P., & Rao, A. L. (2006). Packaging of brome mosaic virus subgenomic RNA is functionally coupled to replication-dependent transcription and translation of coat protein. *J Virol, 80*(20), 10096-10108. doi:10.1128/JVI.01186-06

Campbell, S., Fisher, R. J., Towler, E. M., Fox, S., Issaq, H. J., Wolfe, T., . . . Rein, A. (2001). Modulation of HIV-like particle assembly in vitro by inositol phosphates. *Proc Natl Acad Sci U S A, 98*(19), 10875-10879. doi:10.1073/pnas.191224698

Campbell, S., & Rein, A. (1999). In vitro assembly properties of human immunodeficiency virus type 1 Gag protein lacking the p6 domain. *J Virol, 73*(3), 2270-2279. doi:10.1128/JVI.73.3.2270-2279.1999

Campbell, S., & Vogt, V. M. (1995). Self-assembly in vitro of purified CA-NC proteins from Rous sarcoma virus and human immunodeficiency virus type 1. *J Virol, 69*(10), 6487-6497. doi:10.1128/JVI.69.10.6487-6497.1995

Freed, E. O. (1998). HIV-1 gag proteins: diverse functions in the virus life cycle. *Virology, 251*(1), 1-15. doi:10.1006/viro.1998.9398

Freed, E. O. (2015). HIV-1 assembly, release and maturation. *Nat Rev Microbiol, 13*(8), 484-496. doi:10.1038/nrmicro3490

Fuller, S. D., Wilk, T., Gowen, B. E., Kräusslich, H. G., & Vogt, V. M. (1997). Cryo-electron microscopy reveals ordered domains in the immature HIV-1 particle. *Curr Biol, 7*(10), 729-738. doi:10.1016/s0960-9822(06)00331-9

Ganser, B. K., Li, S., Klishko, V. Y., Finch, J. T., & Sundquist, W. I. (1999). Assembly and analysis of conical models for the HIV-1 core. *Science, 283*(5398), 80-83. doi:10.1126/science.283.5398.80

Gheysen, D., Jacobs, E., de Foresta, F., Thiriart, C., Francotte, M., Thines, D., & De Wilde, M. (1989). Assembly and release of HIV-1 precursor Pr55gag

virus-like particles from recombinant baculovirus-infected insect cells. *Cell, 59*(1), 103-112. doi:10.1016/0092-8674(89)90873-8

Giddings, A. M., Ritter, G. D., & Mulligan, M. J. (1998). The Matrix Protein of HIV-1 Is Not Sufficient for Assembly and Release of Virus-like Particles. *Virology, 248*(1), 108-116. doi:10.1006/viro.1998.9284

Hadravová, R., de Marco, A., Ulbrich, P., Stokrová, J., Dolezal, M., Pichová, I., . . . Rumlová, M. (2012). In vitro assembly of virus-like particles of a gammaretrovirus, the murine leukemia virus XMRV. *Journal of virology, 86*(3), 1297-1306. doi:10.1128/JVI.05564-11

Hammonds, J., Chen, X., Zhang, X., Lee, F., & Spearman, P. (2007). Advances in methods for the production, purification, and characterization of HIV-1 Gag-Env pseudovirion vaccines. *Vaccine, 25*(47), 8036-8048. doi:10.1016/j.vaccine.2007.09.016

Henderson, L. E., Bowers, M. A., Sowder, R. C., Serabyn, S. A., Johnson, D. G., Bess, J. W., . . . Fenselau, C. (1992). Gag proteins of the highly replicative MN strain of human immunodeficiency virus type 1: posttranslational modifications, proteolytic processings, and complete amino acid sequences. *J Virol, 66*(4), 1856-1865. doi:10.1128/JVI.66.4.1856-1865.1992

Hoshikawa, N., Kojima, A., Yasuda, A., Takayashiki, E., Masuko, S., Chiba, J., . . . Kurata, T. (1991). Role of the gag and pol genes of human immunodeficiency virus in the morphogenesis and maturation of retrovirus-like particles expressed by recombinant vaccinia virus: an ultrastructural study. *J Gen Virol, 72 (Pt 10)*, 2509-2517. doi:10.1099/0022-1317-72-10-2509

Hunter, E. (1994). Macromolecular interactions in the assembly of HIV and other retroviruses. *Seminars in Virology, 5*(1), 71-83. doi:10.1006/smvy.1994.1008

Johnston, M. I., & Fauci, A. S. (2007). An HIV vaccine--evolving concepts. *N Engl J Med, 356*(20), 2073-2081. doi:10.1056/NEJMra066267

Jowett, J. B., Hockley, D. J., Nermut, M. V., & Jones, I. M. (1992). Distinct signals in human immunodeficiency virus type 1 Pr55 necessary for RNA binding and particle formation. *J Gen Virol, 73 (Pt 12)*, 3079-3086. doi:10.1099/0022-1317-73-12-3079

Kessans, S. A., Linhart, M. D., Matoba, N., & Mor, T. (2013). Biological and biochemical characterization of HIV-1 Gag/dgp41 virus-like particles expressed in Nicotiana benthamiana. *Plant Biotechnol J, 11*(6), 681-690. doi:10.1111/pbi.12058

Kim, J. H., Rerks-Ngarm, S., Excler, J. L., & Michael, N. L. (2010). HIV vaccines: lessons learned and the way forward. *Curr Opin HIV AIDS, 5*(5), 428-434. doi:10.1097/COH.0b013e32833d17ac

Kräusslich, H. G., Ochsenbauer, C., Traenckner, A. M., Mergener, K., Fäcke, M., Gelderblom, H. R., & Bosch, V. (1993). Analysis of protein expression and virus-like particle formation in mammalian cell lines stably expressing HIV-1 gag and env gene products with or without active HIV proteinase. *Virology, 192*(2), 605-617. doi:10.1006/viro.1993.1077

Ludwig, C., & Wagner, R. (2007). Virus-like particles-universal molecular toolboxes. *Curr Opin Biotechnol, 18*(6), 537-545. doi:10.1016/j.copbio.2007.10.013

Mason, H. S., Lam, D. M., & Arntzen, C. J. (1992). Expression of hepatitis B surface antigen in transgenic plants. *Proc Natl Acad Sci U S A, 89*(24), 11745-11749. doi:10.1073/pnas.89.24.11745

Mervis, R. J., Ahmad, N., Lillehoj, E. P., Raum, M. G., Salazar, F. H., Chan, H. W., & Venkatesan, S. (1988). The gag gene products of human immunodeficiency virus type 1: alignment within the gag open reading frame, identification of posttranslational modifications, and evidence for alternative gag precursors. *J Virol, 62*(11), 3993-4002. doi:10.1128/JVI.62.11.3993-4002.1988

Meyers, A., Chakauya, E., Shephard, E., Tanzer, F. L., Maclean, J., Lynch, A., . . . Rybicki, E. P. (2008). Expression of HIV-1 antigens in plants as potential subunit vaccines. *BMC biotechnology, 8*, 53-53. doi:10.1186/1472-6750-8-53

Morikawa, Y., Goto, T., & Sano, K. (1999). In vitro assembly of human immunodeficiency virus type 1 Gag protein. *J Biol Chem, 274*(39), 27997-28002. doi:10.1074/jbc.274.39.27997

Morikawa, Y., Goto, T., Yasuoka, D., Momose, F., & Matano, T. (2007). Defect of human immunodeficiency virus type 2 Gag assembly in Saccharomyces cerevisiae. *J Virol, 81*(18), 9911-9921. doi:10.1128/JVI.00027-07

Ning, J., Erdemci-Tandogan, G., Yufenyuy, E. L., Wagner, J., Himes, B. A., Zhao, G., . . . Zhang, P. (2016). In vitro protease cleavage and computer simulations reveal the HIV-1 capsid maturation pathway. *Nat Commun, 7*, 13689. doi:10.1038/ncomms13689

Rao, A. L. (2006). Genome packaging by spherical plant RNA viruses. *Annu Rev Phytopathol, 44*, 61-87. doi:10.1146/annurev.phyto.44.070505.143334

Ross, A. L., Bråve, A., Scarlatti, G., Manrique, A., & Buonaguro, L. (2010). Progress towards development of an HIV vaccine: report of the AIDS Vaccine 2009 Conference. *Lancet Infect Dis, 10*(5), 305-316. doi:10.1016/S1473-3099(10)70069-4

Scarlata, S., & Carter, C. (2003). Role of HIV-1 Gag domains in viral assembly. *Biochim Biophys Acta, 1614*(1), 62-72. doi:10.1016/s0005-2736(03)00163-9

Schneider, R., Campbell, M., Nasioulas, G., Felber, B. K., & Pavlakis, G. N. (1997). Inactivation of the human immunodeficiency virus type 1 inhibitory elements allows Rev-independent expression of Gag and Gag/protease and particle formation. *J Virol, 71*(7), 4892-4903. doi:10.1128/JVI.71.7.4892-4903.1997

Scotti, N., Alagna, F., Ferraiolo, E., Formisano, G., Sannino, L., Buonaguro, L., . . . Cardi, T. (2009). High-level expression of the HIV-1 Pr55gag polyprotein in transgenic tobacco chloroplasts. *Planta, 229*(5), 1109-1122. doi:10.1007/s00425-009-0898-2

Smith, A. J., Srinivasakumar, N., Hammarskjöld, M. L., & Rekosh, D. (1993). Requirements for incorporation of Pr160gag-pol from human immunodeficiency virus type 1 into virus-like particles. *Journal of Virology, 67*(4), 2266-2275. doi:doi:10.1128/jvi.67.4.2266-2275.1993

Swanstrom, R., & Wills, J. W. (1997). Synthesis, Assembly, and Processing of Viral Proteins. In J. M. Coffin, S. H. Hughes, & H. E. Varmus (Eds.), *Retroviruses*. Cold Spring Harbor (NY): Cold Spring Harbor Laboratory Press

Tritel, M., & Resh, M. D. (2000). Kinetic analysis of human immunodeficiency virus type 1 assembly reveals the presence of sequential intermediates. *J Virol, 74*(13), 5845-5855. doi:10.1128/jvi.74.13.5845-5855.2000

Vogt, V. M. (1997). Retroviral Virions and Genomes. In: Cold Spring Harbor Laboratory Press, Cold Spring Harbor (NY).

Wills, J. W., & Craven, R. C. (1991). Form, function, and use of retroviral gag proteins. *AIDS, 5*(6), 639-654. doi:10.1097/00002030-199106000-00002

CHAPTER 6

Analysis of Cucumber Mosaic Virus-Q Strain accumulation in local and systemic leaves of S-phase Kinase-associated Protein (SKP1) Silenced *Nicotiana benthamiana* Plants

ABSTRACT

RNA silencing is one of the best-studied antiviral defense mechanisms induced by host plants to combat invading viral pathogens. This mechanism, which plays a critical role in an organism's developmental stages and helps maintain its genome's integrity, depends on a virus or host-derived small RNAs produced from double-stranded RNAs by Dicer-like proteins (DCLs). The small RNAs then guide Argonaute (AGO) proteins in the RNA-induced silencing complex (RISC) to target the cognate RNA or DNA sequence, which may belong to the host or the attacking virus. To combat this host defense strategy, plant viruses have evolved viral suppressors of RNA silencing (VSRs) to inhibit antiviral silencing. These VSRs demonstrate a wide range of mechanisms, including but not limited to targeting small RNAs, AGOs, and DCLs. Some VSRs may target more than one component of the host antiviral silencing pathway. The 2b protein in *Cucumber mosaic virus* has been reported to have a dual mode of VSR activity, achieved either by inhibiting small RNA biogenesis or inhibiting the silencing activity of AGO1 protein. Poleroviruses encode for a P0 VSR that also promotes degradation of AGO1 to suppress antiviral silencing with or without interacting with host S-phase kinase-associated Protein (SKP1), a component of the Ubiquitin-proteosome pathway. This study analyzed the effect of host SKP1 silencing on CMV-Q accumulation in *Nicotiana benthamiana* and investigated the sequence similarity between CMV-Q 2b and Polerovirus P0 for possible functional relevance.

INTRODUCTION

A diverse group of eukaryotic organisms, including fungi, plants, and insects, deploy RNA silencing as an antiviral defense mechanism against attacking viral pathogens. This antiviral defense mechanism starts when either double-stranded or structured single-stranded viral RNA is recognized and host Dicer-like proteins (DCLs) with RNaseIII-like activity process those viral RNAs into 21-26 nucleotide (nt) virus-derived small interfering RNAs (vsiRNAs) (Blevins et al., 2006). Subsequently, the vsiRNAs are loaded into the Argonaute (AGO) protein containing RNA-induced silencing complexes (RISCs) to guide the RISC to target RNA and degrade those RNAs (Carbonell et al., 2012; Garcia-Ruiz et al., 2015).

Plants may have two distinct classes of vsiRNAs: primary siRNA resulting from the DCL-facilitated cleavage of the initial RNA, whereas an RNA-dependent RNA polymerase (RDR) enzyme synthesize secondary siRNAs from the RNA fragments generated by the RISC activity (Donaire et al., 2008; Qu, 2010; Ruiz-Ferrer & Voinnet, 2009; X. B. Wang et al., 2010). DCL2 and DCL4 are the two most essential DCLs involved in antiviral RNA silencing in *Arabidopsis thaliana* (Burgyán & Havelda, 2011; Cuperus et al., 2010; Deleris et al., 2006; Ruiz-Ferrer & Voinnet, 2009). The loading of vsiRNAs onto the AGO complex is determined partially by their 5’-terminal nucleotides, and both AGO1 and AGO7 can clear viral RNAs (Burgyán & Havelda, 2011). The AGO proteins bind to vsiRNAs using their

PAZ domain and cleave the target RNA using their ribonuclease activity (Baulcombe, 2004).

Numerous VSRs have been found in almost all plant virus genera, and their sequence and structural diversity indicate independent evolution (Wu, Wang, & Ding, 2010). *Cucumber mosaic virus* (CMV) is a well-studied plant virus belonging to the genus *Cucumovirus* and the family *Bromoviridae,* infects over 1200 species of monocots and dicots in over 100 families. CMV encodes replicase proteins 1a and 2a, the viral silencing suppressor 2b, movement protein 3a, and a capsid protein (CP), of which 2b and CP are major virulence factors. The disease symptoms caused by CMV vary greatly, ranging from mosaic, stunting, chlorosis to necrosis and severe leaf deformation. Also, the symptoms depend on the strain of CMV and the type of host plant (Jacquemond, 2012; Palukaitis & García-Arenal, 2003).

The CMV 2b is one of the first VSRs to be characterized that blocks siRNA biogenesis, and its ability to bind to siRNA is indispensable for its VSR function (González et al., 2010; Goto, Kobori, Kosaka, Natsuaki, & Masuta, 2007). The 2b protein in CMV-Fny co-localizes with AGO1 in the host cell and physically interacts with the PAZ and part of the PIWI-domain in AGO1 to inhibit its RNA cleavage activity (Mayers, Palukaitis, & Carr, 2000; Zhang et al., 2006). However, neither the nuclear localization signal nor the phosphorylation motif on CMV-Fny 2b is required to interact with AGO1 and AGO4 (González et al., 2010). The 2b protein can also block the salicylic-acid mediated host antiviral defense by reducing the

accumulation of RDRs and potentially blocking transcriptional gene silencing by reducing transgene DNA methylation (Diaz-Pendon, Li, Li, & Ding, 2007; Guo & Ding, 2002; Ji & Ding, 2001). A comparative study between 2b VSRs from a subgroup-I strain (CMV-SD) and subgroup-II (CMV-Q) showed the 2b suppressor activity is more robust in CMV-SD as its 2b contains a domain 3 in the highly variable region (HV2) responsible for blocking antiviral *AGO4* transcription. This domain 3 is absent in less virulent CMV-Q 2b, which has only 100 amino acid (aa) residues than strains in subgroup-I that typically have 2b proteins with 110-111 aa (Y. Wang et al., 2004). However, Q2b can still reduce the level of *AGO4*, although less potently than SD2b (Ye, Qu, Zhang, Geng, & Fang, 2009).

Another class of AGO-1 targeting VSR called P0 is found in poleroviruses that cause severe crop loss under favorable conditions. Although P0 proteins in diverse poleroviruses have little amino acid sequence homology, they contain a conserved F-box-like motif [LPXX(L/I)X_{10-13}P] in the N-terminal region which is essential for its VSR activity (Pazhouhandeh et al., 2006; Zhuo et al., 2014). Unlike 2b, P0 cannot bind siRNAs (Csorba, Lózsa, Hutvágner, & Burgyán, 2010). In the case of *Cucurbit aphid-borne yellows virus* (CABYV), P0 is shown to interact via its minimal F-box like motif with S-phase kinase-associated protein 1 (SKP1), which is a crucial component of the SKP1–Cullin 1–F-box (SCF) E3 ubiquitin ligase family to direct AGO1 degradation (Baumberger, Tsai, Lie, Havecker, & Baulcombe, 2007; Pazhouhandeh et al., 2006). Interestingly, other P0 proteins in poleroviruses like *Pea mild chlorosis virus* and Inner Mongolian isolate of *Potato*

leafroll virus, that lack the L or I residue in the consensus L/I position of F-box motif has silencing suppressor activity independent of its interaction with SKP1 (Sun et al., 2020; Zhuo et al., 2014). Further studies reported P0 to interact and co-localize with AGO1 at least in *Beet western yellows virus* (BWYV), and its degradation of AGO1 is insensitive to proteasome inhibitors (Bortolamiol, Pazhouhandeh, Marrocco, Genschik, & Ziegler-Graff, 2007; Derrien et al., 2012).

Interestingly, an alanine scanning mutagenesis study in 2b protein of CMV-Rs, belonging to subgroup-I, showed ^{55}LPF^{57} is essential for the suppressor function of 2b, and the predicted mutation in these residues reduces the stability of siRNA-RISC complex (Nemes, Gellért, Balázs, & Salánki, 2014). Also, CMV 2b-mediated degradation of host catalase 3 might involve the host proteasome pathway (Murota, Shimura, Takeshita, & Masuta, 2017). Another recent study showed a novel antiviral regulatory mechanism as CMV 1a replicase protein binds to and sequesters 2b to prevent AGO2 mediated resistance against aphids, the insect vector of CMV, and mitigates 2b-induces severe symptoms (Watt et al., 2020). Therefore, the pathways VSRs use to inhibit host antiviral defense are more complex than what we already know, and many VSRs potentially interact with components of RNA-silencing pathways in yet unknown ways.

Based on the collective pieces of evidence that indicate both 2b and P0 co-localize with and uses AGO1 as a substrate, we analyzed the effect of host SKP1 silencing on CMV-Q accumulation in *Nicotiana benthamiana.* Using virus-induced gene silencing (VIGS), we successfully silenced host SKP1, and CMV-Q

accumulation was significantly reduced in the systemic leaves of the silenced plants compared to unsilenced control plants. Subsequently, we investigated the sequence similarity between CMV-Q 2b and polerovirus P0 for possible functional relevance using multiple sequence alignment, and we identified a partially conserved F-box motif located at the N-terminal end of the CMV-Q 2b.

RESULTS AND DISCUSSION

Our preliminary results from the densitometric data generated from a semi-quantitative RT-PCR using ImageJ software showed that the plants with their *NbSKP1* gene silenced using VIGS had a ~95% reduction in SKP1 transcript level compared with plants infiltrated with EV (Fig. 6.1). The transcript levels of housekeeping gene eIF-1 were identical in both unsilenced and silenced plants (Fig. 6.1). The level of CMV-Q accumulation was ~40% reduced in SKP1-silenced systemic leaves (Fig. 6.2, lane 5), while the level of CMV-Q CP remained identical in SKP1-silenced local leaves (Fig. 6.2, lane 4) when compared with control plants (Fig. 6.2, lanes 2 and 3). The observation suggests that silencing NbSKP1 in *N. benthamiana* plants reduced the accumulation of CMV-Q in systemic leaves.

Subsequently, we aligned the conserved F-box-like motifs from ten polerovirus P0 proteins with CMV 2b sequences (Fig. 6.3). The alignments indicate CMV-Q 2b has the conserved LP sequence, which is a part of the [LPXX(L/I)X_{10-13}P] motif and has been reported to be necessary for VSR activity in both CMV and poleroviruses (Fig. 6.3B) (Nemes et al., 2014; Pazhouhandeh et al., 2006; Zhuo et al., 2014). The conserved P residue of the F-box-like motif is also present in CMV-Q 2b and all of the P0 sequences. However, like PMCV, which lacks L/I in the [LPXX(L/I)X_{10-13}P] motif, which might be necessary for physical interaction with SKP1 (Sun et al., 2020), Q 2b does not have a L/I in the predicted F-box motif. However, it seems to have the conserved W present in the 2nd F-box motif of PLRV

and essential for the VSR function (Zhuo et al., 2014) (Fig. 6.3C). In summary, CMV-Q 2b protein has the minimum F-box-like motif like P0 silencing suppressor present in poleroviruses, and residues reported for the VSR activity of P0 are conserved in Q 2b protein.

NbSKP1 is vital for defense against tobacco mosaic virus in *N. benthamiana* plants, as silencing the NbSKP1 makes transgenic plants carrying the resistance gene N lose resistance against the virus (Liu, Schiff, Serino, Deng, & Dinesh-Kumar, 2002). On the other hand, 2b in CMV has been shown to influence both local and systemic movement of CMV (Soards, Murphy, Palukaitis, & Carr, 2002). Therefore, a bimolecular fluorescence complementation (BiFC) assay and a co-immunoprecipitation (Co-IP) assay should be conducted as a logical next step to determine whether Q 2b physically interacts with NbSKP1 or its silencing VSR activity is independent of direct interaction with NbSKP1. Additionally, it will be interesting to investigate whether Q 2b has alternative pathways to target proteins like AGO1, with which it is reported to interact (Zhang et al., 2006), using one or more components of the SCF complex. Furthermore, we can determine the role of SKP1 in the VSR function of Q 2b by silencing SKP1 in 16c transgenic *N. benthamiana* plants that highly and constitutively express a green fluorescent protein (GFP).

MATERIALS AND METHODS

Agroplasmids used in virus-induced gene silencing (VIGS)

The TRV2:*NbSKP1* construct was used to silence the *SKP1* gene in *N. benthamiana* plants using virus-induced gene silencing (VIGS), as reported previously. Briefly, a cDNA fragment of putative *N. benthamiana skp1* (1-411 nt) was amplified and cloned into pTRV2 (Liu et al., 2002). TRV1, TRV2:EV, and TRV2:*EC1* control were used as described previously (Manosalva, Manohar, Kogel, Kang, & Klessig, 2015). A TRV2:*PDS* construct was used as a positive control (Velásquez, Chakravarthy, & Martin, 2009). The VIGS experiment was performed as described previously (Senthil-Kumar & Mysore, 2014).

N. benthamiana plants were grown in a growth chamber under 16-h light/8-h dark at 22°C with 70% relative humidity. Plants used for silencing were three weeks old and infiltrated in two of the most prominent true leaves, an inoculum of *Agrobacterium* cells harboring TRV1 and TRV2:*NbSKP1*. As controls, TRV1+ TRV2:*EV*, TRV1+ TRV2:*EC1*, TRV1+ TRV2:*PDS* and were also infiltrated in individual plants. Plants were maintained at 22°C with a 16-h light/8-h dark cycle and 50% relative humidity for another fourteen days. After 14 days post infiltration (dpi), the upper leaves were mechanically inoculated with 15 µg of purified CMV-Q virions. The inoculated local leaves were harvested at 4 days after virus infection, and the systemic leaves were harvested at 15 days after virus infection.

RNA extraction and semi-quantitative RT-PCR

Total RNA was isolated from local and systemic leaves of control and experimental plants by grinding the frozen leaves in TRIzol™ (Thermo Fisher Scientific) reagent. Briefly, half a leaf was ground in liquid nitrogen in ice-cold mortar and pestle. Approximately 1.5 ml TRIzol™ and 20 ul 5% Bentonite was added to the ground leaf and was ground to a fine powder. The upper phase was collected by centrifuging at 12000 rpm for 15 min at room temperature. Subsequently, 500 ul of chloroform was added to it and was mixed by shaking it for 15 sec. The mixture was incubated undisturbed at room temperature for 5 min and then centrifuged for another 15 min at 12000 rpm. To the resultant upper phase, 500 ul of isopropanol was added and was incubated for 30 min at -80°C. The total RNA was then collected by centrifuging it at 4 ^{o}C for 30 min at 14000 rpm and washing the pellet with 75% ethanol. The air-dried RNA pellet was resuspended in RNAse-free water. 1 ug total RNA from each sample was subjected to RT-PCR using iScript™ cDNA Synthesis Kit (Bio-Rad) and Phusion® High-Fidelity DNA Polymerase (NEB). The resultant PCR products were analyzed using 1% agarose gel. The band intensity was quantified in unsilenced versus silenced plants using ImageJ software (Schneider, Rasband, & Eliceiri, 2012).

Total protein extraction and Western blot analysis

Total protein was extracted in 3 volumes of extraction buffer (20mM Tris-Cl; pH 7.5, 1mM EDTA; pH 8.0, 5mM DTT). The leaf slurry was centrifuged at 14,000 rpm for 5 minutes, and the supernatant was used for downstream analysis of total proteins. Each sample was suspended in SDS-PAGE sample buffer (125mM Tris, pH 6.8, 10% [w/v] glycerol, 2.5% [w/v] DTT, 2% SDS, 0.01% bromophenol blue) and was denatured at 100°C for 5 minutes. The proteins were separated on 12% SDS-PAGE gel, and after separation, the proteins were transferred to a PVDF membrane. Western blot analysis was performed with CMV-Q CP antibody (1:1000 dilution). A secondary antibody conjugated with alkaline phosphatase (BioRad) was used, and bands were visualized by exposing the membrane to a substrate buffer containing NBT (nitro-blue tetrazolium chloride) and BCIP (5-Bromo-4-chloro-3'-indolyl-phosphate, 4-toluidine salt). Following Western blot, the intensity of CMV-Q CP bands was quantified in unsilenced versus silenced plants using ImageJ software (Schneider et al., 2012).

Multiple sequence alignment of CMV-Q 2b sequence with reported polerovirus P0 proteins

Following sequences were downloaded from Genbank: 2b of CMV-Fny (NC002035), CMV-Q (Z21863), P0 of poleroviruses cucurbit aphid-borne yellows virus (CABYV; EU000535), beet mild yellowing virus (BMYV; X83110), beet

western yellows virus (BWYV; NC_004756), cereal yellow dwarf virus-RPV (CYDV-RPV; NC_004751), melon aphid-borne yellows virus (MABYV; EU000534), brassica yellows virus isolate BrYV-ABJ (BrYV-ABJ; HQ388348), maize yellow mosaic virus isolate Yunnan11 (MaYMV-Yunnan11; KU248489), potato leafroll virus isolate PLRV-IM (KC456052), turnip yellows virus (TuYV; NC003743), and pea mild chlorosis virus (PMCV; JF507725). The reported and conserved F-box-like motif [LPXX(L/I)X_{10-13}P] in the N-terminal region of P0 proteins which is essential for its VSR activity, were aligned with 2b protein sequences using the MUSCLE (MUltiple Sequence Comparison by Log- Expectation) tool (https://www.ebi.ac.uk/Tools/msa/muscle/) (Edgar, 2004).

ACKNOWLEDGEMENTS

We thank Dr. Dinesh Kumar (UC Davis) for providing us the TRV2-NbSKP1 construct and Dr. Patricia Manosalva (UC Riverside) for kindly providing us TRV1, TRV2:EV, TRV2:*EC1*, and TRV2:*PDS* constructs.

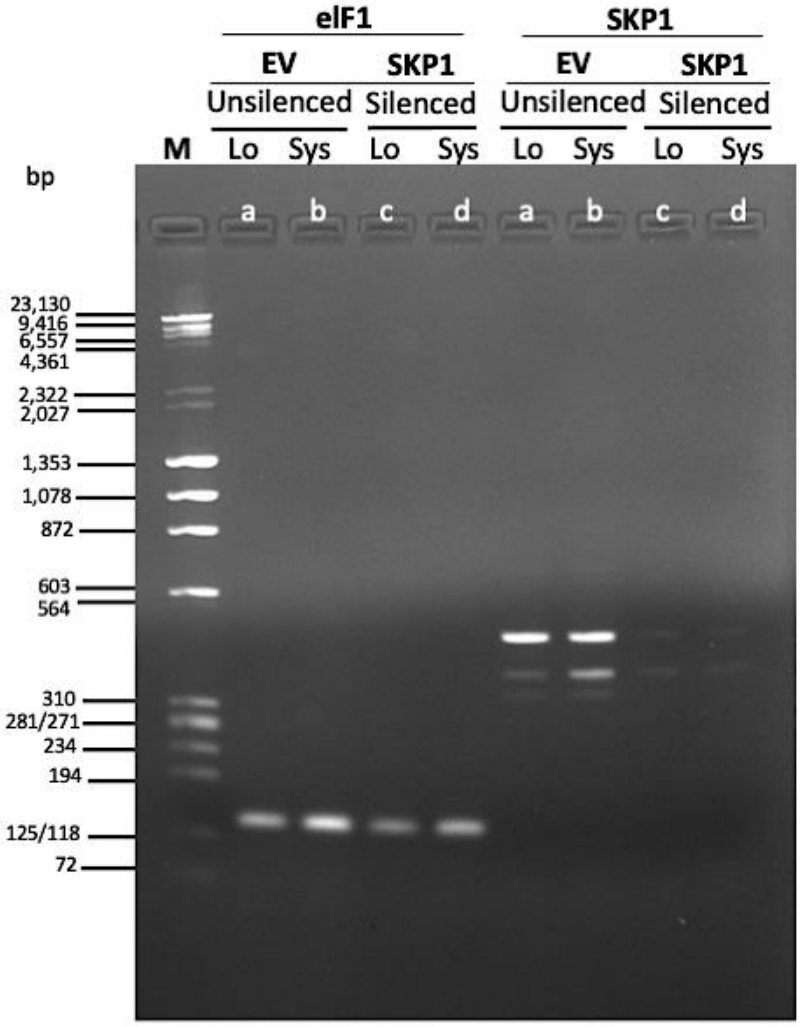

Figure 6.1 Semi-quantitative RT-PCR experiment to quantify the level of housekeeping gene elF1 and SKP1 transcripts in plants either infiltrated with TRV1+ TRV2:*EV* or TRV1+ TRV2:*NbSKP1*. M, marker lane.

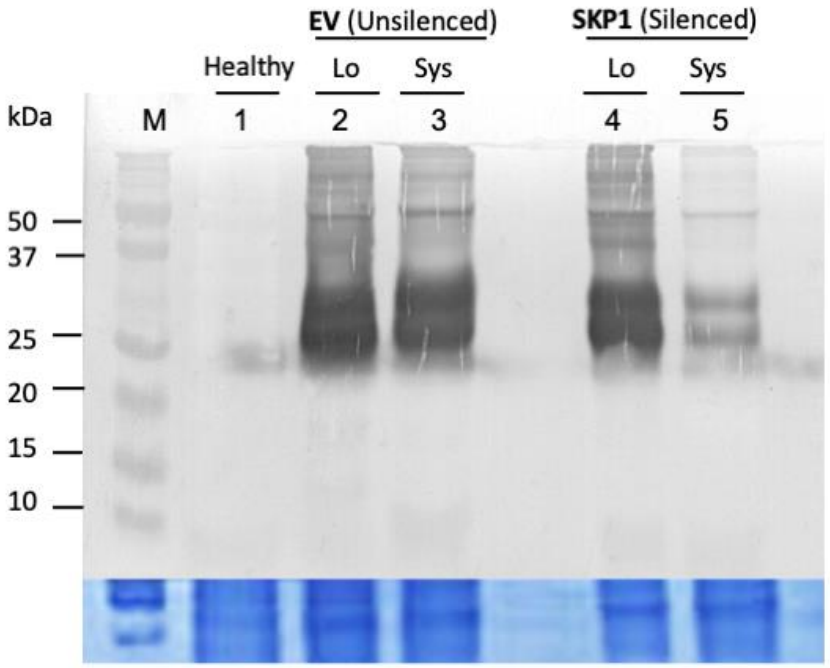

Figure 6.2 Levels of CMV-Q accumulation in local and systemic leaves monitored by Western blotting in plants either infiltrated with empty vector (EV) or in plants with NbSKP1 silenced. Healthy WT *N. benthamiana* leaf of the same developmental stage serves as control (lane 1), EV local leaf (lane 2), EV systemic leaf (lane 3), SKP1 silenced local leaf (lane 4), and SKP1 silenced systemic leaf (lane 5).

Figure 6.3 Alignment of conserved F-box-like motifs from ten polerovirus P0 proteins with CMV 2b sequences. (A) Pairwise alignment between CMV-Q and CMV-Fny 2b sequence shows the absence of domain 3 in CMV-Q 2b. The ^{55}LPF^{57}, essential for the suppressor function of 2b and conserved in both Fny-2b and Q-2b, is highlighted with a black border. (B) The sequence of Q-2b is aligned with F-box motifs of P0 in CABYV (EU000535), BMYV (X83110), BWYV (NC_004756), CYDV-RPV (NC_004751), MABYV (EU000534), BrYV-ABJ (HQ388348), MaYMV-Yunnan11 (KU248489), PLRV-IM (KC456052), TuYV (NC003743), and PMCV (JF507725). The conserved residues are highlighted with a red border. (C) The sequence of Q-2b is aligned with F-box motifs of P0 in PLRV-IM (KC456052) which has two putative motifs and PMCV (JF507725). The conserved residues are highlighted with a red border. See "Results and discussion" for details)

REFERENCES

Baulcombe, D. (2004). RNA silencing in plants. *Nature, 431*(7006), 356-363. doi:10.1038/nature02874

Baumberger, N., Tsai, C. H., Lie, M., Havecker, E., & Baulcombe, D. C. (2007). The Polerovirus silencing suppressor P0 targets ARGONAUTE proteins for degradation. *Curr Biol, 17*(18), 1609-1614. doi:10.1016/j.cub.2007.08.039

Blevins, T., Rajeswaran, R., Shivaprasad, P. V., Beknazariants, D., Si-Ammour, A., Park, H. S., . . . Pooggin, M. M. (2006). Four plant Dicers mediate viral small RNA biogenesis and DNA virus induced silencing. *Nucleic Acids Res, 34*(21), 6233-6246. doi:10.1093/nar/gkl886

Bortolamiol, D., Pazhouhandeh, M., Marrocco, K., Genschik, P., & Ziegler-Graff, V. (2007). The Polerovirus F box protein P0 targets ARGONAUTE1 to suppress RNA silencing. *Curr Biol, 17*(18), 1615-1621. doi:10.1016/j.cub.2007.07.061

Burgyán, J., & Havelda, Z. (2011). Viral suppressors of RNA silencing. *Trends Plant Sci, 16*(5), 265-272. doi:10.1016/j.tplants.2011.02.010

Carbonell, A., Fahlgren, N., Garcia-Ruiz, H., Gilbert, K. B., Montgomery, T. A., Nguyen, T., . . . Carrington, J. C. (2012). Functional analysis of three Arabidopsis ARGONAUTES using slicer-defective mutants. *Plant Cell, 24*(9), 3613-3629. doi:10.1105/tpc.112.099945

Csorba, T., Lózsa, R., Hutvágner, G., & Burgyán, J. (2010). Polerovirus protein P0 prevents the assembly of small RNA-containing RISC complexes and leads to degradation of ARGONAUTE1. *Plant J, 62*(3), 463-472. doi:10.1111/j.1365-313X.2010.04163.x

Cuperus, J. T., Carbonell, A., Fahlgren, N., Garcia-Ruiz, H., Burke, R. T., Takeda, A., . . . Carrington, J. C. (2010). Unique functionality of 22-nt miRNAs in triggering RDR6-dependent siRNA biogenesis from target transcripts in Arabidopsis. *Nat Struct Mol Biol, 17*(8), 997-1003. doi:10.1038/nsmb.1866

Deleris, A., Gallego-Bartolome, J., Bao, J., Kasschau, K. D., Carrington, J. C., & Voinnet, O. (2006). Hierarchical action and inhibition of plant Dicer-like proteins in antiviral defense. *Science, 313*(5783), 68-71. doi:10.1126/science.1128214

Derrien, B., Baumberger, N., Schepetilnikov, M., Viotti, C., De Cillia, J., Ziegler-Graff, V., . . . Genschik, P. (2012). Degradation of the antiviral component ARGONAUTE1 by the autophagy pathway. *Proc Natl Acad Sci U S A, 109*(39), 15942-15946. doi:10.1073/pnas.1209487109

Diaz-Pendon, J. A., Li, F., Li, W. X., & Ding, S. W. (2007). Suppression of antiviral silencing by cucumber mosaic virus 2b protein in Arabidopsis is associated with drastically reduced accumulation of three classes of viral small interfering RNAs. *Plant Cell, 19*(6), 2053-2063. doi:10.1105/tpc.106.047449

Donaire, L., Barajas, D., Martínez-García, B., Martínez-Priego, L., Pagán, I., & Llave, C. (2008). Structural and genetic requirements for the biogenesis of tobacco rattle virus-derived small interfering RNAs. *J Virol, 82*(11), 5167-5177. doi:10.1128/JVI.00272-08

Edgar, R. C. (2004). MUSCLE: multiple sequence alignment with high accuracy and high throughput. *Nucleic Acids Res, 32*(5), 1792-1797. doi:10.1093/nar/gkh340

Garcia-Ruiz, H., Carbonell, A., Hoyer, J. S., Fahlgren, N., Gilbert, K. B., Takeda, A., . . . Carrington, J. C. (2015). Roles and programming of Arabidopsis ARGONAUTE proteins during Turnip mosaic virus infection. *PLoS Pathog, 11*(3), e1004755. doi:10.1371/journal.ppat.1004755

González, I., Martínez, L., Rakitina, D. V., Lewsey, M. G., Atencio, F. A., Llave, C., . . . Canto, T. (2010). Cucumber mosaic virus 2b protein subcellular targets and interactions: their significance to RNA silencing suppressor activity. *Mol Plant Microbe Interact, 23*(3), 294-303. doi:10.1094/MPMI-23-3-0294

Goto, K., Kobori, T., Kosaka, Y., Natsuaki, T., & Masuta, C. (2007). Characterization of silencing suppressor 2b of cucumber mosaic virus based on examination of its small RNA-binding abilities. *Plant Cell Physiol, 48*(7), 1050-1060. doi:10.1093/pcp/pcm074

Guo, H. S., & Ding, S. W. (2002). A viral protein inhibits the long range signaling activity of the gene silencing signal. *EMBO J, 21*(3), 398-407. doi:10.1093/emboj/21.3.398

Jacquemond, M. (2012). Cucumber mosaic virus. *Adv Virus Res, 84*, 439-504. doi:10.1016/B978-0-12-394314-9.00013-0

Ji, L. H., & Ding, S. W. (2001). The suppressor of transgene RNA silencing encoded by Cucumber mosaic virus interferes with salicylic acid-mediated virus resistance. *Mol Plant Microbe Interact, 14*(6), 715-724. doi:10.1094/MPMI.2001.14.6.715

Liu, Y., Schiff, M., Serino, G., Deng, X. W., & Dinesh-Kumar, S. P. (2002). Role of SCF ubiquitin-ligase and the COP9 signalosome in the N gene-mediated resistance response to Tobacco mosaic virus. *Plant Cell, 14*(7), 1483-1496. doi:10.1105/tpc.002493

Manosalva, P., Manohar, M., Kogel, K. H., Kang, H. G., & Klessig, D. F. (2015). The GHKL ATPase MORC1 Modulates Species-Specific Plant Immunity in Solanaceae. *Mol Plant Microbe Interact, 28*(8), 927-942. doi:10.1094/MPMI-12-14-0401-R

Mayers, C. N., Palukaitis, P., & Carr, J. P. (2000). Subcellular distribution analysis of the cucumber mosaic virus 2b protein. *J Gen Virol, 81*(Pt 1), 219-226. doi:10.1099/0022-1317-81-1-219

Murota, K., Shimura, H., Takeshita, M., & Masuta, C. (2017). Interaction between Cucumber mosaic virus 2b protein and plant catalase induces a specific necrosis in association with proteasome activity. *Plant Cell Rep, 36*(1), 37-47. doi:10.1007/s00299-016-2055-2

Nemes, K., Gellért, Á., Balázs, E., & Salánki, K. (2014). Alanine scanning of cucumber mosaic virus (CMV) 2b protein identifies different positions for cell-to-cell movement and gene silencing suppressor activity. *PLoS One, 9*(11), e112095. doi:10.1371/journal.pone.0112095

Palukaitis, P., & García-Arenal, F. (2003). Cucumoviruses. In *Advances in Virus Research* (Vol. 62, pp. 241-323): Academic Press.

Pazhouhandeh, M., Dieterle, M., Marrocco, K., Lechner, E., Berry, B., Brault, V., . . . Ziegler-Graff, V. (2006). F-box-like domain in the polerovirus protein P0 is required for silencing suppressor function. *Proc Natl Acad Sci U S A, 103*(6), 1994-1999. doi:10.1073/pnas.0510784103

Qu, F. (2010). Antiviral role of plant-encoded RNA-dependent RNA polymerases revisited with deep sequencing of small interfering RNAs of virus origin. *Mol Plant Microbe Interact, 23*(10), 1248-1252. doi:10.1094/MPMI-06-10-0124

Ruiz-Ferrer, V., & Voinnet, O. (2009). Roles of plant small RNAs in biotic stress responses. *Annu Rev Plant Biol, 60*, 485-510. doi:10.1146/annurev.arplant.043008.092111

Schneider, C. A., Rasband, W. S., & Eliceiri, K. W. (2012). NIH Image to ImageJ: 25 years of image analysis. *Nat Methods, 9*(7), 671-675. doi:10.1038/nmeth.2089

Senthil-Kumar, M., & Mysore, K. S. (2014). Tobacco rattle virus-based virus-induced gene silencing in Nicotiana benthamiana. *Nat Protoc, 9*(7), 1549-1562. doi:10.1038/nprot.2014.092

Soards, A. J., Murphy, A. M., Palukaitis, P., & Carr, J. P. (2002). Virulence and differential local and systemic spread of cucumber mosaic virus in tobacco are affected by the CMV 2b protein. *Mol Plant Microbe Interact, 15*(7), 647-653. doi:10.1094/MPMI.2002.15.7.647

Sun, Q., Zhuo, T., Zhao, T., Zhou, C., Li, Y., Wang, Y., . . . Han, C. (2020). Functional Characterization of RNA Silencing Suppressor P0 from Pea Mild Chlorosis Virus. *Int J Mol Sci, 21*(19). doi:10.3390/ijms21197136

Velásquez, A. C., Chakravarthy, S., & Martin, G. B. (2009). Virus-induced gene silencing (VIGS) in Nicotiana benthamiana and tomato. *J Vis Exp*(28). doi:10.3791/1292

Wang, X. B., Wu, Q., Ito, T., Cillo, F., Li, W. X., Chen, X., . . . Ding, S. W. (2010). RNAi-mediated viral immunity requires amplification of virus-derived siRNAs in Arabidopsis thaliana. *Proc Natl Acad Sci U S A, 107*(1), 484-489. doi:10.1073/pnas.0904086107

Wang, Y., Tzfira, T., Gaba, V., Citovsky, V., Palukaitis, P., & Gal-On, A. (2004). Functional analysis of the Cucumber mosaic virus 2b protein: pathogenicity and nuclear localization. *J Gen Virol, 85*(Pt 10), 3135-3147. doi:10.1099/vir.0.80250-0

Watt, L. G., Crawshaw, S., Rhee, S. J., Murphy, A. M., Canto, T., & Carr, J. P. (2020). The cucumber mosaic virus 1a protein regulates interactions between the 2b protein and ARGONAUTE 1 while maintaining the silencing suppressor activity of the 2b protein. *PLoS Pathog, 16*(12), e1009125. doi:10.1371/journal.ppat.1009125

Wu, Q., Wang, X., & Ding, S. W. (2010). Viral suppressors of RNA-based viral immunity: host targets. *Cell Host Microbe, 8*(1), 12-15. doi:10.1016/j.chom.2010.06.009

Ye, J., Qu, J., Zhang, J. F., Geng, Y. F., & Fang, R. X. (2009). A critical domain of the Cucumber mosaic virus 2b protein for RNA silencing suppressor activity. *FEBS Lett, 583*(1), 101-106. doi:10.1016/j.febslet.2008.11.031

Zhang, X., Yuan, Y. R., Pei, Y., Lin, S. S., Tuschl, T., Patel, D. J., & Chua, N. H. (2006). Cucumber mosaic virus-encoded 2b suppressor inhibits Arabidopsis Argonaute1 cleavage activity to counter plant defense. *Genes Dev, 20*(23), 3255-3268. doi:10.1101/gad.1495506

Zhuo, T., Li, Y.-Y., Xiang, H.-Y., Wu, Z.-Y., Wang, X.-B., Wang, Y., . . . Han, C.-G. (2014). Amino Acid Sequence Motifs Essential for P0-Mediated Suppression of RNA Silencing in an Isolate of Potato leafroll virus from Inner Mongolia. *Molecular Plant-Microbe Interactions®, 27*(6), 515-527. doi:10.1094/MPMI-08-13-0231-R

CONCLUSIONS AND FUTURE DIRECTIONS

The research presented in this thesis is aimed towards mapping capsid dynamics or the local and global rearrangement of peptides present on the capsid surface and the functional significance of such dynamics in member viruses of the family Bromoviridae. Fluctuating dynamic properties of viral capsids have been well-studied in animal viruses like poliovirus and adeno-associated viruses (Rayaprolu et al., 2013; Roivainen, Piirainen, Rysä, Närvänen, & Hovi, 1993). On the other hand, several reports of dynamics in plant viral capsids used WT BMV and CCMV, a constellation of three types of virions carrying its unique RNA species. Therefore, the reported data was an average of three virion types, obscuring our understanding of possibly existing unique dynamism in each virion type (Calhoun, Speir, & Rao, 2007; Speir et al., 2006). Also, the individual morphologically similar virion types in multicomponent bromoviruses were impossible to separate by known separation techniques like sucrose density gradient centrifugation due to their particle homogeneity.

Chapter 1 of this thesis used a robust agroinfiltration-based strategy to assemble each virion type of BMV independently in *Nicotiana benthamiana.* We established that the virions were pure and free from their other two counterparts using a series of biological and biochemical assays. Analysis of packaged RNA progeny in BMV revealed $B1^V$ and $B2^V$ made up to ~40% of total virions in BMV,

with $B1^V$ being the least abundant virions at ~10%. The remaining ~60% virions were of $B3+4^V$, the predominant virion type in the WT population. Subsequently, using differential scanning fluorimetry and limited proteolysis followed by peptide mass mapping by MALDI-TOF revealed two classes of BMV virions having qualitatively different dynamics: the $B1^V$ and $B2^V$ having higher stability were grouped in class I and $B3+4^V$, which were unstable upon trypsin treatment and had the reported K65, R103, K111, and K165 residues on the capsid surface in class II. Furthermore, we proposed that the class I virions are stable with only their N-ARM to translate the replicase proteins they code for upon entry into the host cell. The unstable class II virions easily dissociate to allow replication of RNA3 to synthesize subgenomic RNA4 and capsid protein to stimulate the synthesis of plus-strand viral RNA over minus-strand (Chakravarty, Reddy, & Rao, 2020). The atomic structure of the $B3+4^V$ was subsequently elucidated, and the RNA inside these virions was highly disordered and associated with the capsid shell compared to monocomponent virions, which follow a different strategy of using “packaging signals” for genome encapsidation (Beren et al., 2020). In the future, the atomic structure of $B1^V$ and $B2^V$ should be determined by single-particle tomography to map the conformational homogeneity in these virion types conclusively. Additionally, our agroinfiltration approach for assembling individual virions and analyzing their capsid dynamics can be extended to CMV, an economically important plant virus causing significant crop loss, and CMV virions containing satellite RNA.

Chapter 2 extended the approach we have used in chapter 1 to assemble the three virion types of CCMV independently in *N. benthamiana*. CCMV is a bromovirus closely related to BMV, and both viruses asymptomatically infect *N. benthamiana*, an experimental dicot host. However, in a natural environment, BMV is a monocot-adapted virus vs. CCMV, which only infects dicots like black-eyed peas. Using the assays introduced in chapter 1, we determined that each type of CCMV virions independently assembled in *N. benthamiana* were pure with identical morphology and electrophoretic mobility profiles and contained the desired RNA progeny. Next, we studied the influence of host species in the dynamic properties of virions (Chakravarty & Rao, 2021) and observed that WT CCMV virions assembled in natural host cowpea were less thermally stable susceptible to extensive proteolysis compared to WT CCMV assembled in an experimental host *N. benthamiana.* The individual virion types also showed identical thermal stability and proteolytic cleavage profile as BMV, with the $C1^V$ and $C2^V$ had higher stability than $C3+4^V$, which were unstable upon trypsin treatment. We also observed the disproportionate distribution of each virion type in the WT CCMV population in cowpea, with $C3+4^V$ being the most prevalent type at ~54%. Therefore, it was expected that the proteolysis profile of $C3+4^V$ would closely mimic that of WT CCMV in cowpea. We speculate that the identical dynamic properties of both bromoviruses, BMV and CCMV, in *N. benthamiana* could be an adaptation to the same host. For future studies, we need to assemble individual virion types

of CCMV in its natural host cowpea and investigate if and how host plants influence capsid dynamics in plant viruses (Verduin, 1978).

Chapter 3 is an extension of studies in bromovirus capsid dynamics, and here we attempted to investigate the comparative dynamics of BMV and CCMV capsids assembled in the presence of heterologous replicase. We assembled BMV and CCMV RNA3+4 containing virions assembled in the presence of heterologous BMV 1a/2a and CCMV 1a/2a replicase exploiting the inherent compatibility of RNA3 between these two viruses (Dinant, Janda, Kroner, & Ahlquist, 1993). We observed that virions assembled in the presence of homologous replicase were different in their stability and dynamics from their counterparts assembled with heterologous replicase, as the latter group showed increased thermal stability and highly resistant to proteolysis as confirmed with EM and MALDI-TOF. The biological relevance of such heightened stability should be investigated *in vivo* infection studies, and the atomic structure of the heterologous virions should be determined to map the rearrangement of residues on the capsid surface.

Chapter 4 investigated the critical reason behind the co-packaging of a genetically redundant subgenomic RNA in B3+4^{V} of BMV, which is not required to initiate infection. We assembled B3+4^{V} and RNA3 only containing virions (B3^{V}) and compared their stability and dynamics to determine the functional relevance

of packaging subgenomic RNA4. The $B3^V$ has previously been reported to be unable to move systemically in *Chenopodium quinoa*. Also, $B3^V$ caused local necrotic lesions in *C. quinoa* compared to $B3+4^{V,}$ which caused chlorotic lesions (Choi & Rao, 2000). We attempted to correlate these phenotypic differences to capsid dynamics and observed that the $B3^V$ had near-identical thermal stability as $B3+4^V$, but the former class was remarkably stable upon trypsin digestion compared to $B3+4^V$, which readily digested as reported previously. Subsequently, we investigated the cell-to-cell movement in $B3^V$ vs. $B3+4^V$. When supplemented with their counterparts $B1^V$ and $B2^V$ via agroinfiltration, $B3+4^V$ moved locally following the timeline of natural BMV infection, whereas $B3^V$ did not move from cell-to-cell beyond six days post infiltration and remained localized only in the infiltrated cells. Based on these observations, we propose that a particular class of virions like RNA3+4 containing virions may not effectively move from cell to cell without subgenomic RNA. Therefore, as a logical next step, we must determine which virion populations moved from the infiltrated area till four days post infiltration to determine which populations did not. For this purpose, virions should be extracted from infiltrated (source) and non-infiltrated (sink) leaf areas. An RT-PCR experiment should be conducted to test which RNA species the virions in each area package.

Chapter 5 characterized Virus-like Particles (VLPs) assembled from the Gag protein of *Human immunodeficiency virus* (HIV-1) in *N. benthamiana*. Plant-based VLPs have been explored as powerful tools to study the maturation process of eukaryotic viruses (Castells-Graells et al., 2021). Prior studies had failed to achieve a high level of Gag expression in plants (Meyers et al., 2008; Scotti et al., 2009). Our results showed that a high level of p55-Gag could be consistently expressed in plants co-expressing p19, a viral silencing suppressor. VLPs were released from infiltrated leaves by enzymatic digestion at four days post-infiltration and pelleted through sucrose cushion followed by another round of sucrose density gradient centrifugation. Electron microscopic examination of the VLPs showed that the wild-type p55-Gag (codon-optimized for humans) assembled into both spherical VLPs of 80 nm diameter and long flexuous rods up to 1 µm in length and 20 nm diameter. These VLPs were susceptible to Proteinase K but not to either DNase or RNase treatment. Analysis of RNA isolated from the VLPs revealed that they encapsidated a single RNA species of approximately 10 kb that contained HIV-1 Gag-specific sequences. As future steps in this research, attempts should be made to determine the assembly phenotype of individual Gag segments like MA and CA-NC in plants to map the entire maturation process of Gag.

Finally, **Chapter 6** attempted to silence the NbSKP1 gene, a component of the SCF complex in *N. benthamiana* using virus-induced gene silencing (VIGS),

and the effect on cucumber mosaic virus-Q strain accumulation was studied. Several viruses use SCF ubiquitin-ligase complex to counter defense against plant antiviral RNA silencing mechanisms (Burgyán & Havelda, 2011). Although the mechanism of VSR function in CMV-Q 2b has been elucidated to a great extent, the pathways VSRs use to inhibit host antiviral defense are more complex than what we already know, and many VSRs potentially interact with components of RNA-silencing pathways in yet unknown ways (Diaz-Pendon, Li, Li, & Ding, 2007; González et al., 2010; Guo & Ding, 2002; Ji & Ding, 2001; Mayers, Palukaitis, & Carr, 2000). Our preliminary data showed *NbSKP1* gene silenced using VIGS had a ~95% reduction in SKP1 transcript level compared with plants infiltrated with an empty vector. We also observed a strong correlation between the reduction of SKP1 transcript level and the level of CMV-Q accumulation being reduced by ~40% in SKP1-silenced systemic leaves. A subsequent multiple sequence alignment determined the minimum F-box-like motif like P0 silencing suppressor present in poleroviruses, and residues reported for the VSR activity of P0 are conserved in Q 2b protein. As the next steps in this project, a bimolecular fluorescence complementation (BiFC) assay and a co-immunoprecipitation (Co-IP) assay should be conducted to determine whether Q 2b physically interacts NbSKP1 or its silencing VSR activity is independent of direct interaction with NbSKP1. Additionally, it will be interesting to investigate whether Q 2b has alternative pathways to target proteins like AGO1, with which it is reported to interact (Zhang et al., 2006) using one or more components of the SCF complex.

Furthermore, we can determine the role of SKP1 in the VSR function of Q 2b by silencing SKP1 in 16c transgenic *N. benthamiana* plants that highly and constitutively express a green fluorescent protein (GFP).

REFERENCES

Beren, C., Cui, Y., Chakravarty, A., Yang, X., Rao, A. L. N., Knobler, C. M., . . . Gelbart, W. M. (2020). Genome organization and interaction with capsid protein in a multipartite RNA virus. *Proc Natl Acad Sci U S A, 117*(20), 10673-10680. doi:10.1073/pnas.1915078117

Burgyán, J., & Havelda, Z. (2011). Viral suppressors of RNA silencing. *Trends Plant Sci, 16*(5), 265-272. doi:10.1016/j.tplants.2011.02.010

Calhoun, S. L., Speir, J. A., & Rao, A. L. (2007). In vivo particle polymorphism results from deletion of a N-terminal peptide molecular switch in brome mosaic virus capsid protein. *Virology, 364*(2), 407-421. doi:10.1016/j.virol.2007.03.034

Castells-Graells, R., Ribeiro, J. R. S., Domitrovic, T., Hesketh, E. L., Scarff, C. A., Johnson, J. E., . . . Lomonossoff, G. P. (2021). Plant-expressed virus-like particles reveal the intricate maturation process of a eukaryotic virus. *Commun Biol, 4*(1), 619. doi:10.1038/s42003-021-02134-w

Chakravarty, A., & Rao, A. L. (2021). The interplay between capsid dynamics and pathogenesis in tripartite bromoviruses. *Curr Opin Virol, 47*, 45-51. doi:10.1016/j.coviro.2020.12.005

Chakravarty, A., Reddy, V. S., & Rao, A. L. N. (2020). Unravelling the stability and capsid dynamics of the three virions of brome mosaic virus assembled autonomously. *J Virol, 94*(8). doi:10.1128/JVI.01794-19

Choi, Y. G., & Rao, A. L. (2000). Molecular studies on bromovirus capsid protein. VII. Selective packaging on BMV RNA4 by specific N-terminal arginine residuals. *Virology, 275*(1), 207-217. doi:10.1006/viro.2000.0513

Diaz-Pendon, J. A., Li, F., Li, W. X., & Ding, S. W. (2007). Suppression of antiviral silencing by cucumber mosaic virus 2b protein in Arabidopsis is associated with drastically reduced accumulation of three classes of viral small interfering RNAs. *Plant Cell, 19*(6), 2053-2063. doi:10.1105/tpc.106.047449

Dinant, S., Janda, M., Kroner, P. A., & Ahlquist, P. (1993). Bromovirus RNA replication and transcription require compatibility between the polymerase- and helicase-like viral RNA synthesis proteins. *J Virol, 67*(12), 7181-7189.

González, I., Martínez, L., Rakitina, D. V., Lewsey, M. G., Atencio, F. A., Llave, C., . . . Canto, T. (2010). Cucumber mosaic virus 2b protein subcellular targets and interactions: their significance to RNA silencing suppressor activity. *Mol Plant Microbe Interact, 23*(3), 294-303. doi:10.1094/MPMI-23-3-0294

Guo, H. S., & Ding, S. W. (2002). A viral protein inhibits the long range signaling activity of the gene silencing signal. *EMBO J, 21*(3), 398-407. doi:10.1093/emboj/21.3.398

Ji, L. H., & Ding, S. W. (2001). The suppressor of transgene RNA silencing encoded by Cucumber mosaic virus interferes with salicylic acid-mediated virus resistance. *Mol Plant Microbe Interact, 14*(6), 715-724. doi:10.1094/MPMI.2001.14.6.715

Mayers, C. N., Palukaitis, P., & Carr, J. P. (2000). Subcellular distribution analysis of the cucumber mosaic virus 2b protein. *J Gen Virol, 81*(Pt 1), 219-226. doi:10.1099/0022-1317-81-1-219

Meyers, A., Chakauya, E., Shephard, E., Tanzer, F. L., Maclean, J., Lynch, A., . . . Rybicki, E. P. (2008). Expression of HIV-1 antigens in plants as potential subunit vaccines. *BMC biotechnology, 8*, 53-53. doi:10.1186/1472-6750-8-53

Rayaprolu, V., Kruse, S., Kant, R., Venkatakrishnan, B., Movahed, N., Brooke, D., . . . Bothner, B. (2013). Comparative analysis of adeno-associated virus capsid stability and dynamics. *J Virol, 87*(24), 13150-13160. doi:10.1128/JVI.01415-13

Roivainen, M., Piirainen, L., Rysä, T., Närvänen, A., & Hovi, T. (1993). An immunodominant N-terminal region of VP1 protein of poliovirion that is buried in crystal structure can be exposed in solution. *Virology, 195*(2), 762-765. doi:10.1006/viro.1993.1427

Scotti, N., Alagna, F., Ferraiolo, E., Formisano, G., Sannino, L., Buonaguro, L., . . . Cardi, T. (2009). High-level expression of the HIV-1 Pr55gag polyprotein in transgenic tobacco chloroplasts. *Planta, 229*(5), 1109-1122. doi:10.1007/s00425-009-0898-2

Speir, J. A., Bothner, B., Qu, C., Willits, D. A., Young, M. J., & Johnson, J. E. (2006). Enhanced local symmetry interactions globally stabilize a mutant virus capsid that maintains infectivity and capsid dynamics. *J Virol, 80*(7), 3582-3591. doi:10.1128/JVI.80.7.3582-3591.2006

Verduin, B. J. M. (1978). Reversible Change in the Nucleoprotein Composition of Bromoviruses after Multiplication in Chenopodium hybridum L. *Journal of General Virology, 38*(3), 571-575. doi:10.1099/0022-1317-38-3-571

Zhang, X., Yuan, Y. R., Pei, Y., Lin, S. S., Tuschl, T., Patel, D. J., & Chua, N. H. (2006). Cucumber mosaic virus-encoded 2b suppressor inhibits Arabidopsis Argonaute1 cleavage activity to counter plant defense. *Genes Dev, 20*(23), 3255-3268. doi:10.1101/gad.1495506

PUBLICATIONS FROM THIS WORK

Peer-reviewed Publications

Chakravarty, A., & Rao, A. L. (2021). The interplay between capsid dynamics and pathogenesis in tripartite bromoviruses. *Curr Opin Virol, 47*, 45-51. doi:10.1016/j.coviro.2020.12.005

Chakravarty, A., & Rao, A. L. N. (2021). Bromoviridae: A family of plant viruses with tripartite genomes. In *eLS (Ed.)* (Accepted, in press)

Chakravarty, A., Reddy, V. S., & Rao, A. L. N. (2020). Unravelling the stability and capsid dynamics of the three Virions of brome mosaic virus assembled autonomously. *J Virol, 94*(8). doi:10.1128/JVI.01794-19

Beren, C., Cui, Y., Chakravarty, A., Yang, X., Rao, A. L. N., Knobler, C. M., . . . Gelbart, W. M. (2020). Genome organization and interaction with capsid protein in a multipartite RNA virus. *Proc Natl Acad Sci U S A, 117*(20), 10673-10680. doi:10.1073/pnas.1915078117

Publications in Preparation

Chakravarty, A., & Rao, A. L. N. (In preparation). Biological significance for co-packaging of a genetically redundant sub-genomic RNA4 in brome mosaic virus.

Chakravarty, A., Seo, J-K., & Rao, A. L. N. (In preparation). Elucidating the effect of replicase-capsid protein interaction on capsid dynamics and pathogenesis using chimeric virions of brome mosaic virus and cowpea chlorotic mottle virus.